Master's Thesis

The response of a semi-submersible floating offshore wind turbine under misaligned wind and waves

MT54035

J. B. van der Spek

Delft University of Technology

TU Delft

SIEMENS Gamesa
RENEWABLE ENERGY

Master's Thesis

The response of a semi-submersible floating offshore wind turbine under misaligned wind and waves

by

J. B. van der Spek

to obtain the degree of Master of Science in Marine Technology
at the Delft University of Technology,
to be defended publicly on Friday October 28, 2022 at 15:45.

October 17, 2022

Document number: MT.22/23.004.M.
Student number: 4444523

Thesis committee:

Dr. C.L. Walters	TU Delft, chair
Dr. H. C. Seyffert	TU Delft
Dr. A. Grammatikopoulos	TU Delft
Dr.ir. A.C. Viré	TU Delft
Q. Shen MSc.	Siemens Gamesa Renewable Energy
N. Maljaars MSc.	Siemens Gamesa Renewable Energy

Institution: Delft University of Technology
Place: Faculty of Mechanical, Maritime and Materials Engineering, Delft
Project Duration: December, 2021 - October, 2022

Cover Photo: Artificial Intelligence (Stable-Diffusion) interpretation of: ”Various floating wind turbine designs in rough seas, in the style of Johannes Vermeer (Dutch painter from Delft)”. The output has been upscaled by AI and the image is colour graded by the thesis author.

TU Delft

SIEMENS Gamesa
RENEWABLE ENERGY

Preface

Dear reader,

The document before you is my master's thesis on "The response of a semi-submersible floating offshore wind turbine under misaligned wind and waves". My interest in floating offshore wind turbines was not self-evident. As many 1st year BSc Maritieme Techniek students I had a background in sailing. During my board year at the study association Scheepsbouwkundig Gezelschap "William Froude" I found out my interest was maybe not in shipbuilding specifically. I started working at Heerema Engineering Solutions and further developed my interests in offshore wind. Coming from a marine technology background, developments in floating offshore wind turbines caught my attention due to its multidisciplinary challenges.

This thesis is written as the concluding step of the master Marine Technology at the Delft University of Technology. For the duration of my thesis I have been supervised by Harleigh Seyffert (Ship Hydromechanics, TU Delft), Apostolos Grammatikopoulos (Ship and Offshore Structures, TU Delft), Qing Shen (Loads Engineer, Siemens Gamesa Renewable Energy), and Nico Maljaars (Loads Engineer, Siemens Gamesa Renewable Energy).

To them, I would like to express my gratitude for the guidance. Harleigh, thank you for keeping me in line and telling me what I needed to hear, not what I wanted to hear. You have supervised me at a time when you had time off and I appreciate that immensely. Apostolos, thank you for your patience and thorough feedback. Your enthusiasm during the progress meetings kept me motivated and looking for new creative solutions. Qing, thank you for your consistent feedback. Your industry experience with hydrodynamics in projects has kept me sharp and helped me maintain a critical attitude towards my results. Finally, I would like to thank Nico for answering my questions and staying after a meeting to exchange ideas with me. Your experience with aerodynamics was invaluable for this project. You helped me find innovative solutions to test my hypothesis and draw more scientifically sound conclusions. Thank you also for introducing me to foosball and trying to teach me. Family and friends know I'm hardheaded at times and you all have kept me sharp. Thanks to all of you I have further developed my interest in this field and learned to look at research from different perspectives.

I would also like to thank Carey Walters for chairing the committee and asking critical questions during the graduation process. I would like to thank Axelle Viré for taking the time to serve on my thesis committee. I would like to acknowledge Matthew Hall from the National Renewable Energy Laboratory for his efforts in resolving aerodynamics and control problems in the RAFT code. I also want to thank Anthony Viselli and Jacob Ward from the Ocean Engineering and Energy Department at the University of Maine for their assistance in resolving confidentiality conflicts. Special thanks to Mick, Bart, Martijn, Cas, Maarten, and Thomas for their help in proofreading.

Finally, I want to thank Mellissa, my family, my friends, and fellow Froude board members for their support, their words of encouragement and all non-academic distractions.

Joep van der Spek
Delft, October 2022

Abstract

Reducing the levelised cost of energy is crucial to accelerating the energy transition. To develop offshore wind solutions in greater water depths, a floating solution is required. The time-domain simulations of these Floating Offshore Wind Turbines (FOWTs) under wind-wave misalignment used in research and industry projects are computationally intensive and limits researchers and industry in their developments. To better understand the sensitivities of the fatigue loads of FOWTs to different parameters and environmental conditions, a computationally efficient method is needed.

The aim of this research is to develop a frequency-domain method to quantify the effects of misaligned wind and waves on the response of a semi-submersible floating offshore wind turbine. Therefore, the following research question is defined: What is the effect of misaligned wind, windsea waves, and swells on the loads at the tower base of a semi-submersible type floating offshore wind turbine?

Several sensitivity studies are conducted to quantify the contribution of yaw-roll coupling effects and aerodynamic damping to the responses and loads. From these studies, it appears that the yaw-roll coupling can increase the response when excited at wind/wave directions in which the structure is asymmetric. The magnitude of this effect is related to the wave peak period (and the resulting wavelength), the angle of misalignment with respect to the structure, and the apparent length of the structure. Also, the lack of aerodynamic damping in the direction of the rotor plane (side-side direction) leads to a noticeable increase in the response, directly or through coupling effects. Finally, the frequency-domain method is compared with the time-domain simulations (BHawC-OrcaFlex) carried out by Siemens Gamesa. Although reasonable agreement is found for the load driving rigid body modes, significant differences in the tower bottom loads are found for the lowest and highest production wind speeds.

These results show that misaligned wind and waves can increase the response for headings where the structure is asymmetric due to coupling effects. Wind-wave misalignment leads to an increased response in the direction of the rotor plane due to the lack of aerodynamic damping. In general, the wind-wave misalignment can also have a mitigating effect on the maximum equivalent moment at the tower base, as the aerodynamic damping also reduces the response in the wave frequency range. Furthermore, the comparison shows the need to extend the frequency-domain method with the first tower bending modes and improvement of aerodynamic/mooring property estimation.

Based on the findings and the conclusions, the recommendation is to investigate the floater specific sensitivities at an early stage of the design. Future research should focus on: the implementation of tower flexibility, improvement of the quasi-static estimation of mooring stiffness, frequency dependent aerodynamic properties, and implementation of second-order wave forcing.

Contents

Nomenclature

Abbreviations

Abbreviation	Definition
CFD	Computational Fluid Dynamics
CPU	Central Processing Unit
DEL	Damage Equivalent Load
DLC	Design Load Case
DOF	Degree of Freedom
FAST	Fatigue Aerodynamics, Structures, and Turbulence
FO	Floater Orientation
FOWT	Floating Offshore Wind Turbine
FPSO	Floating Production Storage and Offloading
IEA	International Energy Agency
IEC	International Electrotechnical Commission
HAMS	Hydrodynamic Analysis of Marine Structures
JIP	Joint Industry Project
JONSWAP	Joint North Sea Wave Project
LCOE	Levelised Cost of Energy
NREL	National Renewable Energy Laboratory
NEAV	New England Aqua Ventus
NTM	Normal Turbulence Model
PM	Pierson-Moskowitz
PSD	Power Spectral Density
RAFT	Response Amplitudes of Floating Turbines
RAO	Response Amplitude Operator
RAM	Random Access Memory
SGRE	Siemens Gamesa Renewable Energy
SoA	State of the Art
SS	Swell System
TLP	Tension Leg Platform
QuLAF	Quick Load Analysis of Floating wind turbines
VRS	Vortex Ring State
WTG	Wind Turbine Generator
WS	(Windsea) Wave System

Symbols

Symbol	Definition
a	Induction factor
A	Turbine rotor area
$\mathbf{A}_{aero}$	Added Mass coefficient matrix for the rotor
$\mathbf{A}_{BEM}$	Added Mass coefficient matrix obtained from potential flow software.
$\mathbf{A}_{Hydro,morison}$	Added Mass coefficient matrix for members approximated by the Morison equation.
$\mathbf{B}_{aero}$	Damping coefficient matrix for the rotor
$\mathbf{B}_{BEM}$	Damping coefficient matrix obtained from potential flow software.

Symbol	Definition
$\mathbf{A}_{Hydro,drag}$	Viscous Damping coefficient matrix for submerged members, approximated by the Morison equation estimate.
$\mathbf{C}_{Hydro}$	Hydrostatic stiffness coefficient matrix.
$\mathbf{C}_{moor}$	(Quasi-static) mooring stiffness coefficient matrix.
$\mathbf{C}_{struc}$	Structural stiffness coefficient matrix for the structure.
$\vec{F}_{aero}$	Aerodynamic excitation vector.
$\vec{F}_{BEM}$	Hydrodynamic excitation vector, Froude-Krylov and diffraction correction.
$\vec{F}_{Hydro,drag}$	Hydrodynamic viscous drag excitation.
$\vec{F}_{Hydro,Inertia}$	Hydrodynamic excitation vector (Froude-Krylov), for Morison members.
h_{hub}	Hub height w.r.t. water line.
$M_{aero,excitation}(\omega)$	Contribution of the aerodynamic excitation to the tower base bending moment.
$M_{aero,response}(\omega)$	Contribution of the aerodynamic response to the tower base bending moment.
M_{FA}/Mt_y	Fore-aft bending moment at the tower base.
$M_{inertia}(\omega)$	Contribution of inertia to the tower base bending moment.
M_{SS}/Mt_x	Side-to-side bending moment at the tower base.
$M_{TB}(\omega)$	Tower base bending moment
$m_{turbine}$	Tower and RNA Mass.
$M_{weight}(\omega)$	Contribution of the total turbine mass to the tower base bending moment
n_i	Counted cycles for stress range i
n_v	Total counted cycles
p_i	Weighting factor for case i
p_{tot}	Sum of the weighting factors
SD_{TT}	Standard Deviation of the time trace
T_p	Wave peak period
$\frac{\delta T}{\delta U}$	Thrust derivative to the wind speed.
U_{ave}	Average wind speed at hub height.
V	Velocity
z_{base}	Tower base height w.r.t. water line.
γ	Peak enhancement factor
θ	Misalignment angle
ρ	Density
σ_i	Stress range of bin i
σ_v	Equivalent stress
ω	Frequency
$\xi_i(\omega)$	Response of DOF i

List of Figures

List of Tables

1 Introduction

1.1. Motivation and Problem Statement

The energy transition and rising energy demand require institutes and industry to innovate and reduce the Levelised Cost of Energy (LCOE) to make it competitive with fossil fuel alternatives and diversify the energy supply. Within the field of offshore wind, one of the possibilities is to further explore winds at greater water depths. As water depth increases, the economic feasibility of bottom-fixed structures decreases, and floating offshore wind turbines (FOWTs) become more cost- effective. Insights into the factors contributing to the fatigue life of these floating turbines can improve the design at an early stage and reduce labour and material costs.

Scientific research on floating offshore wind turbines has taken large steps in recent decades. Recent studies combine knowledge from bottom-fixed wind turbines, oil and gas installations, and advanced aerodynamics to capture the coupled dynamic behaviour of a floating offshore wind turbine. The research presented in this thesis aims to improve the understanding of the coupled behaviour of a semi-submersible floating offshore wind turbine using a frequency-domain method. The main research question is proposed as:

> "What is the effect of misaligned wind, windsea waves and swells on the loads at the tower base of a semi-submersible type floating offshore wind turbine?"

Current frequency-domain methods are constrained by simplified aerodynamics and hydrodynamics, leading to an underestimation of the response [1]. A method developed by Pegalajar-Jurado *et al.* [2] only considers aligned wind and waves, which limits its application to idealised conditions. Furthermore, Hegseth and Bachynski [3] have developed a method applicable only to spar- type floaters, which allows for hydrodynamic simplifications due to its simple substructure.
The hydrodynamic response of a semi-submersible floater depends on the angle of incidence of the waves. A research is proposed to investigate the response characteristics of a semi-submersible floating offshore wind turbine subjected to misaligned wind and waves simultaneously. The frequency-domain method used in this work is an improved version of the Response Amplitudes of Floating Turbines (RAFT) method from the National Renewable Energy Laboratory (NREL) [4].

To answer the research question, sensitivity studies are performed with respect to the contribution of yawing and aerodynamic damping on the tower base bending response. Finally, the response estimates of the frequency-domain method are compared with time domain simulations for an industry demo project.

1.2. Report Outline

The structure of the report is presented in this section. Chapter 2 presents a summary of the literature review on floater designs, wind-wave misalignment and numerical methods for floating offshore wind turbines. In Chapter 3 the research plan is presented.

Chapter 4 presents an overview of the frequency-domain method. This is an overview that covers the estimates of the hydrodynamic characteristics, aerodynamics characteristics and mooring system. Moreover, an overview of improvements and additions to the method and python code are presented.

Chapter 5 presents the base case for the sensitivity studies in this chapter. Followed by the sensitivity study for sub-question 1 in Chapter 6 and sub-question 2 in Chapter 7.

The frequency-domain method is compared to time-domain simulations performed by SGRE in Chapter 8. This chapter answers research sub-question 3 and presents an overview of differences and their contribution to the results.

Chapter 9 presents a discussion of the work. Finally, in Chapter 10, sub-questions and the main research question are answered, followed by recommendations for future work.

Part I

Literature Review

2

Literature Review

This chapter provides a summary of the literature review on the response of a semi-submersible floating offshore wind turbine under misaligned wind and waves. Section 2.1 first provides an overview of the limitations of different floating wind substructures.

Section 2.2 presents a review on identifying the contribution of aerodynamic damping on the response of a semi-submersible floating offshore wind turbine.

Section 2.3 presents the limitations of computationally efficient methods for estimating the response characteristics for a semi-submersible type floating offshore wind turbine. Knowledge gaps related to the modelling of semi-submersible type floating offshore wind turbines in reduced order models are identified. Finally, Section 2.4 provides a summary of the knowledge gaps found with concluding remarks. To address these knowledge gaps, Chapter 3 presents the research plan and methodology that serve as the basis for this research.

2.1. Floater Designs

In recent decades, much research has been done to improve FOWT designs. This mainly concerns the design of floaters and the pitch control of wind turbines. In this section, a brief overview of floater designs is given.

Several floater wind turbine concepts have been considered as possible solutions in the last decades (Figure 2.1 and Figure 2.2). Initial studies have explored the feasibility of the concept of a wind turbine mounted on a semi-submersible platform in deep water. As illustrated by Fulton *et al.* [5], these early feasibility studies presented concepts based on experience from the oil and gas industry. They already concluded that the design of the substructure is important for the cost-effectiveness of the system. However, the study also indicated that whether a bottom-fixed structure or a floating solution is more suitable depends on the marine environment.

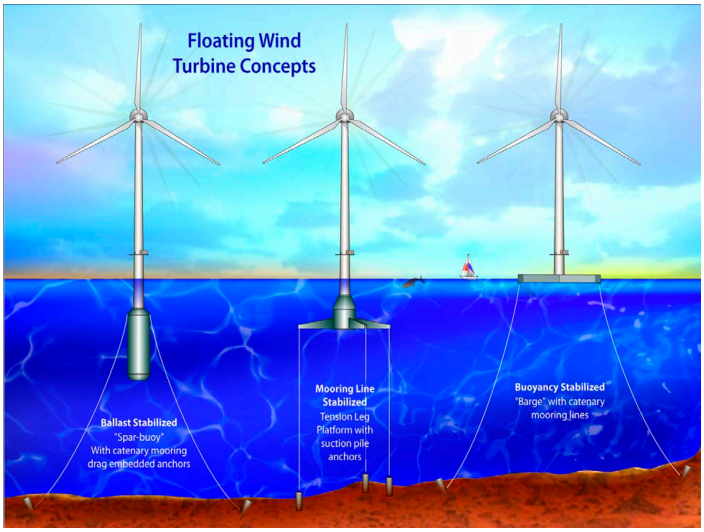

Figure 2.1: Three floater types: Spar-type, TLP and Barge [Retrieved from [6]]

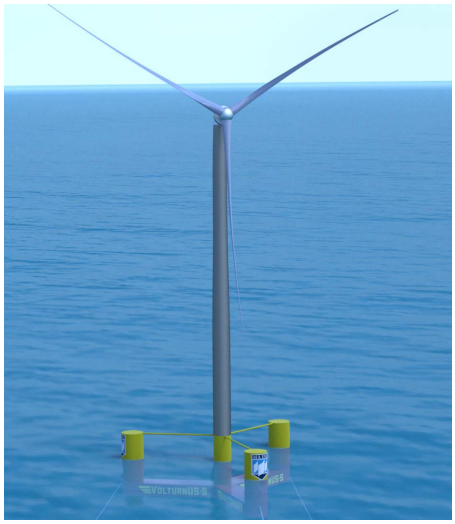

Figure 2.2: VolturnUS-S floater and IEA 15 MW reference turbine [Retrieved from [7]]

In a study by Bagbanci *et al.* [8] and Karmakar *et al.* [9], North Atlantic waves (claimed to have a severe wave climate) are used in a nonlinear time-domain simulation. It was found that the amplitudes of the surge, heave and pitching motions, as well as the bending moment of the tower base, are higher in the case of a semi-submersible floater than in the case of a spar-type floater. This is due to the greater dynamic response. In another study, Nejad *et al.* [10] argued that the use of a spar-type floater leads to the greatest damage to the bearings in the drive train, which are also prone to fatigue.

A recent study by Goupee *et al.* [11] examined the behaviour of three floating designs (spar, TLP and semi-submersible) for a range of wave and wind loads and concluded that preference generally depends on site conditions. In addition, logistical conditions such as installation have been shown to be a limiting factor [12, 13]. Installation location is often a critical factor, and the limited depth in many harbours favours the use of a semi-submersible. Semisubmersibles have a wide application and low cost of the mooring system, as well as low transport/installation costs. It is pointed out by Musial *et al.* [14] that currently 75 % of the installed or planned floating projects use a semi-submerisble floater. Therefore, the use of a semi-submersible floating offshore wind turbine is considered in this work.

2.2. Wind, waves, and misalignment.

Prediction of aerodynamic loads is essential in the initial design phase of floating offshore wind turbines. Sebastian and Lackner [15] present a comparison between different aerodynamic analysis methods and conclude that there are several reasons for the difficult prediction of aerodynamic loads compared to bottom-fixed offshore wind turbines. The first reason is the almost constant non-axial flow field due to the yaw and pitch motions of the platform. Secondly, there are non-uniform winds over the rotor disc due to the tilting motion of the structure. Finally, the angular and translational motions lead to turbulent transient conditions such as the vortex ring state (VRS) [16] and dynamic stall.

An aeroelastic quantity, aerodynamic damping, quantifies the fluid force in phase with the velocity of the oscillating body on which it acts. Wind turbines oscillate in the direction of the wind while they are in operation. This changes the relative wind speed acting on the rotor blades and, consequently, altering the angle of attack and instantaneous lift forces. As a result, the amplitude and speed of the oscillations have a direct influence on the magnitude of the aerodynamic forces [17].

The importance of estimating the aerodynamic damping of a FOWT is often stressed, but it is often analysed only for a simple unidirectional load case [18]. Misalignment of the wind direction with respect to the floater orientation changes the direction in which the aerodynamic damping is acting, since the aerodynamic damping occurs perpendicular to the rotor plane. This reduced aerodynamic damping in the direction of the rotor plane can increase the response when excited in that direction. Barj *et al.* [19] confirmed the effects of limited aerodynamic damping on the side-to-side motion of a spar floater. The increased side-to-side motion is attributed to the limited aerodynamic damping, but the magnitude of this effect for a semi-submersible has not been investigated.

Furthermore, the increased dynamic response of the platform can result in hydrodynamic radiation forces, due to the motion of the body through the water, and the disturbance of the water radiates kinetic energy from the structure. Due to the complexity of the substructure, it is common practice to precompute the linearised radiation and diffraction problems using a panel method [2, 20, 21]. It is argued by Lupton [1] and Jonkman [20] that for relatively small structures the use of Morison's equation with correction terms for drag and hydro static restoring can be sufficient, while for larger floating structures the use of potential flow methods is recommended. However, this can be very computationally intensive if a small panel size is chosen to capture details of the structure. This suggests the possibility of a hybrid approach where relatively small, connecting members are modelled using Morison equation. However, this approach has not yet been verified for a floating offshore wind turbine.

Finally, there are the hydrodynamic viscous forces that act on the structure. Viscous forces consist of a damping and an excitatory part. Journée and Massie [22] and Robertson *et al.* [23] state that viscous damping is caused by the waves dissipating energy from the moving structure and by viscous effects such as sheath friction and vortices. In general, viscous damping is neglected when the motions of a large structure (e.g. an anchored FPSO) are small.

Jonkman [20] notes that implementing some form of viscous drag may be important because it is a major source of hydrodynamic damping in some situations. The viscous drag can be implemented by using Morison equation [20], performing free decay tests in time-domain simulations, or performing a full CFD analysis [24]. Since estimation with the Morison equation can underestimate the drag for an oscillating structure and free decay tests and a full CFD analysis are computationally efficient, a novel approach is presented to estimate drag damping and drag excitation using an iterative approach [25].

In contrast to spar-type floaters, the hydrodynamic response of semi-submersible platforms depends on the orientation of the float with respect to the waves. In this, the global orientation of a semisubmersible is determined by the mooring system. The direction of wind and waves is relative to this orientation. This is the result of the asymmetric structure for certain misalignment angles, as shown in Figure 2.3.

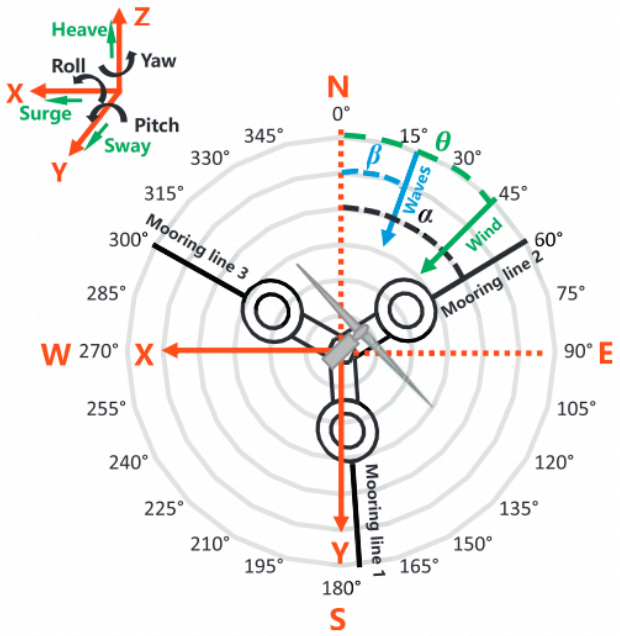

Figure 2.3: Orientation definition semi-submersible [Retrieved from [26]].

Bachynski *et al.* [27] investigate the motions and tower loads for four types of floating wind turbines using time-domain simulations at different locations. In this study, JONSWAP and Kaimal spectra are used for waves and wind respectively. For the limited load cases, increased motions are observed for the semisubmersible under misaligned conditions.

Semi-submersible designs show a maximum lateral bending moment at the tower base for a 60° misalignment between waves and wind (shown in Figure 2.4). At this angle of the incoming wave, two of the columns are excited by an in-phase wave force, resulting in an increased response of the structure. The time-domain simulations show that the lack of aerodynamic damping at in the side-side direction increases the fatigue damage when the tower is subjected to a misaligned wave system. This has been attributed to aerodynamic damping, but the exact mechanism has not been isolated.

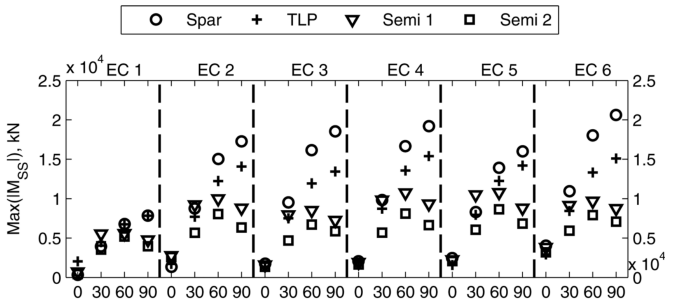

Figure 2.4: Maximum side-side bending moments for four different floater concepts [Retrieved from Bachynski *et al.* [27]].

A subsequent study by Bachynski *et al.* [28] examines the effect of wind-wave misalignment on fatigue damage. This study evaluated only 5 load cases using time-domain simulations. The study concludes that the misalignment of waves and wind and their coupling play an important role in the assessment of fatigue damage but the magnitude of this effect is not isolated due to the computational expense of time-domain simulations.

However, these recent studies on the loads at the tower base [19, 27, 28] assume that the structure is exposed to only a single wave spectrum propagating in one direction. No additional wave systems are included, therefore limiting the conclusion to these idealised environmental conditions.

Kang *et al.* [29] study the effect of multiple wave systems on the motion response by using time-domain simulations. They showed that there is an increase in pitch motion for a semi-submersible FOWT excited by wind-sea waves and a swell system. The authors argue that this increase in pitching motion and the surge-pitch coupling increases the dynamic response compared to just a windsea wave case. They concluded that if this swell is present all the time, the FOWT is a sensitive to a change of swell misalignment, fatigue-related and structural problems could occur. However, these effects where only analysed for 7 load cases and therefore the magnitude of change in swell misalignment to the response is not quantified.

Zhou *et al.* [26, 30] discuss the importance of floater orientation for a Y-type semi-submersible with respect to aligned wave and wind systems using time-domain simulations. In this study, the response of the floater is evaluated in time-domain simulations for three directions (0, 60 and 90 degrees with respect to one of the mooring lines). The results of both the experimental and numerical tests showed that the orientation of the floater has a noticeable effect on the RAO magnitudes. It is concluded that for the Y-type semisubmerisble under aligned waves, a difference of 25% is observed in the accumulated fatigue damage at the tower base between 4 possible orientations. However, this study is limited in the amount of evaluated orientations and mainly aligned winds and waves are considered.

In summary, the importance of aerodynamic damping for the fore-aft and side-to-side tower base bending moments is noted by Barj *et al.* [19]. The increase in side-to-side of the tower response due to lack of aerodynamic damping is investigated by misalignment of a single wave system by Bachynski *et al.* [27, 28]. However, due to the high computational cost of the time-domain simulations, only up to five wind-wave system combinations are analysed. The difference between the accumulated fatigue damage in the different cases is attributed to the lack of aerodynamic damping in the side-to-side direction, but the exact mechanism is not isolated due to the computational expense. Furthermore, these studies do not take into account the constant presence of swell sea, which is later found to be a major factor in the fatigue damage [29]. Zhou *et al.* [26, 30] find that the floater orientation can also contribute and limit the accumulated fatigue damage at the tower base . However, for these studies only aligned wind

and waves are considered and the previously described contribution of misalignment between wind and waves is therefore not considered.

Research has not isolated the mechanism with which aerodynamic damping effects the response because they are limited by the computational cost of time-domain simulations. Section 2.3 discusses the possibility of quantifying this contribution using a frequency-domain method.

2.3. Numerical methods for floating offshore wind turbines.

The dynamic response of a floating offshore wind turbine contains many nonlinearities. These include the geometric nonlinearity of the mooring system, the hydrodynamic viscous drag, and the aeroelastic modelling of the turbine [6, 31]. To account for the resulting coupled dynamics, time-domain methods for the design process of floating offshore wind turbines have been developed and verified [32].

These fully coupled nonlinear simulations may require extensive calculations when evaluated for the required design load cases (DLCs) (presented in IEC 61400-3) [33]. This can amount to about 20000 simulations with a processing speed of 1-3 times real time [2] and about 6-8 weeks of computation time for a single design iteration [21, 34]. This considerable simulation time is a constraint for research and leads to increased development costs if many iterations of the floater design of offshore wind turbines are performed. Therefore, there are developments to capture this non-linear behaviour in a computationally efficient model using a computationally efficient method.

One of the ways to reduce the computation time for fatigue damage estimation is to use a surrogate model, such as neural networks [35]. However, these methods use a black-box approach and therefore do not contribute to a better understanding of the physics in such a system.

Another approach is to estimate the response of the FOWT in the frequency domain. Using a frequency-domain method requires linearisation of the non-linear loads and response characteristics around an average operating point. Recent frequency-domain methods by Lupton [1], Pegalajar-Jurado *et al.* [2], and Hegseth and Bachynski [3] are developed for different and specific applications. They consider different linearisation techniques and degrees of freedom present in the methods. Their respective limitations are discussed in this section.

Considerable simplifications are assumed in the methods by Lupton [1]. The hydrodynamic excitation and response are estimated using only the Morison equation. This limits the application to relatively small and slender structures, since diffraction and radiation effects occur for large structures [22].

In addition, there are developments for the QuLAF method (Quick Load Analysis of Floating wind turbines) [2, 36, 37], a model with four degrees of freedom (DOF) (floater surge, heave and pitching, and the first fore-aft tower bending mode). This method only considered four DOFs and is therefore not suitable for considering misaligned wave and wind cases. One of the recommendations is to add out-of-plane degrees of freedom to include calculations for misaligned wind and waves [2]. The required degrees of freedom for such an extended method have not been presented in the research.

The method by Hegseth and Bachynski [3] is developed for spar-type floaters. It proposes a method with seven degrees of freedom, namely rotor speed, surge,sway, roll, pitch, and 1st fore-aft and side-side bending modes. Based on previous studies for a spar-buoy type floating wind turbine [38], the heave and yaw responses are assumed to be relatively small. An earlier study by Ramachandran *et al.* [39] has shown that although the hydrodynamic yaw force is zero for a floating wind turbine of the spar-buoy type, there is excitation from the aerodynamics of the rotor and couplings with other DOFs are present.

In contrast, the axial symmetry of a semi-submersible floater increases the hydrodynamic coupling effects. Also, there may be hydrodynamic yaw excitations at asymmetric angles of incidence [23, 29, 40]. At these asymmetric wave misalignment angles, the mooring system and hydrodynamic coupling effects may contribute to the roll and pitch response. In addition, it is observed that misaligned waves with respect to the wind can excite yaw natural frequencies, which can increase roll via coupling effects [41]. The effects have been observed, but their physical cause and the relationship to the platform properties has not been investigated. These coupling effects are only observed and it is not quantified how these yaw coupling effects contribute to the response of a semi-submersible floater.

Based on the previously presented literature on FOWT modelling, several limitations of existing methods are identified. Time-domain methods have been shown to capture nonlinear behaviour well, but they are very computationally intensive [28, 32]. Frequency-domain are proposed to reduce the computational expense. However, these models have several limitations, namely: highly simplified aerodynamics and/or hydrodynamics [1], only aligned wind and waves [2, 36], or only applicable to a slender spar-type floater [3]. Therefore, an extended or new method is required to estimate the response under misaligned wind and waves. However, this development is limited by the selection of the degrees of freedom, as it cannot be clearly established if the inclusion of the yaw DOF is required to best estimate the loads at the tower base in misaligned winds and waves. The coupling between yaw and pitch and yaw and roll is present, but the contribution of multiple wave components that excite the structure cannot be determined from the existing literature. This suggests that the influence on the response at the tower base resulting from the contribution of the yaw motions due to the yaw-pitch and yaw-roll coupling remains to be investigated.

In summary, the existing methods are not directly applicable to estimate the response of a semi-submersible under misaligned wind and waves. Such a method must estimate the response characteristics with reasonable accuracy. This requires research into the contribution of the yaw DOF to the response of a semi-submersible type floating offshore wind turbine.

2.4. Concluding remarks

Based on the literature discussed and analysed in the previous sections, this section provides a summary of the identified scientific knowledge gaps. Therefore, this chapter summarises the scientific justification of the proposed research. Section 2.1 provides an overview of different floating solutions currently being considered by researchers and industry. As a semi-submersible floater is less constrained by logistical challenges, it is considered the floater of interest for this thesis.

Section 2.2 discusses the external loads on a floating offshore wind turbine. First, the environmental conditions are discussed. However, the contribution of wind, wind-sea waves and swell waves to the response of a semi-submersible FOWT has only been analysed for misalignment between wind and a single wave system. The contribution of multiple swell systems to the response of a floating offshore wind turbine has not yet been investigated, but has been shown to be significant in industry demonstration projects.

As far as the author is aware, no literature addresses the effects of wind and wave systems on a semi-submersible type floating offshore wind turbine. Furthermore, considering the coupling effects of semi-submersible floaters with respect to wind and waves, it is concluded that there is a scientific knowledge gap in estimating the contribution of aerodynamic damping to fatigue damage under misaligned wind and waves.

Section 2.3 presents a gap in knowledge to determine the contribution of aerodynamic damping on the fatigue life. For time-domain simulations, performing simulations for research and industry purposes is very computationally expensive. A more flexible and computationally efficient method is found by using a frequency-domain method.

Current frequency-domain methods are not suitable for these calculations because the literature assumes very limited degrees of freedom or only considers a spar-like floater, which allows for considerable hydrodynamic simplifications. The effects of aerodynamic-hydrodynamic coupling between different degrees of freedom in computationally efficient methods that occur with a semi-submersible floater, is an open research topic.

A scientific knowledge gap is found in determining the contribution of aerodynamic damping and yawing to the tower base bending moment under misaligned wind and waves. Finally, a frequency-domain methods for semi-submersible floating offshore wind turbines is not yet developed and compared with time-domain simulations for multidirectional wind, wind-sea waves and swells. In the next chapter, a research plan is presented to fill the knowledge gaps summarised in this section.

3

Research Plan

Chapter 2 presented scientific knowledge gaps. In this chapter, a research plan is presented to fill these knowledge gaps. Section 3.1 presents research questions and objectives to fill knowledge gaps. Furthermore, the methodology is presented in Section 3.2. The numerical experimental setup and confidentiality are discussed in Section 3.3.

3.1. Research question, project aim and project objectives

3.1.1. Research questions and objectives

From the literature review, the following research question is presented.

> "What is the effect of misaligned wind, windsea waves, and swells on the loads at the tower base of a semi-submersible type floating offshore wind turbine?"

This main research question is supported by three sub-questions. The first sub-question aims to quantify the contribution of yawing and yaw-related couplings and their physical cause to the response characteristics, thus filling the knowledge gap found in Section 2.3. The second sub-question aims to fill the knowledge gap identified in Section 2.2 and identify the contribution of aerodynamic damping to the fatigue response for misaligned wind and waves and for different floater orientations.

The last sub-question aims to compare the developed frequency-domain method with time-domain simulations. The aim is to identify any differences and evaluate how they affect the estimation of the equivalent moment at the tower base.

SQ1 How does inclusion of the yaw motion of a semi-submersible FOWT contribute to the rotational dynamic response under misaligned wind and waves in a frequency-domain method?

SQ2 What is the contribution of aerodynamic damping to the response of a semi-submersible floating offshore wind turbine, considering misalignment of wind and waves with respect to floater orientation?

SQ3 How effective is a frequency-domain method compared to a time-domain method at estimating the equivalent bending moment at the tower base for misaligned wind, windsea waves, and swells?

These research questions are formulated to support the goal of this thesis:

> "To develop a computationally efficient method to quantify the effect of misaligned wind, windsea waves, and swells on the tower base response of a semi-submersible type floating offshore wind turbine."

In order to successfully achieve this project goal, several project objectives are defined. The first objective is to investigate the contribution of yaw and yaw-coupling effects to the floater motion to best estimate the response of the tower base to misaligned waves and wind.

Secondly, the objective is to investigate the effect of aerodynamic damping in the presence of wind and wave misalignment. Misalignment of wind and wave loads with respect to the orientation of the

floater increases the contribution of coupling between the degrees of freedom of the floater. There is a particular interest in identifying the change in fore-aft and side- to- side bending moments for different orientations of the platform.

Finally, the frequency-domain method is compared with time-domain simulations. The objective is to evaluate the differences between the methods to better understand and assess how these differences contribute to the response at the tower base.

3.2. Methodology

Based on the knowledge gap summarised in Chapter 2, and using the research questions and accompanying research objectives, this section presents a methodology to answer the research question.

3.2.1. Sub-question 1: Yaw-DOF and yaw coupling effects

Industry projects and literature [29, 42] have recently shown the effects of swell waves on a semi-submersible floating offshore wind turbine. The coupling between the degrees of freedom of the floater for an asymmetric incidence angle of the waves can excite the natural frequency of the structure in the roll and pitch directions. The existing frequency-domain method RAFT (Response Ampltidues of Floating Turbines) by the National Renewable Energy Laboratory (NREL) [4] is extended to include and investigate the above phenomena. A sensitivity study is carried out to find out the contribution of the yaw degree of freedom to the response of a semi-submersible floating offshore wind turbine. Due to the asymmetry of a semi-submersible at certain wave incidence angles, yaw-roll and yaw-pitch coupling is present [41]. The contribution to the motion response when including the yaw DOF under misaligned wind and waves is not understood. A sensitivity study is conducted to quantify the contribution of this DOF for different wind and wave parameters.

3.2.2. Sub-question 2: Aerodynamic damping

The current literature is limited in evaluating load cases to quantify the contribution of aerodynamic damping due to the high computational cost of performing time-domain simulations. Therefore, the contribution of aerodynamic damping to the fatigue response is not evaluated for several misaligned wind/wave systems and floater orientations. Since aerodynamic and hydrodynamic responses are coupled, the resulting aerodynamic damping in pitch and roll direction influences this response [43]. The magnitude of this effect when subject to an additional swell system is not yet quantified, but a better understanding could be valuable for float design. A sensitivity study is conducted for several different wind and wave parameters.

3.2.3. Sub-question 3: Comparison

The estimation of system characteristics for an open-source configuration and an industry project configuration is compared.

The mean response and dynamic response estimated are compared with existing results of time-domain simulations carried out in a joint industry project (NEAV). Finally, the tower base bending moment estimates are compared. Any limitations and differences between the results are evaluated and possible improvements are suggested. Further details on the setup of the comparison are discussed in Section 3.3.

3.3. Numerical experiments, set-up and confidentiality

3.3.1. Numerical experiment/set-up

To answer the sub-questions and research question, numerical experiments are performed. The setup of those experiments and comparisons are discussed in this section.

As this thesis is time limited, the frequency-domain method is an extension of the RAFT (Response Amplitudes of Floating Turbines) modelling package (figure 3.1). In contrast to QuLAF [2], this is open-source python code developed by the NREL. This code uses existing and verified packages to linearise the rotor aerodynamics (CCBlade), obtaining a quasi-static estimate of the mooring system (MoorPy). Furthermore, it uses a potential flow hydrodynamics package based on the Hydrodynamic Analysis of Marine Structures (HAMS) tool [44]. Furthermore, a description of the VolturnUS-S is already included

in the code.

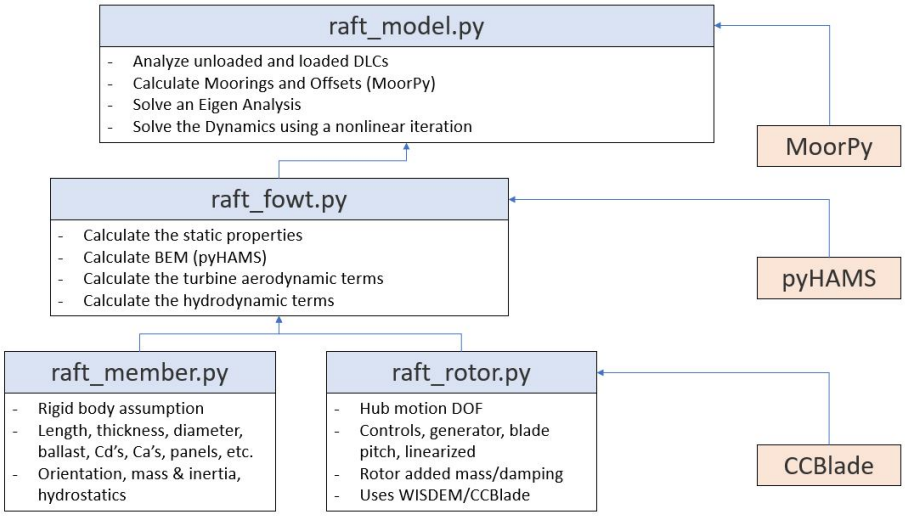

Figure 3.1: Structure of RAFT model [Retrieved from [4]].

Currently, RAFT is under development for the assessment of Response Amplitude Operators (RAOs) of floating offshore wind turbines. In order to perform the numerical expirements and answer the research questions, some extensions are planned. The following extensions and post-processing steps are expected, but not limited to:

- Modifying the method to include misalignment of wind
- Additional first order wave force by JONSWAP or PM.
- Side-to-side bending moment at the tower base.
- Stress distribution around tower base circumference.
- Estimation of fatigue damage for misaligned response spectra.
- Wrapper module to evaluate for different parameters and visualise the results.

Currently, the RAFT model only allows for aligned winds and a single aligned wave system. The inclusion of additional wave spectra from another direction is implemented. In addition, the model only allows external forces from one direction per evaluated load case. This requires the evaluation of the tower base bending moments for the different directions and plotting capabilities to present the resulting equivalent stress estimates and/or fatigue damage over the circumference of the tower base.

As discussed, the RAFT model is developed mainly to investigate the motion response of a floating offshore wind turbine. In the method it is assumed that the floater, tower, and blades are rigid bodies.

The comparison is done in three parts: comparison of system characteristics, comparison of response characteristics from a set of load cases and the comparison of a full DLC set. For the comparison of system characteristics, such as natural frequencies, (hydrodynamic added) mass and inertia estimates, and wind and wave spectra are compared.

3.3.2. Confidentiality

For the sensitivity studies, publicly available design data for the VolturnUS-S semi-submersible floater [7] and the IEA 15 WM reference turbine [45] is used. A concrete, patented version of this floater (VolturnUS) is used for the comparison.

Data related to this floater that is included in this thesis is approved by Anthony Viselli and Jacob Ward of the University of Maine.

SGRE data includes the design data of the 11 MW RNA used in the NEAV project, as well as RAOs and/or response data from time-domain simulations performed by SGRE in BHawC/Orcaflex DLC 1.2. In order to ensure the publication of this thesis, appropriate measures are taken in the report not to breach confidentiality.

Part II

Model Description

4

Method Description

4.1. Frequency-Domain Method

This section gives an overview of the frequency-domain method. The various dependencies (structural, mooring, hydrodynamic, and aerodynamic) will be introduced.

The general equation of motion for the a 6 degree of freedom system is given by Equation 4.1. In these equations $\vec{\xi}(t)$ represents the response for the 6 floater degrees of freedom (surge, sway, heave, roll, pitch, and yaw).

$$(\mathbf{m} + \mathbf{a}) \cdot \ddot{\vec{\xi}}(t) + \mathbf{b} \cdot \dot{\vec{\xi}}(t) + \mathbf{c} \cdot \vec{\xi}(t) = \vec{F}(t) \tag{4.1}$$

If a linear(ised) system is considered, this can be presented in the frequency domain using Equation 4.2.

$$(\mathbf{M} + \mathbf{A}) \cdot -\omega^2 \cdot \vec{\xi}(\omega) + \mathbf{B} \cdot j\omega \cdot \vec{\xi}(\omega) + \mathbf{C} \cdot \vec{\xi}(\omega) = \vec{F}(\omega) \tag{4.2}$$

The various matrices for mass (**M**), added mass (**A**), damping (**B**) and stiffness (**C**), presented in Equation 4.2, are the linearised system properties of the terms presented in Equation 4.1. Each matrix (indicated in bold) consists of 6-by-6 coefficients, considering the 6 floater DOFs. The description of the aerodynamic terms is presented in Section 4.1.1. The estimation of the hydrodynamic terms are estimated in Section 4.1.2 and Section 4.1.3. The estimation of the structural and mooring stiffness is presented in Section 4.1.4.

$$\begin{aligned}
\mathbf{M} &= \mathbf{M}_{struc} \\
\mathbf{A} &= \mathbf{A}_{aero} + \mathbf{A}_{BEM} + \mathbf{A}_{Hydro,morison} \\
\mathbf{B} &= \mathbf{B}_{aero} + \mathbf{B}_{BEM} + \mathbf{B}_{Hydro,drag} \\
\mathbf{C} &= \mathbf{C}_{struc} + \mathbf{C}_{moor} + \mathbf{C}_{Hydro} \\
\vec{F} &= \vec{F}_{aero} + \vec{F}_{BEM} + \vec{F}_{Hydro,Inertia} + \vec{F}_{Hydro,drag}
\end{aligned} \tag{4.3}$$

4.1.1. Aerodynamic excitation vector and coefficient matrices.

The aerodynamic excitation and load derivatives are calculated using the Blade Element Momentum (BEM) method CCBlade. This method is developed by the NREL and is based on the work of [46], which describes a BEM with guaranteed convergence and superlinear rate and continuously differentiable output. This method requires several predefined properties as input, such as blade geometry, pitch angle at an average wind speed, and rotational speed at a given average wind speed. This method returns mean aerodynamic loads such as thrust and torque. Furthermore, this method returns derivatives of thrust and torque with respect to wind velocity, rotational speed, and blade pitch angle. The aerodynamic damping is set to the derivative of thrust with respect to wind speed ($\frac{\delta T}{\delta v}$). This is a reasonable estimation and gives a reasonable estimation of the response [47].

To rotate the aerodynamic damping, it is rotated from the hub reference frame to the floater reference frame to account for a wind heading (θ) with respect to the floater orientation. This is done by multiplying

the excitation force and aerodynamic matrices with a rotation matrix, as presented in Equation 4.4 and Equation 4.5. In these equations F_x, F_y, and F_z is the force vector.

$$\begin{bmatrix} cos(\theta) & -sin(\theta) & 0 \\ sin(\theta) & cos(\theta) & 0 \\ 0 & 0 & 1 \end{bmatrix} \begin{bmatrix} F_x \\ F_y \\ F_z \end{bmatrix} \tag{4.4}$$

$$\begin{bmatrix} cos(\theta) & -sin(\theta) & 0 \\ sin(\theta) & cos(\theta) & 0 \\ 0 & 0 & 1 \end{bmatrix} \begin{bmatrix} c_{11} & \cdots & c_{13} \\ \vdots & \ldots & \vdots \\ c_{31} & \cdots & c_{33} \end{bmatrix} \begin{bmatrix} \xi_1 \\ \xi_1 \\ \xi_1 \end{bmatrix} \tag{4.5}$$

4.1.2. Hydrodynamic excitation and coefficient matrices.

For the hydrodynamics, the diagonals in the coefficient matrices can either be calculated using (1) the Morison's equation, a (2) potential flow software ([44, 48], based on the work by Newman [49]) and the calculating the drag components using the Morison's equation representation. An alternative option is to evaluate complex members in a potential flow package and use the Morison's equation for select members. Previous literature [31] has shown that for surface piercing members with a member diameter that can disturb the waves (G.I. Taylor's long-wavelength approximation) potential flow software is recommended. However, for slender members, the Morison's equation can estimate the hydrodynamic added mass coefficients and the Froude-Krylov force.

The VolturnUS-S floater is described by various members, such as different columns and braces that are either circular or rectangular. The members for the VolturnUS-S floater and 15MW turbine are visualised in Figure 4.1.

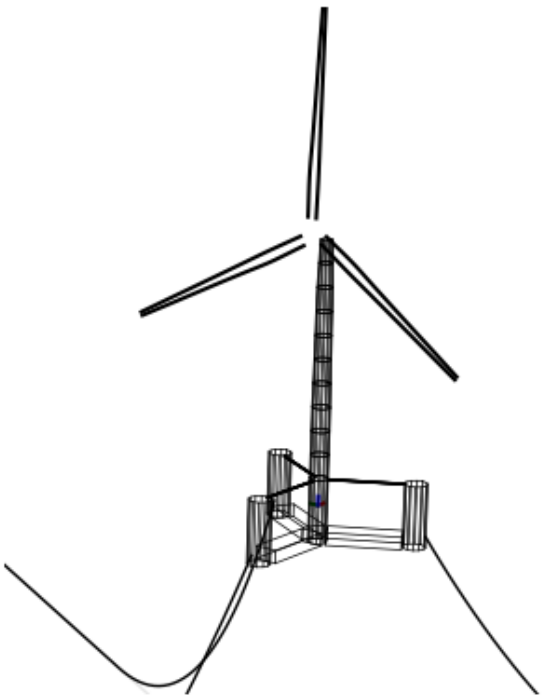

Figure 4.1: VolturnUS-S Floater and IEA 15MW turbine, visualised by RAFT.

Potential flow members
Using specified dimensions on the platform geometry, a panel mesh description is created. For previously set wave headings, the potential flow solver software [44] evaluates the frequency dependent aerodynamic added mass, aerodynamic damping and excitaion RAO's for the six degrees of freedom of the floater. The contribution of those members to the response matrix $\mathbf{A}_{BEM}$ and damping matrix $\mathbf{B}_{BEM}$ are retrieved from a WAMIT-like *".1-file"*. In this file, the contribution to $\mathbf{A}_{BEM}(\omega)$ and $\mathbf{B}_{BEM}(\omega)$ for each mode pair ($i, j = 1, 2, ..., 6$) for a range of frequencies is determined.

In the resulting *".3-file"* the directional dependent real and imaginary parts of the excitation force RAO $\vec{X_{BEM}}(\omega)$ are present. For the wave headings present in the case, the force/moment RAO for each DOF is retrieved. The frequency dependent wave headings are retrieved over the frequency range using either a JONSWAP spectrum for a given significant wave height (H_s), peak period (T_p) and peak enhancement factor (γ), or a constant wave height over the frequency range.

Multiplying this frequency dependent wave height height from the wave spectrum ($\eta(\omega)$), the resulting wave force $\vec{F}_{BEM}(\omega)$ is calculated for each degree of freedom.

Morison's equation members
As a rule of thumb, members are considered slender if the extension along the wave direction D is significantly smaller than the wavelength λ (i.e. if $\frac{D}{\lambda} < 0.2$ [31]. For such members, the added mass/inertia and Froude-Krylov (FK) excitation can be estimated using an analytical approach. This requires a numerically or experimentally determined added inertia coefficient. In the preprocessor of the frequency-domain method, it can be determined for each member (column, connecting pontoon, etc.) whether the hydrodynamic properties are estimated using the Morison equation or whether the members are included in the potential flow solver. When estimating with the Morison equation, the hydrodynamic added mass and the FK force are estimated for the orientation and position of the member in relation to the floater origin frame.

For each wave system present in the case, the frequency-dependent wave height is determined. Using this wave height, the water depth and the wave elevation in dispersion relation are used to calculate the wave kinematics (local velocity, acceleration and dynamic pressure) at the location of the member. Using these values, the frequency-dependent FK force and the hydrodynamic mass force are calculated for the simplified members in the member reference frame. The estimated added mass and FK force are then rotated and translated into the floater reference frame as a contribution to $\mathbf{A}_{Hydro,morison}$ and $\vec{F}_{Hydro,Inertia}$ respectively.

4.1.3. Viscous drag damping and excitation
For a moving body in oscillatory flow, the (viscous) hydrodynamic drag depends on the relative velocity between the flow and the structure. The only models that may directly integrate viscous effects on submerged bodies are time-domain models because they depend nonlinearly on the relative velocities of the wave particles and the structure. State-of-the-art frequency-domain methods for floating wind turbines assume that the floating structure has small displacements and velocities relative to the fluid velocity, since the hydrodynamics are dominated by inertia. Therefore, the direction of the viscous drag can therefore reasonably assumed in the direction of the fluid.

The method estimates the viscous drag matrix ($\mathbf{B}_{Hydro,drag}$) and the hydrodynamic drag excitation force ($\vec{F}_{Hydro,drag}$) by an iterative step that solves the system response (and thus velocity at every frequency). Using the solved response velocity, the damping coefficient for each degree of freedom is estimated at the reference frame of the submerged member using the relative velocity between the wave velocity and the velocity of the submerged member. The viscous drag excitation force is then obtained my multiplying the viscous drag damping coefficient by the wave particle velocity at the member origin.

In other words, the viscous damping coefficients depend on the relative velocity and the (angular) velocity of the structure. The viscous drag force depends on the relative velocity and the wave kinematics. If it does not converge, a combination of the last and current response is used to recalculate the viscous drag damping and excitation, and the linearised system is solved again until the required convergence tolerance is achieved. A detailed description of this approach is presented by Pegalajar-Jurado *et al.* [2].

4.1.4. Structural and mooring coefficient matrices.

The structural mass matrix ($\mathbf{M}_{struc}$) is calculated by the mass of the structure, which is either input or calculated from the dimensions of the structure. In addition, the hydrostatic coefficients for heave, pitch and roll in the matrix $\mathbf{C}_{hydro}$ are calculated from the mean position of the floater in the water for small displacements and rotations using the approach presented by Lee and Newman [48]. In $\mathbf{C}_{struc}$ a P-delta small angle approximation term for small angles is introduced to account for the (reverse) pendulum effect for slender structures.

Finally, the mooring forces are estimated using a quasi-static approach by the open source package MoorPy. Here, the mooring design is specified in an input file containing the depth, the position of the anchors, the position of the fairlead, the line types and the anchor type. The stiffness of the mooring $\mathbf{C}_{moor}$ is assessed at a mean position assumed to be excited by the wind only. Currently, the simplified assumption is that the wave forces excite the structure only locally and have no influence on the mean position of the structure.

4.2. Equivalent stress/bending moment estimation

This section presents the equivalent stress calculations performed in the method. A rigid tower is considered and therefore the bending moment is derived from the contributions of the (added) mass/inertia of the turbine and the aerodynamic excitation contribution at the tower base. This is justified on the work by Pegalajar-Jurado *et al.* [2], where it was observed that for a tower supporting a 10 MW turbine, the first fore-aft and side-to-side tower bending frequencies were observed at approximately 4.4 rad/s, which is outside the range of wind and wave excitation. However, industry projects try to reduce the tower mass in order to reduce costs. This reduction in tower mass reduces the first bending natural frequency, which could affect the overall pitch and roll if it is much closer to the wind and wave excitation. Any differences in response due to this rigid/flexible tower are discussed in Chapter 8, where the method is compared to time-domain simulations.

The complex, frequency-dependent fore-aft and side-to-side bending moments are used to calculate the stress power spectral density (PSD) around the tower base circumference. Using this stress response PSD, the Tovo-Benasciutti method [50] is applied to estimate the equivalent stress levels at each location around the tower base.

4.2.1. Tower base bending moments.

As described in section Section 4.1, the 6 degrees of freedom of the floater are considered as the degrees of freedom of the method. The tower base bending moments of the rigid tower are calculated by Equation 4.6. In this equation, M_{weight} represents the contribution of the turbine mass with the arm resulting from the pitch/roll motion (Equation 4.7). $M_{inertia}$ represents the dynamic contribution due to the inertia of the RNA and the tower from the pitch/roll motion (Equation 4.8). In addition, $M_{aero,excitation}$ (Equation 4.9) and $M_{aero,response}$ (Equation 4.10) and Equation 4.11) represent the aerodynamic excitation and the contribution of the response due to the coupled aerodynamic added mass and damping, respectively. The aerodynamic response consists of a contribution of the diagonal term (Equation 4.10) and a contribution of the coupling coefficient to the bending moment in that direction (Equation 4.11).

$$M_{TB}(\omega) = M_{weight}(\omega) + M_{inertia}(\omega) + M_{aero,response}(\omega) + M_{aero,excitation}(\omega) \tag{4.6}$$

$$M_{weight}(\omega) = m_{turbine} * g * h_{bottom} * \xi_{pitch/roll}(\omega) \tag{4.7}$$

$$\begin{aligned} M_{inertia}(\omega) = &- m_{turbine} * -\omega^2 * (\xi_{surge/sway}(\omega) + z_{turbine,CG} * \xi_{pitch/roll}(\omega)) \\ &- I_{turbine}(\omega) * (-\omega^2 * \xi_{pitch/roll}(\omega) \end{aligned} \tag{4.8}$$

$$M_{aero,excitation}(\omega) = \vec{F}_{aero,pitch/roll}(\omega) * (h_{hub} - z_{base}) \tag{4.9}$$

$$\begin{aligned} M_{aero,response,diag}(\omega) = &- \omega^2 * \mathbf{A}_{aero,diagonal} * (h_{hub} - z_{base})^2 * \xi_{pitch/roll}(\omega) \\ &- j\omega * \mathbf{B}_{aero,diagonal} * (h_{hub} - z_{base})^2 * \xi_{pitch/roll}(\omega) \end{aligned} \tag{4.10}$$

$$M_{aero,response,coupling}(\omega) = \omega^2 * \mathbf{A}_{roll/pitch} * (h_{hub} - z_{base})^2 * \xi_{roll/pitch} - j\omega * \mathbf{B}_{aero,coupling} * (h_{hub} - z_{base})^2 * \xi_{roll/pitch}(\omega) \tag{4.11}$$

4.2.2. Equivalent stress estimation.

The equivalent stress range is calculated by using Palmgren-Miner rule and a rainflow counting equivalent method such as the Dirlik method, the Tovo-Benasciutti method or the Zhao-Baker method [51]. To estimate the stress range PSD from the stress PSDs in this method, the Tovo-Benasciutti approach is used. This method has been shown to be effective for different response spectra and for a range of k-factors [51]. From the stress PDF ($P_{\text{TB}}\ (S_i)$) calculated using the Tovo-Benasciutti approach for a random process, it can be seen that not all stress ranges have an equal amount of cycles. To compare the fatigue performance of a structure over its lifetime, the variable stress range can be represented by an equivalent stress range. The equivalent stress range σ_v is proportional to the number of cycles experienced and is denoted by Equation 4.12 [52]. In this equation, σ_i^m is the stress range at cycles i, n_i is the number of cycles in the stress range σ_i. n_v is the total number of cycles experienced, and m is the crack growth rate. For each angle around the tower base circumference α_i, the equivalent stress σ_v can be calculated (Palmgren-Miner).

$$\sigma_v = \left(\sum_{i=1}^{n} \left(\sigma_i^m n_i \right) / n_v \right)^{1/m} \tag{4.12}$$

Since this is a frequency domain approach only, the stress range has to be estimated from the spectral information (variance/spectral moment). The maximum value of the wave height can reasonably be assumed by $H_{max} = 8 \cdot \sqrt{m_{0,E(f)}}$ [53]. Since a long-term stress range is considered, a similar estimate of the maximum stress of the stress range is considered as $\sigma_{max} = 8 \cdot \sqrt{m_{0,PSD_\sigma}}$. However, it must be ensured that this maximum stress is lower than the yield stress of the steel structure.

Since an average pitch and roll angle is known for each case, the average bending moments in fore-aft and side-to-side can be calculated using the RNA weight and mean thrust estimated in equations Equation 4.7 and Equation 4.9 respectively. From these mean bending moments, the contribution of these components at each location around the tower base mean bending moment can be calculated with Equation 4.13.

$$M_{avg}(\theta) = ((M_{FA,avg} * sin(\theta))^2 + (M_{SS,avg} * cos(\theta))^2)^{0.5} \tag{4.13}$$

From this mean bending at each location, the mean stress can be estimated since the tower properties at the tower base are known. Using the approach presented by Niesłony and Böhm [54], a corrected stress PSD is estimated by applying a mean stress correction factor. Here the Goodman correction factor is used as it has given good results for asymmetric stress cases [55]. For the estimated stress PSDs around the tower base circumference (Section 4.2), the resulting equivalent stress levels around the tower base are estimated using the Palmgren-Miner rule (Equation 4.12) at each location around the tower base.

4.3. Method improvements

The method presented in section Chapter 4 is developed from the existing method with the acronym RAFT[1] (Response Amplitudes of Floating Turbines), an open-source method developed by NREL. In its current form, it has been developed mainly for low-level motion analysis at an early stage of floating wind turbine development. However, several shortcomings have been identified and modified for this analysis[2].

The first modification was the implementation of a second wave system, as found in areas with strong swell. The method was not suitable to account for misaligned wave systems when using the potential flow method. This required changes in the accounting of the hydrodynamic excitation vector. In addition, corrections were made to the analytical analysis of the non-potential flow members to account for the misalignment of the waves.

The method was not developed with misalignment of wind in mind and it required modifications to account for wind directions other than zero. Additional modifications were made to account for the resulting mean roll angle when estimating the mean wind excitation.

Furthermore, the calculation of the side-to-side bending moment required a modification of the code to account for wind misalignment. As the rotor yaws with changing wind heading, the direction of the rotor plane changes and so does the aerodynamic damping and thrust. Improvements were also needed to correct the direction of rotation.

The calculation of the tower base bending moment was implemented, as well as the calculation of the equivalent stress using the Palmgren-Miner rule. This required the implementation of the Tovo-Benasciutti method for estimating the probability density of the rainflow cycle amplitude from the spectral density of the stress PSD (Section 4.2).

Finally, improvements were made to further reduce computation time on multicore CPU's (Central Processing Unit). Using a novel Python package "joblib" [56], parallel calculation of cases was been achieved. This required major revisions to the method to take into account the correct allocation of random access memory (RAM) to store results and prevent memory leaks. Given enough RAM, parallelisation reduces computation time linearly with the number of cores available for computation. On a laptop with 10 cores, the computation time was reduced from about 15 seconds per case (2-16 hours in the time domain) to approximately 1.5 seconds. Since the overhead in the RAM decreases as the number of cases increases, the relative improvement increases even more as the number of cases increases. To put this in perspective, DLC 1.2 requires an average of 10,000 cases for a full hindcast, which is a reduction from about 42 hours to 4 hours and 10 minutes.

[1] https://github.com/WISDEM/RAFT

[2] All of the developments and code for the reproduction of the sensitivity studies are available and open-source on: https://github.com/JoepvdSpek/RAFT/tree/joep_dev

4.4. Method application and limitations

This section explains the intended application of the model and several limitations. The frequency-domain method is intended to evaluate fatigue behaviour over the lifetime of the structure at an early design stage. It is known that extreme events due to failures, emergency stops, parking or transport conditions contribute to accumulated fatigue damage. These conditions can, for example, crack initiation and thus shorten the life of the structure. However, these effects are rather rare compared to the lifetime of the structure. As this study focuses on lifetime and production stage of a FOWT to compare possible designs, the above conditions and modelling considerations are not taken into account. Based on the expected conditions at the offshore site, the normal power production case can be evaluated (DLC 1.2). These load cases represent power production during normal operation, extreme turbulence and heavy seas, respectively. Since no controller action is currently applied in the method, DLC 1.3 and DLC 1.6 (extreme condition cases) can not be evaluated.

Furthermore, this method can be used independent of time-domain simulations as response estimations can be calculated independently of time-domain simulations. This is useful for academic purposes and/or if limited information on turbine is known. However, if turbine characteristics are known, it is recommended to take them from a parent-model using an approach such a presented by Pegalajar-Jurado *et al.* [2].

In addition, no wave current is taken into account in this method as the focus is on pitch and roll response. Wave current mainly affects the mean response in surge and sway direction.

Lastly, as a rigid tower is considered no tower modes are present in the method as the contribution to the floater motion is limited. However for relatively soft tower designs, the first bending mode can be excited by second-order wave forces. This is evaluated in Section 8.7. The contribution of these limitations in light of the comparison are discussed in Section 8.1.

5

Sensitivity Study Setup

5.1. Sensitivity study

First, basic operating/idling design conditions are established for the system. The floater and mooring system in the sensitivity studies is the VolturnUS-S as defined by Allen *et al.* [7]. This is a four-column, three radial and one central, semi-submersible platform with a three-line catenary mooring system. The turbine in this study is the IEA 15 MW reference turbine defined by Gaertner *et al.* [45]. The RAFT visualisation of this system is displayed in Figure 4.1. Full details are presented in the respective technical reports.

The reference operating conditions are defined in accordance with the DLC 1.2, defined in the IEC 61400-3 guideline. The results of the sensitivity studies in Chapter 6 and Chapter 7 will be presented relative to this base case.

5.2. Base case

To perform the sensitivity studies in Chapter 6 and Chapter 7, base environmental conditions have to be established from which parameters are varied. Literature [19, 27, 34] states that that aligned wind and windsea waves result in the largest response, but it is recommended to take a 90 degree wave misalignment angle into account. Given these factors, a base case is established that with an aligned (turbulent) wind and a windsea wave from a 0 degree misalignment and a swell sea approaching from a 90 degree angle.

As the scope of this project is limited to relatively near-shore locations that are selected for their wind energy potential, the base case is defined accordingly. The design driving cases from industry projects are defined to be within the scope of the sensitivity study. The base case is defined in Table 5.1. In this table the wind and wave conditions are presented. In this table, U_{ave} represents the average wind speed. Furthermore, θ represents the heading of the wind/wave with respect to the floater orientation. H_s, T_P, and γ represent the significant wave height, wave peak period, and peak enhancement factor of the JONSWAP spectrum.

Table 5.1: Base Case input values

	Value	Unit
Wind:		
U_{ave}	10.5	m/s
Turbine Class	II	
Turbulence class	B	
Turbulence Model	NTM	
$\theta_{FO,U_{ave}}$	0	deg
Windsea:		
H_s	2	m
T_P	6	s
γ	3.3	-
$\theta_{FO,WS}$	0	deg
Swell:		
H_s	1.5	m
T_P	10	s
γ	1.0	-
$\theta_{FO,SS}$	90	deg

For the floater and turbine presented in RAFT, the axis system and definitions are used which are presented in Figure 5.1. Wind and waves are defined as propagating towards. By this reasoning, a 0 degree angle ($\theta_{FO,U_{ave}}$/$\theta_{FO,WS}$) means excitation in positive x-direction and a 90 degree angle ($\theta_{FO,SS}$) means excitation in positive y-direction.

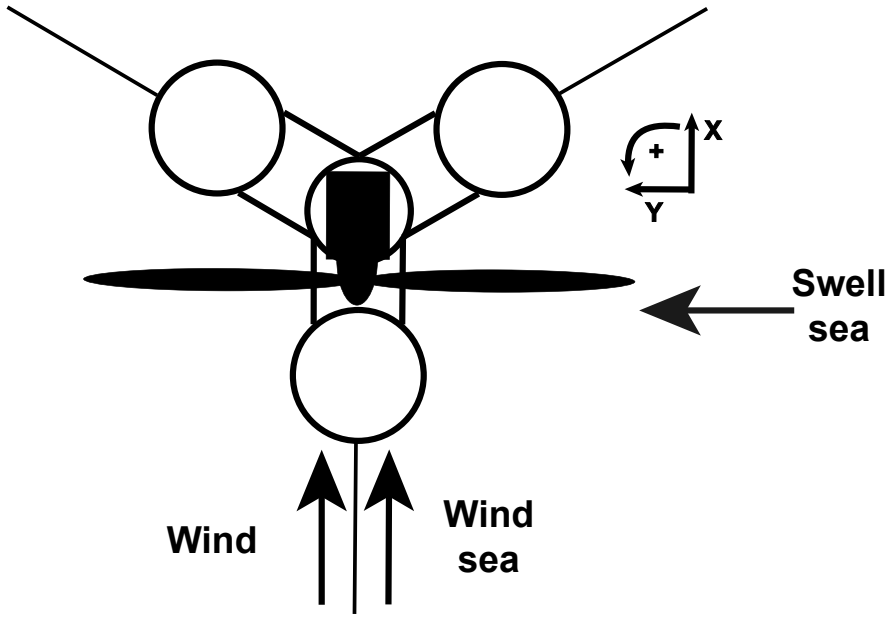

Figure 5.1: Base case wind and wave directions with respect to floater reference system.

5.2.1. Potential Flow coefficient matrices

The central column and the three outer columns are evaluated using the potential flow software, while the added mass and FK excitation of the connecting pontoons are estimated using the Morison equation. This improves computational time of the potential flow software (by reducing the number of panels) and is considered reasonable as they are located -16.5 metres below the waterline and therefore the contribution of wave excitation is limited. However, this approach does not estimate hydrodynamic damping (radiation) and coupling terms (added mass and damping).

In this section, the focus is exclusively on the resulting coefficient matrices for the added mass and damping calculated with the potential flow software [44]. The Morison equation represents only the viscous damping, but this is evaluated in an iterative step (Section 4.1.3).

Figure 5.2 shows the coefficients in both $\mathbf{A}_{BEM}$ and $\mathbf{B}_{BEM}$. It can be observed that the diagonal terms in these matrices of the rotational DOF's, have the highest numerical value. This is to be expected for this size of structure, since the magnitude of the moment is proportional to the size of the structure.

The hydrodynamic coupling coefficients for added mass and damping are shown in Figure 5.3. From these figures it can be seen that for roll motion the coupling term between sway and roll is largest for both added mass and damping. For the pitch motion, the largest coupling term is the surge-pitch coupling term. In general, it can be stated that for roll and pitch, the largest coupling term is for sway and surge, respectively. Furthermore, the magnitude of these coupling terms for sway-roll and surge-pitch is smaller ($10^1 - 10^2$) than that of the diagonal terms for roll-roll and pitch-pitch terms.

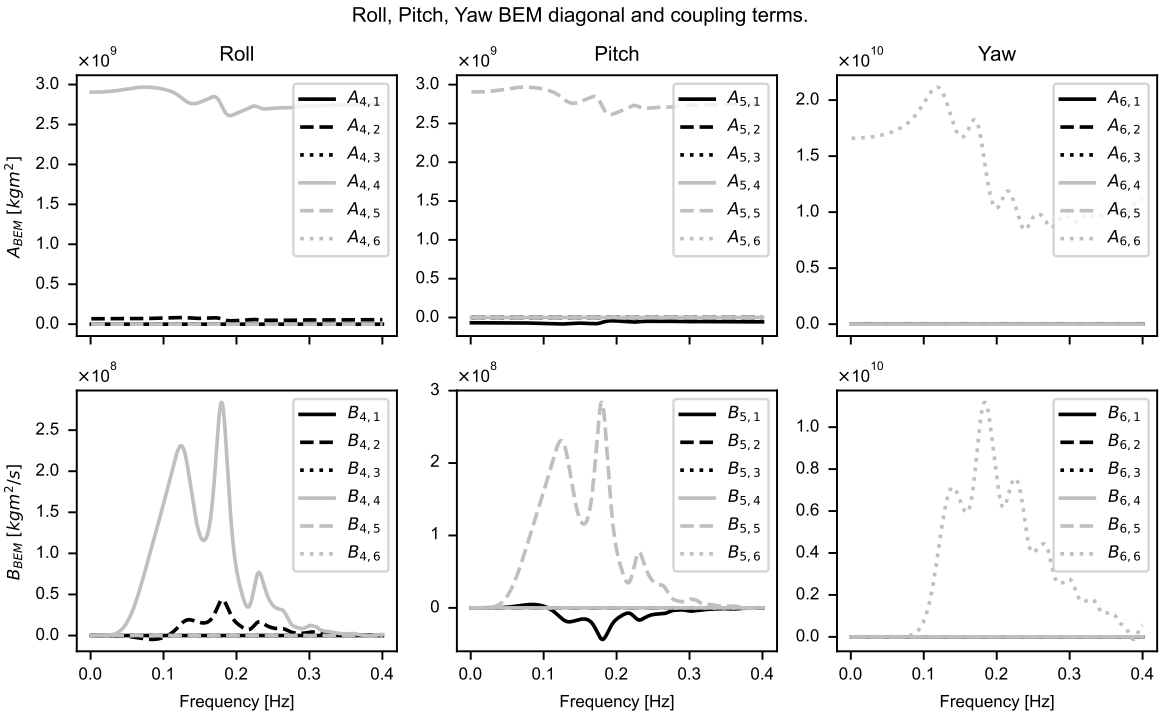

Figure 5.2: Potential flow, diagonal and coupling terms.

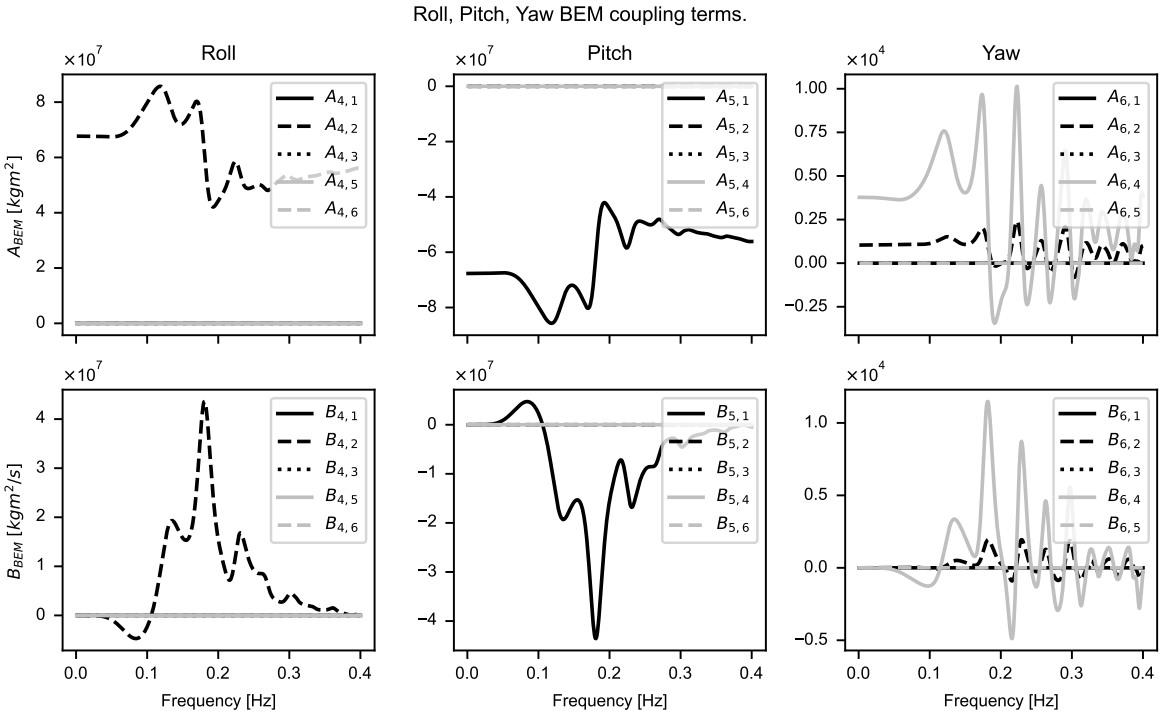

Figure 5.3: Potential flow coupling terms.

5.2.2. Aerodynamic coefficient matrices

For the aerodynamic added mass and damping terms (Figure 5.4) it can be stated that for no wind misalignent only aerodynamic damping is present in the pitch direction. As it is assumed that the damping terms are only present perpendicular to the rotor plane [47, 57]. Furthermore, the aerodynamic damping terms in the direction of the rotor plane are considered negligible when compared to the direction perpendicular to the rotor plane.

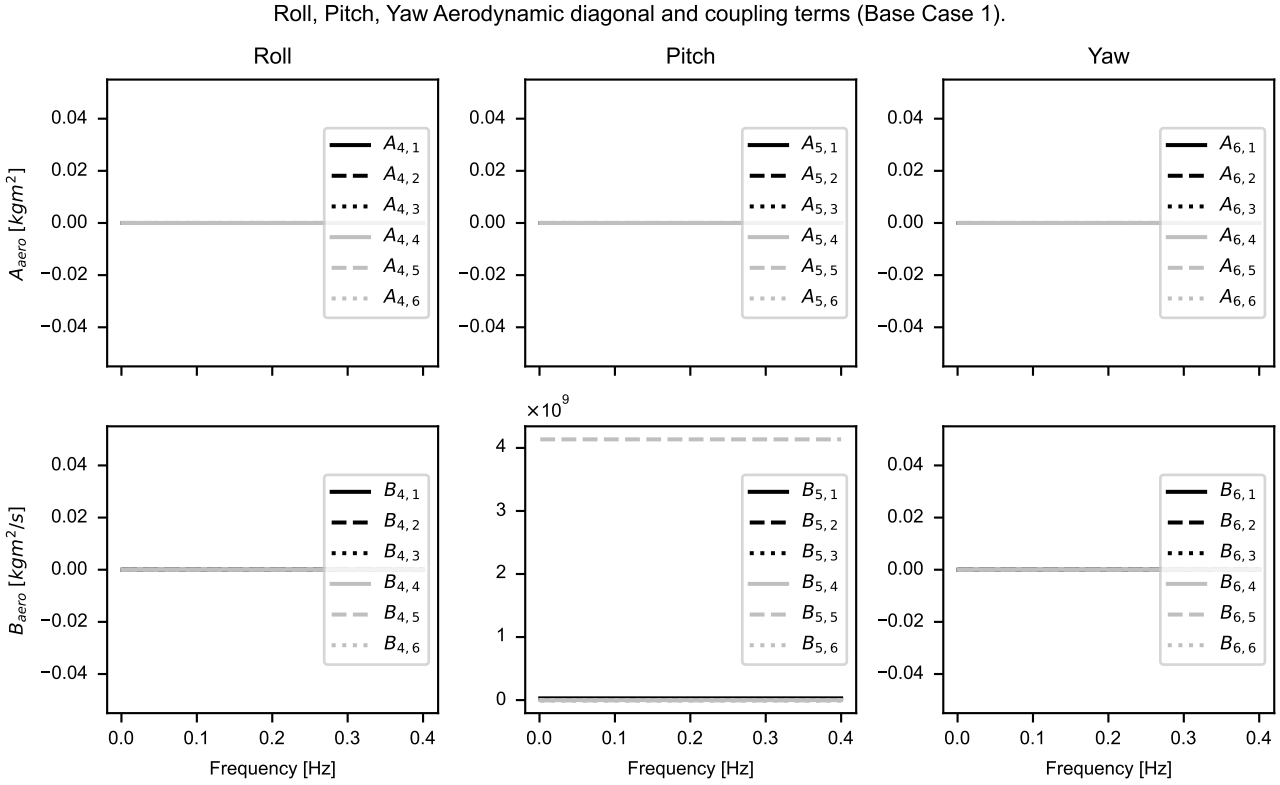

Figure 5.4: Aerodynamic added mass and damping coefficients: diagonals and coupling terms.

5.2.3. Total coefficient matrices

After evaluating the potential flow and aerodynamic contributions to the response matrices, the overall coefficient matrices are plotted in Figure 5.5. Several phenomena can be observed in this figure. As shown in Equation 4.3, the (added) mass consists of a structural mass matrix, the aerodynamic added mass, the hydrodynamic added mass calculated using the potential flow software and the added mass calculated using Morison equation for the connecting pontoons.

For the (added) mass/inertia terms, the largest contribution is due to the structural mass/inertia matrix. The system contains an RNA mass of nearly 1000 mT, an out of rotor plane and in rotor plane inertia of 220,000 $mT \cdot m^2$ and 120,000 $mT \cdot m^2$, respectively. The contribution of these members, located at a hub height of 150 metres, to the pitch and roll terms of the (added) mass matrices is considerable. In addition, the yaw (added) mass shows noticeable contributions from the structural mass matrix and the previously observed hydrodynamic added mass (Figure 5.2).

As for the damping terms, it can be observed that for the roll terms, that a considerable contribution of the hydrodynamic damping is present. Furthermore, the hydrodynamic drag calculated using the iterative steps is present. For this specific base case, the pitch damping is dominated by the aerodynamic damping (observed in Figure 5.4). The yaw terms for damping show that the yaw damping is dominated by the hydrodynamic damping (Figure 5.2).

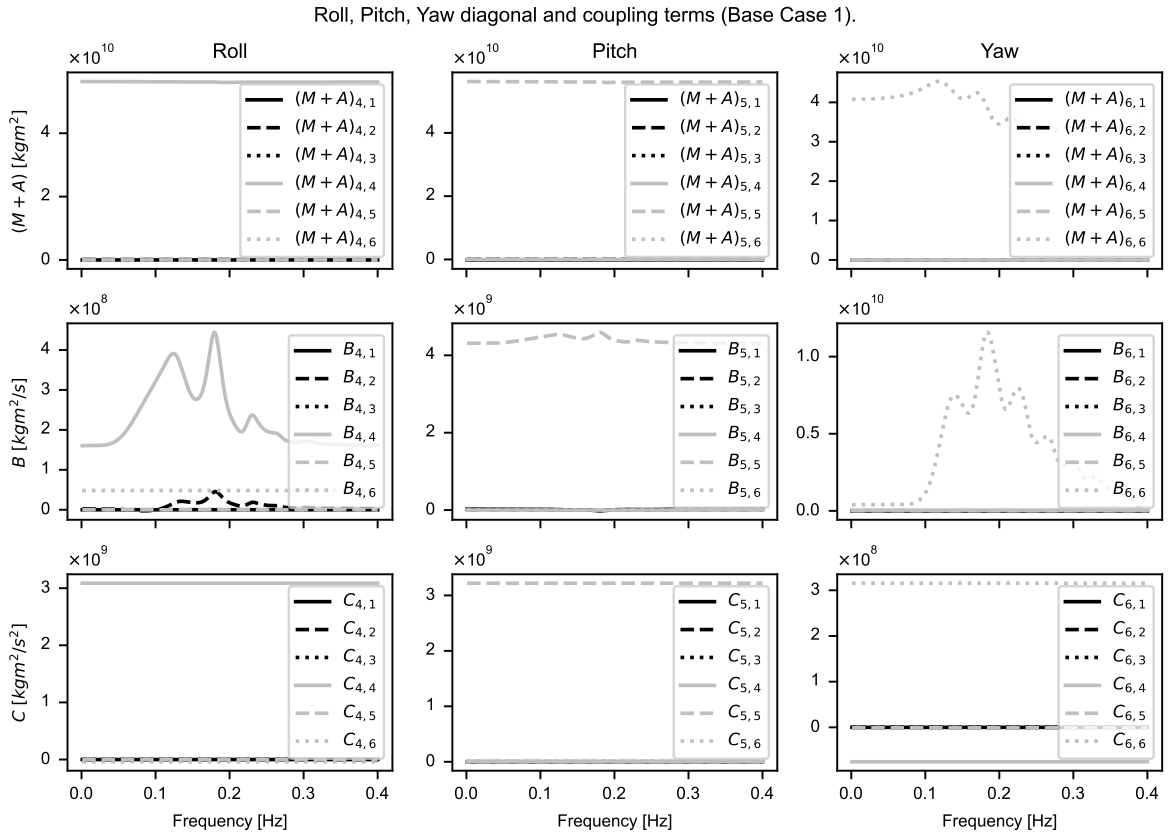

Figure 5.5: Coefficient matrix components, diagonal and coupling terms.

The stiffness terms for pitch and roll are dominated by hydrodynamic stiffness, whereas the stiffness in the yaw direction is dominated by the mooring system. This can be observed in Equation 5.1 Equation 5.2, and Equation 5.3.

$$\mathbf{C}_{moor} = \begin{bmatrix} \mathbf{1.54e{+}05} & -4.01e+02 & 3.54e+04 & -7.68e+03 & 2.40e+06 & 2.60e+04 \\ -4.03e+02 & \mathbf{5.37e{+}04} & 5.00e+02 & -8.08e+05 & -5.16e+03 & -1.83e+05 \\ 3.55e+04 & 4.93e+02 & \mathbf{6.91e{+}04} & -1.47e+02 & 6.84e+05 & 2.69e+04 \\ -7.66e+03 & -8.06e+05 & -2.14e+02 & \mathbf{2.38e{+}08} & 2.41e+05 & -4.67e+07 \\ 2.38e+06 & -5.82e+03 & 6.80e+05 & 1.51e+06 & \mathbf{3.98e{+}08} & 4.80e+05 \\ 1.90e+04 & -2.70e+05 & 2.51e+04 & -9.10e+07 & -1.26e+06 & \mathbf{3.32e{+}08} \end{bmatrix} \tag{5.1}$$

$$\mathbf{C}_{struc} = \begin{bmatrix} \mathbf{0.00e{+}00} & 0.00e+00 & 0.00e+00 & 0.00e+00 & 0.00e+00 & 0.00e+00 \\ 0.00e+00 & \mathbf{0.00e{+}00} & 0.00e+00 & 0.00e+00 & 0.00e+00 & 0.00e+00 \\ 0.00e+00 & 0.00e+00 & \mathbf{0.00e{+}00} & 0.00e+00 & 0.00e+00 & 0.00e+00 \\ 0.00e+00 & 0.00e+00 & 0.00e+00 & \mathbf{4.96e{+}08} & 0.00e+00 & 0.00e+00 \\ 0.00e+00 & 0.00e+00 & 0.00e+00 & 0.00e+00 & \mathbf{4.96e{+}08} & 0.00e+00 \\ 0.00e+00 & 0.00e+00 & 0.00e+00 & 0.00e+00 & 0.00e+00 & \mathbf{0.00e{+}00} \end{bmatrix} \tag{5.2}$$

$$\mathbf{C}_{hydro} = \begin{bmatrix} \mathbf{0.00e{+}00} & 0.00e+00 & 0.00e+00 & 0.00e+00 & 0.00e+00 & 0.00e+00 \\ 0.00e+00 & \mathbf{0.00e{+}00} & 0.00e+00 & 0.00e+00 & 0.00e+00 & 0.00e+00 \\ 0.00e+00 & 0.00e+00 & \mathbf{4.49e{+}06} & -7.45e-09 & 1.12e-08 & 0.00e+00 \\ 0.00e+00 & 0.00e+00 & -7.45e-09 & \mathbf{2.35e{+}09} & 0.00e+00 & 0.00e+00 \\ 0.00e+00 & 0.00e+00 & 1.12e-08 & 0.00e+00 & \mathbf{2.35e{+}09} & 0.00e+00 \\ 0.00e+00 & 0.00e+00 & 0.00e+00 & 0.00e+00 & 0.00e+00 & \mathbf{0.00e{+}00} \end{bmatrix} \tag{5.3}$$

Figure 5.6 presents solely the coupling terms present in the coefficient matrices for roll, pitch, and yaw, respectively. Comparing this with the magnitude of the diagonals (presented in Figure 5.5), it can be observed that yaw-roll coupling and sway-roll coupling in the damping matrix is of comparable magnitude.

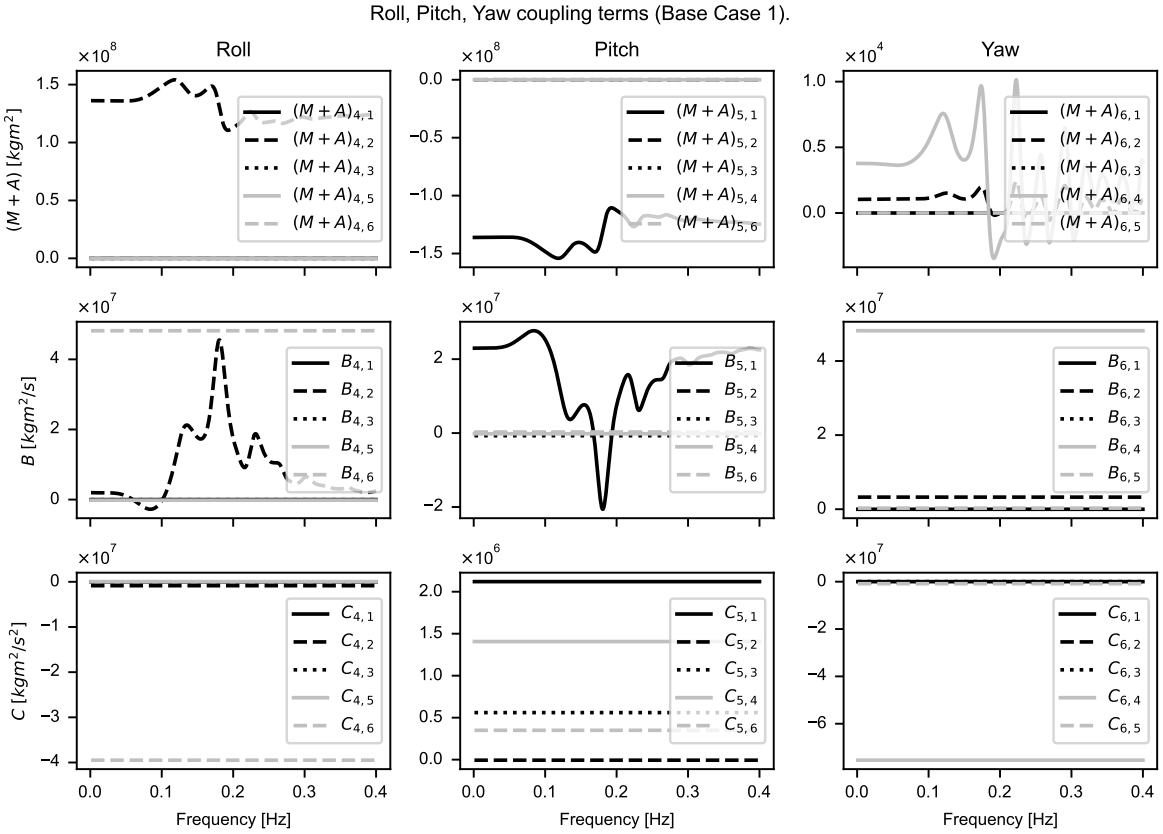

Figure 5.6: Coefficient matrix components, diagonal and coupling terms.

The sway-roll coupling is observed in Figure 5.2 due to the asymmetry of the structure about the y-axis (pitch axis). The yaw-roll coupling is the result of the iterative step in the calculation (Section 4.1.3). In other words, the connecting pontoons between the columns were not included in the potential flow calculation and their contribution to the damping was estimated only as viscous damping (Section 5.2.1). The resulting linearised hydrodynamic drag is a combination of these members and the columns as shown in Equation 5.4 (bold term). Finally, the roll-yaw coupling in the stiffness matrix comes from the mooring stiffness matrix (Equation 5.1).

$$\mathbf{B}_{linearised,drag} = \begin{bmatrix} 2.68e+05 & -1.12e+02 & -1.44e-12 & -1.84e+03 & -3.70e+06 & -8.14e+03 \\ -1.12e+02 & 1.21e+05 & 2.77e-13 & 1.51e+06 & 1.84e+03 & 2.98e+06 \\ -1.44e-12 & 2.77e-13 & 2.13e+05 & -5.11e+04 & -9.86e+05 & 5.05e-28 \\ -1.84e+03 & 1.51e+06 & -5.11e+04 & 1.75e+08 & 1.48e+05 & 4.51e+07 \\ -3.70e+06 & 1.84e+03 & -9.86e+05 & 1.48e+05 & 1.71e+08 & 1.47e+05 \\ -8.14e+03 & 2.98e+06 & 5.05e-28 & \mathbf{4.51e+07} & 1.47e+05 & 3.35e+08 \end{bmatrix} \tag{5.4}$$

Part III

Research

6

Yaw DOF and Yaw-Coupling.

This chapter answers the subquestion related to the yaw degree of freedom in the modelling of a floating offshore wind turbine:

> "How does inclusion of the yaw motion of a semi-submersible FOWT contribute to the rotational dynamic response under misaligned wind and waves in a frequency-domain method?"

A selection of relevant parameters is made for the sensitivity study. These parameters influence the coefficient matrices and/or influence the excitation in such a way that the response changes. The base case is defined in Section 5.2 and the coordinate system is defined in Figure 5.1. Based on this base case, several parameters are identified that could influence the yaw response and yaw coupling effects. The following parameters were selected for this study:

- Wind heading ($\theta_{FO,U_{ave}}$)
- Swell misalignment ($\theta_{FO,SS}$)
- Swell peak period (T_p)
- Floater orientation (θ_{FO})

Here the angles are defined as misalignment with respect to the floater orientation.

6.1. Yaw DOF: Wind heading

For a misaligned wind direction the aerodynamic damping and the aerodynamic excitation are rotated with respect to the floater reference frame. To capture the resulting change in response characteristics, the change in response can be quantified by the standard deviation (SD). The SD of a PSD (power spectral density) is a measure of the energy under the area of the PSD. In this case, it is used to assess the change in rotational energy for different wind headings. Since they are direction dependent, the L2 norm[1] of these respective SD values is used to compare the total rotational energy of the rotational components.

The results of this analysis are shown in Figure 6.1. From this analysis it can be seen that as the heading increases (away from 0 degrees) the pitch response decreases and the roll response increases. The pitch response is greatest at a wind heading of 0 degrees and the roll response is greatest at a wind heading of 90 degrees. This corresponds to a wind-wave misalignment of 0 degrees with respect to the wind-sea component or the swell-sea component. In addition, the yaw response increases initially but decreases again at wind directions where the floater is symmetrical.

It can also be seen that the L2 norm of the standard deviations increases for wind directions away from 0 degrees wind heading. As the L2 norm of the pitch and roll SD increases, this indicates an increase in rotation response in these degrees of freedom.

[1] The L2 norm (or Euclidean norm) is the distance of the vector coordinate from the origin of the vector space.

Overall, changing the wind heading increases the total rotational response and the yaw response increases at wind directions where the floater is not symmetrical. With increased roll response, the yaw response also increases due to the coupling terms identified in Section 5.1, as the yaw excitation is not changed.

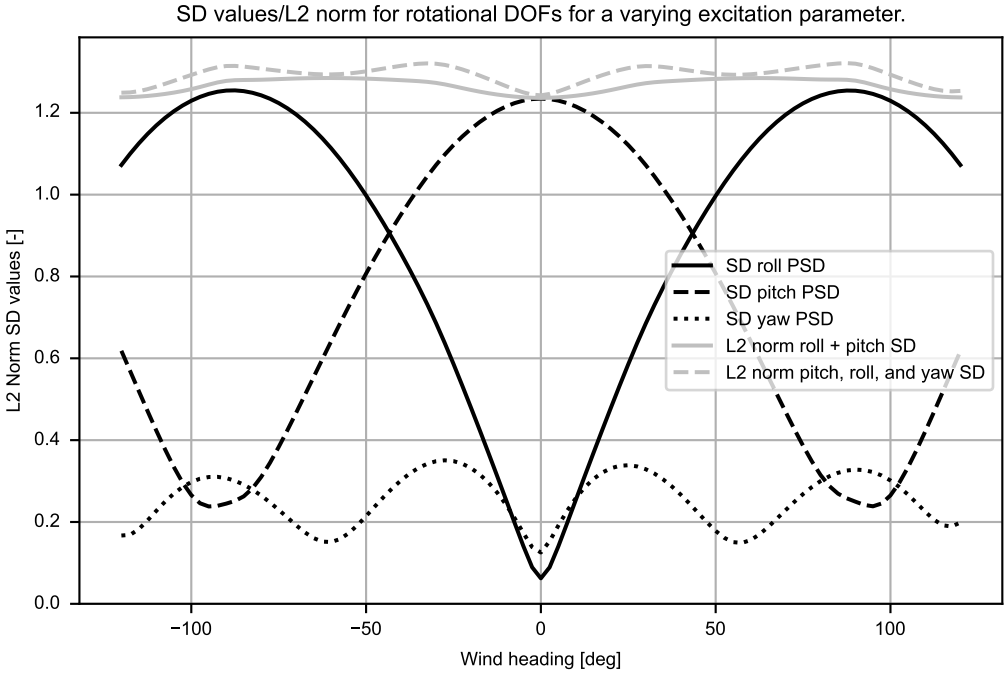

Figure 6.1: SD of roll, pitch, and yaw for wind heading of -120 deg to +120 deg.

To identify the cause of the change in response, the response spectra for wind headings of 0 degree (base case) and 30 degree are plotted in Figure 6.2. From this figure it can be seen that for a wind heading of 0 degrees, there is only an observable response in roll direction around the wave frequency (0.1-0.2 Hz). However, for a wind heading of 30 degrees a noticeable roll response is observed around the wind turbulence range (up to 0.05 Hz). Since there is no yaw excitation from the wind, the roll-yaw coupling in the stiffness terms (identified in Section 5.2.3) also leads to an increased yaw response at low frequencies for $theta_{Wind} = 30$ degrees. This is the result of the limited damping is present at low frequencies, as presented in Figure 5.5.

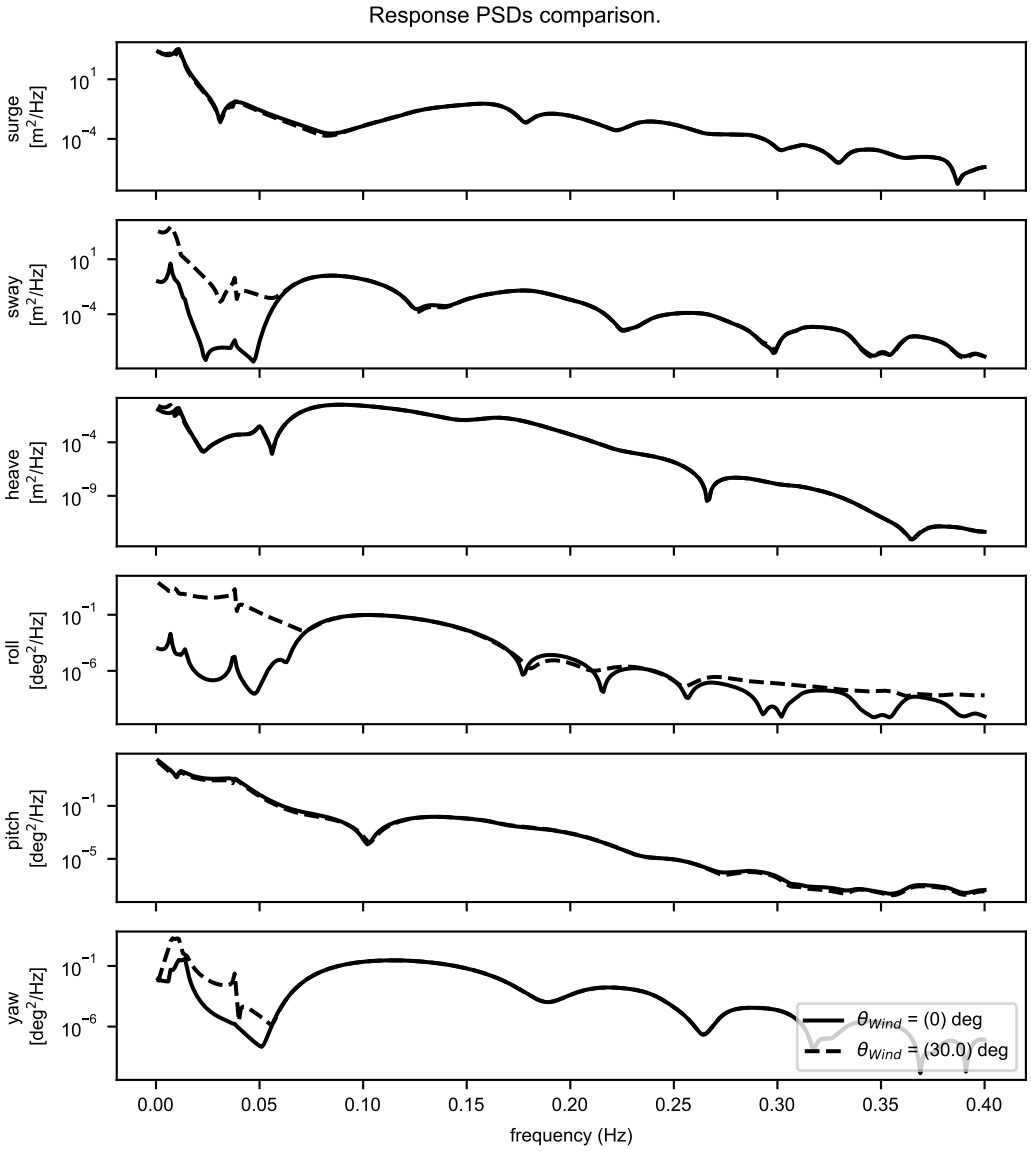

Figure 6.2: Response PSDs for $\theta_{wind} = 0deg$ and $\theta_{wind} = 30deg$.

6.2. Yaw DOF: Swell misalignment

In this section a change of swell heading ($\theta_{FO,SS}$) implies a different direction of a wave excitation component. It is a change of wave direction from pitch/surge direction (0 degrees) to roll/ swing direction (90 degrees). From Figure 5.5, it is clear that yaw-roll and roll-yaw couplings exist. Therefore, changing the swell heading and thus the excitation also affects the contribution of these coupling effects to the rotational response. This section examines the change in roll response and the contributions to the rotational DOFs (roll, pitch, and yaw).

To illustrate the different components of the wave excitation, the wave excitation on the structure for a JONSWAP spectrum with $T_p = 10\ s$, $H_s = 1\ m$, and $\gamma = 1$ is plotted in Figure 6.3. This figure shows for this particular floater type, significant wave height, and peak period, the real part of the wave excitation for 0 degrees to 180 degrees of swell direction. Therefore, this figure shows how the wave excitation changes at different wave angles.

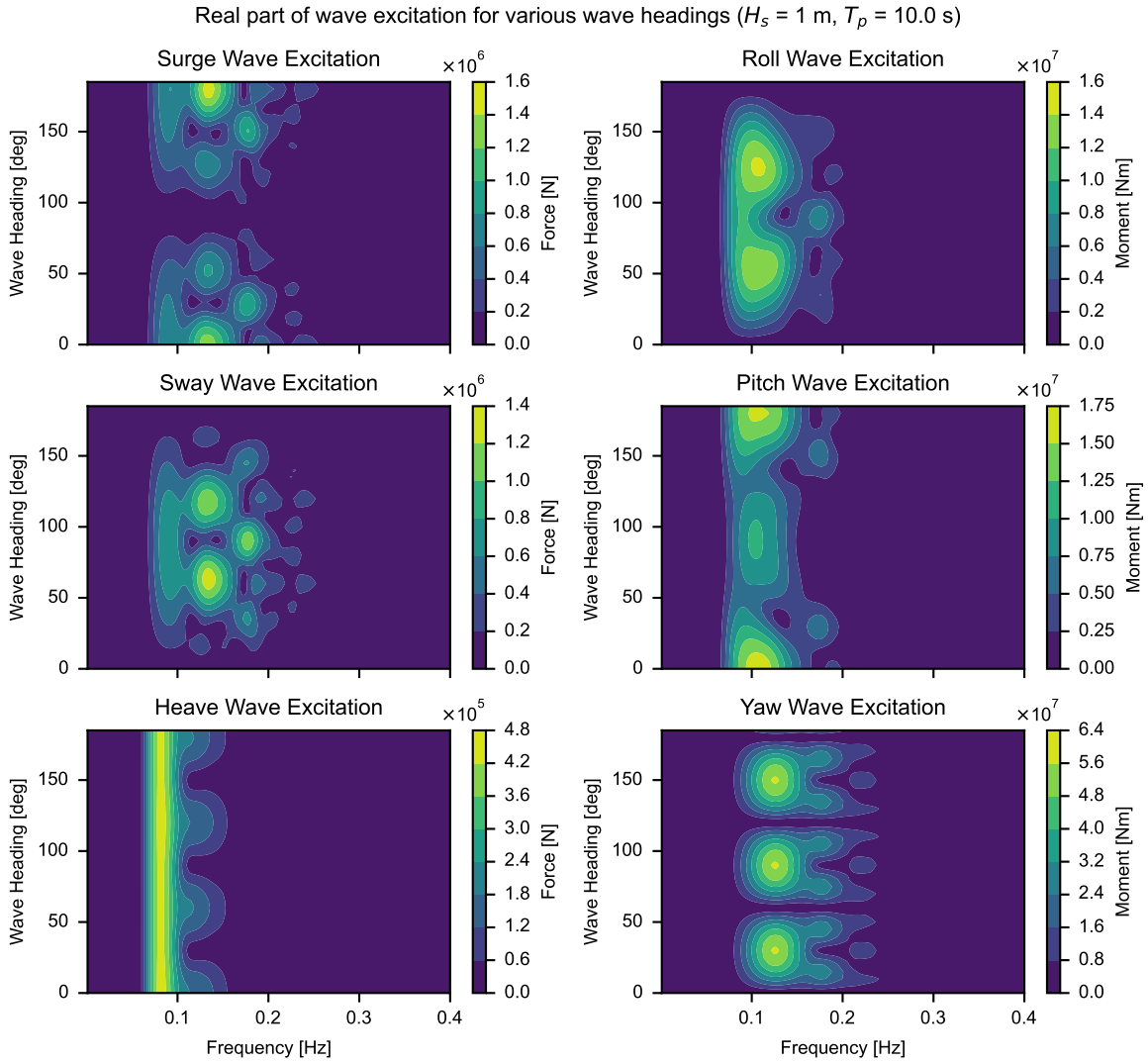

Figure 6.3: Wave excitation for various wave headings ($T_p = 10$, $\gamma = 1$).

Yaw-excitation occurs when there is a resulting moment around the z-axis of the floater. From Figure 6.3 it can be observed that for a wave peak period of 10 seconds, the yaw wave excitation is largest for swell headings in which the floater is not symmetric (30, 90. and 150 degree). For a swell misalignment of 90 degrees, the resulting projection of the wave crests on the structure is illustrated in Figure 6.4. This combination of wavelength and peak period results in a moment around the z-axis due to the difference in pressure on the outer columns.

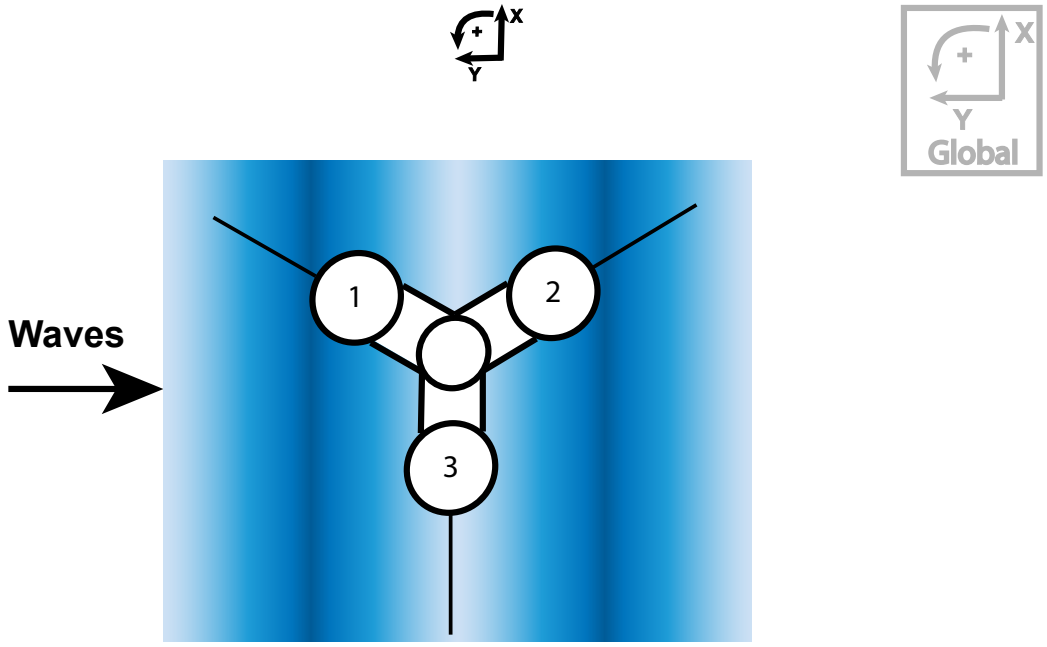

Figure 6.4: Maximum yaw excitation for a wave direction in which floater is asymmetric.

Furthermore, in Figure 6.3 it is seen that a swell heading of 60 degree and 120 degree results in the largest wave excitation. A wave heading of 120 degrees results in columns 1 and 3 being in phase with the wave direction as shown in Figure 6.5. This explains why 60 degree and 120 degree wave direction result in the largest roll excitation.

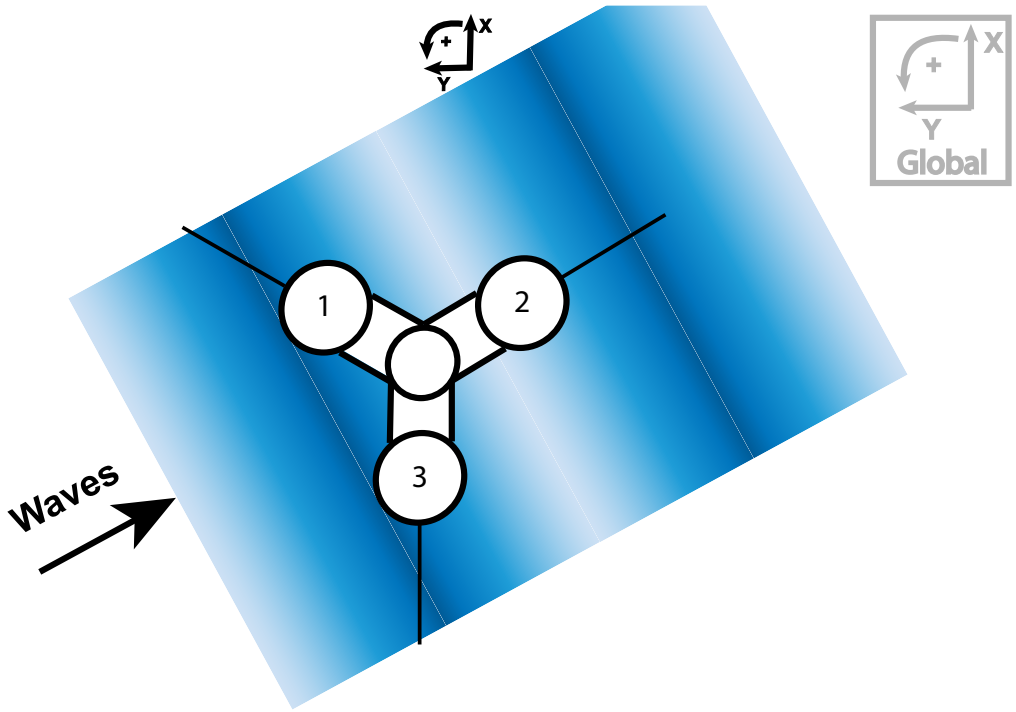

Figure 6.5: Maximum roll excitation occurs for the wave direction in which the excitation of two columns is in phase.

To further analyse this changing behaviour, the response PSDs are plotted in Figure 6.6. The contribution of the maximum roll excitation and its distribution along the wave frequency range can be observed. No wave excitation around the wave frequency range in yaw is seen for 60 degrees swell misalignment ($\theta_{swell} = 60°$). The (negligible) response around the wind turbulence range is contributed to pitch-yaw coupling terms in the mooring stiffness (Equation 5.1) and the linearised drag estimate (Equation 5.4). However, for a swell misalignment of 90 degrees ($\theta_{swell} = 90°$) a yaw response around the wave frequency range can be observed. Furthermore, an increased roll-response is present around the wave frequency range too.

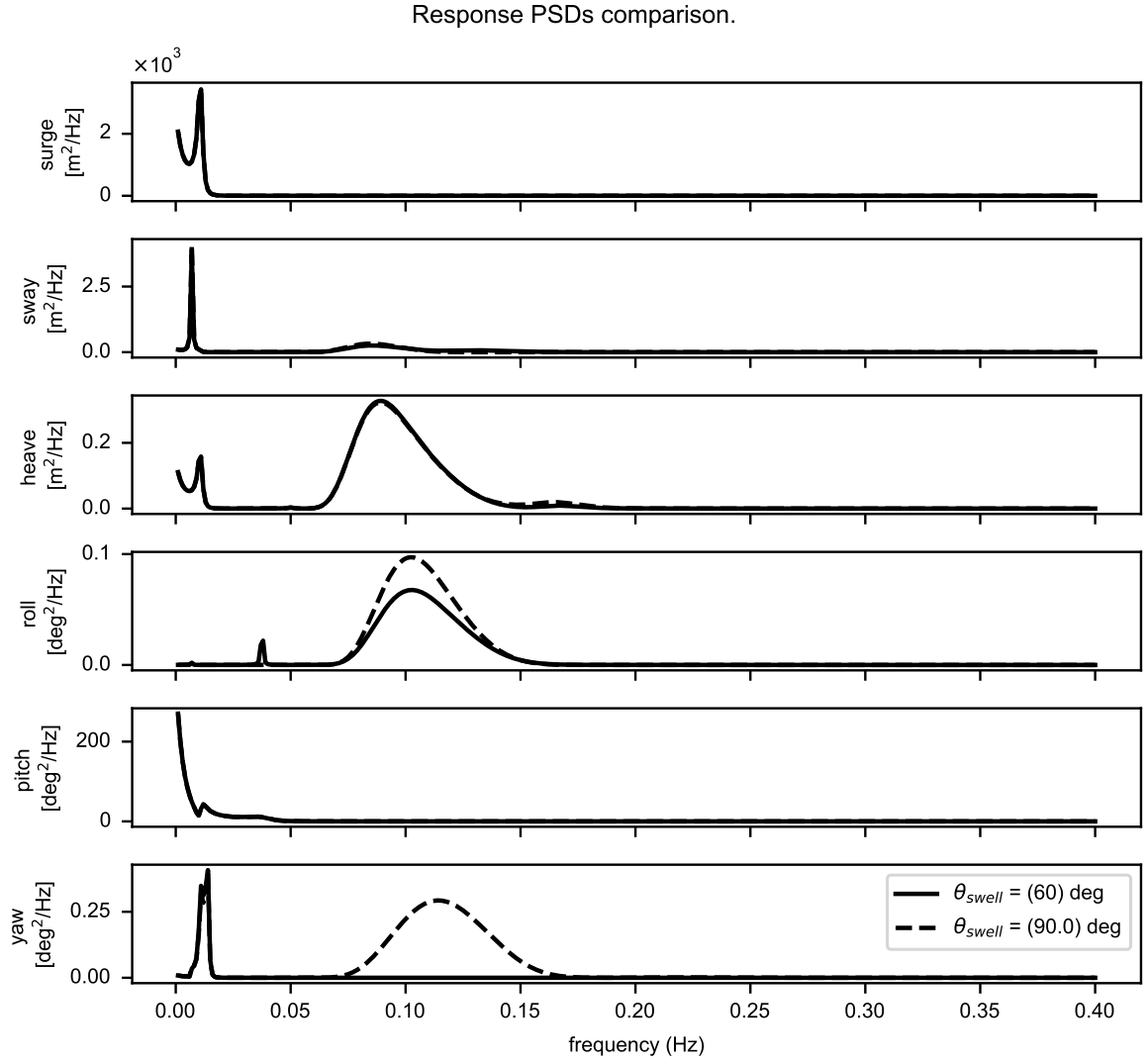

Figure 6.6: Response PSDs for $\theta_{swell} = 60deg$ and $\theta_{swell} = 90deg$.

For the swell misalignment of 0 degree to 180 degree, the SDs of the rotational DOFs are plotted in Figure 6.7. From this figure it can be seen that as the misalignment with respect to the floater origin system increases, the yaw response increases at angles where the floater is not symmetrical. The roll excitation seen in Figure 6.3 results in an increased roll response.

However, the lower roll excitation at a 90 degrees swell misalignment (compared to 60 degree and 120 degree) does not lead to a lower roll response. Since a noticeable yaw-roll coupling was observed in Section 5.2.3, it can be concluded that the increase in roll response at 90 degrees swell misalignment is because of the increased yaw excitation via yaw-roll coupling effects.

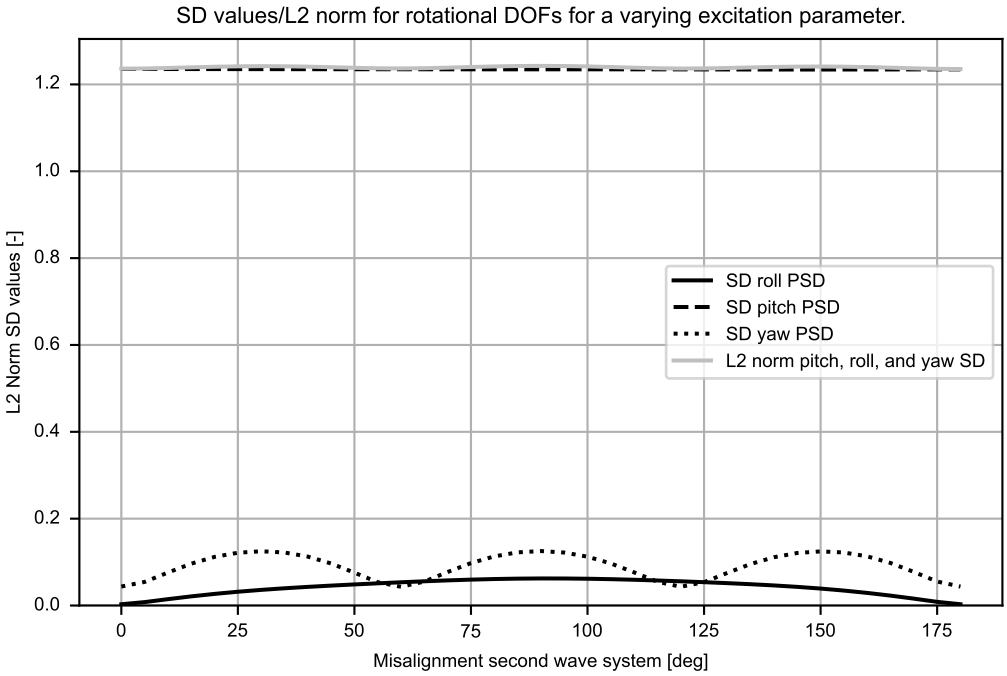

Figure 6.7: SD-values for roll, pitch, and yaw for swell misalignment of 0 degrees to 180 degrees.

6.3. Yaw DOF: Swell peak period

Furthermore, the wave period of the misaligned wave component is varied. The natural period of roll and pitch is about 26 seconds. The natural period of yaw is about 60 seconds, which is outside the likely peak periods of waves in coastal waters [53]. To include the roll response around its natural period, the maximum swell peak period is set at 30 seconds. The SDs for the range of swell periods are shown in Figure 6.8.

Although the natural period of the yaw period is about 60 seconds, the wave force in the yaw direction is greatest at a peak period of 8.0 seconds. This can be observed in Appendix B, Figure B.1 to Figure B.10, where the wave force calculated by the potential flow software is shown for a range of wave headings and a range of wave peak periods. It can be observed that for a wave misalignment of 90 degrees and a wave peak period of 8 seconds, the wave excitation is greater than for lower and higher wave peak periods (seen in Figure B.13 to Figure B.23).

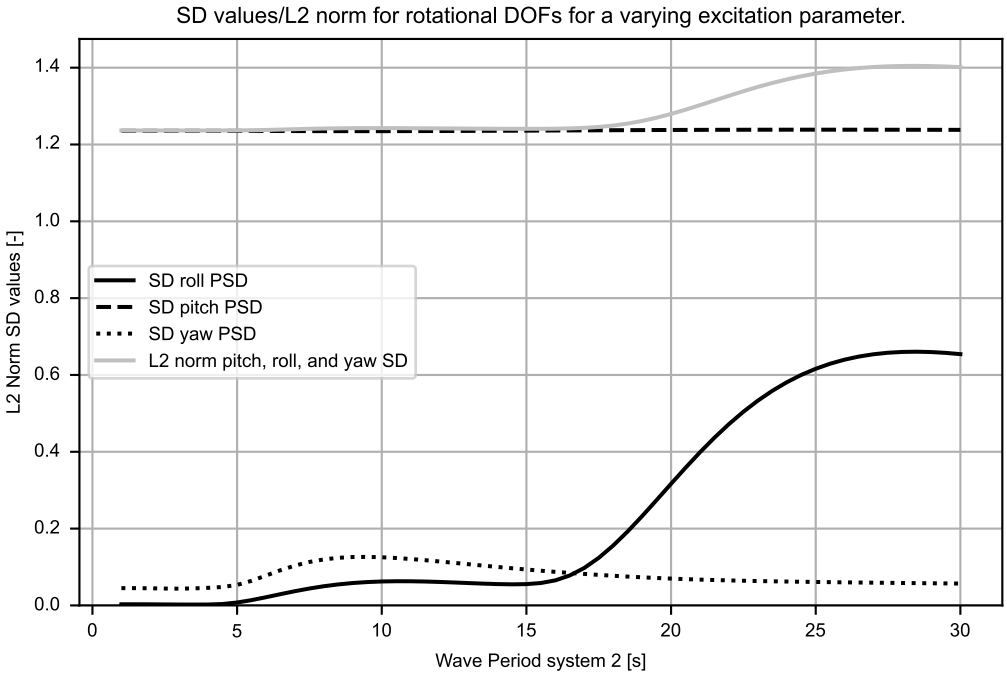

Figure 6.8: Standard deviations for roll, pitch, and yaw for swell periods from 1 to 30 seconds.

Since deep water is considered, the deep water frequency dispersion relation applies [53]. From this relationship, for a peak period of 8, it can be estimated that the wavelength is about 100 metres. At this incident angle, this wavelength corresponds to the apparent length of the structure in that direction. This is illustrated in Figure 6.9. In the figure it can be seen that due to the symmetry of the structure, column 1 and column 2 experience a maximum pressure because there is a wave crest at that location. Column 3 experiences a minimum pressure on the column because it is located in a wave trough. The resulting moment around the centre of gravity leads to an oscillatory excitation. Thus, if the peak period of the spectrum is around this apparent length, increased excitation is expected compared to shorter waves (lower T_p) and longer waves (higher T_p).

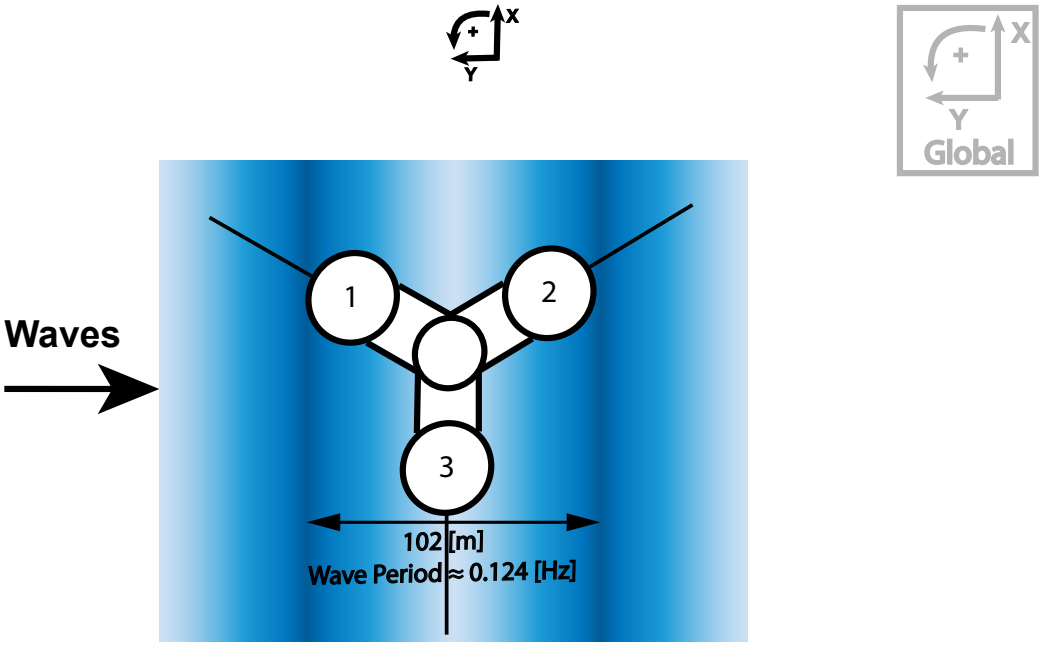

Figure 6.9: Maximum yaw excitation occurs for a wave peak period equal to the apparent length of the structure.

To illustrate the differences to a lower wave peak period of 5.0 seconds (Figure B.3), the wavelength for this wave period is illustrated in Figure 6.10. From this figure it can be seen that the three columns are each located on a crest of the wave. Together with the shorter wave period results in a smaller oscillatory moment around the z-axis.

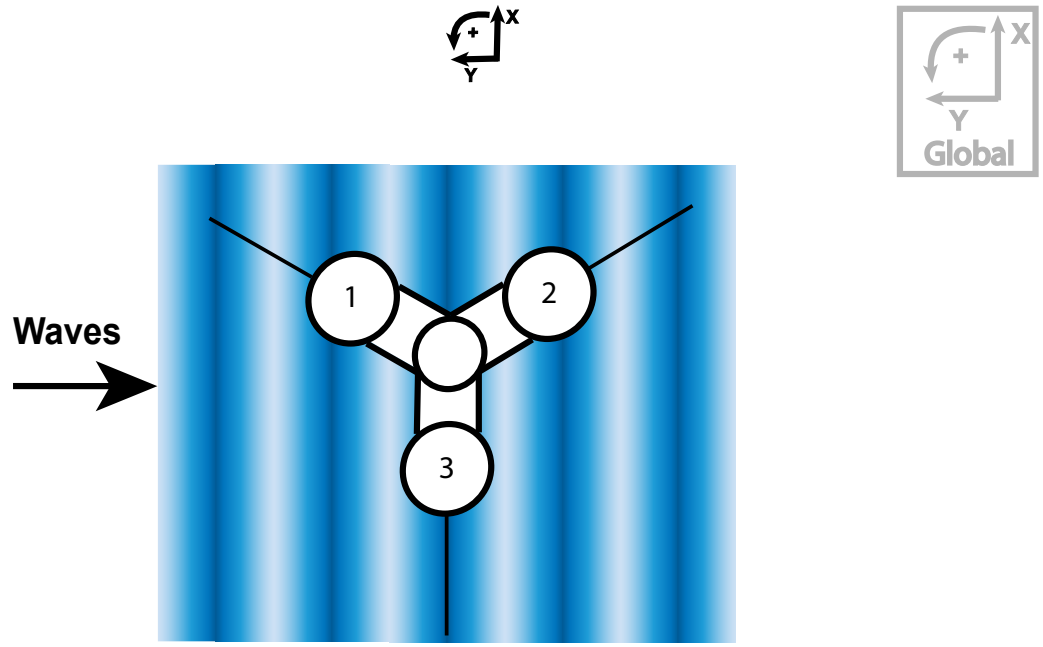

Figure 6.10: Minimum yaw excitation for a wave peak period of 5 seconds which corresponds to a wavelength of $39m$.

Since the yaw-roll coupling (mooring stiffness) is observed in Equation 5.1, a large yaw excitation compared to the roll excitation also leads to an increased roll response. To quantify this, Figure 6.11 shows the response spectra for a wave period of 5.0 and a wave period of 8.0 seconds. From these PSDs it can be concluded that an increased yaw response occurs for the wave peak period of 8 seconds. This increased yaw response also increases the roll response due to coupling effects present as the roll excitation for this wave period and misalignment angle is small (Figure B.6).

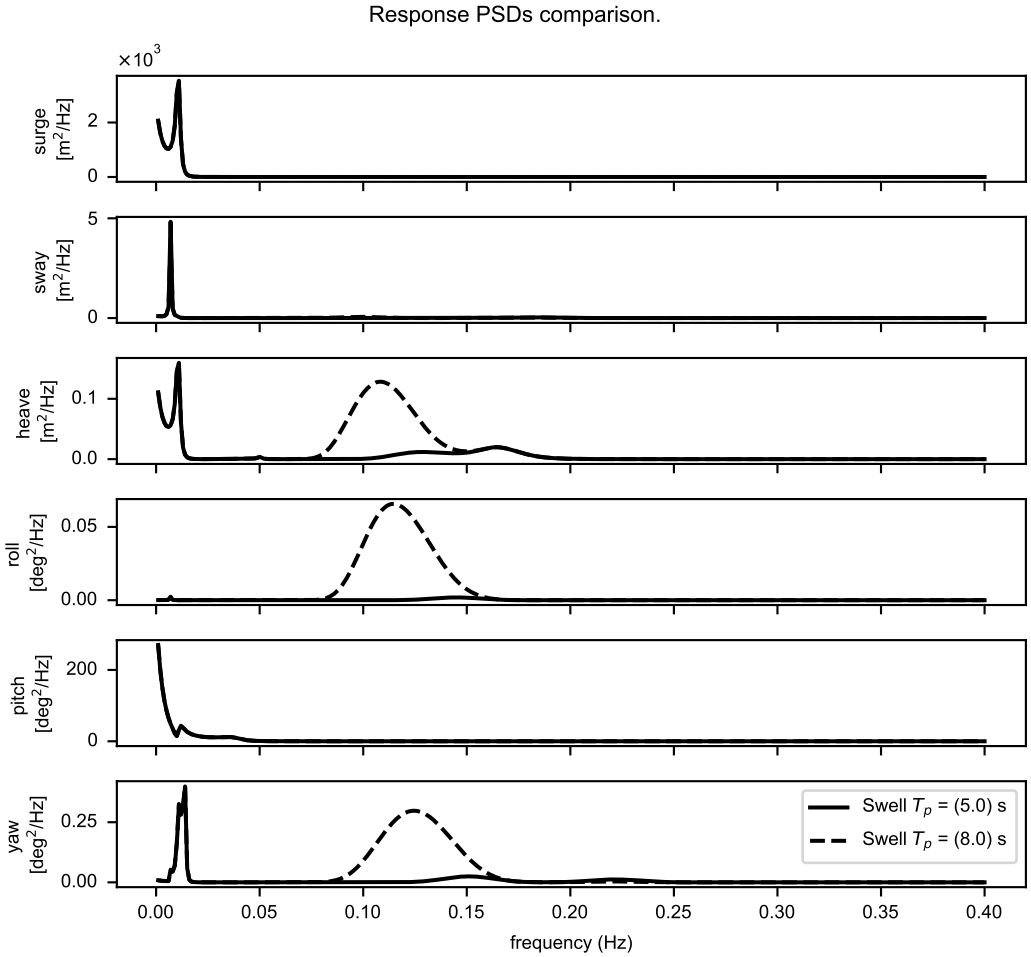

Figure 6.11: Response PSDs for $SwellT_p = 5.0[s]$ and $SwellT_p = 5.0[s]$.

6.4. Yaw DOF: Floater orientation

Finally, the response for different floater orienatations is evaluated. A different orientation of the floater changes the wind and waves directions with respect to the floater orientation. This can be observed as a combination of the change in wind heading (Section 6.1), wind-sea direction and swell direction (Section 6.2).

To evaluate the combination of these changes, Figure 6.12 shows the SD values for different floater orientations. From this figure it can be seen that the SD value for yaw increases with increasing floater orientation up to 30 degrees. This increased SD value visible for 30 degrees and 90 degrees, was also previously observed in Section 6.1 and corresponds to the wind direction in which the structure is not symmetrical.

Furthermore, this figure shows that there is an increased rotational response (L2 norm of roll, pitch. and yaw) when the floater is rotated 30 degrees and 90 degrees compared to the base case. This is consistent with the observations in Section 6.1, as a wind heading of 30 degrees resulted in an increased rotational response due to roll-yaw coupling.

However, this rotation of 30 degrees also results in a misalignment angle of the wind-sea component

of 30 degrees. With a peak period of 6 seconds, this has a relatively low yaw excitation compared to the swell sea component (10 seconds) (Figure B.4 and Figure B.8). Since the 30 degrees rotation leads to a 120 degrees swell heading, this swell component does not excite in the yaw direction (Figure B.8). Overall, this leads to a reduced yaw excitation by the wave components, but to an increased response due to the roll-yaw coupling.

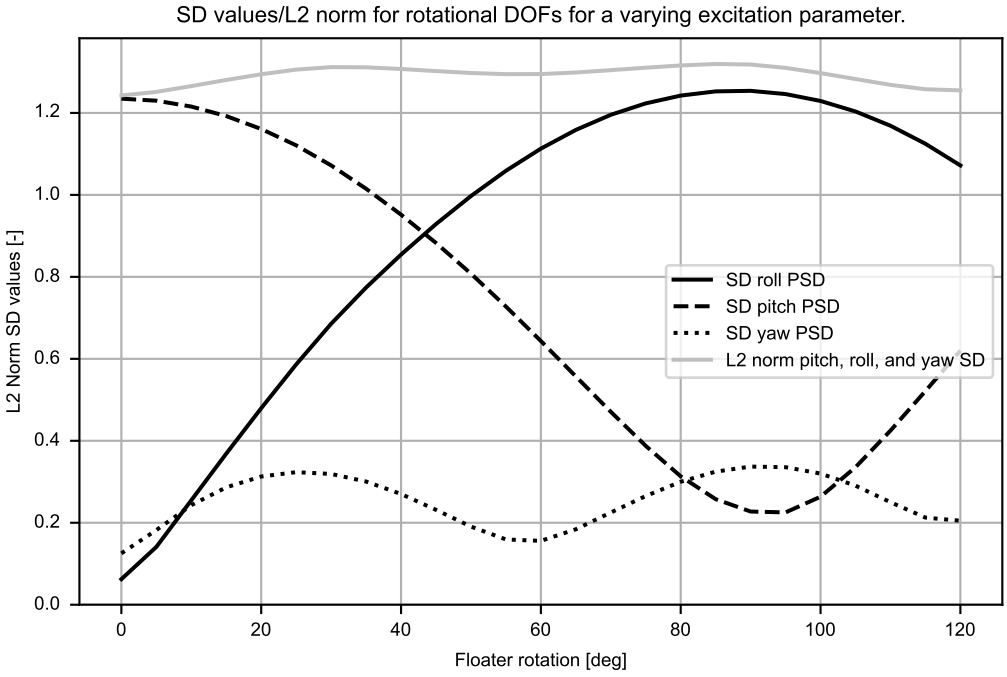

Figure 6.12: SD values of roll, pitch, and yaw response for a floater rotation from 0 degrees to 120 degrees.

6.5. Yaw DOF: Concluding remarks

To summarise, this chapter presented a sensitivity study for various wind and wave parameter to investigate the contribution of yawing and yaw-related coupling effects to the total motion response of the structure.

Several conclusions are drawn from this sensitivity study. First, it is concluded from Section 6.1 that the yaw response increases with increasing wind direction at angles where the floater is not symmetrical. This increase in yaw response increases the roll response for these directions due to yaw-roll coupling terms identified in Section 5.2.3.

Furthermore, varying the heading of the swell system (Section 6.2) only changes the wave excitation. The yaw response increases at angles where the floater is not symmetrical. This increase in yaw response, even at small angles, increases the roll response through coupling effects.

In Section 6.3 it has been shown that at different wave peak periods the rotational response increases due to increased wave excitation. This change in wave excitation is dependent on the angle of incidence (shown in Section 6.2), wave period and geometry of the floater. It has been identified that the yaw wave excitation is the largest when the length of the waves equals the length of the structure and excites at an angle in which the floater is asymmetrical. Due to the yaw-roll coupling effects the roll excitation also increases.

In Section 6.4 the floater is rotated. It is found that floater rotation can result in an increase in excitation, as a rotation can result in an unfavourable wave direction with respect to the floater orientation. This can increase or decrease the response of the yaw degree of freedom due to coupling effects.

7

The Effect of Aerodynamic Damping on the Response

This chapter describes the research to answer the sub-question of the effect of aerodynamic damping on the overall motion response under misaligned wind and waves:

> "What is the contribution of aerodynamic damping to the response of a semi-submersible floating offshore wind turbine, considering misalignment of wind and waves with respect to floater orientation?"

To answer this sub-question, a sensitivity study is conducted to quantify the contribution of (reduced) aerodynamic damping to the tower base bending moment response. The base case is defined in Section 5.2 and the coordinate system is defined in Figure 5.1. Four input parameters are identified that contribute to aerodynamic damping and\or misalignment. The following parameters are selected for this sensitivity study:

- Wind speed (U_{ave})
- Wind heading ($\theta_{FO,U_{ave}}$)
- Swell sea heading ($\theta_{FO,SS}$)
- Floater orientation (θ_{FO})

The headings are defined as misalignment with respect to the floater orientation.

7.1. Aerodynamic damping: Average wind speed

It is assumed that damping is independent of frequency and that the average aerodynamic thrust on the rotor depends on the average wind speed. Both variables can be plotted for a range of wind speeds as shown in Figure 7.1. From this figure it can be seen that as the wind speed increases, the estimated aerodynamic damping increases. Secondly, the damping decreases slightly above the rated wind speed, but remains approximately the same until the cut-off wind speed is reached.

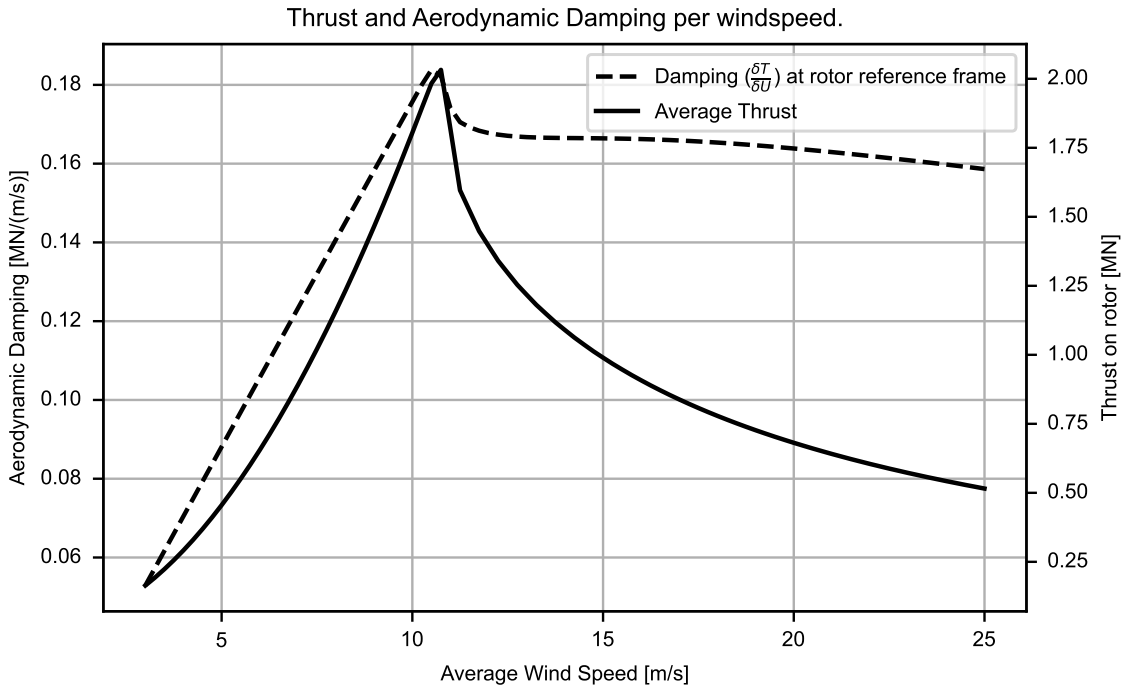

Figure 7.1: Aerodynamic damping and thrust on the rotor the operational wind speeds.

Above the rated wind speed, the blades are pitched to maintain a constant torque (rated power) at the turbine. Therefore, the thrust at the rotor initially increases up to the rated wind speed, after which it decreases significantly. This is the effect of pitching of the blades above the rated wind speed to keep the torque approximately constant. The decrease in average thrust excitation reduces the mooring stiffness in the surge direction when the mooring line is lowered back to the seabed. This effect is shown in Figure 7.2, where the black turbine illustrates the situation for reduced thrust and the grey situation displays the mean response at maximum thrust.

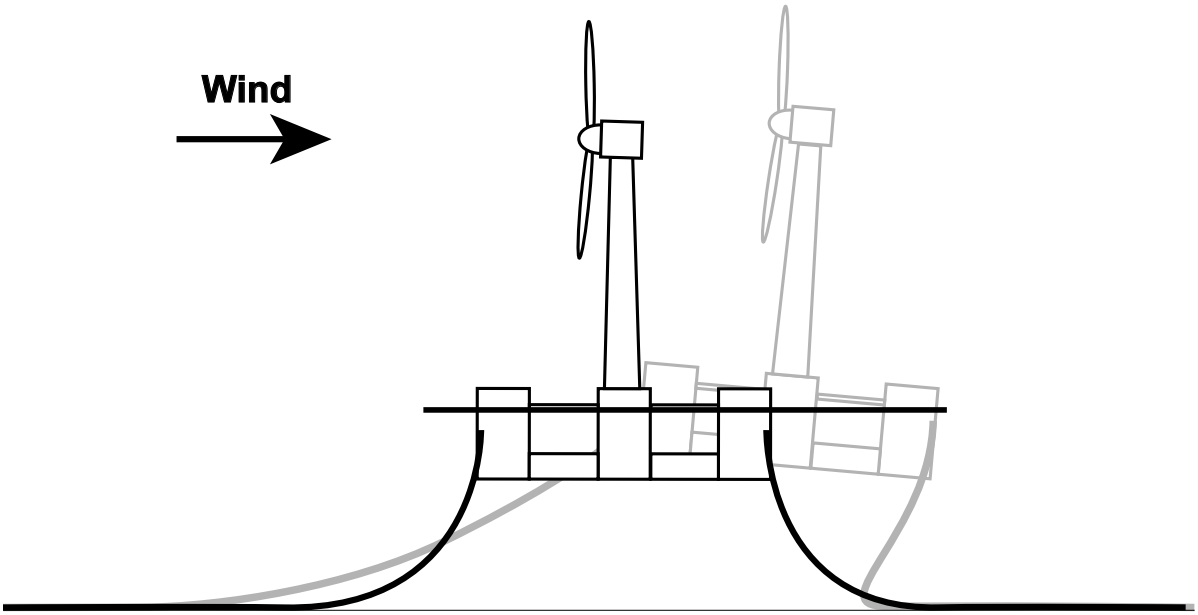

Figure 7.2: Decreased thrust on the rotor results in a reduced mooring stiffness in surge direction.

For the same range of wind speeds presented in Figure 7.1, the SD of rotational responses are plotted in Figure 7.3. It can be seen that as the wind speed increases, the SD of the pitching motion increases up to the rated wind speed. Above the rated wind speed, the maximum equivalent stress decreases slightly before increasing again.

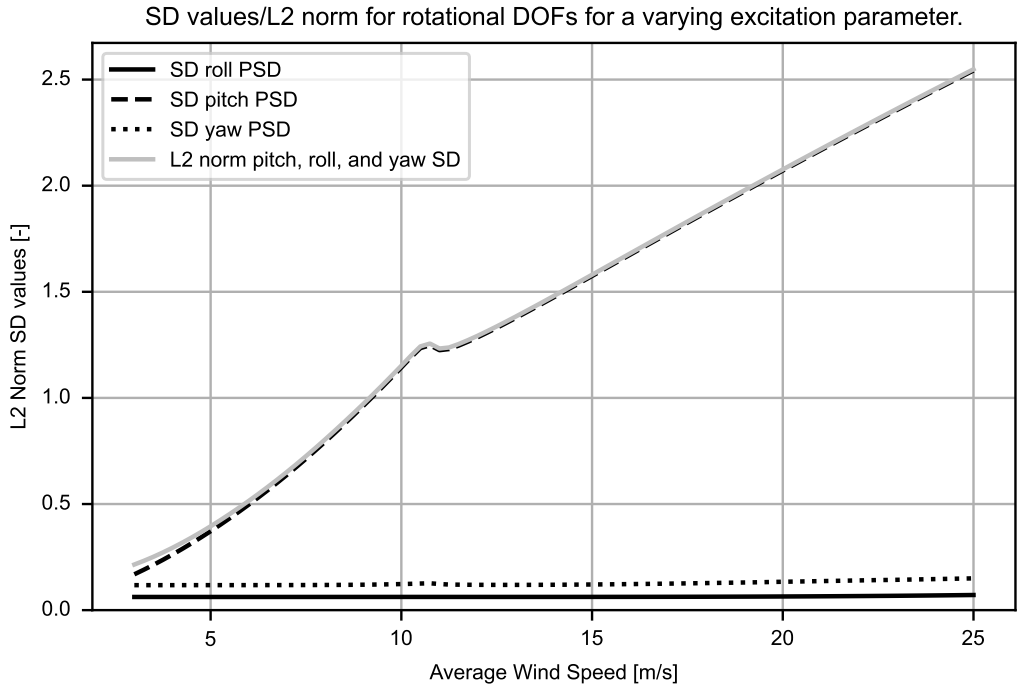

Figure 7.3: SD values/L2 norm of SD for a range of average wind speeds.

To evaluate this increase, the PSDs of the response are plotted in Figure 7.4. It can be seen that at low frequencies (below 0.05 Hz), the reduced mooring stiffness increases the response at low frequencies for all degrees of freedom. Furthermore, the increased damping effect around the pitch natural frequency (0.38 Hz (Section 8.3.1)) can be seen, which reduces the response around the natural frequency.

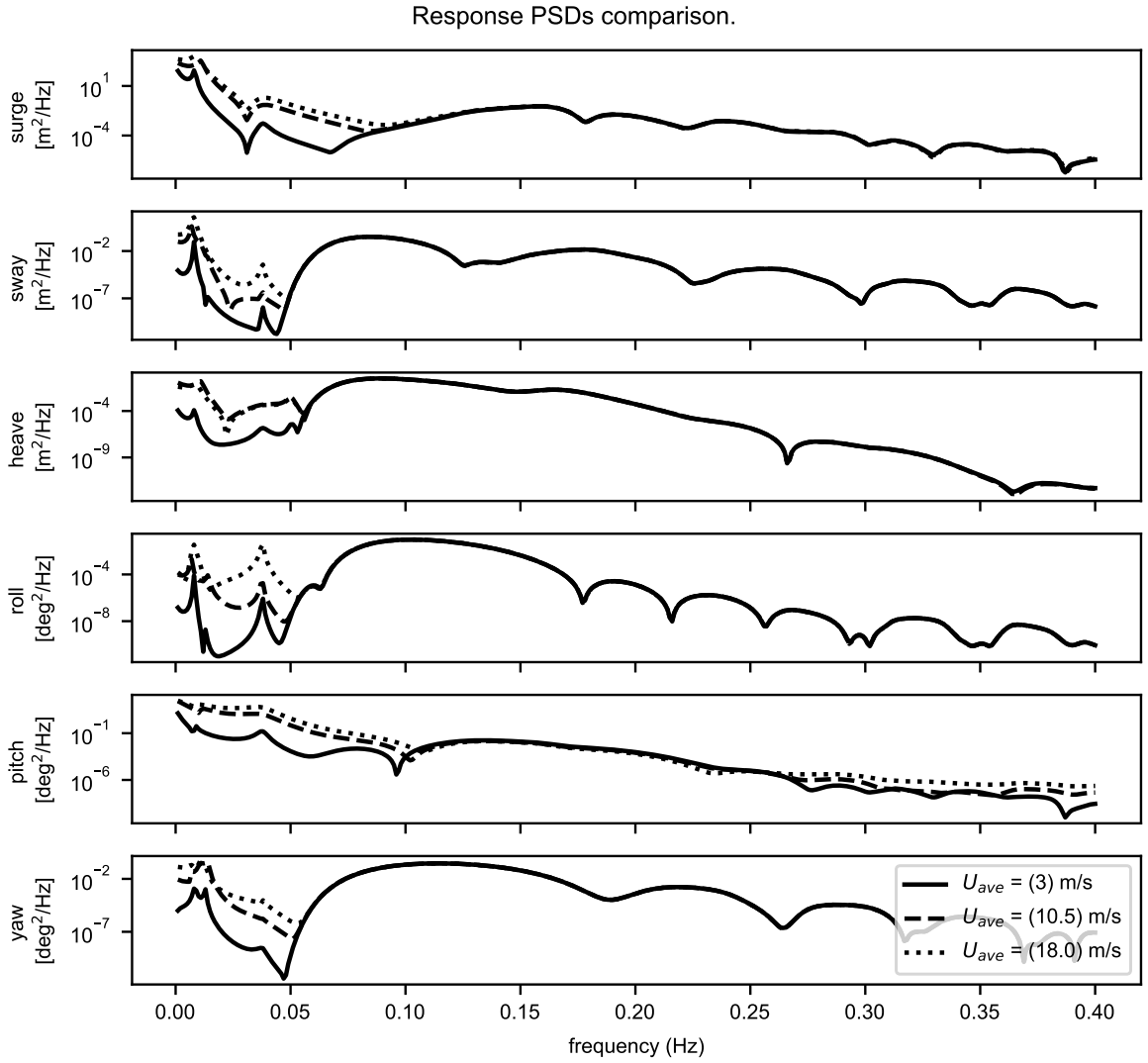

Figure 7.4: Response PSDs for an average wind speed of 3, 10.5, and 18 m/s.

It is found that the thrust decreases at higher wind speeds. However, the dynamic response perpendicular to the rotor plane (pitch and surge) increases. The effect of this on the tower base bending moments is shown in Figure 7.5. This figure shows the contribution of the difference in aerodynamic damping on the tower base bending moments.

The average wind speed of 3 m/s showed the lowest damping, resulting in a noticeable response around the pitch natural frequency (approximately 0.038 Hz). At an average wind speed of 10.5 m/s and 18 m/s, the aerodynamic damping is greater, and therefore the response around the pitch natural frequency is more clearly damped.

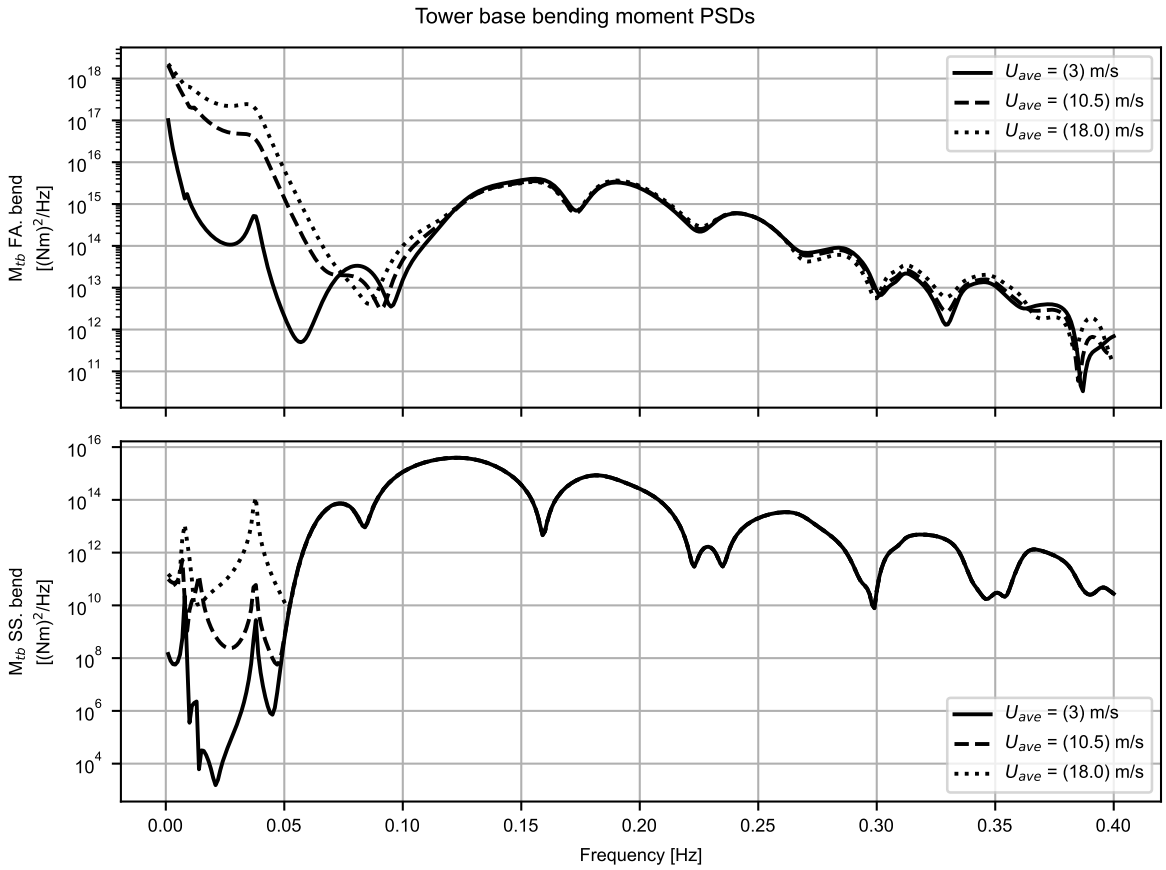

Figure 7.5: Tower base bending moment PSDs for an average wind speed of 3, 10.5, and 18 m/s.

The effect of this observation on the estimation of the equivalent stress at tower base is shown in Figure 7.6. In this figure it can be seen that the maximum equivalent stress does not increase as much as the dynamic response (Figure 7.3). This is contributed to the increased aerodynamic damping and to the lower mean pitch response above the rated wind speed, which reduces the mean stress effect at the tower base. Therefore, the increase in equivalent stress is contributed to the decrease in the mooring stiffness above rated wind speeds and the reduced aerodynamic damping above rated wind speeds.

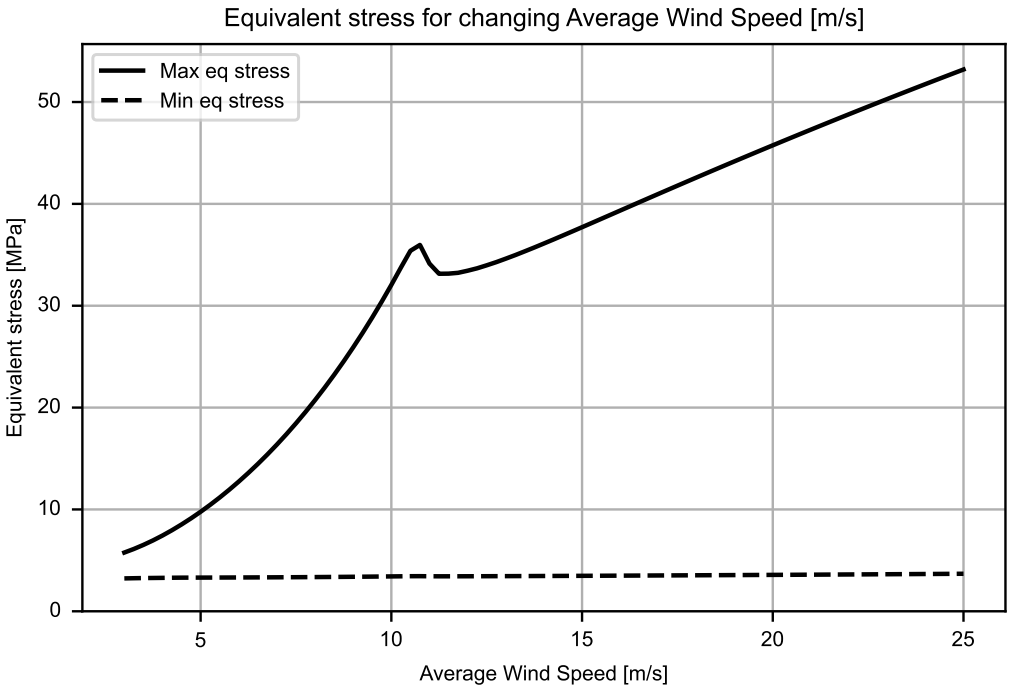

Figure 7.6: Maximum and minimum equivalent stress estimates at the tower base for the operational wind speed range.

For the system under consideration, it is concluded that the wind direction is decisive for the maximum equivalent stress. The response due to the misaligned swell is small compared to the significant excitation around rated wind speed. The effect of aerodynamic damping is observed around the pitch/roll natural frequency.

To summarise, for a range of wind speeds the effect of aerodynamic damping and change in aerodynamic thrust is investigated. It is found that the maximum equivalent stress increases for increasing wind speeds. The reduced thrust above rated wind speed reduces the mooring stiffness, increasing the dynamic response for all degrees of freedom. However, the reduced thrust also reduces the mean stress effect for pitch/roll. The change in aerodynamic damping was observed for a range of wind speeds. The contribution of aerodynamic damping to the tower base bending moments is mostly observed around the pitch and roll natural frequencies.

7.2. Aerodynamic damping: Wind heading

For a range of wind directions, the response characteristics are shown in Figure 6.1. In this figure it can be seen that as the wind misalignment with respect to the floater orientation system increases, the pitch response decreases but the roll response increases. To evaluate the influence of aerodynamic damping at different wind directions on the response, the maximum and minimum equivalent stress at the tower base is plotted in Figure 7.7 for a range of wind headings.

From this figure, it can be seen that the maximum equivalent stress at the tower base is greatest when the wind heading angle coincides with the wind sea (0 degrees) and the swell sea (90 degrees).

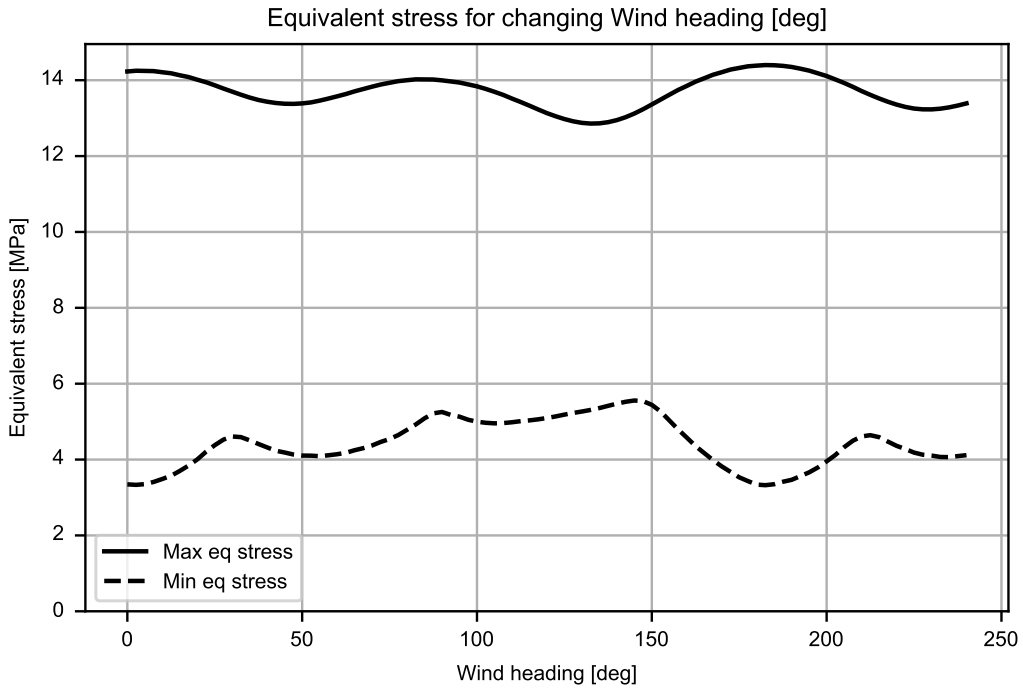

Figure 7.7: Equivalent stress at the tower base for a wind direction with respect to the floater reference frame (0 degrees to 240 degrees).

To identify how this change in wind heading influences the response, the tower base bending moment PSDs are plotted for 0 degree, 45 degree, and 90 degree wind heading (Figure 7.8). Below 0.10 Hz, a difference in response characteristics can be observed, which is due to the directionality of the response characteristics of the structure. Above 0.10 Hz the response appears to be comparable, but at 45 degrees wind direction a slight reduction in wave response is observed compared to 0 degrees wind direction. This is contributed to the rotation in which the aerodynamic damping affects the response. For a non-zero degrees wind direction it affects the response due to the swell component.

At a wind heading of 0 degrees (base case), the damping around the roll natural frequency is dominated by the hydrodynamic damping effects. As the wind heading changes, aerodynamic damping starts affecting the roll natural frequency (around 0.38 Hz (Section 8.3.1)).

At this 45 degrees wind heading, the reduced aerodynamic damping results in an increased pitch response around the pitch natural frequency, indicated by the dotted line in the fore-aft bending moment PSD. At this angle, the aerodynamic damping affects the wind sea (now misaligned with 45 degrees) and the swell sea (now misaligned with 45 degrees), resulting in a reduced response.

With a wind heading of 90 degrees there is a greater response around the pitch natural frequency as there is no aerodynamic damping in pitch direction anymore. However, it is excited due to pitch couplings in the mooring system (Equation 5.1). As the aerodynamic damping now affects only in the swell sea direction, the maximum equivalent stress is reduced.

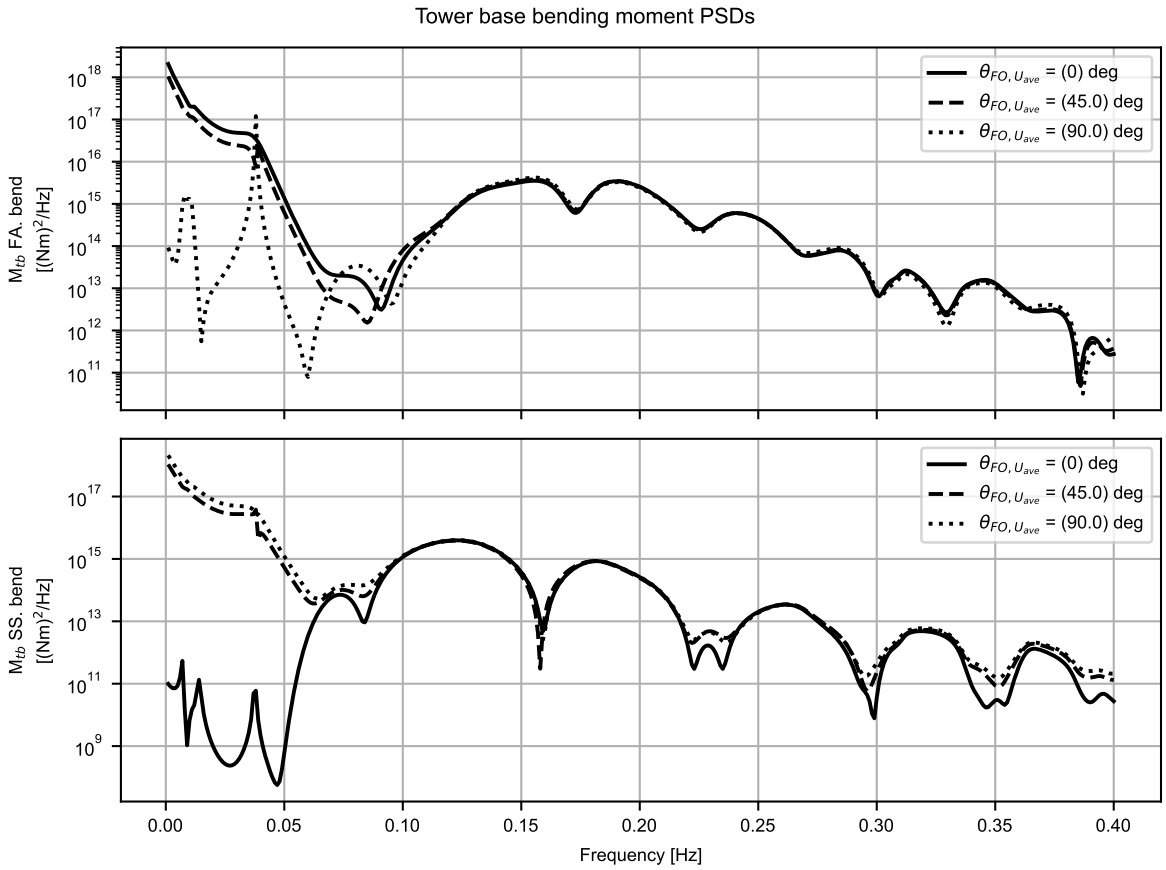

Figure 7.8: Tower base bending moment PSD's for different wind headings.

7.3. Aerodynamic damping: Swell misalignment

From Figure 6.7 it can be seen that as the swell misalignment increases with respect to the floater orientation, the SD of the roll response increases up to a swell misalignment of 90 degrees. For a swell misalignment angle from 90 to 180 degrees, the roll response decreases. Figure 7.9 shows the equivalent stress at the tower base (Section 4.2.1). From this figure it can be seen that the maximum equivalent stress decreases with increasing wave misalignment up to 120 degrees.

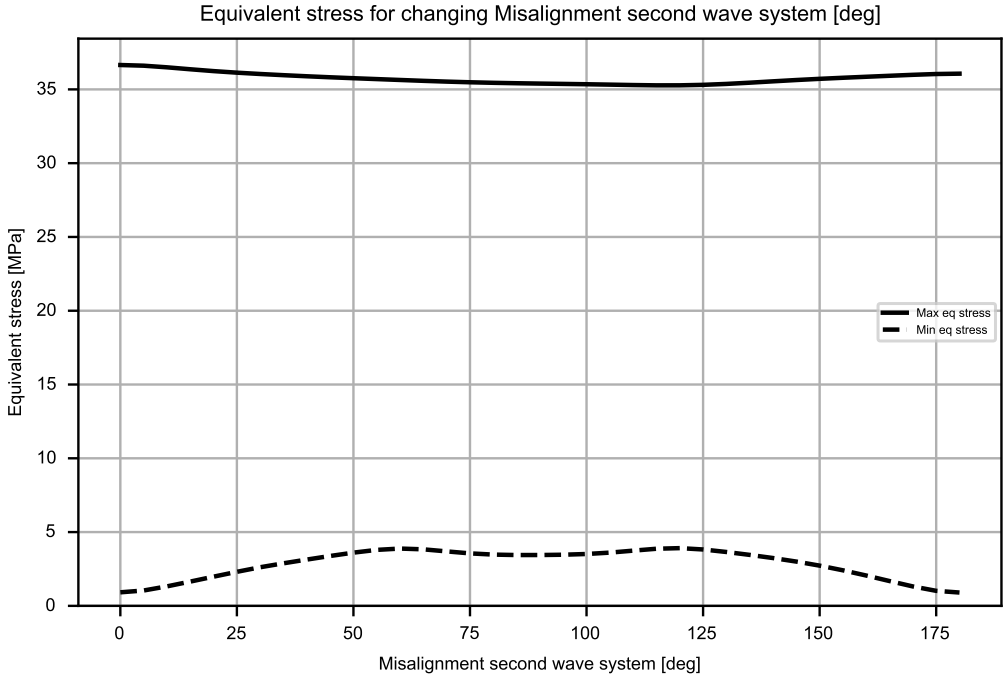

Figure 7.9: Equivalent bending stress at the tower base for different swell misalignment angles.

This decrease in equivalent stress is the result of the decrease in pitch excitation for this wave peak period. From Appendix B, Figure B.8 and Figure B.9, it can be seen that the pitch excitation decreases but the roll excitation does not increase proportionally.

For 0, 30, 60, and 90 degrees alignment angles, the tower base bending moment spectra are plotted in Figure 7.10. In this figure it can be seen that in the range of wind frequency (below 0.05 Hz) the contribution of wind excitation is dominant. In the wave frequency range, the fore-aft bending moment decreases with increasing swell misalignment.

For the side-to-side bending moment, there is a clear increase in response in the range of wave frequency. Also the roll natural frequency (0.38 Hz (Section 8.3.1)) is excited more noticeable around the wind frequency range. A significant increase in side-to-side response from 30 to 60 degrees misalignment at low frequencies is visible. This is a contribution of slightly increased pitch response, as the viscous drag damping in pitch direction decreases for increasing swell misalignment angles.

The contribution of aerodynamic damping to the response for increasing swell misalignment is small, as the damping effects mainly contribute to the response around the natural frequency, which is below the wave frequency range. Second-order wave excitation is not considered in the method but it is expected to make a noticeable contribution to the pitch/roll natural frequency outside the wave frequency range.

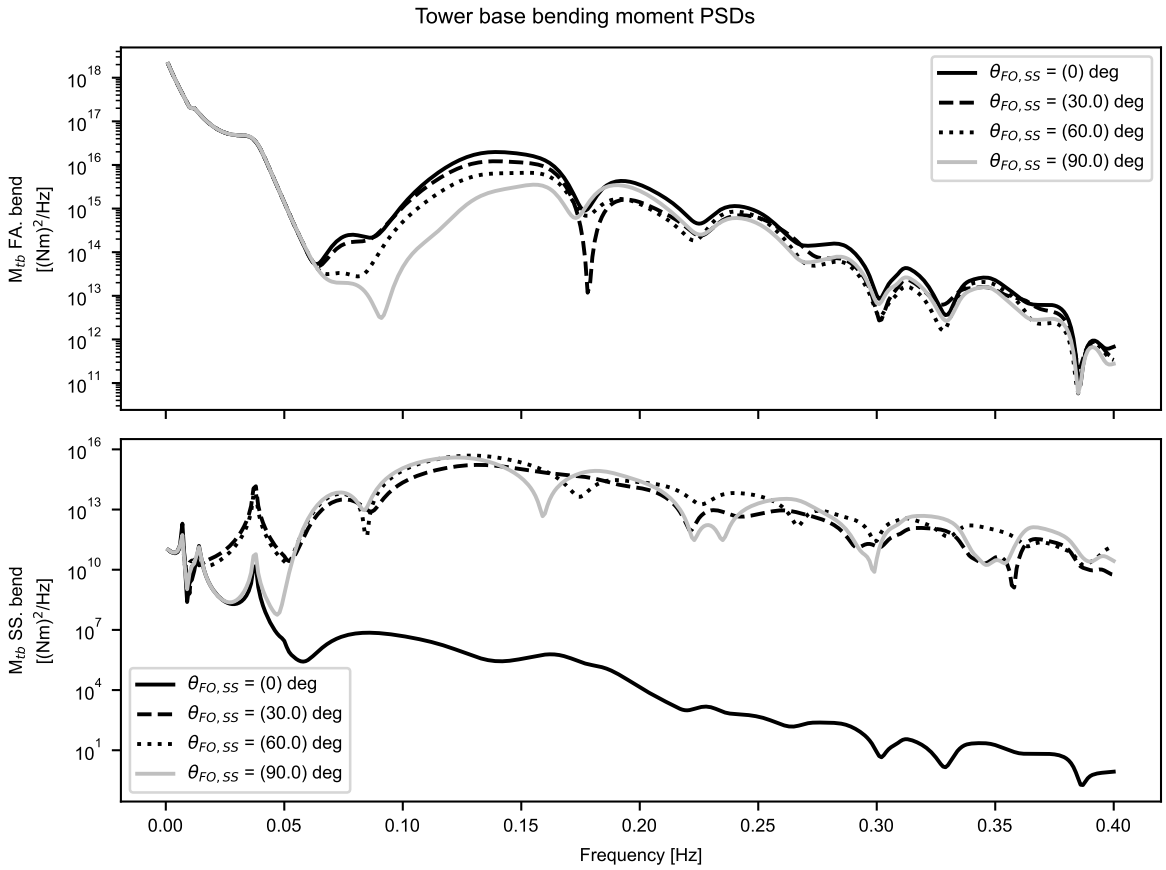

Figure 7.10: Tower base bending moment PSD's for different swell misalignment angles.

However, the base case considers excitation around rated wind speed and it is found to be the main contributor to equivalent stress (Section 7.1). Therefore, it is useful to evaluate the effect of a higher significant wave height and a lower wind speed. Since the wave excitation is a transfer function with respect to the crest height (Appendix B), a larger significant wave height leads to a further decrease in this maximum equivalent stress. This is seen in Figure 7.11, which shows the equivalent stress levels for a significant wave height at sea state of 4 metres.

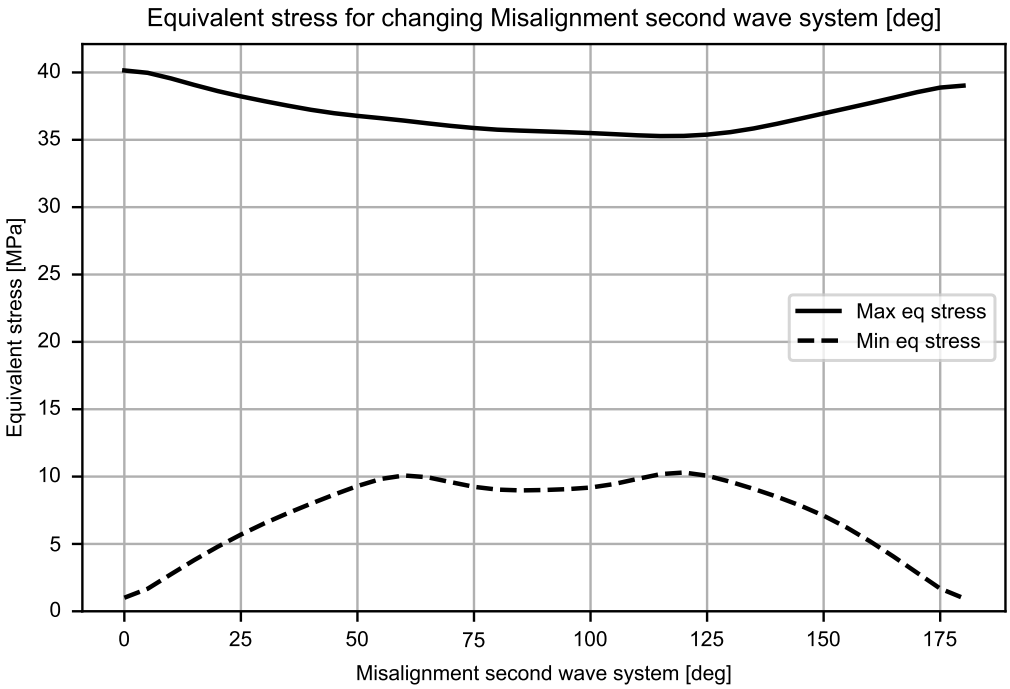

Figure 7.11: Equivalent bending stress at the tower base for different wave misalignment angles (Swell $H_s = 4[m]$).

Finally, reducing the mean wind speed does not affect these results for the same reason, which is shown in Figure 7.12. A lower equivalent stress is also observed with a mean wind speed of 5 m/s (instead of 10.5).

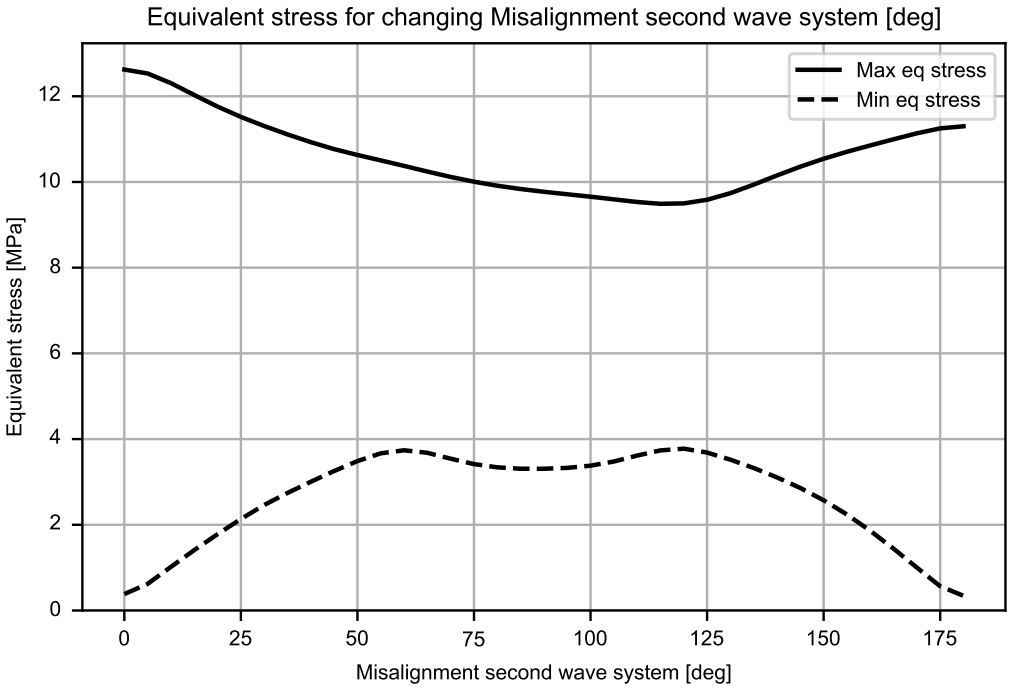

Figure 7.12: Equivalent bending stress at the tower base for different wave misalignment angles ($U_{ave} = 5[m/s]$).

In summary, the minimum equivalent stress is increased slightly for increasing swell misalignment. Around rated wind speed, the maximum equivalent stress is dominated by wind excitation as it excites the pitch/roll natural frequency and introduces the largest mean stress effect. The investigation of the effect of aerodynamic damping is limited by this frequency-domain method. Since no second-order effects are included, the excitation of natural frequencies outside the wave frequency range are not considered.

7.4. Aerodynamic damping: Floater orientation

In Section 6.4, Figure 6.12, the response characteristics for a range of floater orientations is presented. This figure shows that for increasing floater orientation (or rotating the wind and wave systems), the pitch response decreases and the roll response increases. The effect of this changing floater orientation is presented in Figure 7.13. In this figure it can be seen that a change in floater orientation affects both the maximum and minimum equivalent stress. With respect to the original floater orientation (0 degrees rotation), the equivalent stress decreases with increasing angles of rotation up to about 45 degrees. The maximum equivalent stress increases at a rotation of 90 degrees.

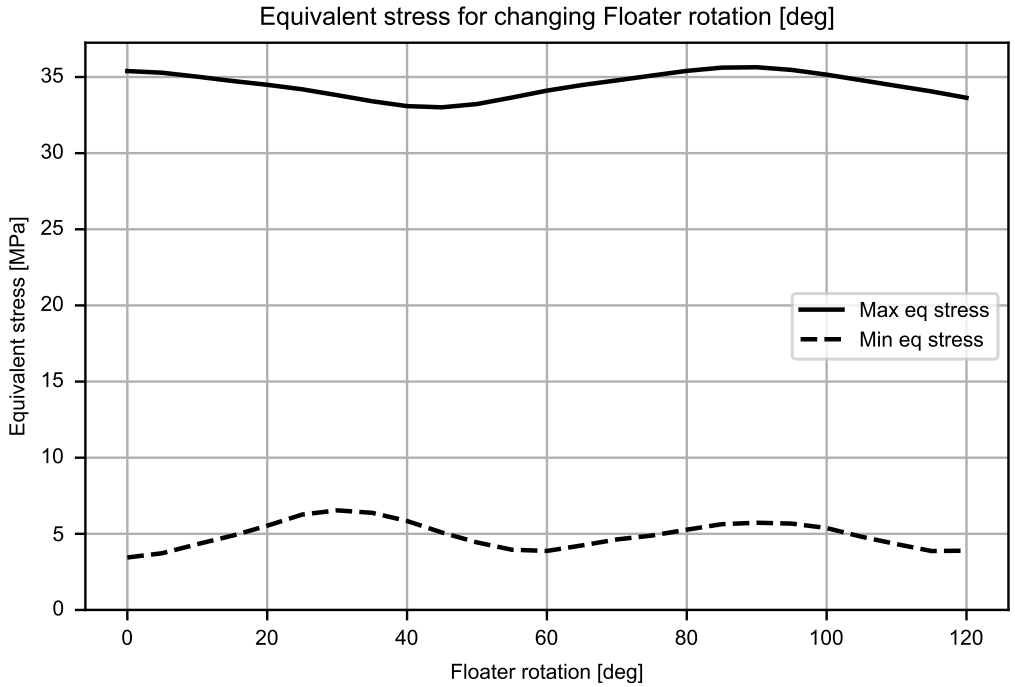

Figure 7.13: Equivalent bending stress at the tower base for different floater orientations.

For 0, 45, and 90 degree floater rotation, the tower base bending spectra are plotted in Figure 7.14. In this figure, it can be seen that at a rotation of 45 degrees (dashed line), both the fore- aft and side-to-side bending moments show an increased damping effect around the pitch/roll natural frequency. This is due to aerodynamic damping, as it now affects the roll and pitch response. The 90 degrees rotation resulted in an increase in the maximum equivalent stress, and using Figure 7.14 it can be concluded that this is most likely due to the increased low- frequency response of the fore-aft bending moment. This is due to the increased roll-yaw and yaw-pitch coupling effects for this 90 degrees rotation of the floater and the resulting lack of aerodynamic damping in the pitch direction. This effect is also observed in the PSDs in Section 7.2.

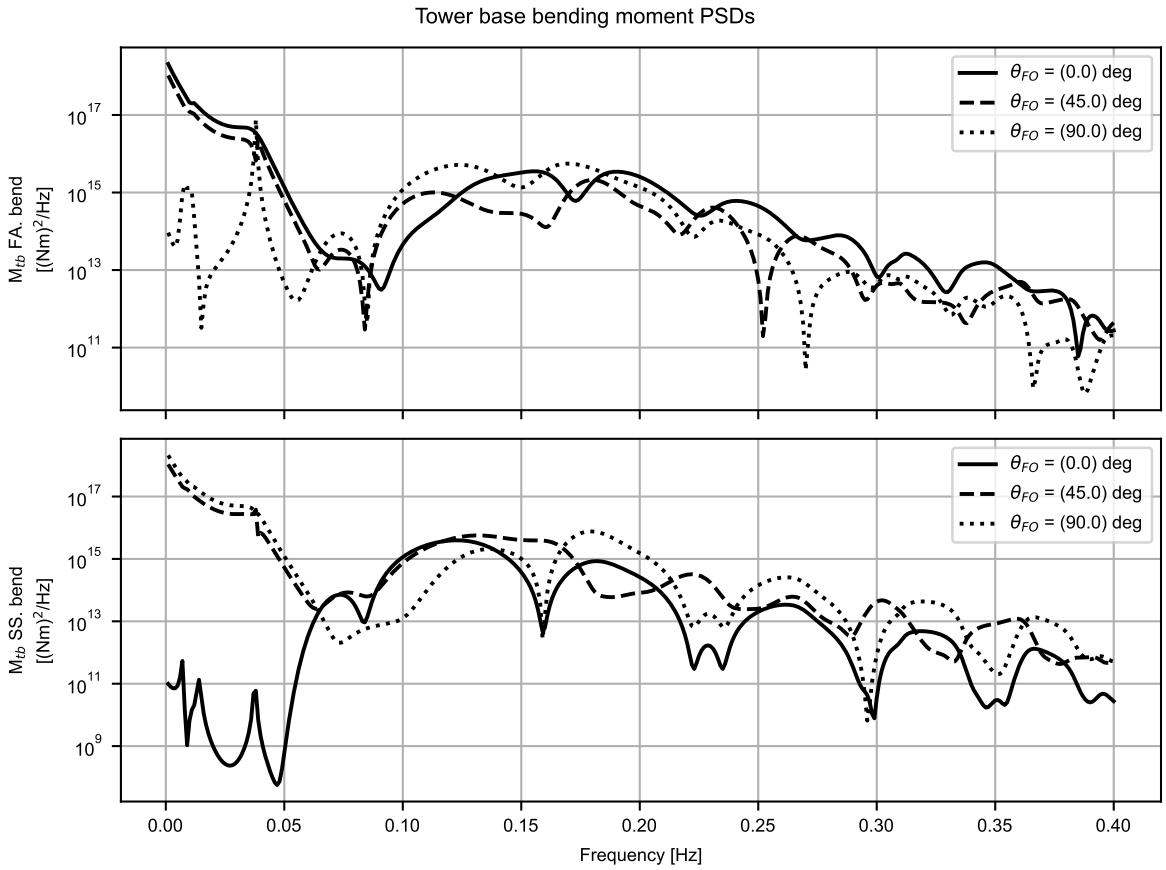

Figure 7.14: Tower base bending moment PSD's for floater rotations of 0, 45, and 90 degree with respect to the base case.

7.5. Aerodynamic damping: Conclusion

In this chapter, the contribution of aerodynamic damping to the response of a semi-submersible FOWT is evaluated.

In Section 7.1 the influence of wind speed on aerodynamic damping and thrust is analysed. Up to the rated wind speed, the damping increases. Above the rated wind speed, the damping decreases slightly. It is found that this change in damping mainly influences the response around the pitch/roll natural frequency.

Section 7.2 presents how a change in wind direction, and hence the change in direction for aerodynamic damping and excitation, affects the equivalent stress. It is found that a change in wind direction can reduce the maximum equivalent stress as aerodynamic damping begins to affect the out-of-plane response. However, it is also found that the wind excitation increases the response at the natural frequencies of the degree of freedom perpendicular to the wind direction due to coupling effects in the system.

The contribution of aerodynamic damping to the response in the wave frequency range is investigated for a range of swell misalignments (Section 7.3). It is found that the change in wave misalignment increases the equivalent stress in the rotor plane direction more than the decrease in maximum equivalent stress. However, this observation is limited by the simplifications of the method, as no second order wave force is considered.

Finally, the effect of floater rotation on aerodynamic damping is evaluated in Section 7.4. It is found that the maximum equivalent stress is mainly due to a reduction of the response in the wave frequency range. However, it can also increase the minimum equivalent stress because the response is increased in the direction of the rotor plane due to coupling effects. This direction then has no aerodynamic damping.

8

Frequency-Domain Method and Time-Domain Method Comparison

This chapter presents the comparison of the method against time-domain simulations performed in BHawC-Orcaflex by Siemens Gamesa Renewable Energy. The comparison of the method is split up in three parts, namely; a comparison of the system properties, comparing a set of four load cases and comparing the equivalent stress around the tower for the full hindcast dataset. Using the insights and conclusions from Section 6.5 and Section 7.5, four comparison cases have been selected. This chapter answers the research question related to the effectiveness of the method to estimate the tower base bending response:

> "How effective is a frequency-domain method compared to a time-domain method at estimating the equivalent bending moment at the tower base for misaligned wind, windsea waves, and swells?"

8.1. Comparison conditions and known limitations

This section lists some conditions and limitation of the comparison due to assumptions and modelling differences. Their contribution to the differences will be evaluated for the four cases.

First off, the frequency-domain method assumes no current is present, even though they are included in the time-domain simulations of Siemens Gamesa. This assumption will result in difference in mean operating conditions, especially for the surge and sway direction. Due to couplings in the stiffness terms (mostly due to the mooring system), this can also effect mean offsets of roll, pitch and yaw.

Secondly, the frequency-domain method uses a hybrid analytical and numerical approach to estimate the hydrodynamic added mass and damping. The centre and outer columns of the floaters are modelled in the potential flow software and therefore include coupling effects and hydrodynamic damping due to radiation. The hydrodynamic added mass and excitation of the connecting pontoons is estimated using the Morison equation. Therefore, there is no hydrodynamic coupling or radiation damping for these members in the equations of motion of the system.

Thirdly, no controller action is assumed in the frequency domain method (Section 4.1.1). This will mostly affect differences at low frequencies as no aerodynamic added mass is assumed and the damping is overestimated [47].

Furthermore, the tower used in the industry project is relatively soft compared to towers used in the literature [7]. However, the time-domain simulations performed by SGRE are carried out with a flexible tower and blades, whereas the frequency-domain method assumes only rigid body modes for the floater. Therefore, the response around the first bending mode of the tower is not estimated in the frequency-domain method.

Lastly, there is no second-order wave force in the method. Degrees of freedom with a natural frequency below the wave frequency range can be significantly excited by the second-order wave force. As presented in the Section 8.3.2, all natural frequencies except one (heave) are relatively low (outside the range of wave excitation) and can therefore be excited by a second-order wave force.

8.2. Comparison case selection

Four cases are selected from the DLC 1.2 load case set performed for the industry project. These cases are selected using the observations of Chapter 6 and Chapter 7. The case set consist of two cases below and two cases above the rated wind speed with wind-wave misalignment angles varying from small (< 14 degrees) to large (up to $\approx$ 107 degrees). An overview of the load cases is presented in Table 8.1. The wind and wave directions in this table are with respect to the local floater reference frame, where ”counterclockwise” is a positive angle and is defined as ”towards”, which is the same definition as in Section 5.2. An illustration of the wind and wave headings with respect to the floater orientation is given in Figure 8.1.

Table 8.1: Comparison of platform property estimates between TD and FD estimates.

Property	**Case 1**	**Case 2**	**Case 3**	**Case 4**
Wind excitation:				
U_{ave} [m/s]	4.00	9.00	15.00	25.00
Turbulence Intensity [-]	0.17	0.10	0.09	0.09
$\theta_{FO,U_{ave}}$ [deg]	262.50	292.50	292.50	352.50
Yaw error [deg]	0.00	0.00	0.00	5.60
Wave system 1:				
T_p system 1 [s]	6.67	5.98	6.14	9.18
H_s system 1 [m]	0.94	1.02	1.54	3.40
γ system 1 [-]	1.46	1.42	1.44	1.99
$\theta_{FO,WS}$ [deg]	338.21	327.29	313.37	349.84
Wave system 2:				
T_p system 2 [s]	10.15	9.86	10.26	9.18
H_s system 2 [m]	0.74	0.83	0.65	2.66
γ system 2 [-]	2.05	1.70	2.03	1.87
$\theta_{FO,SS}$ [deg]	9.24	12.78	10.74	339.38

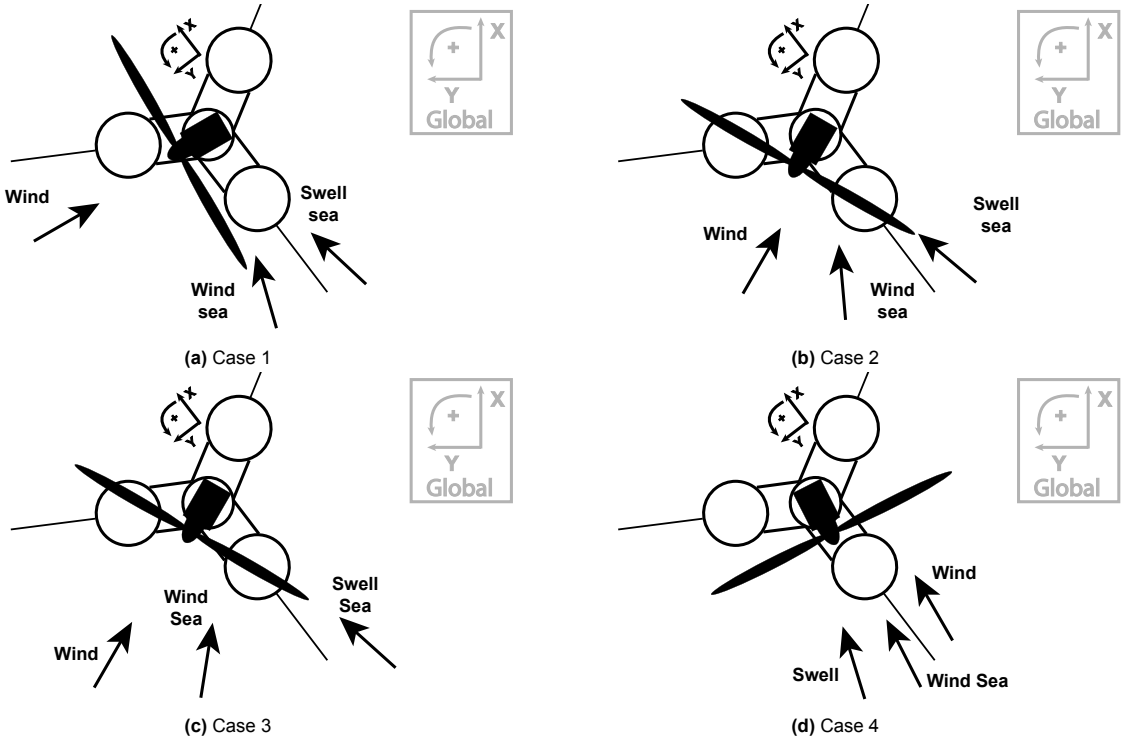

Figure 8.1: Relative wind and wave directions with respect to floater orientation for each case.

From these figures it can be seen that in case 1 the wind and waves have the greatest misalignment, with the wind coming from a relative angle of -90 degrees with respect to the wave components. Case 2 shows a smaller misalignment angle between the wind and waves. Case 3 shows a relatively similar wind and wave misalignment angle to Case 2, but has a higher wind speed. Finally, in case 4, the wind and the waves are mostly aligned. The wind speed is near the cut-off speed and the significant wave height is the highest of all the cases.

8.3. Comparison of system properties and wind/wave spectra

The comparison of system properties is divided into two parts. The first part includes a comparison of the estimated system properties of the UMaine VolturnUS-S (steel version) reference floater [7] in combination with the IEA 15 MW offshore wind turbine [45]. The second part contains a comparison of the system characteristics of the SGRE configuration.

As shown in Section 4.1, the mass and inertia in RAFT are estimated based on the dimensions and characteristics of the floater, such as the diameter of the columns, the column spacing and the ballast settings. Instead of directly specifying the terms for mass, inertia and hydrostatic stiffness, this method allows for parametric studies of these parameters.

8.3.1. System properties: open-source configuration

Several system characteristics of the steel floater are presented by Allen *et al.* [7]. These include mass/inertia, hydrostatic stiffness estimates and natural frequencies of the rigid body. A comparison of the mass and inertia estimates is presented in Table 8.2. This table shows that based on the given geometry, a reasonable estimate is made for the mass, inertia and hydrostatic stiffness terms resulting from the floater. A comparable estimate for the heave hydrostatic stiffness is expected, since it is equal to the total waterplane area of the submerged floater [48]. Due to the symmetrical nature of the tri-floater, the inertia terms of roll and pitch are the same. The slight differences in the hydrostatic stiffness of roll and pitch are because of slight differences in the anchor positions of the implemented mooring design.

Table 8.2: Comparison of platform property estimates between TD and FD estimates.

Property	Technical Report	Estimate RAFT/FD	Difference FD to TD
Platform mass [mt]	17,854	17,671	-0.9 %
Platform roll inertia [kgm2]	1.251E+10	1.20E+10	-4.2 %
Platform pitch inertia [kgm2]	1.251E+10	1.20E+10	-4.2 %
Platform yaw inertia [kgm2]	2.367E+10	2.24E+10	-5.6 %
Heave hydrostatic stiffness terms [N/m]	4.47E+06	4.49E+06	+0.5 %
Roll hydrostatic stiffness terms [Nm]	2.19E+09	2.35E+09	+7.3 %
Pitch hydrostatic stiffness terms [Nm]	2.19E+09	2.35E+09	+7.3 %

Table 8.3 presents the comparison of the added mass and added inertia terms between the technical report (estimated with WAMIT) and the Morison equation estimate of the frequency-domain method. Reasonable agreement is found these estimates with the main differences present in surge, sway, and yaw.

Table 8.3: Comparison of platform property estimates between TD and FD estimates.

Infinite Frequency added mass/inertia	Technnical Report (WAMIT)	Estimate RAFT/FD	Difference FD to TD
Surge [kg]	9.640E+06	1.02E+07	+6.2 %
Sway [kg]	9.640E+06	1.02E+07	+6.2 %
Heave [kg]	2.480E+07	2.49E+07	+0.3 %
Roll [kgm]	1.160E+10	1.19E+10	+3.0 %
Pitch [kgm]	1.160E+10	1.19E+10	+3.0 %
Yaw [kgm]	2.010E+10	2.19E+10	+8.9 %

The rigid-body natural frequencies obtained using a free decay simulation and the estimates using the RAFT method are presented in Table 8.4. Since the TD estimate is obtained from a numerical free-decay test, it is actually a comparison between a damped natural frequency (TD) and a natural frequency in free vibration (FD). Since the damping is relatively small (underdamped system), it is to be expected that the magnitudes of the natural frequencies are comparable. In general, it can be stated that there is a reasonable agreement between the heave, roll, and pitch natural frequencies. The roll and pitch show a reasonable estimate of the natural frequency. The combined platform inertia and the hydrodynamic added inertia for these degrees of freedom are comparable. However, the hydrostatic stiffness term dominates the stiffness in these degrees of freedom and already shows a difference of 7.3 %.

This agreement for the heave DOF is mainly the result of the comparable mass, the estimate of the heave added mass and the hydrodynamic stiffness terms of heave. All observed differences are due to the different estimation of the mooring stiffness. The natural frequencies of surge and sway are difficult to compare due to the limited decimal numbers in the technical report; all differences are mainly due to the estimation of the mooring system. For the yaw DOF, there is no hydrostatic stiffness and negligible structural stiffness due to the symmetry of the structure. Therefore, the natural frequency of the yaw DOF is dominated by the mooring stiffness and the (added) yaw inertia. The limited accuracy of the technical report makes the comparison difficult, but the main differences are due to the estimation of the mooring system, whose quasi-static stiffness terms are not available.

Table 8.4: Comparison or Rigid-Body Natural Frequencies between TD and FD estimates.

Rigid-Body mode	Estimate free-decay (OpenFAST/TD) [Hz]	Estimate (RAFT/FD) [Hz]	Difference FD to TD
Surge	0.007	0.0080	+15.7 %
Sway	0.007	0.0080	+15.7 %
Heave	0.049	0.0508	+3.67 %
Roll	0.036	0.0380	+5.56 %
Pitch	0.036	0.0381	+5.83 %
Yaw	0.011	0.0125	+13.64 %

8.3.2. System properties: SGRE configuration

This section compares system property estimates for the VoluturnUS (concrete) and SGRE turbine and tower configurations. Using the (confidential) information on the RNA, tower, floater, and mooring system provided by SGRE and the University of Maine, the configuration is recreated using the frequency-domain method. Good agreement of the properties is observed for the estimation by the preprocessor of the frequency-domain method.

Table 8.5: Difference of platform property estimates SGRE (TD) and RAFT (FD) estimates.

Property	Difference FD to TD
Platform mass [mt]	+0.1 %
Platform COG [m]	-0.5 %
Platform roll & pitch inertia [1000·mt·m]	+0.2 %
Platform yaw inertia [1000·mt·m]	-4.8 %

Table 8.6: Difference in hydrostatic property estimates SGRE (TD) and RAFT (FD) estimates.

Property	Difference FD to TD
Submerged Volume [m^3]	+0.2 %
Platform COB [m]	+0.2 %
Heave hydrostatic stiffness [mt]	+0.9 %
Roll/Pitch hydrostatic stiffness [1000·mt·m]	+2.9 %

Table 8.7 gives an overview of the differences in natural frequency estimation between the two methods. As with the combination of open-source turbine and floater, the heave natural frequency is estimated quite well. The natural frequencies of roll and pitch are also estimated with a deviation of 5.4 and 5.1 %, respectively. However, the underestimation of the natural frequencies of surge, sway and yaw is very noticeable. These underestimations are the result of an underestimation of the mooring stiffness. Due to a limitation of the quasi-static mooring estimation in the frequency-domain method, it was not possible to model a mooring system with more than 1 chain type. The influence of the mooring system and the total stiffness on the heave, roll and pitch motion is limited (Section 5.2.3).

Another factor contributing to the differences in mooring stiffness is the non-linearity of the mooring stiffness. The frequency-domain method estimates the mooring stiffness from the stiffness at the undisplaced position, while the time-domain estimate is obtained from a free-decay simulation that includes an mooring stiffness dependent on the displaced system at each time step. Compared to the

200-metre water depth considered in the open-source configuration, this effect is more noticeable at shallower water depths (100 metres for the SGRE configuration), as illustrated by Xu *et al.* [58].

Table 8.7: Difference in rigid-body natural frequency estimates SGRE (TD/free-decay) and RAFT (FD) estimates.

Rigid-Body mode	Estimate free-decay (TD) [Hz]	Estimate (RAFT/FD) [Hz]	Difference FD to TD
Surge	0.0118	0.0061	-48.3 %
Sway	0.0073	0.0061	-16.4 %
Heave	0.0532	0.0527	-0.9 %
Roll	0.0377	0.0357	-5.4 %
Pitch	0.0377	0.0358	-5.1 %
Yaw	0.0117	0.0075	-35.8 %

8.3.3. Wind and wave spectra

This section provides an overview of the differences between wind turbulence and wave height spectra for four different average wind speeds. Wind excitation and wave height are compared to better understand the differences in response. In the time-domain simulations, the wind speed time traces are generated as a stochastic process around a mean value using a turbulence seed. The time trace of the wave elevation is generated from a JONSWAP spectrum. An example of these time traces is plotted in Figure 8.2.

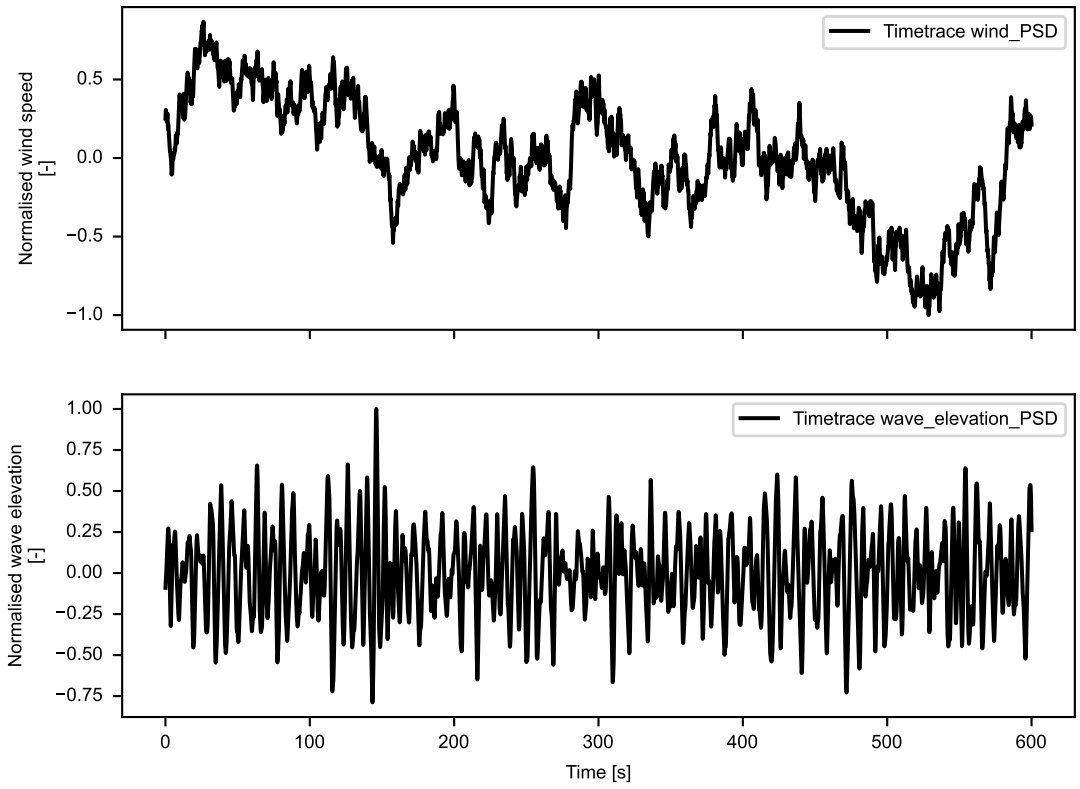

Figure 8.2: An example of a time trace of relative wind speed and relative wave elevation.

A PSD is obtained from the Fourier transform of the wind and wave speed time traces using an FFT algorithm. This is compared with the PSDs of the wind speed and the wave elevation PSD's from the frequency-domain method. In the case of a relatively low wind speed ($U_{ave} = 4\ m/s$), this comparison is presented in Figure 8.3. It can be observed that there is a difference in the wind turbulence spectrum, while the wave spectrum has a comparable magnitude. For the load case with an average wind speed of $25\ m/s$ (Figure 8.4), it can be seen that the difference between the time-domain spectrum and the frequency domain approximation is smaller.

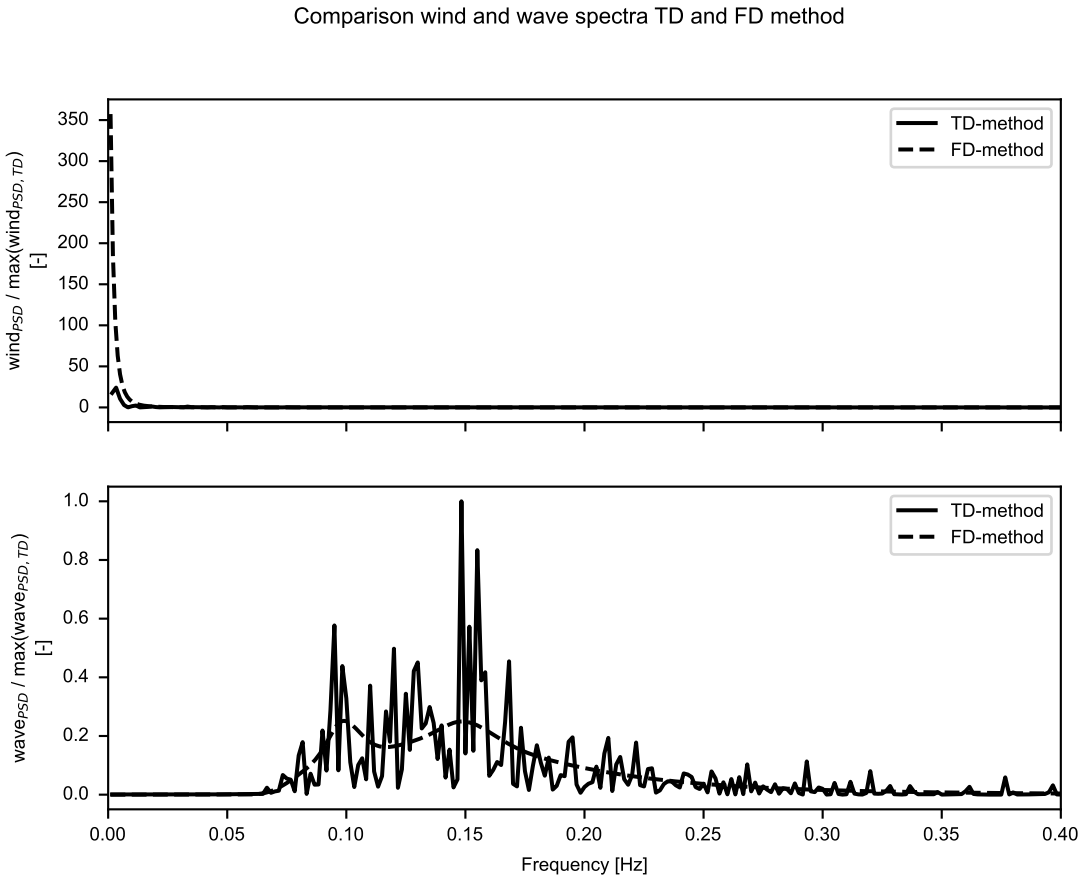

Figure 8.3: Normalised Wind and Wave PSD comparison, comparison case 1.

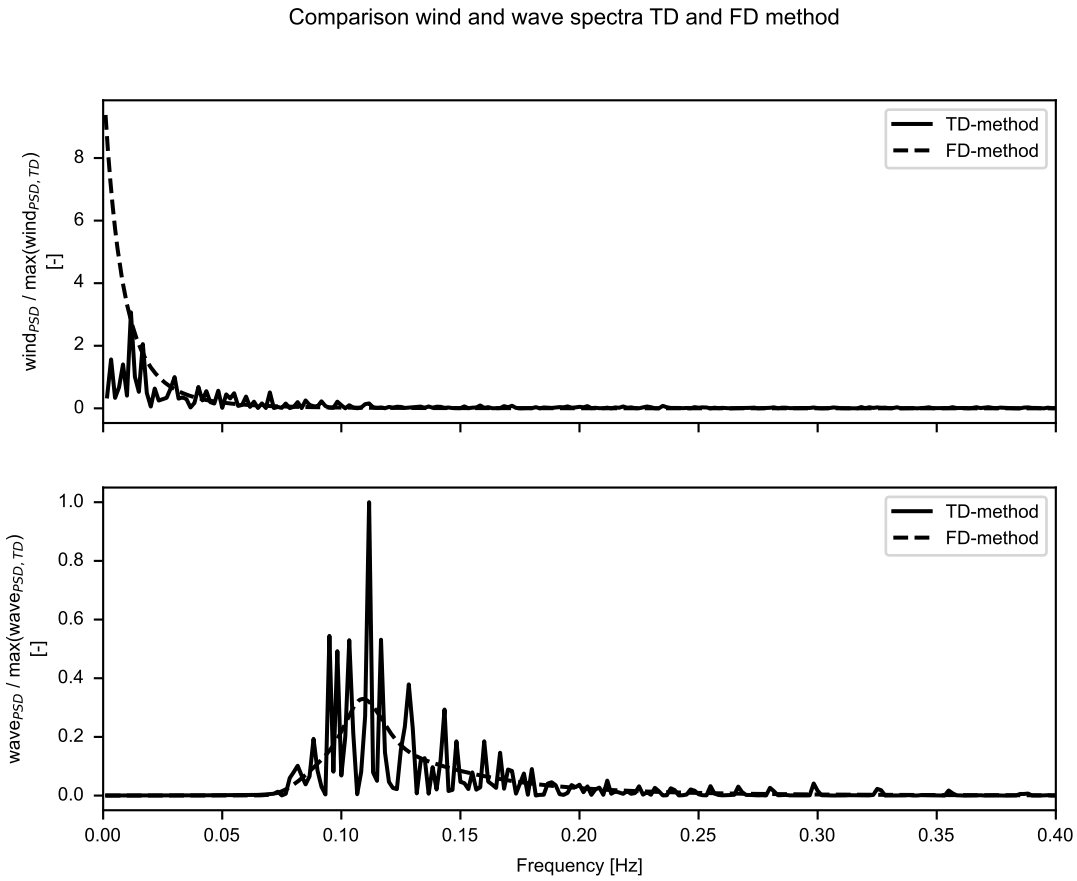

Figure 8.4: Normalised Wind and Wave PSD comparison, comparison case 4.

For the four selected load cases, the standard deviation of the time-domain signal and the frequency domain approximation as well as their difference are presented in Table 8.8. This table shows that the standard deviation for the wind spectra has a difference, but it decreases with increasing wind speed. From the environmental conditions, it appears that the turbulence of the wind decreases with increasing wind speed. In addition, low frequencies may not be accurately captured as the time trace has a finite duration of 600 seconds and therefore only limited cycles may have occurred. It is expected that the difference in wind excitation spectra at low frequencies will affect the response characteristics, especially for the degrees of freedom whose natural frequencies are in the wind frequency range. In order to make a reasonable comparison, the lowest comparison frequency is set to $1/60 \approx 0.01667\ Hz$.

Table 8.8: Comparison of standard deviations of wind and wave spectra for the four load cases.

DOF	SD_{FD}	$SD_{TD,FFT}$	Difference FD to TD
PSD_{wind} Case 1	1.912 [m/s]	0.713 [m/s]	168.20 %
PSD_{waves} Case 1	0.298 [m]	0.309 [m]	-3.76 %
PSD_{wind} Case 2	1.651 [m/s]	0.719 [m/s]	129.77 %
PSD_{waves} Case 2	0.324 [m]	0.307 [m]	5.80 %
PSD_{wind} Case 3	2.197 [m/s]	1.435 [m/s]	53.08 %
PSD_{waves} Case 3	0.412 [m]	0.381 [m]	7.99 %
PSD_{wind} Case 4	3.266 [m/s]	2.287 [m/s]	42.86 %
PSD_{waves} Case 4	1.073 [m]	1.063 [m]	0.93 %

It is concluded that the frequency-domain method overestimates wind spectra. As can be seen in Figure 8.3 and Figure 8.4, this overestimation occurs mainly at very low frequencies. This is a direct consequence of the limited duration (600s) of the time trace. In Figure 8.4 it can be seen that there seems to be a reasonable estimate of the wind spectrum for frequencies above $0.02\ Hz$. For this reason, the comparison of the motion response (Section 8.6) is performed using the shift of the lower frequency limit from 0.001 Hz to about 0.01667 Hz. This is the lower limit when calculating the standard deviation values from the PSD and the Fourier transform of the time trace of the motion response. For this lower limit, the updated standard deviations of the wind and wave spectra are presented in Table 8.9. This table also shows small differences in the relative difference for the wave PSD, as this frequency range has also been slightly changed. The updated PSDs can be found in Appendix A, Figure A.1 to Figure A.4. In general, more comparable standard deviations are observed for wind, but a difference of about 20 % is still present for the two cases with the lowest wind speed.

Table 8.9: Comparison of standard deviations of wind and wave spectra for the four load cases.

DOF	SD_{FD}	$SD_{TD,FFT}$	Difference FD to TD
PSD_{wind} Case 1	0.237 [m/s]	0.297 [m/s]	-20.07 %
PSD_{waves} Case 1	0.298 [m]	0.309 [m]	-3.75 %
PSD_{wind} Case 2	0.436 [m/s]	0.598 [m/s]	-27.02 %
PSD_{waves} Case 2	0.324 [m]	0.307 [m]	5.80 %
PSD_{wind} Case 3	0.861 [m/s]	0.885 [m/s]	-2.64 %
PSD_{waves} Case 3	0.412 [m]	0.381 [m]	8.00 %
PSD_{wind} Case 4	1.740 [m/s]	1.905 [m/s]	-8.68 %
PSD_{waves} Case 4	1.073 [m]	1.063 [m]	0.96 %

The difference in wind excitation spectra and its contribution to the response is evaluated in Section 8.6. Consequently, it is difficult to compare the dynamic motion characteristics of surge, sway, and yaw as their natural frequencies are estimated below this frequency. This is justified for this study by the fact that the main interest is in the roll and pitch motions, as the responses in these degrees of freedom contribute most to the tower base bending moment estimate.

8.4. Floater response comparison: wind only

This section gives an overview of the floater's response when excited only by wind. Since the simulation of the load case in the time domain includes second-order effects and current, it is inherently difficult to compare this with the frequency-domain method, where only the mean wind speed results in a mean response. Since there is still a difference in the wind speed spectra, the focus here is on the mean response of the floater to investigate any differences in estimates of mooring, structural and hydrodynamic stiffness.

As mentioned in Section 8.1 and observed in Section 8.3.2, there are inherent differences between the two methods and system properties. For surge, sway and yaw, this is primarily the stiffness of the moorings. In each of the respective cases, this contributes to a difference between the mean response of the structure in that specific DOF. Figure 8.1 gives an overview of the relative direction of wind excitation. Case 1 is mainly excited in the negative sway direction, while case 4 is mainly excited in the positive surge direction. Case 2 and case 3 are excited in both positive surge and negative sway direction.

In each of these cases the direction of the mean response is correctly estimated. What is very striking here, however, is the clear underestimation of the sway excitation. Although it shows more agreement at the natural frequency (Section 8.3.2). In contrast, it can be observed that the roll response is overestimated. For mean surge/sway, only the stiffness of the mooring system affects the structure. For roll/pitch, the contributions of hydrostatic stiffness and structural stiffness dominate (p-delta effect). Since reasonable agreement has been found between the mass/inertia and the natural frequency estimate, any differences in the mean roll/pitch response are likely to be the result of differences in the estimate of the mean thrust of the turbine. This overestimation around the cut-in wind speed (case 1) leads to an overestimation of roll (and pitch due to coupling effects). This overestimation is therefore also visible (to a lesser extent) in the mean sway response. This overestimation of sway is amplified by the underestimation of stiffness.

A hand calculation to check the contribution of underestimation of the mooring system in sway direction (case 1) is as follows: As the mooring system is underestimated by 16.4%*, this suggests that for equal (added) mass the mooring stiffness is approximately underestimated by about* 30% *(*$\omega = \sqrt{\frac{K}{M+A}}$*). For an approximately equal and low mean thrust on the rotor and assuming an reasonably sparse and linear mooring system, this suggests an overestimation of 43 %, solely due to the difference in mooring system estimate. (*$1/(1-0.30) = 1/0.7 = 1.43 = 43\%$*, where mean response is found by* $x = \frac{F}{K}$*).*

Table 8.10: Comparison of the mean response: case 1

DOF	Mean response: FD	Mean response: TD	Difference FD to TD
surge	0.023 [m]	-0.478 [m]	-104.86 %
sway	-4.064 [m]	-2.822 [m]	44.00 %
heave	-0.271 [m]	-0.043 [m]	529.60 %
roll	0.779 [deg]	0.213 [deg]	266.21 %
pitch	-0.939 [deg]	-0.281 [deg]	234.11 %
yaw	0.032 [deg]	-0.902 [deg]	-103.50 %

In the cases closer to the rated wind speed, Case 2 and Case 3, the differences in the estimated mean pitch are much smaller. This is even more noticeable for the roll response. One of the reasons for this is the accuracy with which the generated power is estimated at rated wind speed. Above rated wind speed, the blade pitch control aims to keep the torque constant. The thrust and power generated can be approximated by Equation 8.1 and Equation 8.2, where a represents the induction factor (related to the change in wind velocity due to the power extracted at the turbine).

$$T = 1/2 \cdot \rho \cdot U^2 \cdot A \cdot 4 \cdot \mathsf{a}(1-\mathsf{a}) \tag{8.1}$$

$$P = 1/2 \cdot \rho \cdot U^3 \cdot A \cdot 4 \cdot \mathsf{a}(1 - \mathsf{a})^2 \tag{8.2}$$

The estimated power at a wind speed of 15 m/s is approximately equal to the turbine's rated power of 11 MW. Since thrust and power are related to velocity by a quadratic and cubic relationship respectively, this suggests that the estimate of thrust is also reasonable. Since the natural frequencies of pitch and roll are comparable, this also results in a comparable mean response. Finally, the comparable mean response is also due to the smaller coupling effects as the structure is excited by wind from a relative wind angle of about 300 degrees, which is one of the angles for which the structure is symmetrical. In addition, the mean yaw response is underestimated. This can be explained by two factors, namely the asymmetric aerodynamic response to the blades in the time-domain estimate and the influence of the overestimation of the surge/sway and the contribution of the mooring stiffness. In the time-domain method, the excitation of the turbine is asymmetrical. In other words, the distribution of the aerodynamic force is not uniform due to blade geometry, angle of attack and rotational speed, as well as other factors. Secondly, the increased mean surge and sway response compared to the time-domain simulation increases the mooring stiffness. As can be seen in Figure 8.5, the increased mean surge/sway response lifts the mooring line off the seabed, which, among other things, increases the stiffness in the yaw direction. This displacement of the mooring line also increases the heave stiffness and therefore leads to an increased downward heave response.

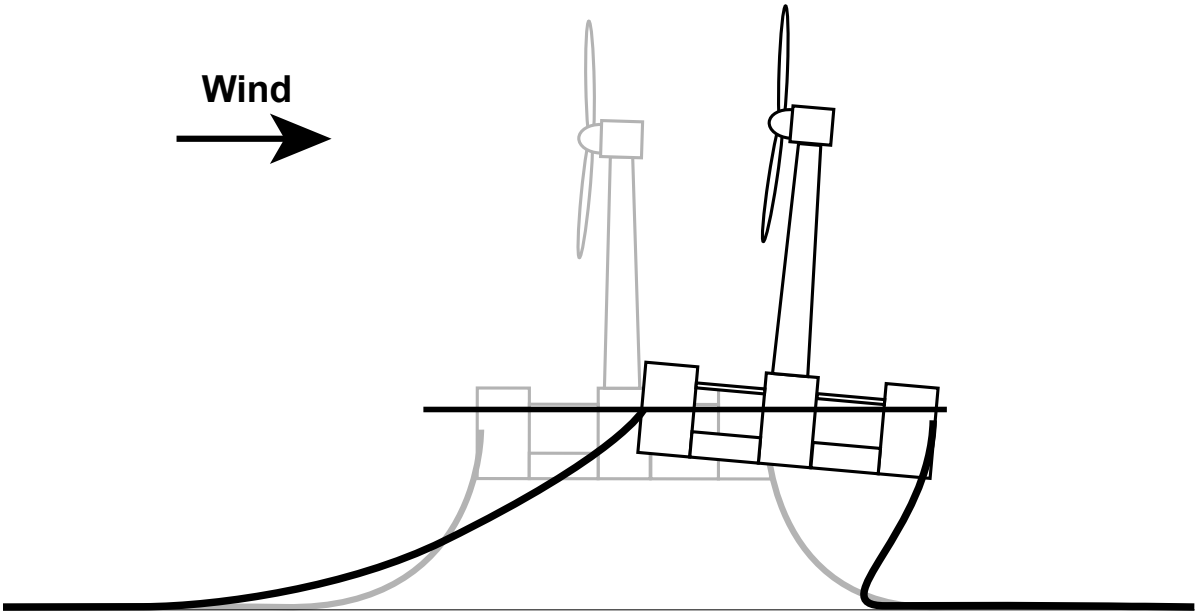

Figure 8.5: Increased horizontal response and the resulting mooring line displacement.

Table 8.11: Comparison of the mean response: case 2

DOF	Mean response: FD	Mean response: TD	Difference FD to TD
surge	10.142 [m]	3.442 [m]	194.63 %
sway	-19.127 [m]	-10.966 [m]	74.41 %
heave	-0.342 [m]	-0.138 [m]	148.28 %
roll	3.630 [deg]	3.658 [deg]	-0.76 %
pitch	0.649 [deg]	1.125 [deg]	-42.26 %
yaw	0.221 [deg]	-4.884 [deg]	-104.52 %

Table 8.12: Comparison of the mean response: case 3

DOF	Mean response: FD	Mean response: TD	Difference FD to TD
surge	9.300 [m]	3.032 [m]	206.74 %
sway	-17.440 [m]	-10.059 [m]	73.38 %
heave	-0.329 [m]	-0.120 [m]	173.33 %
roll	3.414 [deg]	3.272 [deg]	4.34 %
pitch	0.544 [deg]	0.691 [deg]	-21.29 %
yaw	0.201 [deg]	-4.649 [deg]	-104.33 %

For a near solely surge direction exciation (case 4, Table 8.13), a similar calculation by hand (as for case 1) would give an overestimation of 275 %due to the difference in stiffness of the mooring in the surge direction. However, since the pitch response is also underestimated, this indicates an underestimation of the mean thrust at an average wind speed of $25\ m/s$.

As the turbine operates close to cut-off speed, an attempt is made to keep the torque constant at rated power. However, the frequency-domain method underestimates the power generation at this wind speed at approximately 9.4 MW (instead of the rated power of 11 MW). Using Equation 8.1 and Equation 8.2, this underestimation of the power also results in an underestimation of the mean thrust. The reason for this underestimation is found in the approximation of the turbine model (Section 8.3.2).

Table 8.13: Comparison of the mean response: case 4

DOF	Mean response: FD	Mean response: TD	Difference FD to TD
surge	7.733 [m]	3.219 [m]	140.24 %
sway	-1.054 [m]	-1.931 [m]	-45.41 %
heave	-0.280 [m]	-0.054 [m]	415.39 %
roll	0.280 [deg]	1.026 [deg]	-72.69 %
pitch	1.175 [deg]	1.714 [deg]	-31.44 %
yaw	-0.468 [deg]	-2.598 [deg]	-82.00 %

8.5. Floater response comparison: waves only

This section provides a comparison of load case estimates when only waves excite the structure. This comparison provides insight into the contribution of the mooring system and hydrodynamic properties, as no aerodynamic excitation, added mass, and aerodynamic damping are considered. Around the wave frequency range, the motions are dominated by inertial effects, but the underestimation of the mooring system presented in Section 8.4 is expected to contribute at very low frequencies. The response PSDs of the four cases are presented in Figure 8.6 to Figure 8.9. Standard deviations are presented in Table 8.14 to Table 8.17.

As shown in Figure 8.1a, the wave components act mostly in a positive surge direction (floater reference frame). As shown in Section 8.4, the mooring system is underestimated for both surge and sway directions. This leads to an overestimation of the surge response around the wave frequency range. Furthermore, it can be observed that the surge natural frequency is excited by the second-order difference frequency wave force, which is not present in the frequency-domain method.

In contrast to the overestimation of the surge response at the wave frequencies, the sway response at the wave frequencies is underestimated. Since there is no coupling in the hydrodynamic added mass due to the absence of the pontoons (submerged connecting members) in the potential flow software, this results in an underestimation of the contribution of roll to the sway response. The presence of the submerged pontoons leads to an increased roll-sway coupling and thus a lower response in the time-domain method.

The heave response is very comparable. Since both the natural frequency and the stiffness terms (Section 8.3.2) are predicted with reasonable accuracy, only minor differences are to be expected here.

In the case of the roll response, the differences are related to the differences in hydrodynamic properties. Very noticeable is the excitation of the roll natural frequency below the wave frequency range due to the second-order wave excitation. In general, the difference here is relatively small because the magnitude of the dynamic response is small compared to the pitch response (Table 8.14). However, the differences in the wave frequency range are likely the result of underestimated wave excitation, as the structure is excited by waves around the apparent length of the structure, an effect highlighted in Section 6.3.

The pitch response shows an overestimation by the frequency-domain method in the wave frequency range. Two possible differences in the hydrodynamic response and excitation properties explain this difference, namely: the ratio of diameter to wave length at high frequencies is relatively small for the connecting pontoons, and the Morison equation does not correct for diffraction and radiation effects. This suggests that the added mass in the wave frequency range is underestimated. Secondly, the frequency-domain method does not estimate radiation damping for the connecting pontoons, which leads to an underestimation of the response at higher frequencies.

For the yaw DOF, the response in the wave frequency range is comparable. Here, the excitation of the yaw natural frequency by the second-order wave force is noticeable, which is absent in the frequency-domain method.

Similar trends are observed for case 2 (Figure 8.7) and case 3 (Figure 8.8). Since the wave excitation increases linearly with the crest height of the wave, this trend is to be expected. However, case 4 (Table 8.17) shows very clearly that the time-domain estimates noticeable responses around 0.09 Hz, which corresponds to a wavelength twice the apparent length of the structure. The frequency-domain method estimates responses around 0.15-0.16 Hz, which corresponds to an apparent length of the structure approximately equal to the wavelength.

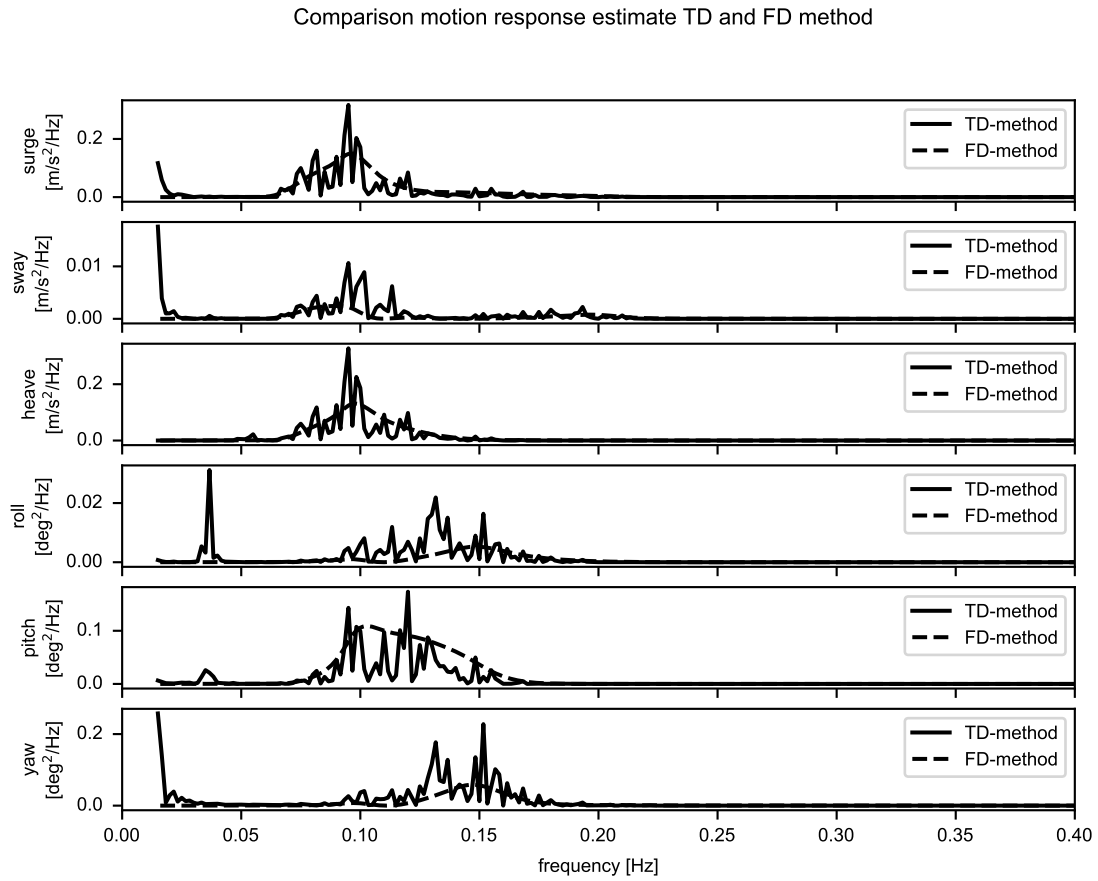

Figure 8.6: Floater Response PSD comparison for load case 1 (Waves only, no wind or current).

Table 8.14: Comparison of standard deviations of motion response characteristics case 1 (Waves only, no wind or current).

DOF	SD_{FD}	$SD_{TD,FFT}$	Difference FD to TD
surge	0.074 [m]	0.070 [m]	6.22 %
sway	0.010 [m]	0.015 [m]	-35.55 %
heave	0.066 [m]	0.064 [m]	3.07 %
roll	0.015 [deg]	0.023 [deg]	-33.14 %
pitch	0.074 [deg]	0.057 [deg]	29.88 %
yaw	0.046 [deg]	0.069 [deg]	-33.94 %

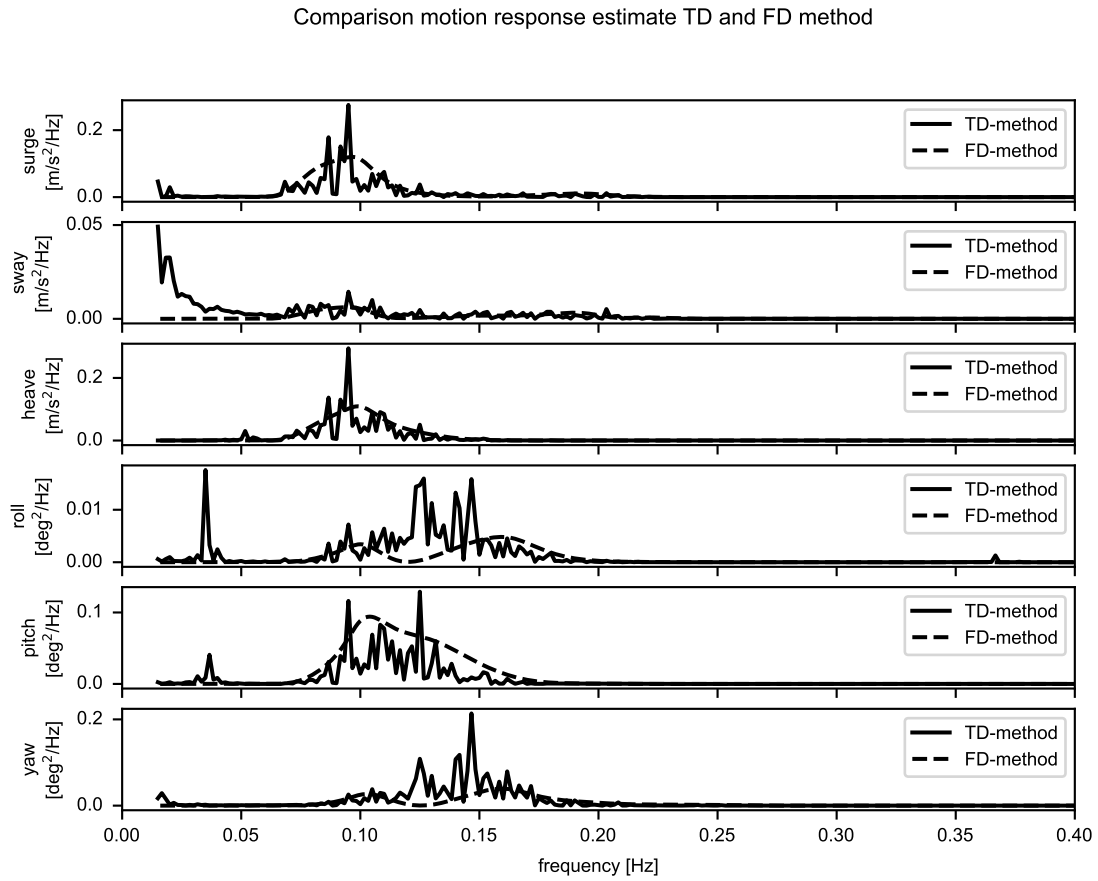

Figure 8.7: Floater Response PSD comparison for load case 2 (Waves only, no wind or current).

Table 8.15: Comparison of standard deviations of motion response characteristics case 2 (Waves only, no wind or current).

DOF	SD_{FD}	$SD_{TD,FFT}$	Difference FD to TD
surge	0.067 [m]	0.059 [m]	14.08 %
sway	0.019 [m]	0.030 [m]	-36.73 %
heave	0.062 [m]	0.055 [m]	11.74 %
roll	0.016 [deg]	0.022 [deg]	-25.96 %
pitch	0.067 [deg]	0.049 [deg]	37.95 %
yaw	0.047 [deg]	0.061 [deg]	-23.50 %

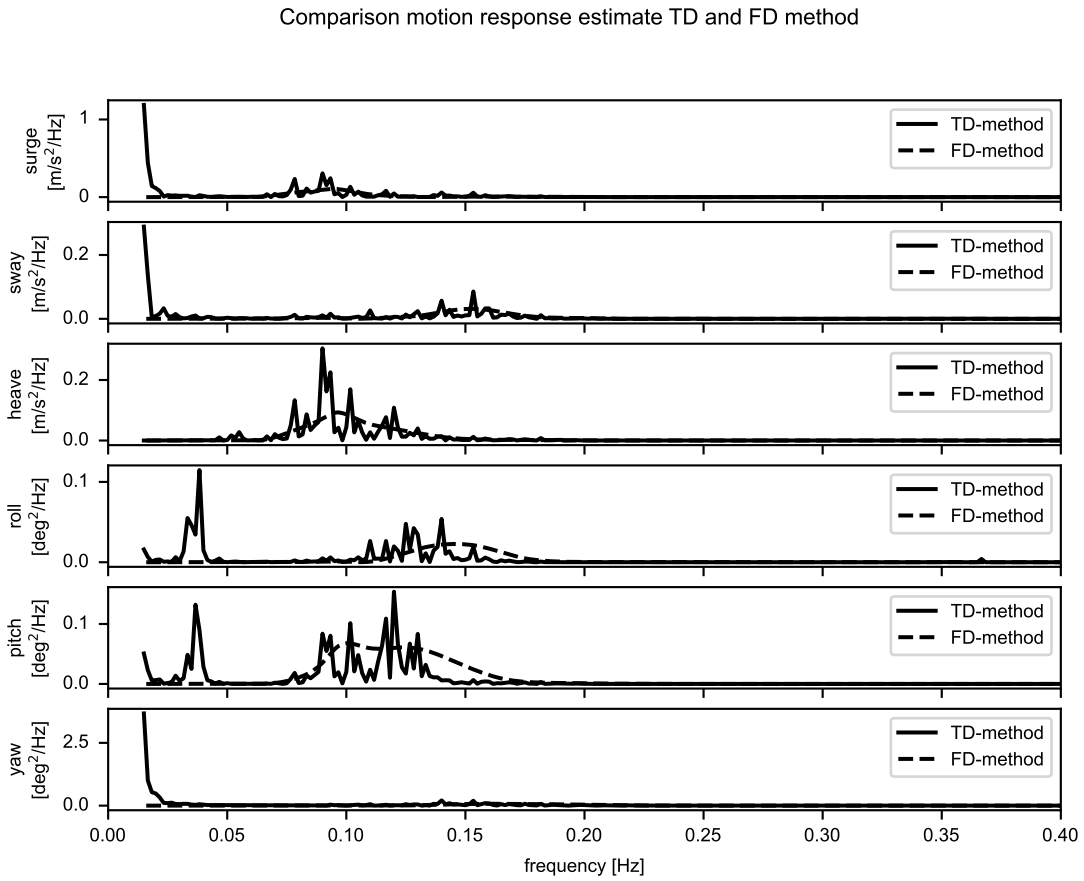

Figure 8.8: Floater Response PSD comparison for load case 3 (Waves only, no wind or current).

Table 8.16: Comparison of standard deviations of motion response characteristics case 3 (Waves only, no wind or current).

DOF	SD_{FD}	$SD_{TD,FFT}$	Difference FD to TD
surge	0.059 [m]	0.089 [m]	-33.27 %
sway	0.036 [m]	0.046 [m]	-21.55 %
heave	0.059 [m]	0.062 [m]	-4.19 %
roll	0.031 [deg]	0.037 [deg]	-14.73 %
pitch	0.062 [deg]	0.056 [deg]	11.89 %
yaw	0.068 [deg]	0.128 [deg]	-46.72 %

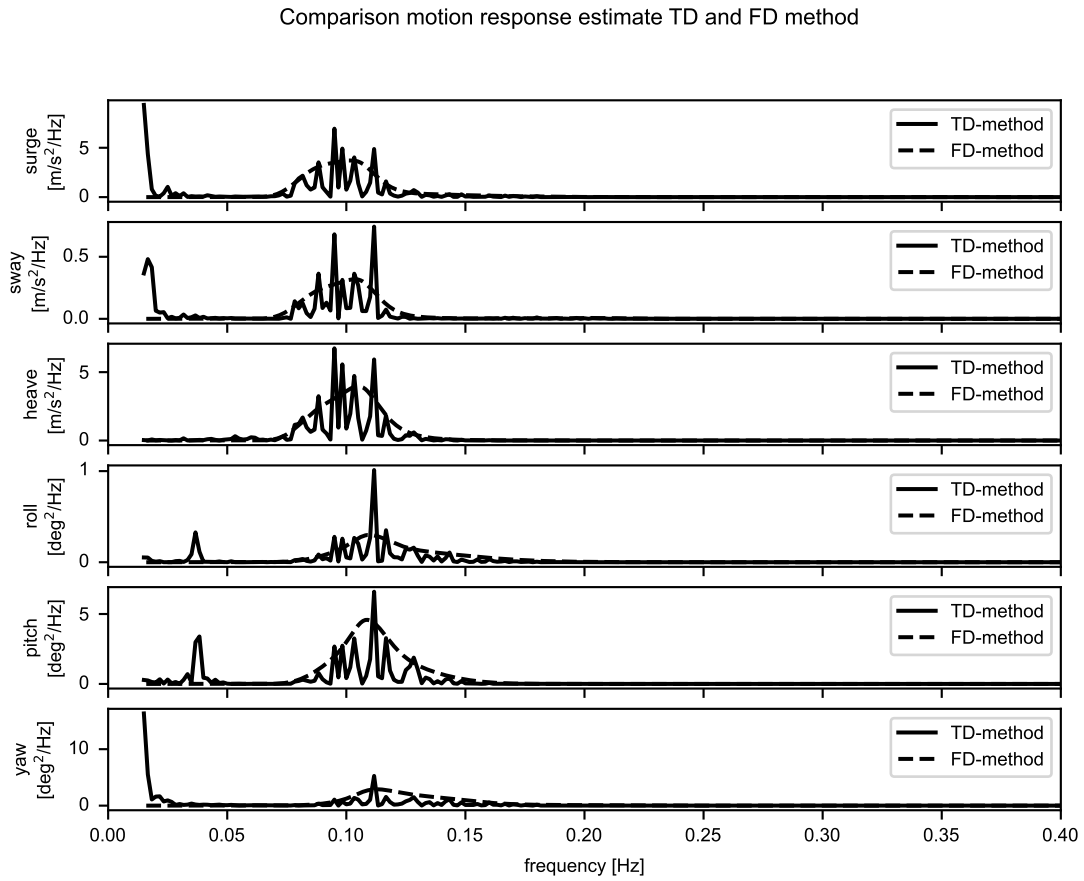

Figure 8.9: Floater Response PSD comparison for load case 4 (Waves only, no wind or current).

Table 8.17: Comparison of standard deviations of motion response characteristics case 4 (Waves only, no wind or current).

DOF	SD_{FD}	$SD_{TD,FFT}$	Difference FD to TD
surge	0.370 [m]	0.337 [m]	9.91 %
sway	0.103 [m]	0.100 [m]	3.00 %
heave	0.355 [m]	0.290 [m]	22.38 %
roll	0.109 [deg]	0.094 [deg]	14.88 %
pitch	0.374 [deg]	0.282 [deg]	32.98 %
yaw	0.347 [deg]	0.316 [deg]	9.91 %

8.6. Floater response comparison: wind and waves

For the cases presented in Table 8.1 the response spectra and standard deviations of the floater's 6 DOF motion response are compared using both the time-domain method and the frequency-domain method. The power spectral densities and their standard deviations for the 6 floater DOFs are compared to identify additional differences not identified in Section 8.3, Section 8.4 and Section 8.5.

The PSDs of the four different cases are shown in Figure 8.10 to Figure 8.13. The comparison between the standard deviations is presented in Table 8.18 to Table 8.21.

Comparison Case 1

When comparing the surge response, it can be seen that the surge and sway responses are comparable in the wave frequency range. The natural frequency of the surge DOF (0.012-0.013 Hz) is outside the observable range, but its excitation can be observed. Since the natural frequency is estimated quite well by the frequency-domain method, the increased response at these low frequencies can be observed in both methods.

The heave response is estimated with reasonable accuracy, even though the standard deviation is overestimated by 22 % (Table 8.8). The first reason for this comparable response is the negligible aerodynamic excitation, aerodynamic added mass and aerodynamic damping for this degree of freedom. In other words, both the excitation and the response for this degree of freedom are dominated by hydrodynamic excitation and hydrostatic stiffness in this direction (Appendix C, Figure C.1).

The roll response shows differences in the frequency range of the wind turbulence frequency range (below 0.05 Hz). Since these differences occur at very low frequencies and around the roll natural frequency, these differences are probably due to an underestimation of the stiffness and damping terms. Differences in the mean response of the mooring system are found for this case (Section 8.4). It is therefore expected that differences are present in the linearised mooring system at that mean response. Furthermore, the differences affecting the overestimation of thrust may also contribute to the underestimation of aerodynamic damping. Another reason for the underestimation is the lack of hydrodynamic damping due to the connecting pontoons. Since they are relatively wide and tall compared to the wavelength, but are only modelled by the Morison equation, the hydrodynamic damping due to radiation is not estimated. Finally, no hydrodynamic coupling terms are estimated for these connecting pontoons. Because of time limitations the contribution of these differences to the disagreement in role responses cannot be quantified.

In the pitch response, the excitation is increased around the natural pitch frequency compared to Figure 8.6. The pitch natural frequency is excited by second-order difference frequency excitation, which is not included in this frequency-domain method. In the wave frequency range, the response is comparable to the case without wind, since there is negligible aerodynamic damping in this direction due to the turbine's orientation (Figure 8.1a).

Finally, the yaw response at low frequencies is underestimated by the frequency-domain method. This is due to the exclusion of the second-order wave drift force in the frequency-domain method (observed in Section 8.5). Furthermore, no aerodynamic yaw excitation is estimated since the aerodynamic code assumes a symmetric thrust distribution across the rotor plane.

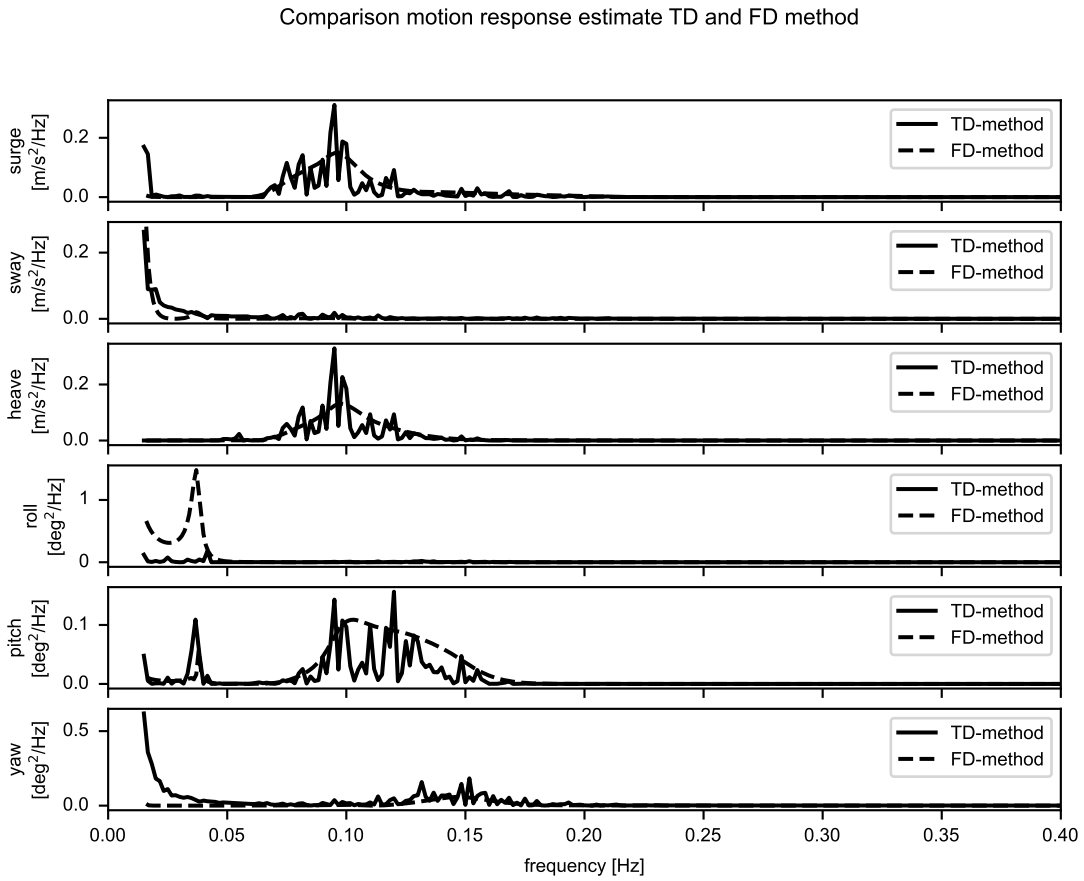

Figure 8.10: Floater Response PSD comparison for load case 1

Table 8.18: Comparison of standard deviations of motion response characteristics case 1

DOF	SD_{FD}	$SD_{TD,FFT}$	Difference FD to TD
surge	0.074 [m]	0.071 [m]	4.08 %
sway	0.028 [m]	0.045 [m]	-38.75 %
heave	0.066 [m]	0.064 [m]	3.14 %
roll	0.139 [deg]	0.038 [deg]	266.16 %
pitch	0.076 [deg]	0.059 [deg]	28.72 %
yaw	0.046 [deg]	0.092 [deg]	-50.17 %

Comparison Case 2 and 3

For case 2 and case 3, the results show more similarities, as was also observed for the mean response and the response to waves only. However, there are clear differences for roll and pitch in the frequency range of the wind turbulence. The differences around the natural frequency of pitch and roll are due to the differences in aerodynamic damping and hydrodynamic damping already noted for roll in Section 8.6. In general, the magnitude of these responses is estimated with reasonable accuracy in the wind turbulence frequency range, as the thrust is estimated with reasonable accuracy (Section 8.4).

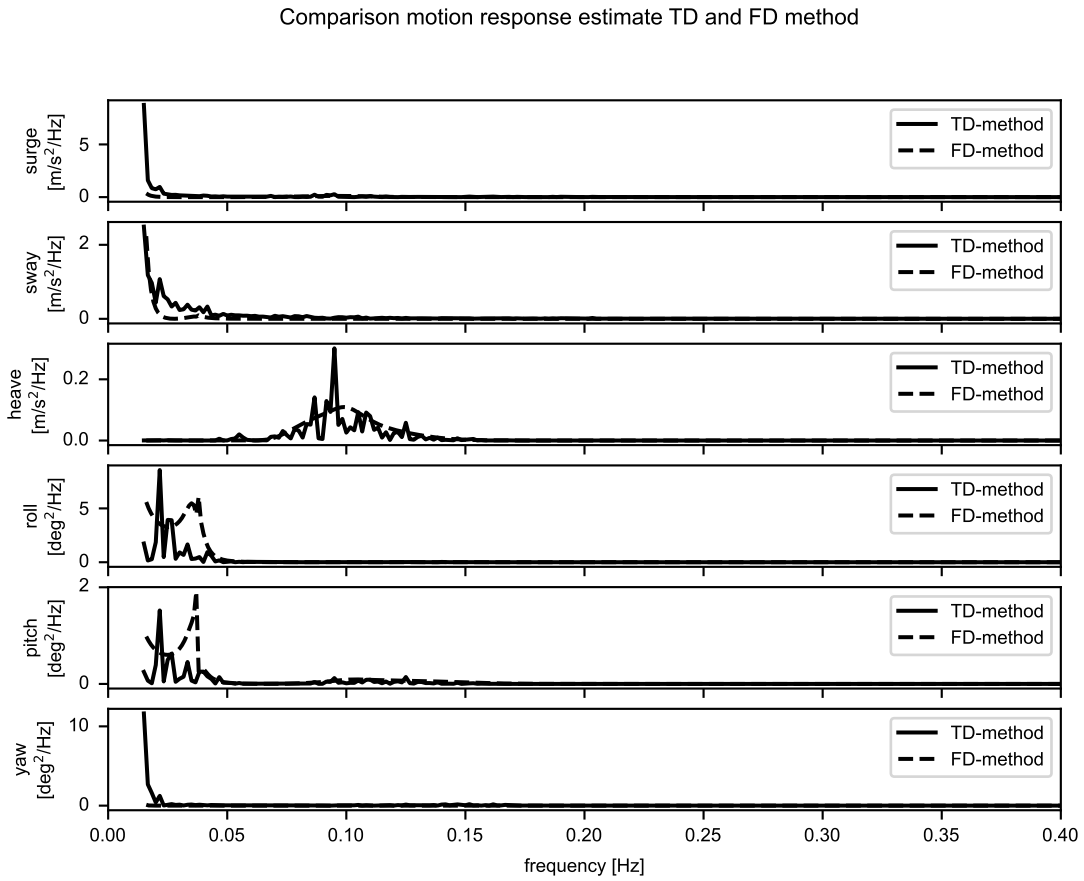

Figure 8.11: Floater Response PSD comparison for load case 2

Table 8.19: Comparison of standard deviations of motion response characteristics case 2

DOF	SD_{FD}	$SD_{TD,FFT}$	Difference FD to TD
surge	0.074 [m]	0.177 [m]	-57.85 %
sway	0.079 [m]	0.153 [m]	-47.96 %
heave	0.062 [m]	0.056 [m]	11.17 %
roll	0.363 [deg]	0.217 [deg]	67.27 %
pitch	0.184 [deg]	0.106 [deg]	73.13 %
yaw	0.047 [deg]	0.195 [deg]	-75.96 %

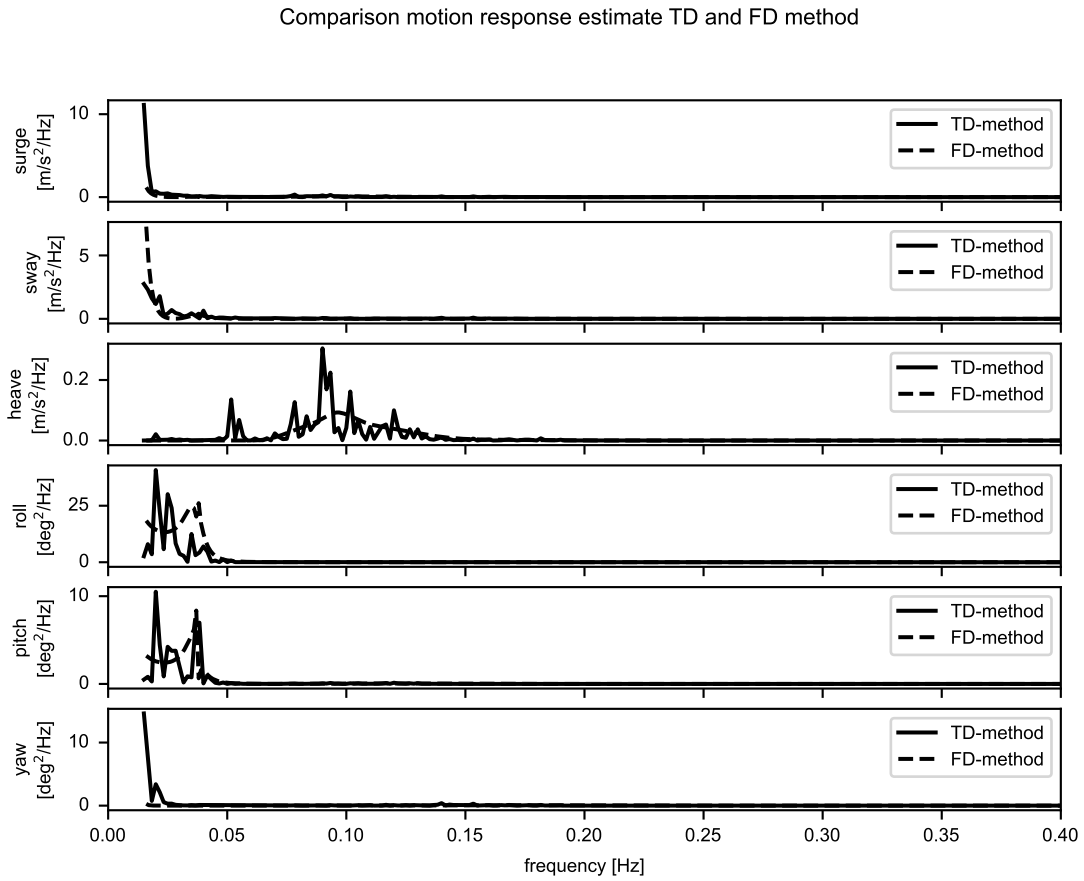

Figure 8.12: Floater Response PSD comparison for load case 3

Table 8.20: Comparison of standard deviations of motion response characteristics case 3

DOF	SD_{FD}	$SD_{TD,FFT}$	Difference FD to TD
surge	0.084 [m]	0.194 [m]	-56.71 %
sway	0.148 [m]	0.166 [m]	-10.54 %
heave	0.059 [m]	0.064 [m]	-6.99 %
roll	0.742 [deg]	0.561 [deg	32.17 %
pitch	0.354 [deg]	0.289 [deg]	22.46 %
yaw	0.068 [deg]	0.243 [deg]	-71.87 %

Comparison Case 4

In this case, the wind and wave components mainly excite the surge and pitch degrees of freedom (Figure 8.1d). In this particular case, the frequency-domain method estimates the surge response quite well in both the wind frequency range (below 0.05 Hz) and wave frequency range (0.07- 0.15 Hz). What is very striking here, however, is the overestimation of the pitch response at low frequencies. This overestimation is similar to the response found for case 1 and is contributed to the underestimation of the mooring system and the underestimation of the hydrodynamic and aerodynamic damping.

This underestimation of the pitch response is because of the underestimation of the response at low frequencies (below natural frequency). This is contributed to the underestimation of the mooring stiffness. Furthermore, the underestimation of the hydrodynamic radiation damping and the different estimation of the viscous drag leads to an increased response around the pitch natural frequency.

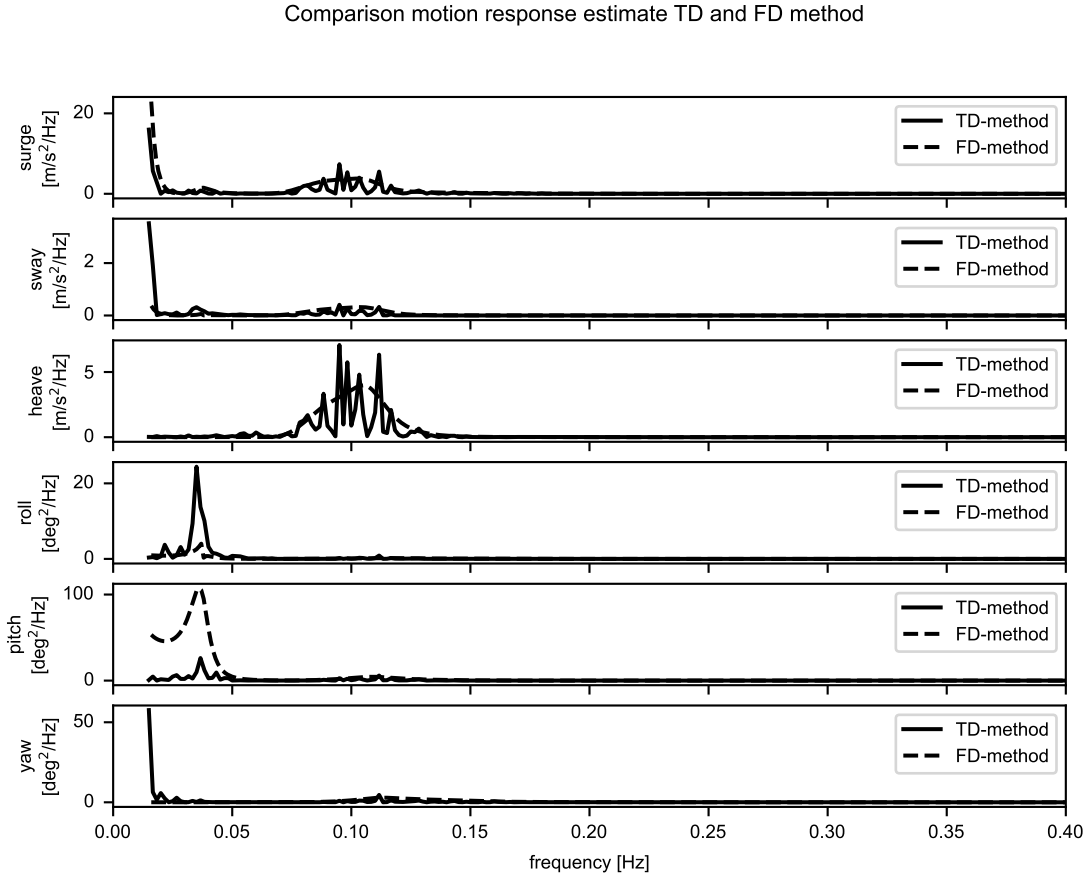

Figure 8.13: Floater Response PSD comparison for load case 4

Table 8.21: Comparison of standard deviations of motion response characteristics case 4

DOF	SD_{FD}	$SD_{TD,FFT}$	($SD_{TD,FFT,all}$/ $SD_{TD,TT}$)	Difference FD to TD
surge	0.461 [m]	0.374 [m]	(0.729/0.729 [m])	23.32 %
sway	0.109 [m]	0.129 [m]	(0.978/0.978 [m])	-15.27 %
heave	0.355 [m]	0.298 [m]	(0.299/0.299 [m])	19.30 %
roll	0.228 [deg]	0.384 [deg]	(0.409/0.409 [deg])	-40.49 %
pitch	1.526 [deg]	0.476 [deg]	(0.507/0.507 [deg])	220.71 %
yaw	0.347 [deg]	0.419 [deg]	(1.696/1.696 [deg])	-17.02 %

In general, it is concluded that the frequency-domain method does not provide a satisfactory estimate of the dynamic response when turbulent wind excitation is taken into account. Section 8.1 gives a detailed overview of the inherent differences and their contribution to the (dynamic) response of the structure. The effect of these differences on the tower base bending moment and equivalent stress estimates is discussed in Section 8.7.

8.7. Comparison of the tower base bending moments

The aim of this research is to provide a computationally efficient estimate of the equivalent bending moment, this section provides a comparison of the estimated tower base bending moments. For case 1, the PSDs of the tower base bending moments is shown in are presented in Figure 8.14. For case 2, case 3, and case 4 the PSDs are presented in Appendix D, Figure D.1 to Figure D.3.

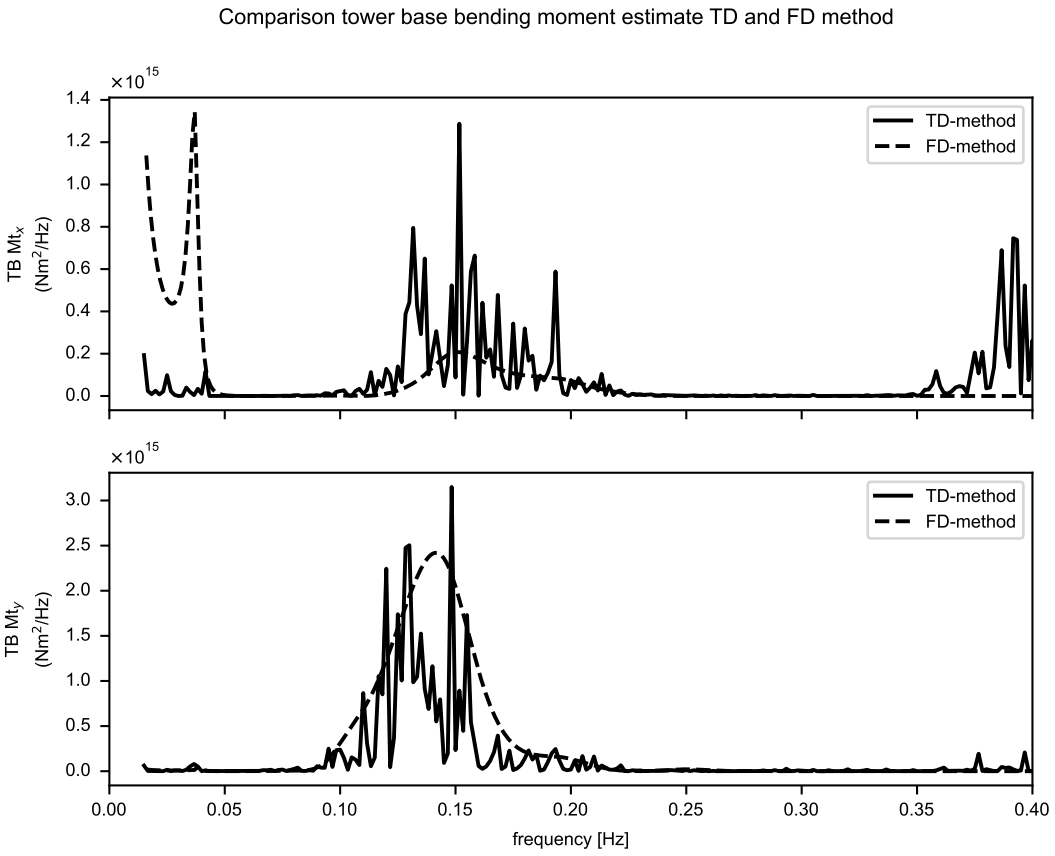

Figure 8.14: Tower base bending PSD's (case 1).

To get an indication of the differences, the standard deviations of these response spectra are presented in Table 8.22. In the case of Mt_x (side-to-side) (case 1), the bending moment about the y-axis of the float, has contributions from sway and rotation about the y-axis (roll). From the response spectra and standard deviations in Section 8.6, it can be seen that the sway response is underestimated and the roll response is overestimated. These contributions are opposite and therefore counteract each other in the tower base bending response. This leads to an apparently accurate estimate of the spectrum of the tower base bending response for this case. However, this is an incorrect conclusion as the tower base bending response results from the contributions of these components, but is not a linear superposition and these effects do not cancel each other out. In fact, this analogy does not hold for the Mt_y response. The sway and pitch responses are estimated with greater accuracy compared to the roll and roll responses. However, the estimated Mt_y (fore-aft bending moment) has a larger error. An equivalent interaction is observed for cases 2 and 4, where the PSDs are also under- and overestimated, respectively.

To summarise, the individual bending moments spectra show limited similarity due to (1) underestimation at low frequencies due to second-order wave force excitation (Section 8.5), (2) overestimation of the response at low frequencies (Section 8.6) and (3) the underestimation around the first tower bending natural frequency, which is assumed to be rigid in the frequency-domain method (Section 4.1).

Table 8.22: Comparison of standard deviations of tower base bending moment PSD's.

DOF	SD_{FD} [MNm]	$SD_{TD,FFT}$ [MNm]	Difference FD to TD
Case 1:			
Mt_x	5.51	5.92	-6.89 %
Mt_y	10.37	7.69	34.81 %
Case 2:			
Mt_x	12.85	15.45	-16.85 %
Mt_y	10.83	8.67	24.99 %
Case 3:			
Mt_x	26.10	24.77	5.35 %
Mt_y	13.82	13.88	-0.46 %
Case 4:			
Mt_x	15.55	25.46	-38.93 %
Mt_y	62.66	40.00	56.66 %

From the obtained PSDs of the tower base bending moments, the equivalent stresses/moments are estimated using the Tovo-Benasciutti method (Section 4.2.1). In Figure 8.14 to Figure D.3 the contribution of the equivalent bending moment around the tower base is plotted for the four cases. The equivalent moment around the tower base is estimated in the local floater reference frame, as presented in Figure 8.1.

In case 1 (Figure 8.14), the magnitude of overestimation is limited, as it is mainly the fore-aft (Mt_y) component that is overestimated. This fore-aft bending moment is overestimated by 22%. From Figure 8.15 it is concluded that this overestimation is the result of the overestimation of the pitch response around the wave frequency.

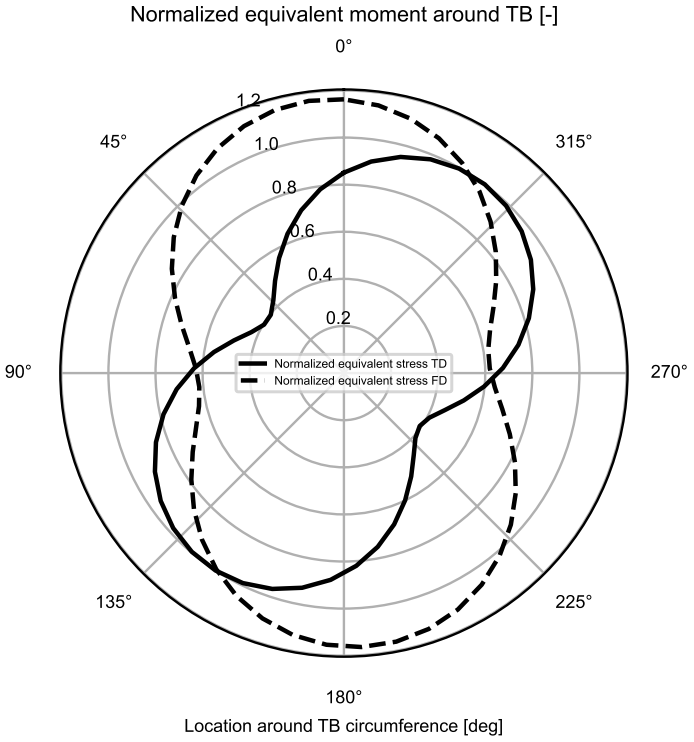

Figure 8.15: Normalised tower base bending moment estimates around the tower base (case 1).

In case 2 the direction of the maximum/minimum equivalent bending moment is reasonably well estimated (Figure 8.16). For the case below the rated wind speed (case 2), the standard deviation of the fore-aft bending moment is overestimated by 25 %, while the standard deviation of the side-to-side bending moment is underestimated by about 17 %. The equivalent bending moment in fore-aft direction is overestimated by 14 % and the side-to-side equivalent bending moment is underestimated by 22 %. The maximum equivalent bending moment is underestimated by about 21 %. The underestimation in side-to-side is contributed to the response around the first tower base bending frequency.

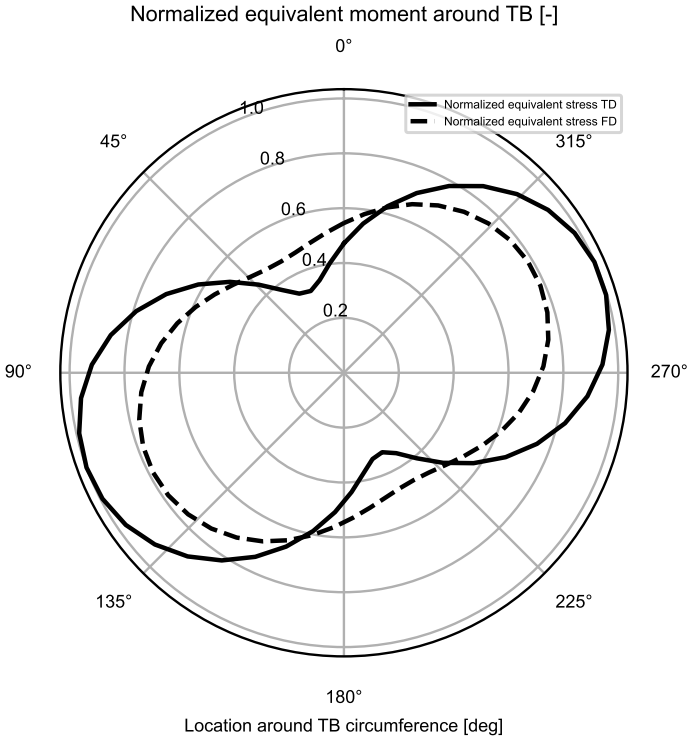

Figure 8.16: Normalised tower base bending moment estimates around the tower base (case 2).

Case 3 (Figure 8.17) shows the most reasonable estimate of the equivalent tower base bending moment, within an error of 2 %. The main reason for this is the reasonable approximation of the power and hence the thrust on the rotor. This results from a reasonable estimate of the mean response characteristics for pitch and roll (Table 8.11 and Table 8.12) and the reasonable estimate of the dynamic response characteristic Section 8.6. Finally, the response around the first tower base bending frequency is limited.

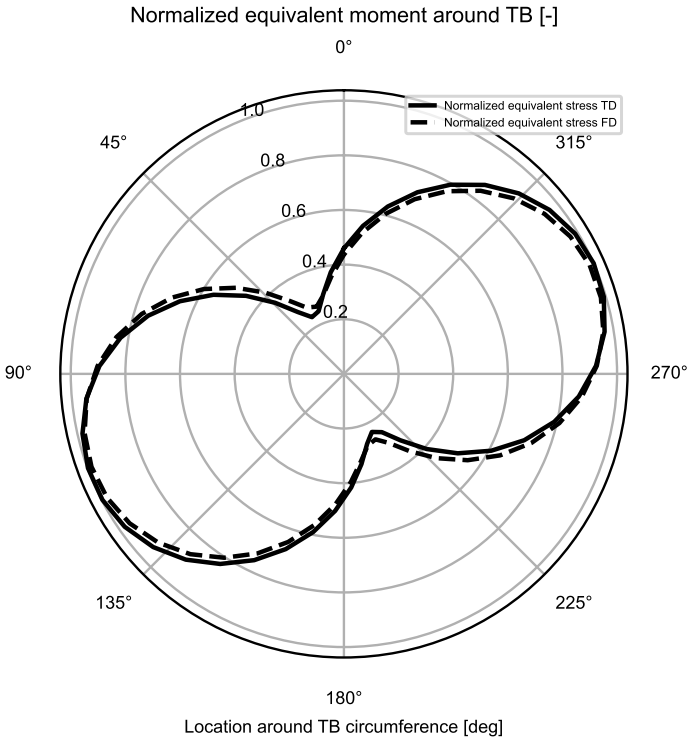

Figure 8.17: Normalised tower base bending moment estimates around the tower base (case 3).

The equivalent bending moment at the tower base for case 4 is plotted in Figure 8.18. The fore-aft bending moment is overestimated by 50 % due to the overestimation of the dynamic response in the pitch direction in the range of the wind turbulence frequency range (Figure D.3). The side-to-side bending moment is significantly overestimated (-53 %) as no response due to a flexible tower is assumed.

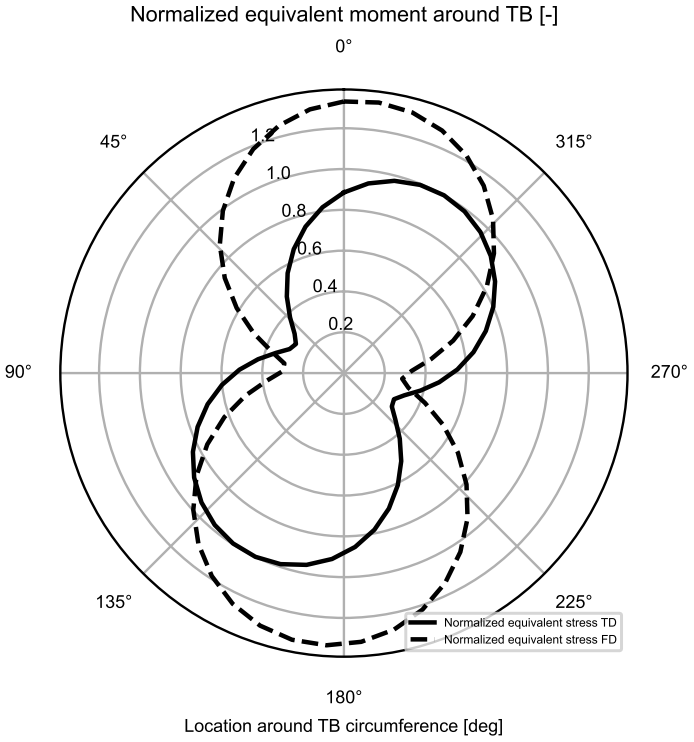

Figure 8.18: Normalised tower base bending moment estimates around the tower base (case 4).

For the different load cases, the overestimation is mostly observed outside the rated wind speed. For load cases 1 and 4, the dynamic response of roll/pitch is overestimated. However, near the rated wind speed (cases 2 and 3), the tower base bending moment shows a better estimate.

To conclude, the frequency-domain method is unable to estimate the equivalent bending moment away from the rated wind speed. However, it can estimate the tower base bending moment around the rated wind speed quite well. This suggests that the frequency-domain method can be used to estimate the equivalent bending moment for a complete set of load cases when most cases occur around the rated wind speed. In other words: If the wind speeds that are well below and above the rated speed can be considered as outliers, then their contribution to the equivalent bending moment is small anyway and a reasonable estimate for a full set of DLCs might be possible. This will be evaluated for SGRE project data in the Section 8.8.

8.8. Comparison of bending moment estimate for DLC 1.2

In the time-domain simulations, rain flow counting is performed to obtain the equivalent stress of the bending moment time traces at every 30 degrees around the tower. This is estimated for each load case within the design load case set (about 5000 cases in DLC 1.2). As this load case set is based on hindcast data, a probability factor is known for each case. The resulting equivalent stress can then be converted to an equivalent bending moment to compare the performance of the designs for a DLC.

As discussed in Section 8.7, a reasonable estimate of the equivalent bending moment at the tower base might be possible if the load cases operate near the rated wind speed, where the torque and hence thrust are estimated with reasonable accuracy. Thus, if the probability of occurrence of these load cases is relatively high compared to wind speeds outside this range, it might be possible to estimate the total equivalent moment with reasonable accuracy.

The distribution of the probability compared to the wind speeds is displayed in Figure 8.19. This figure shows that the majority of wind speeds, including those with the highest weighting factor, are within the range of 8 m/s to 15 m/s. This is approximately within the wind speed ranges of Comparison Case 2 and Case 3, which had reasonable accuracy.

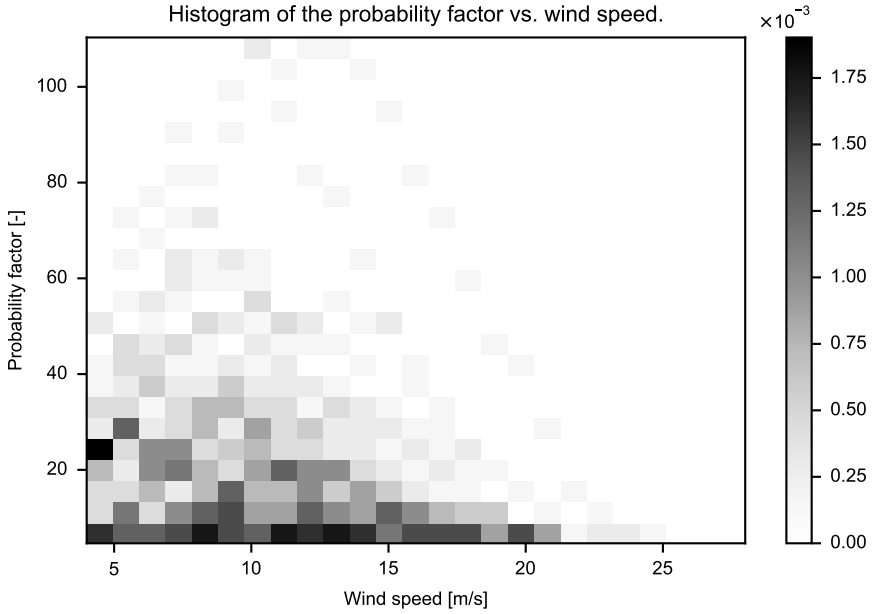

Figure 8.19: Histogram with the probability of all cases per wind speed range.

However, the total equivalent bending moment is estimated by an analogy similar to the Palmgren-Miner rule. The actual cumulative damage from the stress estimation of the sum must be weighted by the probability of occurrence of a given bending moment over the total probability. Equation 8.3 shows the estimate of the total equivalent bending moment $M_{eq,tot}$ by the estimated bending moment for each case $M_{eq}(i)$ for case probability p_i. In this equation p_{tot} is the sum of all probability factors.

$$\sum_{i=1}^{n} M_{eq}^{m} \cdot p_i = M_{eq,tot}^{m} \cdot p_{tot} \tag{8.3}$$

Rewriting this equation gives an expression for the total equivalent bending moment for n load cases (Equation 8.4). From these equations it can be seen that the equivalent bending moment of a single case is taken to the power of m (the crack growth constant). For a crack growth constant $k = 4$, by analogy with the Palmgren-Miner rule, this means that the contribution of an estimated equivalent bending moment is actually taken to the power of 4. Any difference in the estimate of the equivalent bending moment of a case, even for the outliers, contributes significantly to the total equivalent bending moment if the probability factor is large.

$$M_{eq,tot} = \left(\sum_{i=1}^{n} \left(M_{eq}(i)^m \cdot p_i \right) / p_{tot} \right)^{1/m} \tag{8.4}$$

The estimate of the equivalent bending moment about the tower base is shown in Figure 8.20. From this figure it can be seen that the total estimated equivalent bending moment is underestimated by 50 to 56 %, depending on the location around the tower base. The direction around the tower base in which the maximum bending moment occurs is also incorrectly estimated.

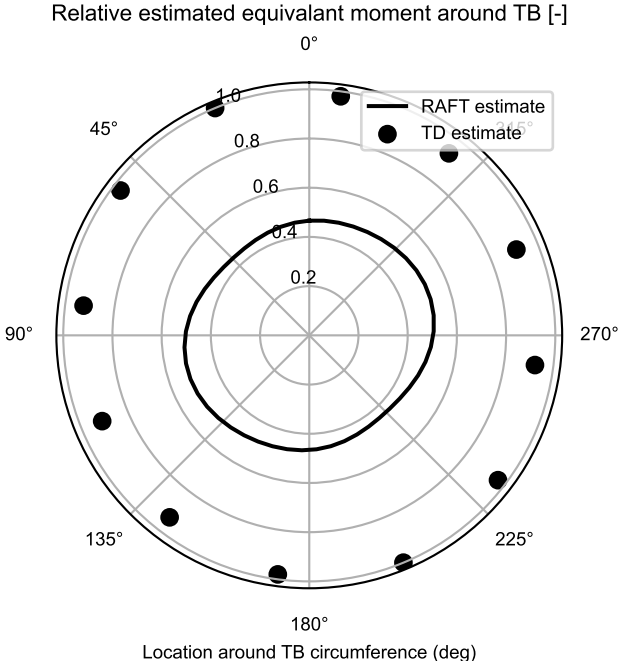

Figure 8.20: Normalised equivalent bending moment around the tower base for the complete DLC 1.2 estimate.

Several causes have been identified for this underestimation. As mentioned in the last paragraph, the differences in the estimated bending moment contribute exponentially with the power of the crack growth constant. Although a significant number of cases were between the wind speeds of case 2 and case 3, outliers still contribute significantly. This also applies to the differences in the direction of the equivalent bending moment in case 1 and case 4, as these differences also contribute exponentially.

Secondly, there are inherent differences between the Rainflow counting method and the spectral method used in this section. In the spectral approach, the stress range is estimated from the spectral moments instead of being derived from the rainflow counting. There are also differences in the mean response (Section 8.4) and hence differences in the mean stress.

Thirdly, although the Tovo-Benasciutti method is a proven approach for different stress signals [51] and gives comparable results when estimating the equivalent bending moment directly from the PSDs, it has not been directly verified for this type of signal, so there could be differences.

Furthermore, these differences are accumulated in addition to the differences in static and dynamic response between the two methods discussed in this chapter.

In summary, the frequency-domain method is currently unable to accurately estimate the equivalent bending moment for a complex and diverse set of load cases with a range of wind speeds and misalignment angles. Main differences were presented for load cases away from the rated wind speed. However, its exact cause can not be isolated at this time as it is an accumulation of differences presented in this comparison.

8.9. Comparison: concluding remarks

In this section concluding remarks on the comparison of the frequency-domain method estimate to the time-domain estimates are presented.

System characteristics and wind/wave spectra.
From Section 8.3 it can be concluded that the frequency domain is effective in estimating characteristics such as mass/inertia terms, hydrostatic properties, and hydrostatic stiffness terms. The main reason for this comparable result is the relatively simple and linear underlying physics [48]. However, one of the limitations of the method is the estimation of mooring system stiffness for complex mooring systems. Currently, the mooring system is limited by its ability to evaluate simple geometries and line types. This limitation leads to differences in the estimated natural frequencies for sway, surge, and yaw.

Furthermore, the estimation of the wind speed and wave height characteristics introduces differences in the excitation part. The wave height, when compared to the PSD of the limited time trace, is estimated reasonably well. However, the limited duration of the time traces used in this comparison (600 seconds) results in inherent differences at very low frequencies. This makes it inherently difficult to compare the response characteristics at these low frequencies.

Wind response only (mean response).
For the evaluation of the mean response, simulations are carried out by SGRE where only wind excitations are present. The mean wind speed results in a mean response to which the frequency-domain method estimate is compared. In this comparison, two main differences between the methods become apparent, namely the difference in the mooring stiffness and the difference in the thrust estimation aerodynamic module. Away from rated wind speed, the thrust is not estimated accurately. Together with the differences in the mooring stiffness, this leads to a difference in the mean response of the structure. Around the nominal wind speed, the thrust estimate is more accurate and the mean roll and pitch response is estimated with reasonable accuracy. The surge and sway response present differences in the mean surge and sway response that are proportional to the differences in the natural frequency estimates for these degrees of freedom.

Wave-only response (dynamic response).
Separately, the dynamic response characteristics due to wave only excitation are compared. Several inherent differences in the hydrodynamic properties are shown in Section 8.5. The largest differences were again observed in the response to surge and sway, with differences in mooring stiffness and underestimation of aerodynamic/hydrodynamic damping being the most noticeable. In the case of sway, it was observed that even a slight wave misalignment resulted in a significant response. However, for this wave only case, the dynamic responses to roll and pitch were estimated quite well in the wave frequency range. The main differences presented for these degrees of freedom are the absence of the second-order wave force and the simplified hydrodynamic approximation of the connecting pontoons (reduced coupling effects in the FD method).

Response to wind and waves (dynamic response).
Based on these findings, the response characteristics of the floater are compared when it is excited by both the turbulent wind and the wave components. In this comparison, it was found that at low frequencies the pitch/roll response is overestimated due to the excitation by turbulent wind. This is mainly due to differences in the estimation of the mooring stiffness caused by differences in the thrust estimation for the frequencies below the natural frequency. In addition, differences in aerodynamic damping (simplified approach) and the lack of hydrodynamic radiation damping for the contribution are considered to be the main causes of the overestimation at the natural frequencies. Since the thrust is reasonably estimated around the rated wind speed, case 2 and case 3 show a more comparable approach. Due to the time constraints of this work, the magnitude of these effects has not been quantified.

Equivalent bending moment response at the tower base.
The differences between the two methods for the four different cases accumulate when estimating the bending moment response of the tower base. For mean wind speeds away from the rated wind speed, the pitch/roll response is overestimated. This, and the assumption of a rigid tower, lead to differences in the estimation of the equivalent moment at the tower base. This leads to both an overestimation of the wind direction and a change in the angle at which the maximum equivalent bending moment is estimated. However, when a load case around the rated wind speed is considered, both the mean response and the dynamic response are estimated with reasonable accuracy.

Inherent differences between the frequency-domain method and the time-domain method have led to differences in response away from the rated wind speed. Finally, due to the exponential relationship (crack growth slope/k-factor) between the equivalent bending moment and the accumulated damage, the frequency-domain method in its current form is not able to estimate the accumulated damage and the equivalent stress/bending moment for a semi-submersible type floating offshore wind turbine.

Main limitations
The main limitations of the frequency-domain method are: the simplicity of the mooring system, the rigid tower, the simplified aerodynamics, the sensitivity to blade geometry parameters and the under-estimation of hydrodynamic properties due to the hybrid analytical/numerical approach. Each of these individual differences add up to differences in the estimated equivalent bending moment. Due to their cumulative but coupled effects, the individual contributions of the differences are not separable without further analysis. This opens up research opportunities to improve the method on:

- Mooring stiffness estimation for complex configurations.
- Improved modelling of aerodynamics (improving turbine design).
- Implementation of a flexible tower.
- The contribution of a hybrid hydrodynamic property estimation.
- Comparison of the spectral approach to estimate the bending moment of the tower base to rain-flow counting for this approach.

These possibilities and suggestions for future work are presented in more detail in Section 10.3.

Part IV

Judgement

9 Discussion

This chapter provides a reflection on the results of this work. Section 9.1 provides a summary of the key findings of this thesis. A reflection of these findings in light of the literature is presented in Section 9.2. Finally, the limitations of the study are evaluated in Section 9.3.

9.1. Key findings

The goal of this work was to develop a computationally efficient method to quantify the effects of misaligned wind, windsea, and swell waves on a floating offshore wind turbine. The results of this work have determined the sensitivities of the structure using a frequency-domain method and compared the response estimates with time-domain simulations carried out for an industry project.

The results from Chapter 6 demonstrated that increased roll response is present via yaw-roll coupling effects. The results indicate that this is a correlation between the wavelength, apparent length of the structure, and wave direction with respect to the floater reference frame.

Chapter 7 showed the influence of aerodynamic damping on the equivalent stress at the tower base. The analysis showed that above the rated wind speeds, the reduced aerodynamic damping leads to an increased response to the bending moment at the tower base. In addition, it was found that aerodynamic damping can have a mitigating effect on the response to misaligned wind and waves. However, the absence of aerodynamic damping in the direction of the rotor plane (side-side direction) also leads to an increased response because of coupling effects in this direction.

Lastly, in Chapter 8, the frequency-domain method is compared with time-domain simulations performed with BHawC-OrcaFlex for cases of an industry project. This served as a verification of the method. The results show that while reasonable agreement was found for the pitch/response rigid body modes, noticeable differences were found in the equivalent bending moment estimates for the lowest and highest production wind speeds. In these cases, it is found that differences in the thrust estimation and the non-linear effect of the mooring system leads to differences in mooring stiffness. Furthermore, this leads to differences in the estimate of aerodynamic damping which, together with the differences in hydrodynamic damping, lead to noticeable differences in the response around the natural frequencies of pitch and roll natural frequencies.

9.2. Reflection on literature

While previous studies [19, 28] identified that the lack of aerodynamic damping increases the response in side-side direction, the magnitude of this effect was not quantified due to the computational cost of time-domain simulations. The results of a frequency-domain method contributes to a better understanding of how different environmental conditions influence the aerodynamic damping and how it contributes to the equivalent loads at the tower base.

This work confirms the challenges presented in the literature regarding hydrodynamic modelling in computationally efficient methods [31]. In line with the recent findings of Souza [59], it was found that the complex substructure of semisubmersibles requires computations in potential flow software as the Morison equation neglects the diffraction and radiation effects of the structure in the waves.

While previous research on a frequency-domain method for spar-type FOWT [3] did not take yaw into account, the results of this work show that taking yaw into account improves the estimate of roll due to yaw-roll coupling effects. This also sheds light on the improvements proposed for the QuLAF method by Pegalajar-Jurado *et al.* [2]. Where it was stated that the out-of-plane degrees of freedom should be considered to account for the wind-wave misalignment.

The results comparison shows that reasonable approximation is possible of the excitation spectra and rigid body natural frequencies. Furthermore, it is found that the frequency-domain method estimates the response of the load driving modes (pitch/roll) reasonably well. Therefore, for the load cases around and above rated wind, a reasonable estimation is found for the equivalent bending moment. However, differences in the energy distribution of the bending moment estimation show the need for better estimations of the aerodynamic thrust for the lowest and highest production wind speed cases. In addition, it is recommended to extend the frequency domain method with the first tower bending mode in fore-aft and side-to-side direction. Based on the findings by Pegalajar-Jurado *et al.* [2], this should improve the estimation of the tower base bending moment for softer tower designs used in the industry projects.

9.3. Limitations

Second-order wave forcing
The time-domain simulations performed by SGRE in Chapter 8 showed that second-order wave forces can excite natural frequencies outside of the wave frequency range. However, the sensitivity studies presented in Chapter 6 and Chapter 7 were limited by the exclusion of second-order wave forces. As yaw-roll coupling effects were observed at low frequencies due to the mooring system it could have affected the results if the second-order effects were considerable. Furthermore, the contribution of the (aerodynamic) damping effect to the response to second-order wave forcing around the the rigid body natural frequencies was not quantified.

Time-trace duration
Section 8.3.3 provided a comparison of the wind and wave excitation spectra for the frequency and time-domain method. Due to the limited duration of the timetraces low frequencies were not captured accurately. Therefore, it was also inherently difficult to compare the low-frequency response of the structure. This limited the research in comparing the very low frequency response of the structure, making it difficult to compare the response around the surge, sway, and yaw natural frequencies.

Mooring stiffness for complex configurations
When comparing with the time-domain simulations, the mooring system had to be simplified. The MoorPy code used by RAFT did not allow the modelling of a complex configuration of the mooring system. This led to an underestimation of the surge and sway stiffness by up to 43 %. Furthermore, as the response was assessed using a quasi-static approach, this led to an underestimation of the contribution of the mooring stiffness when the mean surge/sway response was substantial (Section 8.4).

Linearised aerodynamic damping
It was beyond the scope of this study to include a frequency-dependent approach for the aerodynamic added mass and aerodynamic damping [47]. Instead, the aerodynamic response characteristics were linearised by a simple constant aerodynamic damping coefficient for all frequencies. This approach is appropriate at higher frequencies, but does not account for nacelle motion and blade pitch control interaction at lower frequencies. This could have resulted underestimate the actual response of the structure at low frequencies.

Hydrodynamic characteristics
The frequency-domain method was limited by a hybrid analytical/potential-flow approach for the hydrodynamic properties. For slender structures with respect to the wave length, the Morison equation is often sufficient to estimate the hydrodynamic added mass and the hydrodynamic excitation force. However, for complex structures this equation does not correct for the diffraction of the waves by the structure and does not correct the added mass and damping effects due to the radiation of the waves from the structure. Furthermore, hydrodynamic coupling coefficients are not calculated for these parts of the structure.

For the semisubmersible in this work, the connecting pontoons is specified as Morison equation members, resulting in a hybrid approach between potential flow software and an analytical approximation. This resulted in differences in the hydrodynamic properties and coupling effects for these connecting pontoons, which was particularly noticeable for the rotational degrees of freedom of the structure, as the added mass and damping is underestimated.

Equivalent moment estimation

The frequency-domain method was limited by estimation of only rigid body modes for the floater. Therefore, the response around the first bending mode of the tower was not estimated in the frequency-domain method. Especially for relatively soft towers, as used in the industry project, this underestimated the response around the first bending mode of the tower.

Furthermore, for the cases with the lowest and highest wind speed noticeable differences were present around the wind frequency range. These differences are the result of accumulated differences found in the comparisons of the mean response and rigid-body mode response. Therefore, it was inherently difficult to compare these statistics and determine the main contributors to the difference in response.

Finally, in Section 8.8 the estimation of the equivalent bending moment of the frequency-domain method was compared with the results of the time-domain simulations. In this comparison the equivalent stress was underestimated by the frequency-domain method. As there were already differences observed for equivalent bending moment, the differences in the total DLC 1.2 equivalent bending moment were inseparable from possible differences resulting from the spectral approach used for the cycles counting estimate.

10

Conclusion and Recommendations

This thesis is concluded by answering the research questions and recommendations for future work. Section 10.1 answers the sub-questions in consideration of the limitations presented in Chapter 9. This leads answering the main research question in Section 10.2. Finally, based on the limitations and the answers of the research questions, recommendations for future work are presented in Section 10.3

10.1. Sub-questions

The research performed for sub-questions 1, 2, and 3 is presented in Chapter 6, Chapter 7, and Chapter 8 respectively. The sub-questions and the answer to those questions are as follows:

SQ1: How does inclusion of the yaw motion of a semi-submersible FOWT contribute to the rotational dynamic response under misaligned wind and waves in a frequency-domain method?

The yaw response can increase the roll response at excitation angles where the structure is not symmetrical. Furthermore, waves with peak periods associated with wavelengths around the apparent wavelength of the structure noticeably increase the yaw response and the roll response via yaw-roll coupling. Therefore, it is recommended to consider this degrees of freedom in a frequency-domain method when the roll response is of interest and the structure is subjected to misaligned wind and wave conditions.

SQ2: What is the contribution of aerodynamic damping to the response of a semi-submersible floating offshore wind turbine, considering misalignment of wind and waves with respect to floater orientation?

Up to rated wind speed the aerodynamic damping increases proportional to the thrust. Above rated wind speed the aerodynamic damping reduces slightly while the thrust reduces noticeably. This results in an increased low frequency response due to a lower mooring stiffness and an increased excitation around and above the natural frequency due to the reduced aerodynamic damping.

Furthermore, a change in wind direction changes the angle in which aerodynamic damping is present. This increases the response to wave excitations that are misaligned to the wind only slightly as no second-order excitation is considered.

SQ3: How effective is a frequency-domain method compared to a time-domain method at estimating the equivalent bending moment at the tower base for misaligned wind, windsea waves, and swells?

For load cases slightly above the rated wind speed the frequency-domain method can estimate the equivalent bending moment within an error of 5%. For the lowest and highest production wind speeds errors ranging from an underestimation of 22% to an overestimation of 50% are observed. Furthermore, this frequency domain this method is not effective in estimating the equivalent bending moment at the tower base for a set of industry project load cases (DLC 1.2) where an error of 56% is observed.

10.2. Main research question

By analysing the response characteristics of a semi-submersible floating offshore wind turbine using a frequency-domain method, this thesis has quantified the contribution of yawing and aerodynamic damping to the response. Furthermore, a comprehensive comparison of the frequency-domain method against time-domain simulations has shown that a reasonable response is possible in the wave frequency range. However, significant differences are found in the wind frequency range. The contribution to the loads at the tower base is identified and this leads to answering the research question:

What is the effect of misaligned wind, windsea waves, and swells on the loads at the tower base of a semi-submersible type floating offshore wind turbine?

Misalignment of wind and waves can increase the response at the tower base due to coupling effects and reduced aerodynamic damping in the direction of the rotor plane. A misalignment of the wind direction with respect to a floater symmetry axis may increase the response perpendicular to the rotor plane (side-side direction). If the wavelength is equal to the apparent length of the floater and the wave heading is misaligned with respect to a floater symmetry axis, the yaw excitation may increase the roll response due to yaw-roll coupling effects. However, the wind-wave misalignment may also have a mitigating effect on the maximum response as aerodynamic damping also reduces the response in the wave frequency range.

This research quantifies the sensitivities of floating offshore wind turbines under misaligned wind and waves using a frequency-domain method. A frequency-domain method is developed which showed its potential for load estimation in an early design stage, sensitivity studies, and optimisation tasks due to its computationally efficiency.

However, the accuracy of the estimated response depends on many variables due to the complexity of the system. To improve the estimated response by the method it is recommended to improve the mooring stiffness estimation, aerodynamic properties, and tower base bending moment estimate in future research. Concrete proposals are presented in Section 10.3.

10.3. Recommendations for future work

This section provides recommendations for future work. These recommendations are divided into recommendations for fundamental research and suggestions for applied research on the frequency-domain method. These suggestions are based on the limitations presented in Chapter 9.

Future work: fundamental research

The sensitivity studies were limited by the lack of second order wave forces. It is recommended for future work to implement this into the frequency domain method and quantify the effects of an increased response around the yaw natural frequency on the roll response. As the (aerodynamic) damping effects are most pronounced around the natural frequencies, it is also recommended to evaluate the damping effects on the second order wave excitation for different wave conditions.

Furthermore, the comparison of the frequency-domain method was limited by the comparison of very low frequencies by the duration of the time traces in the time-domain method. To compare these low frequencies it is recommended to increase the duration of the time-domain simulations for the cases. Instead of simulating 10 minutes (600 seconds) it is recommended to simulate 1 hour (3600 seconds). This would result in a lowest comparable frequency of 1/3600 Hz, which is lower than the 1/1000 Hz used as the lower frequency limit in the frequency-domain method. It should then be possible to compare starting from this lower limit and also compare the response in the range of the surge, sway, and yaw natural frequencies.

The research on the effect of floater orientation was compared with existing time-domain simulations. However, as differences were found, it is recommended to improve such a frequency-domain method and then focus on a more comprehensive comparison of the results with time-domain simulations. As only four individual cases were compared in this study, it was not possible to specify which cases contribute most significantly to the difference in the total equivalent bending moment estimated in Section 8.8. It is recommended to increase the number of cases used in a comparison/verification to better indicate what the main factors are for the difference in the bending moment estimate.

Future work: applied research

As discussed in Chapter 9, several limitations are identified that results in differences between the frequency-domain method and time-domain method.

A first recommendation is to improve the mooring stiffness estimation. As presented by Xu *et al.* [58], mooring systems for FOWTs in shallower water depths show more non-linear behaviour of the mooring line tension for increasing surge/sway offset. Furthermore, it was not possible to configure complex mooring systems, such as different chain/line types. The combination of shallower water depth and the simplification of the mooring system led to an underestimation of the mooring system, resulting in an overestimation of the mean response and the low-frequency dynamic response of sway and pitch. Through coupling effects this also affected the overestimation of the pitch and roll responses, which were found to be the load driving modes.

Secondly, it is recommended to implement the first tower bending modes (fore-aft and side-to-side) as degrees of freedom of the method. The softer tower design of industry projects compared to research reference designs [7] results in noticeable response around the first tower bending frequency. An approach to implement this first tower bending mode is provided by Pegalajar-Jurado *et al.* [2].

Lastly, capturing the aerodynamics of a floating offshore wind turbine in the frequency-domain method is an ongoing field of research [47]. The main reason for this is the dynamic behaviour of the system due to turbulence and dynamic response of the structure, resulting in increased controller action. To improve the response characteristics and account for controller action it is recommended to consider a frequency dependent aerodynamic coefficients [47] or consider the use of a parent model [2].

References

[1] R. Lupton, “Frequency-domain modelling of floating wind turbines,” Ph.D. dissertation, University of Cambridge, Cambridge, Dec. 2014.

[2] A. Pegalajar-Jurado, M. Borg, and H. Bredmose, “An efficient frequency-domain model for quick load analysis of floating offshore wind turbines,” *Wind Energy Science*, vol. 3, no. 2, pp. 693–712, 2018, ISSN: 23667451. DOI: 10.5194/wes-3-693-2018.

[3] J. M. Hegseth and E. E. Bachynski, “A semi-analytical frequency domain model for efficient design evaluation of spar floating wind turbines,” *Marine Structures*, vol. 64, pp. 186–210, Mar. 2019, ISSN: 09518339. DOI: 10.1016/j.marstruc.2018.10.015.

[4] National Renewable Energy Laboratory, *RAFT*, 2021.

[5] G. R. Fulton *et al.*, “Semi-Submersible Platform and Anchor Foundation Systems for Wind Turbine Support,” Tech. Rep., 2004. [Online]. Available: http://www.osti.gov/bridge.

[6] J. M. Jonkman and M. L. Buhl, “Development and Verification of a Fully Coupled Simulator for Offshore Wind Turbines: Preprint,” in *45th AIAA Aerospace Sciences Meeting and Exhibit, Wind Energy Symposium*, Reno, Nevada: NREL, Jan. 2007. [Online]. Available: http://www.osti.gov/bridge.

[7] C. Allen *et al.*, “Definition of the UMaine VolturnUS-S Reference Platform Developed for the IEA Wind 15-Megawatt Offshore Reference Wind Turbine Technical Report,” Tech. Rep., 2020. [Online]. Available: www.nrel.gov/publications..

[8] H. Bagbanci, D. Karmakar, and C. G. Soares, “Comparison of spar and semisubmersible floater concepts of offshore wind turbines using long-term analysis,” *Journal of Offshore Mechanics and Arctic Engineering*, vol. 137, no. 6, 2015, ISSN: 1528896X. DOI: 10.1115/1.4031312.

[9] D. Karmakar, H. Bagbanci, and C. Guedes Soares, “Long-term extreme load prediction of spar and semisubmersible floating wind turbines using the environmental contour method,” *Journal of Offshore Mechanics and Arctic Engineering*, vol. 138, no. 2, Apr. 2016, ISSN: 1528896X. DOI: 10.1115/1.4032099.

[10] A. R. Nejad *et al.*, “Stochastic dynamic load effect and fatigue damage analysis of drivetrains in land-based and TLP, spar and semi-submersible floating wind turbines,” *Marine Structures*, vol. 42, pp. 137–153, Jul. 2015, ISSN: 09518339. DOI: 10.1016/j.marstruc.2015.03.006.

[11] A. J. Goupee, B. J. Koo, R. W. Kimball, K. F. Lambrakos, and H. J. Dagher, “Experimental comparison of three floating wind turbine concepts,” *Journal of Offshore Mechanics and Arctic Engineering*, vol. 136, no. 2, Mar. 2014, ISSN: 1528896X. DOI: 10.1115/1.4025804.

[12] S. Butterfield, W. Musial, J. Jonkman, and P. Sclavounos, “Engineering Challenges for Floating Offshore Wind Turbines,” in *Copenhagen Offshore Wind Conference*, Boulder: NREL, Sep. 2005. [Online]. Available: http://www.osti.gov/bridge.

[13] M. Leimeister, A. Kolios, and M. Collu, “Critical review of floating support structures for offshore wind farm deployment,” in *Journal of Physics: Conference Series*, vol. 1104, Institute of Physics Publishing, Nov. 2018. DOI: 10.1088/1742-6596/1104/1/012007.

[14] W. Musial *et al.*, “Offshore Wind Market Report: 2021 Edition,” Tech. Rep., 2021.

[15] T. Sebastian and M. A. Lackner, “A Comparison of First-Order Aerodynamic Analysis Methods for Floating Wind Turbines,” Tech. Rep., 2010.

[16] D. A. Peters and C. Shyi-Yuang, “Momentum Theory, Dynamic Inflow, and the Vortex-Ring State,” *JOURNAL OF THE AMERICAN HELICOPTER SOCIETY*, vol. 27, no. 3, pp. 18–24, Jul. 1982.

[17] R. Fontecha, F. Kemper, and M. Feldmann, “On the Determination of the Aerodynamic Damping of Wind Turbines Using the Forced Oscillations Method in Wind Tunnel Experiments,” *Energies*, vol. 12, Jun. 2019. DOI: https://doi.org/10.3390/en12122452. [Online]. Available: www.mdpi.com/journal/energies.

[18] L. S. Silva, B. S. Cazzolato, N. Y. Sergiienko, and B. Ding, “Efficient estimation of the nonlinear aerodynamic loads of floating offshore wind turbines under random waves and wind in frequency domain,” *Journal of Ocean Engineering and Marine Energy*, vol. 7, no. 3, pp. 287–303, Aug. 2021, ISSN: 21986452. DOI: 10.1007/s40722-021-00203-0.

[19] L. Barj *et al.*, “Wind/Wave Misalignment in the Loads Analysis of a Floating Offshore Wind Turbine,” in *32nd ASME Wind Energy Symposium*, 2014. [Online]. Available: www.nrel.gov/publications..

[20] J. M. Jonkman, “Dynamics Modeling and Loads Analysis of an Offshore Floating Wind Turbine,” Ph.D. dissertation, 2007. [Online]. Available: http://www.osti.gov/bridge.

[21] D. Matha, F. Sandner, and D. Schlipf, “Efficient critical design load case identification for floating offshore wind turbines with a reduced nonlinear model,” in *Journal of Physics: Conference Series*, vol. 555, Institute of Physics Publishing, 2014. DOI: 10.1088/1742-6596/555/1/012069.

[22] J. M. J. Journée and W. W. Massie, *OFFSHORE HYDROMECHANICS*, 1st ed. Delft: Delft University of Technology, Jan. 2001.

[23] A. N. Robertson *et al.*, “OC5 Project Phase II: Validation of Global Loads of the DeepCwind Floating Semisubmersible Wind Turbine,” in *Energy Procedia*, vol. 137, Elsevier Ltd, 2017, pp. 38–57. DOI: 10.1016/j.egypro.2017.10.333.

[24] M. A. Benitz *et al.*, “Validation of Hydrodynamic Load Models Using CFD for the OC4-DeepCwind Semisubmersible: Preprint,” Tech. Rep., 2015. [Online]. Available: www.nrel.gov/publications..

[25] F. Lemmer, W. Yu, and P. W. Cheng, “Iterative frequency-domain response of floating offshorewind turbines with Parametric drag,” *Journal of Marine Science and Engineering*, vol. 6, no. 4, Oct. 2018, ISSN: 20771312. DOI: 10.3390/jmse6040118.

[26] S. Zhou, C. Li, Y. Xiao, and P. W. Cheng, “Importance of platform mounting orientation of Y-shaped semi-submersible floating wind turbines: A case study by using surrogate models,” *Renewable Energy*, vol. 156, pp. 260–278, Aug. 2020, ISSN: 18790682. DOI: 10.1016/j.renene.2020.04.014.

[27] E. E. Bachynski, M. I. Kvittem, C. Luan, and T. Moan, “Wind-wave misalignment effects on floating wind turbines: Motions and tower load effects,” *Journal of Offshore Mechanics and Arctic Engineering*, vol. 136, no. 4, Nov. 2014, ISSN: 1528896X. DOI: 10.1115/1.4028028.

[28] E. E. Bachynski, M. I. Kvittem, C. Luan, and T. Moan, “Fatigue damage characteristics of a semisubmersible-type floating offshore wind turbine at tower base,” *Journal of Renewable and Sustainable Energy*, vol. 8, no. 5, Sep. 2016, ISSN: 19417012. DOI: 10.1063/1.4964366.

[29] T. w. Kang, E. s. Kim, and H. i. Yang, “Effects of Dynamic Motion and Structural Response of a Semi-submersible Floating Offshore Wind Turbine Structure Under Waves Generated in a Hurricane Environment,” *International Journal of Precision Engineering and Manufacturing - Green Technology*, 2021, ISSN: 21980810. DOI: 10.1007/s40684-021-00331-w.

[30] S. Zhou *et al.*, “Directionality effects of aligned wind and wave loads on a Y-shape semi-submersible floating wind turbine under rated operational conditions,” *Energies*, vol. 10, no. 12, Dec. 2017, ISSN: 19961073. DOI: 10.3390/en10122097.

[31] D. Matha, M. Schlipf, G. Hassan, P. R. Ltd Pereira, and J. Jonkman, “Challenges in Simulation of Aerodynamics, Hydrodynamics, and Mooring-Line Dynamics of Floating Offshore Wind Turbines,” Tech. Rep., 2011. [Online]. Available: http://www.osti.gov/bridge.

[32] A. Robertson *et al.*, “OFFSHORE CODE COMPARISON COLLABORATION CONTINUATION WITHIN IEA WIND TASK 30: PHASE II RESULTS REGARDING A FLOATING SEMISUBMERSIBLE WIND SYSTEM,” in *ASME 2014 33rd International Conference on Ocean, Offshore and Arctic Engineering*, San Francisco, California, USA: ASME, Jun. 2014. [Online]. Available: http://www.asme.org/about-asme/terms-of-use.

[33] A. Natarajan, M. H. Hansen, and S. Wang, “Design Load Basis for Offshore Wind turbines: DTU Wind,” Tech. Rep., 2016.

[34] G. M. Stewart, “Design Load Analysis of Two Floating Offshore Wind Turbine Design Load Analysis of Two Floating Offshore Wind Turbine Concepts,” Tech. Rep., 2016. [Online]. Available: https://scholarworks.umass.edu/dissertations_2.

[35] C. B. Li and J. Choung, “Fatigue damage analysis for a floating offshore wind turbine mooring line using the artificial neural network approach,” *Ships and Offshore Structures*, vol. 12, S288–S295, Mar. 2017, ISSN: 17445302. DOI: 10.1080/17445302.2016.1254522.

[36] A. Pegalajar-Jurado and H. Bredmose, “Reproduction of slow-drift motions of a floating wind turbine using second-order hydrodynamics and Operational Modal Analysis,” *Marine Structures*, vol. 66, pp. 178–196, Jul. 2019, ISSN: 09518339. DOI: 10.1016/j.marstruc.2019.02.008.

[37] F. J. Madsen *et al.*, “D7.8 Required numerical model fidelity in various design phases,” Tech. Rep., 2018.

[38] J. M. Hegseth, E. E. Bachynski, and J. R. Martins, “Integrated design optimization of spar floating wind turbines,” *Marine Structures*, vol. 72, Jul. 2020, ISSN: 09518339. DOI: 10.1016/j.marstruc.2020.102771.

[39] G. Ramachandran, A. Robertson, J. Jonkman, and M. Masciola, “Investigation of Response Amplitude Operators for Floating Offshore Wind Turbines,” in *Twenty-third (2013) International Offshore and Polar EngineeringAnchorage, Alaska, USA*, International Society of Offshore and Polar Engineers, 2013, pp. 369–376, ISBN: 9781880653999.

[40] M. Borg *et al.*, “D4.7 Models for advanced load effects and loads at component level,” DTU, Copenhagen, Tech. Rep., 2018.

[41] S. Ahmada, N. Islam, and A. Ali, “Wind-induced response of a tension leg platform,” *Journal of Wind Engineering and Industrial Aerodynamics*, vol. 72, pp. 225–240, 1997.

[42] T.-W. Kang, H.-I. Yang, and E.-S. Kim, “Evaluation of the effect of hurricane induced swell on the global response of floating offshore wind turbine,” Incheon, 2018.

[43] E. E. Bachynski, “Design and Dynamic Analysis of Tension Leg Platform Wind Turbines,” Ph.D. dissertation, Norwegian University of Science and Technology, Trondheim, Mar. 2014, ISBN: 978-82-326-0096-0.

[44] Y. Liu, “HAMS: A frequency-domain preprocessor for wave-structure interactions-Theory, development, and application,” *Journal of Marine Science and Engineering*, vol. 7, no. 3, 2019, ISSN: 20771312. DOI: 10.3390/jmse7030081.

[45] E. Gaertner *et al.*, “Definition of the IEA Wind 15-Megawatt Offshore Reference Wind Turbine Technical Report,” Tech. Rep., 2020. [Online]. Available: www.nrel.gov/publications..

[46] S. A. Ning, “A simple solution method for the blade element momentum equations with guaranteed convergence,” *Wind Energy*, vol. 17, no. 9, pp. 1327–1345, 2014, ISSN: 10991824. DOI: 10.1002/we.1636.

[47] C. E. S. Souza, J. M. Hegseth, and E. E. Bachynski, “Frequency-Dependent Aerodynamic Damping and Inertia in Linearized Dynamic Analysis of Floating Wind Turbines,” in *Journal of Physics: Conference Series*, vol. 1452, Institute of Physics Publishing, Mar. 2020. DOI: 10.1088/1742-6596/1452/1/012040.

[48] C. Lee and J. Newman, “WAMIT USER MANUAL Version 7.4,” WAMIT, Inc., Chestnut Hill, MA, Tech. Rep., 2020. [Online]. Available: www.wamit.com.

[49] J. N. Newman, *Marine Hydrodynamics*, 40th Ann. Edition. Massachusetts: The MIT Press, 1977.

[50] D. Benasciutti and R. Tovo, “Fatigue life assessment in non-Gaussian random loadings,” *International Journal of Fatigue*, vol. 28, no. 7, pp. 733–746, Jul. 2006, ISSN: 01421123. DOI: 10.1016/j.ijfatigue.2005.09.006.

[51] M. Mršnik, J. Slavič, and M. Boltežar, “Frequency-domain methods for a vibration-fatigue-life estimation - Application to real data,” *International Journal of Fatigue*, vol. 47, pp. 8–17, Feb. 2013, ISSN: 01421123. DOI: 10.1016/j.ijfatigue.2012.07.005.

[52] A. S. H. Makhlouf and M. Aliofkhazraei, *Handbook of materials failure analysis : with case studies from the chemicals, concrete and power industries*. Oxford: Elsevier, 2016, ISBN: 9780081001165.

[53] L. H. Holthuijsen, *Waves in Oceanic and Coastal Waters*. Delft: Cambridge University Press, 2007.

[54] A. Niesłony and M. Böhm, "Mean stress value in spectral method for the determination of fatigue life," *Acta Mechanica et Automatica*, vol. 6, no. 2, 2012. [Online]. Available: https://www.researchgate.net/publication/266886683.

[55] T. Łagoda, E. Macha, and R. Pawliczek, "The influence of the mean stress on fatigue life of 10HNAP steel under random loading," Tech. Rep., 2001, pp. 283–291. [Online]. Available: www.elsevier.com/locate/ijfatigue.

[56] Joblib Development Team, *Joblib: running Python functions as pipeline jobs*, 2020. [Online]. Available: https://joblib.readthedocs.io/.

[57] X. Li, C. Zhu, Z. Fan, X. Chen, and J. Tan, "Effects of the yaw error and the wind-wave misalignment on the dynamic characteristics of the floating offshore wind turbine," *Ocean Engineering*, vol. 199, Mar. 2020, ISSN: 00298018. DOI: 10.1016/j.oceaneng.2020.106960.

[58] K. Xu *et al.*, "Design and comparative analysis of alternative mooring systems for floating wind turbines in shallow water with emphasis on ultimate limit state design," *Ocean Engineering*, vol. 219, Jan. 2021, ISSN: 00298018. DOI: 10.1016/j.oceaneng.2020.108377.

[59] C. E. S. Souza, "Structural modelling, coupled dynamics, and design of large floating wind turbines," Ph.D. dissertation, 2022, ISBN: 978-82-326-6551-8.

A

Updated wind and wave PSDs

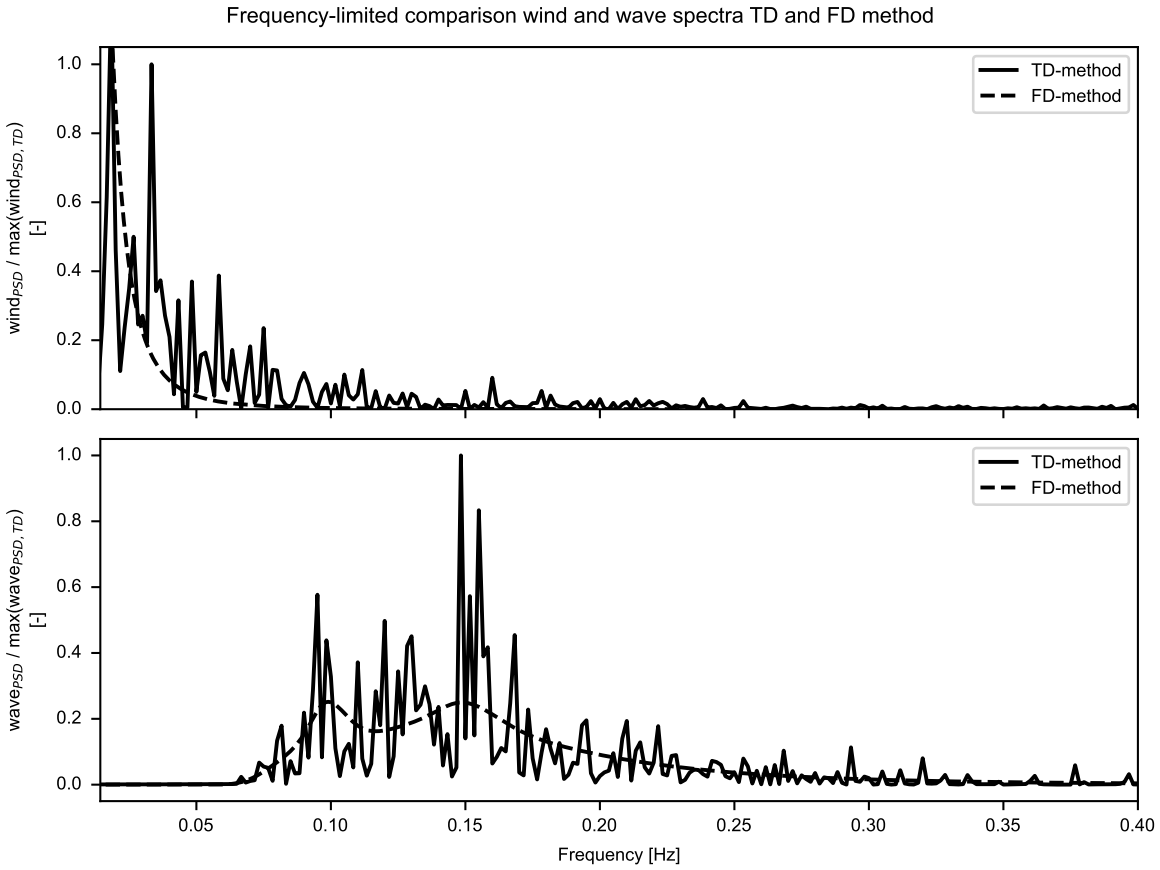

Figure A.1: Updated normalised Wind and Wave PSD comparison, comparison case 1.

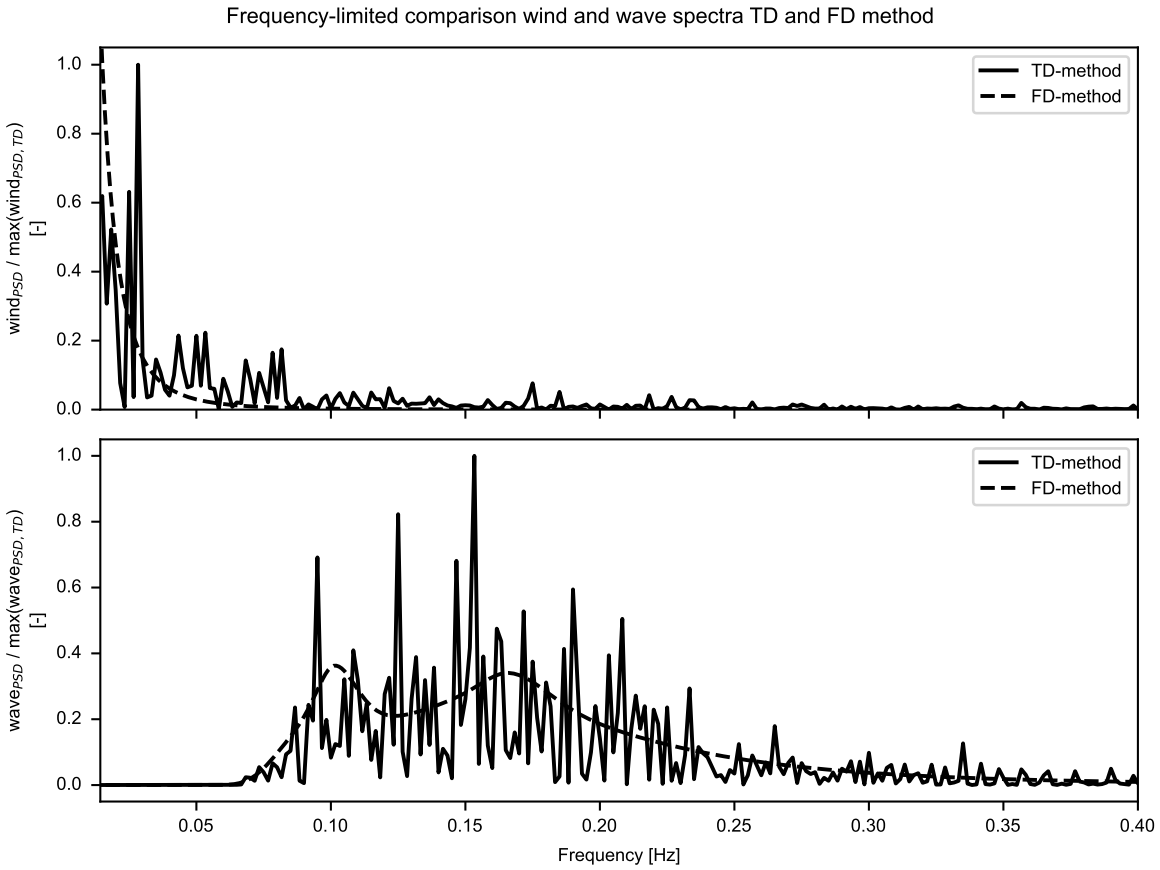

Figure A.2: Updated normalised Wind and Wave PSD comparison, comparison case 2.

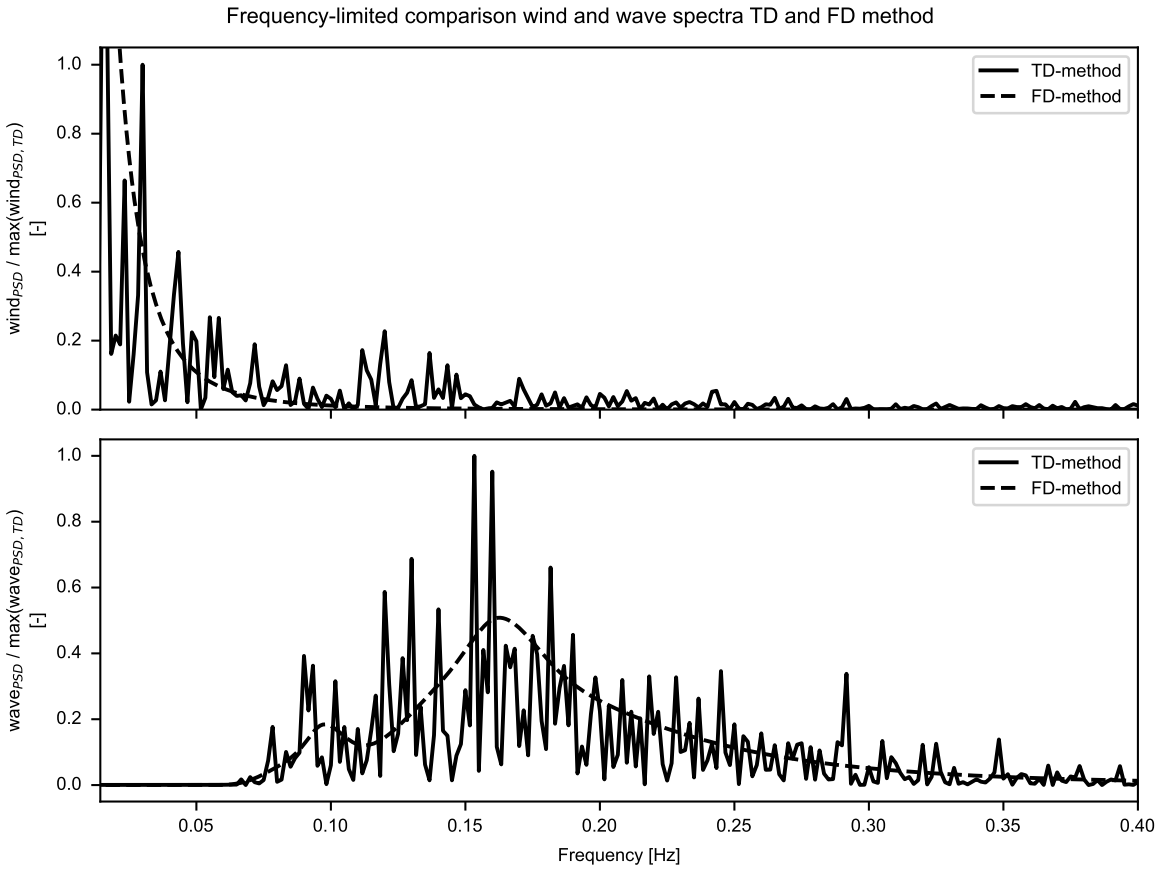

Figure A.3: Updated normalised Wind and Wave PSD comparison, comparison case 3.

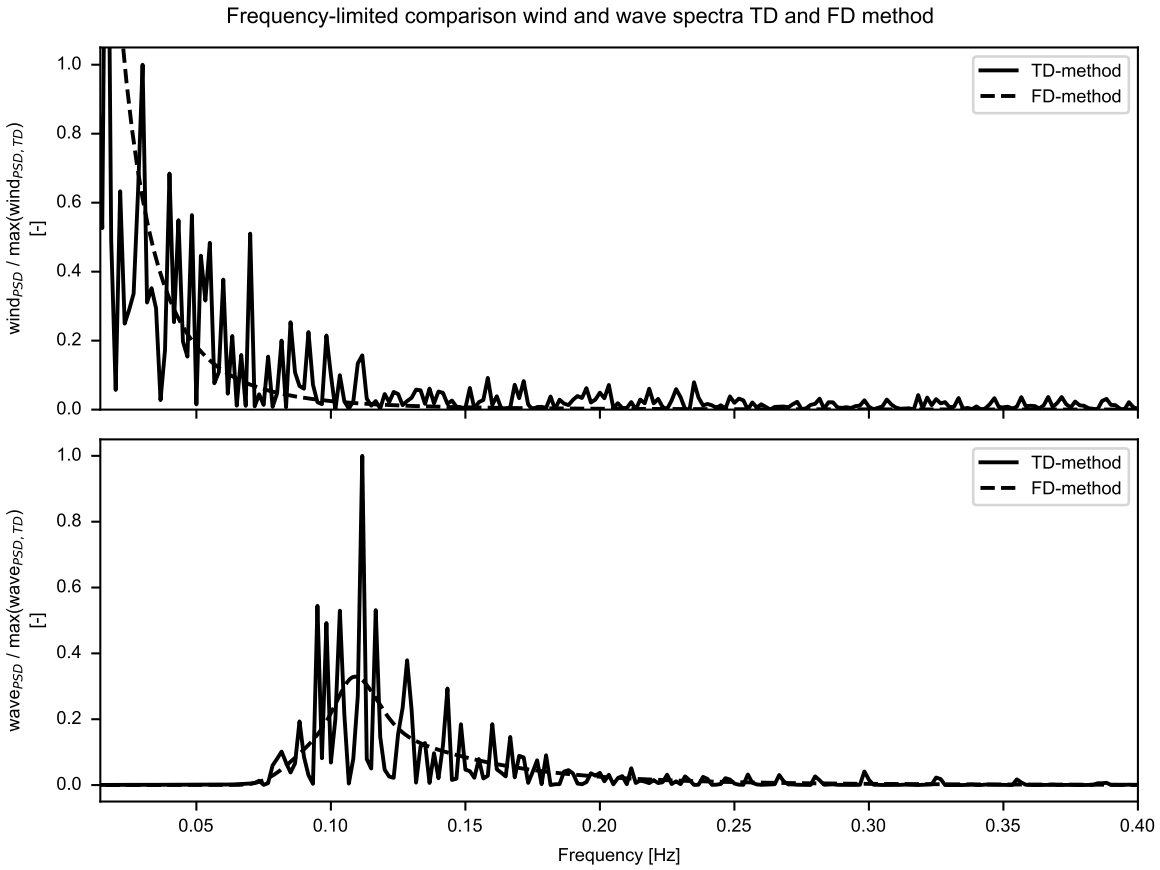

Figure A.4: Updated normalised Wind and Wave PSD comparison, comparison case 4.

B

Wave excitation potential flow

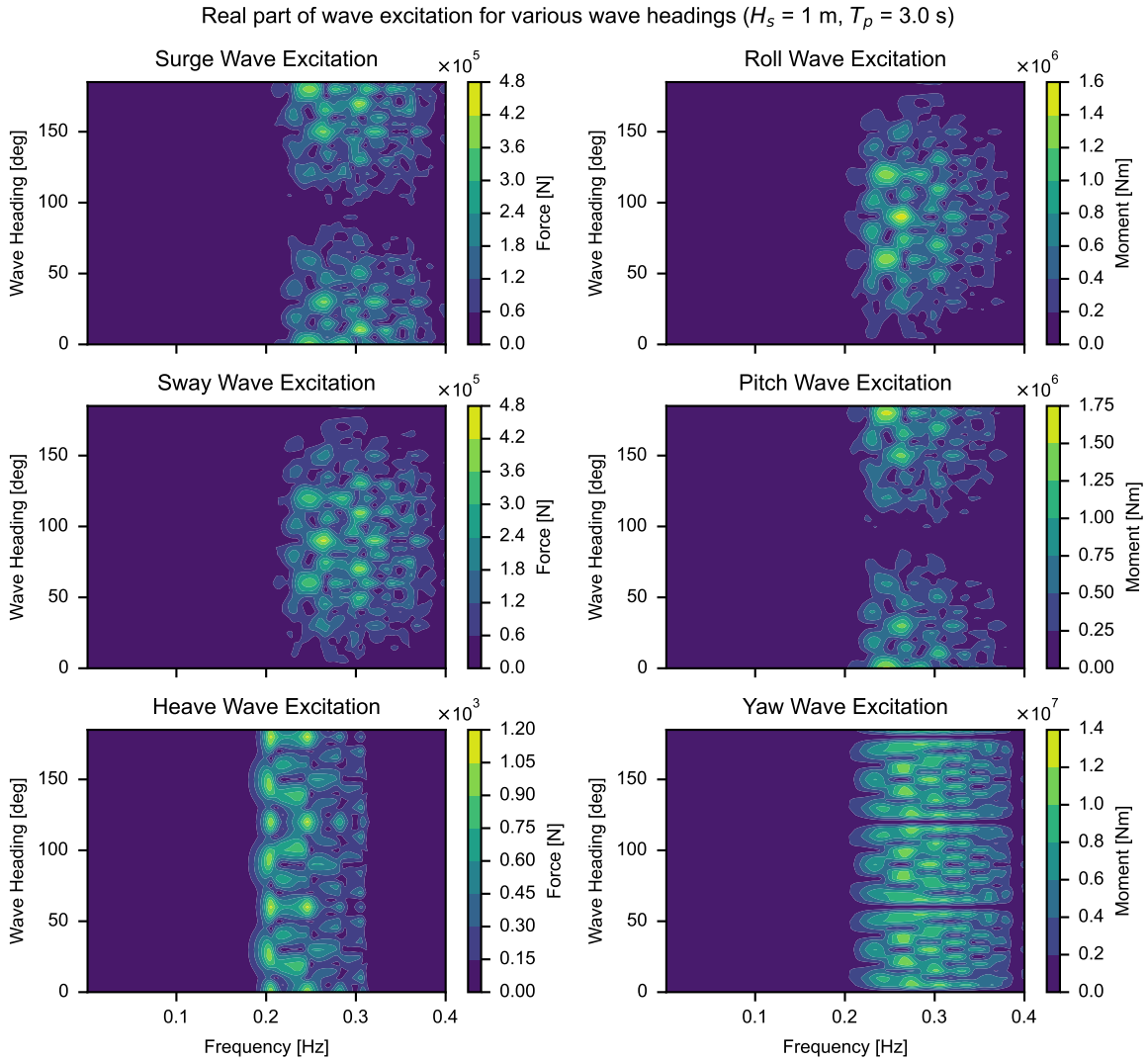

Figure B.1: Wave excitation RAO for 6 DOF's, multiplied by wave elevation from JONSWAP ($T_p = 3.0$, $H_s = 1$, $\gamma = 1$).

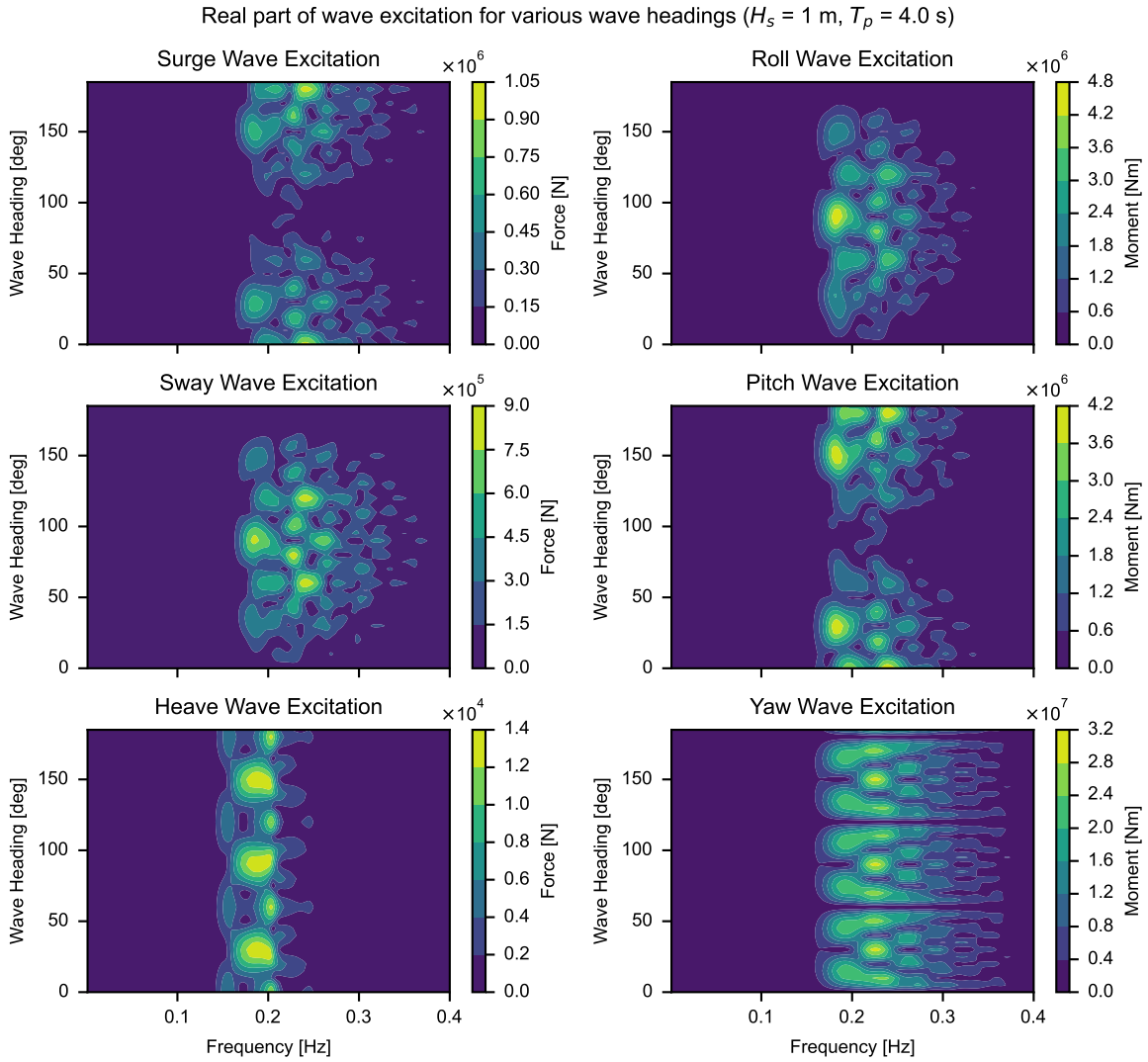

Figure B.2: Wave excitation RAO for 6 DOF's, multiplied by wave elevation from JONSWAP ($T_p = 4.0$, $H_s = 1$, $\gamma = 1$).

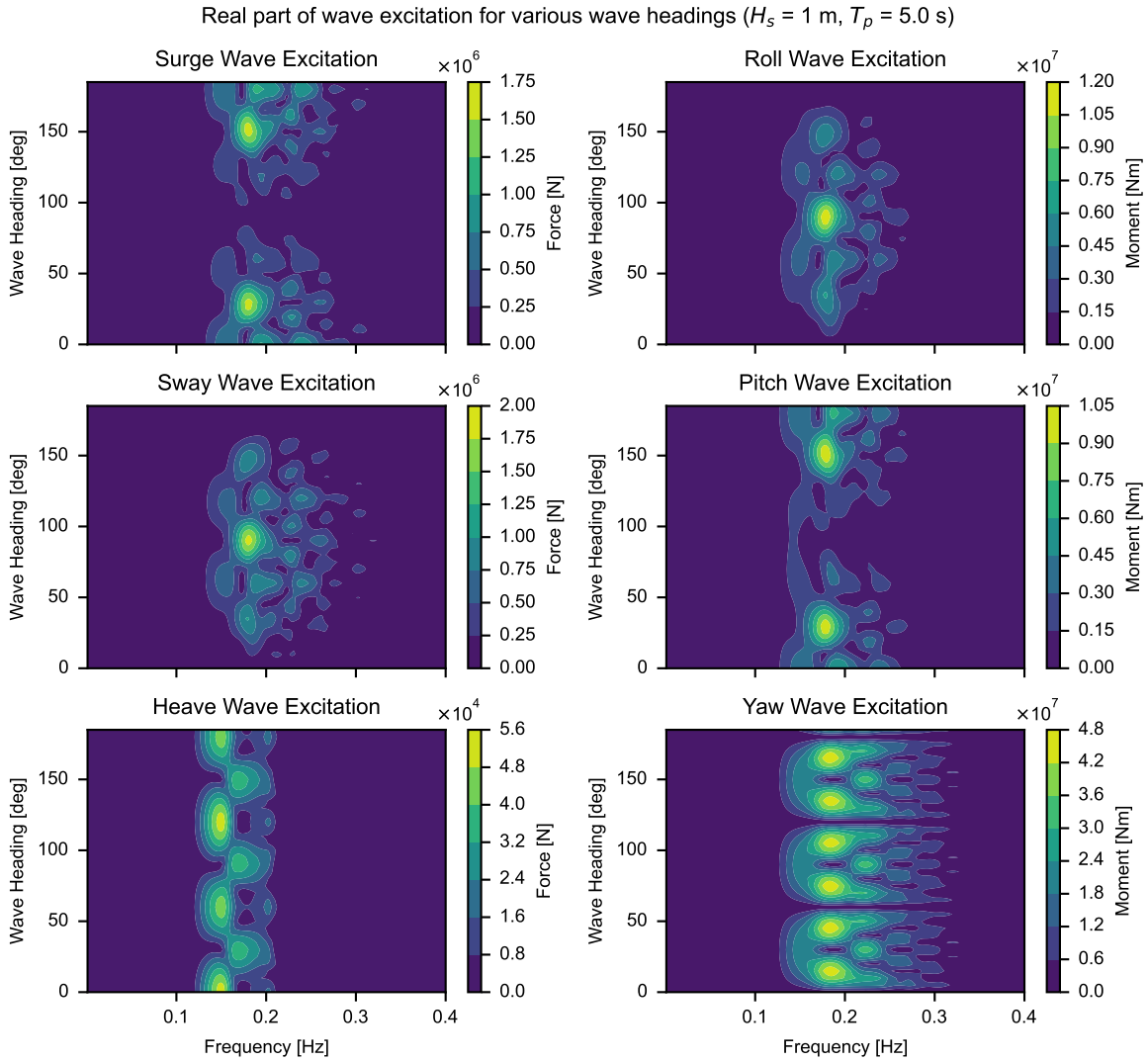

Figure B.3: Wave excitation RAO for 6 DOF's, multiplied by wave elevation from JONSWAP ($T_p = 5.0$, $H_s = 1$, $\gamma = 1$).

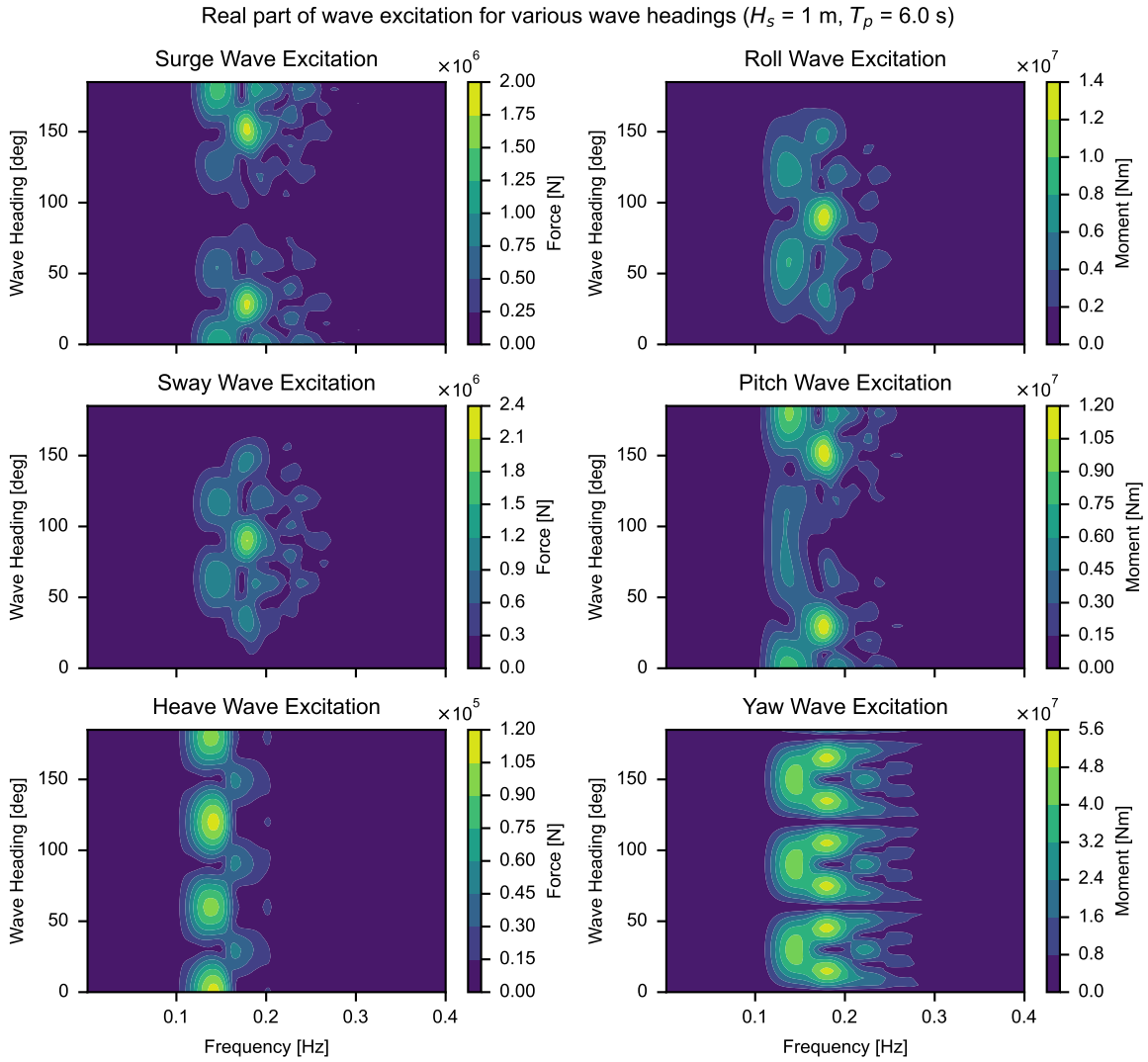

Figure B.4: Wave excitation RAO for 6 DOF's, multiplied by wave elevation from JONSWAP ($T_p = 6.0$, $H_s = 1$, $\gamma = 1$).

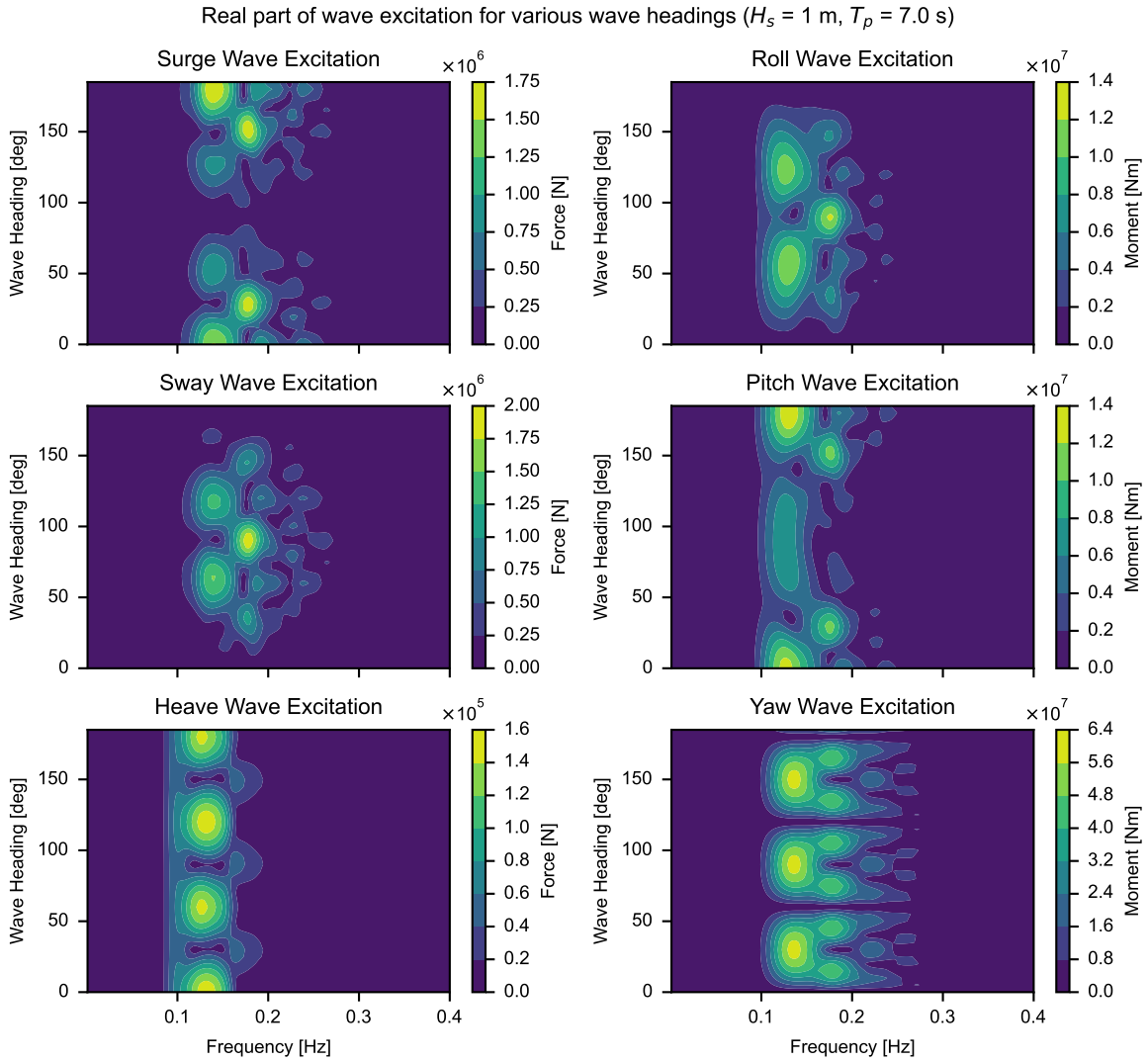

Figure B.5: Wave excitation RAO for 6 DOF's, multiplied by wave elevation from JONSWAP ($T_p = 7.0$, $H_s = 1$, $\gamma = 1$).

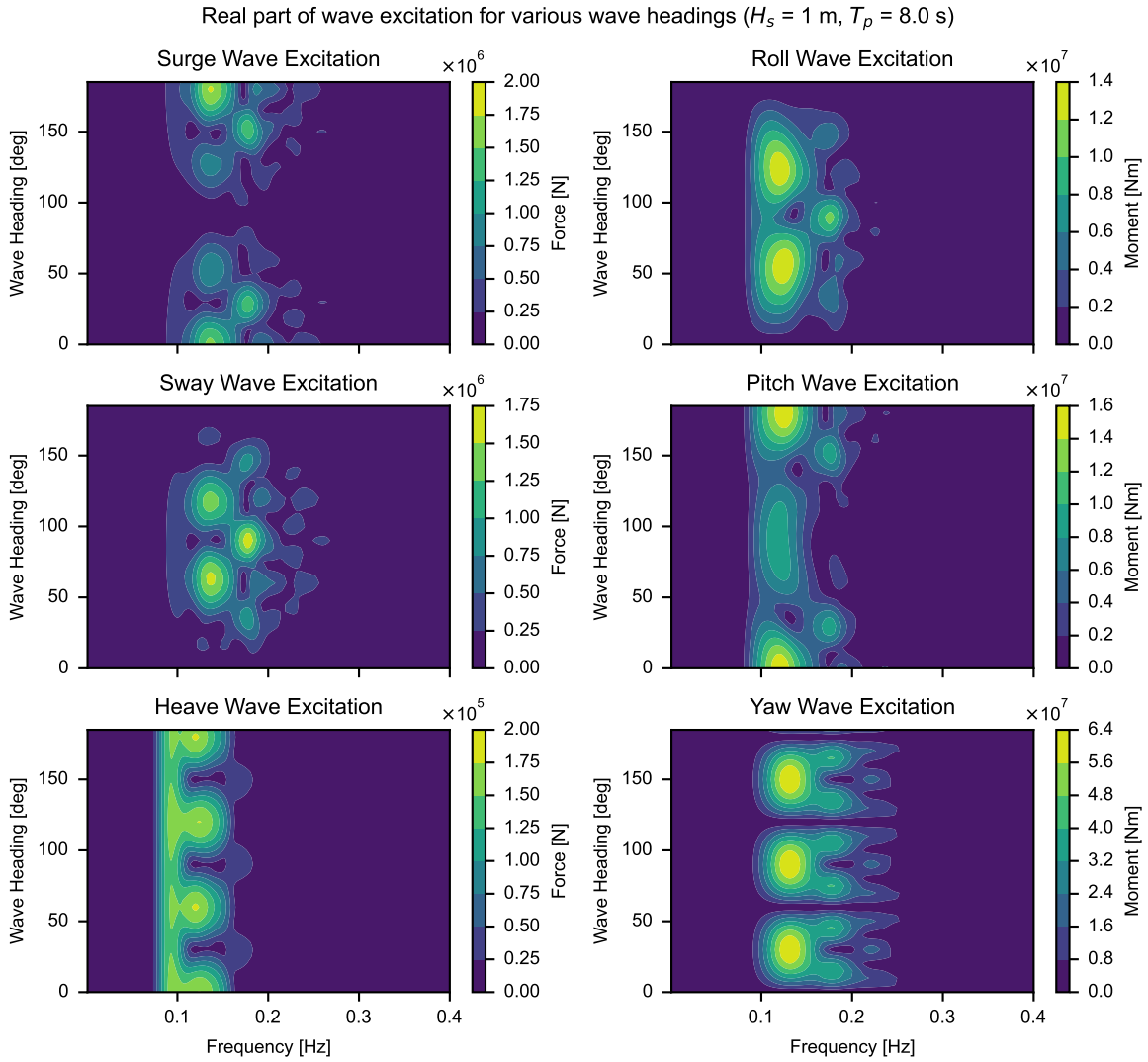

Figure B.6: Wave excitation RAO for 6 DOF's, multiplied by wave elevation from JONSWAP ($T_p = 8.0$, $H_s = 1$, $\gamma = 1$).

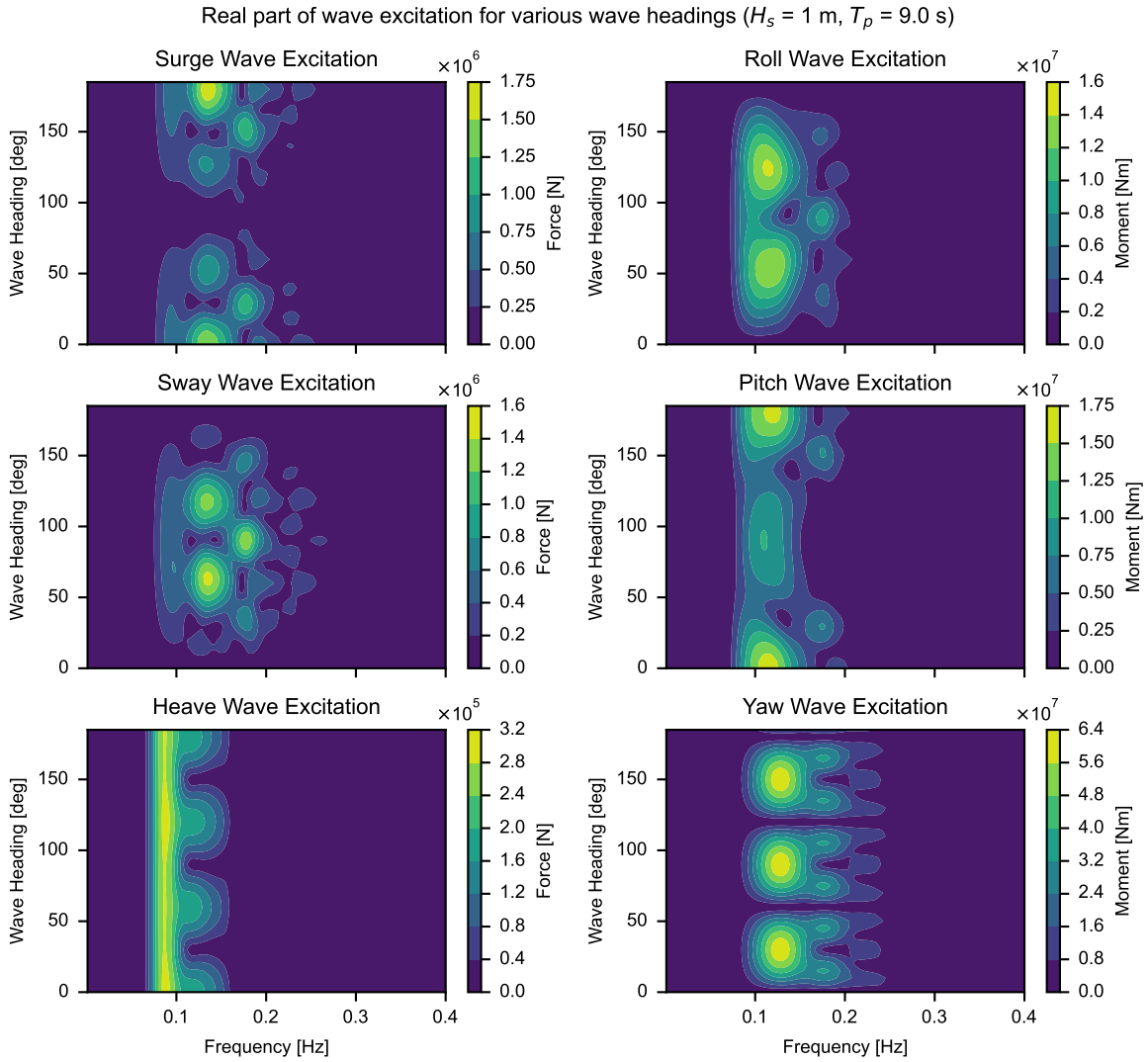

Figure B.7: Wave excitation RAO for 6 DOF's, multiplied by wave elevation from JONSWAP ($T_p = 9.0$, $H_s = 1$, $\gamma = 1$).

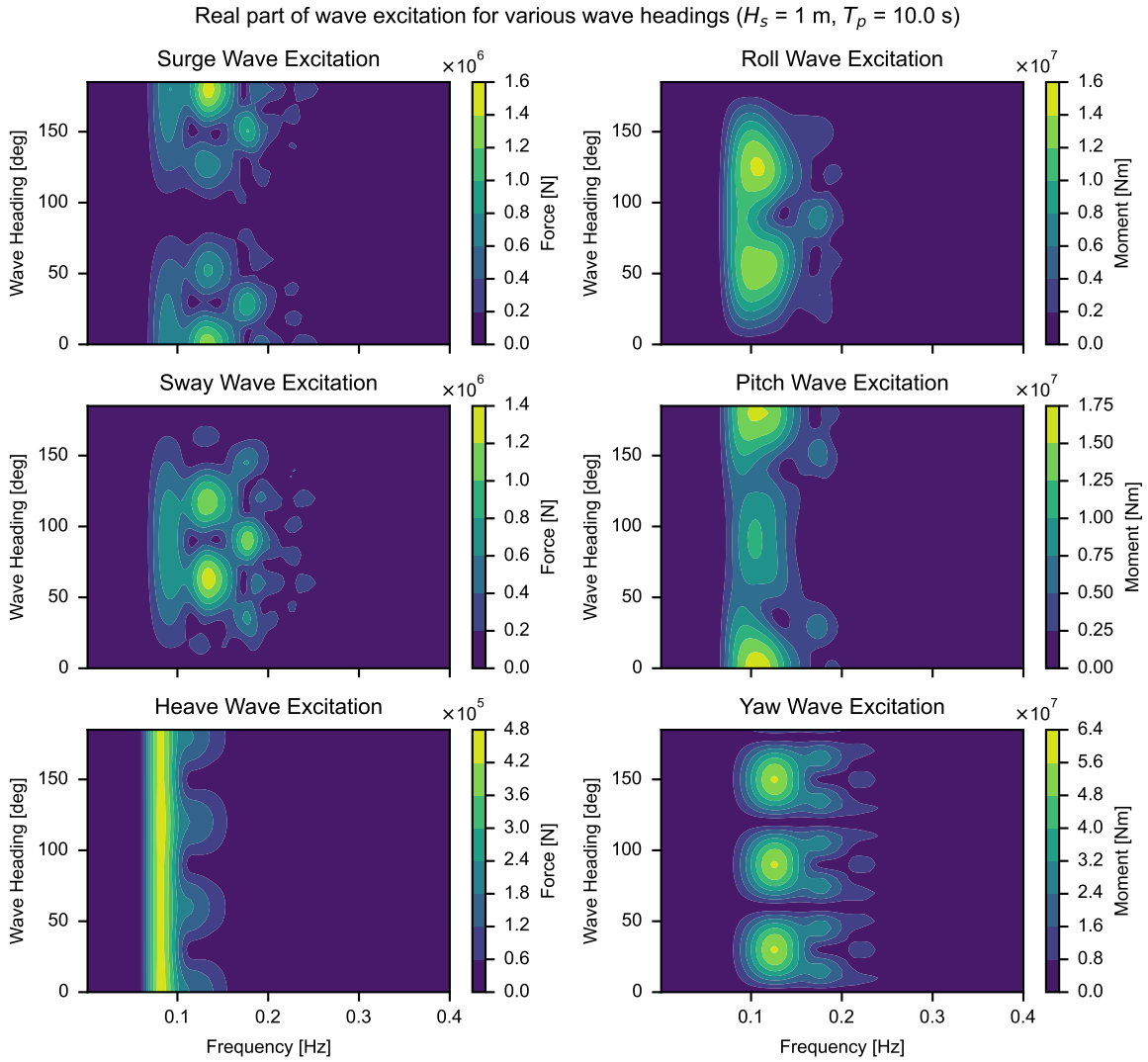

Figure B.8: Wave excitation RAO for 6 DOF's, multiplied by wave elevation from JONSWAP ($T_p = 10.0$, $H_s = 1$, $\gamma = 1$).

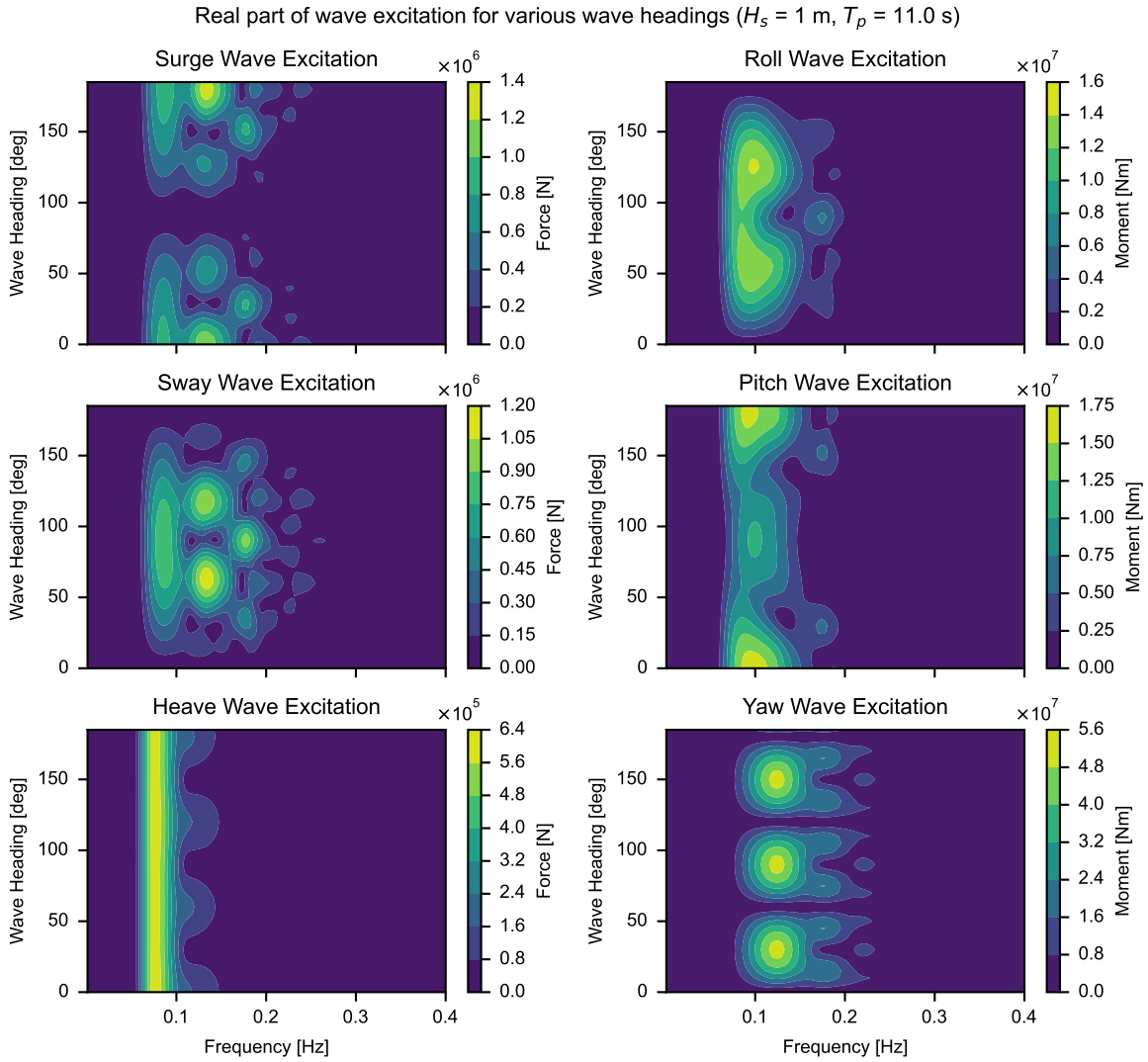

Figure B.9: Wave excitation RAO for 6 DOF's, multiplied by wave elevation from JONSWAP ($T_p = 11.0$, $H_s = 1$, $\gamma = 1$).

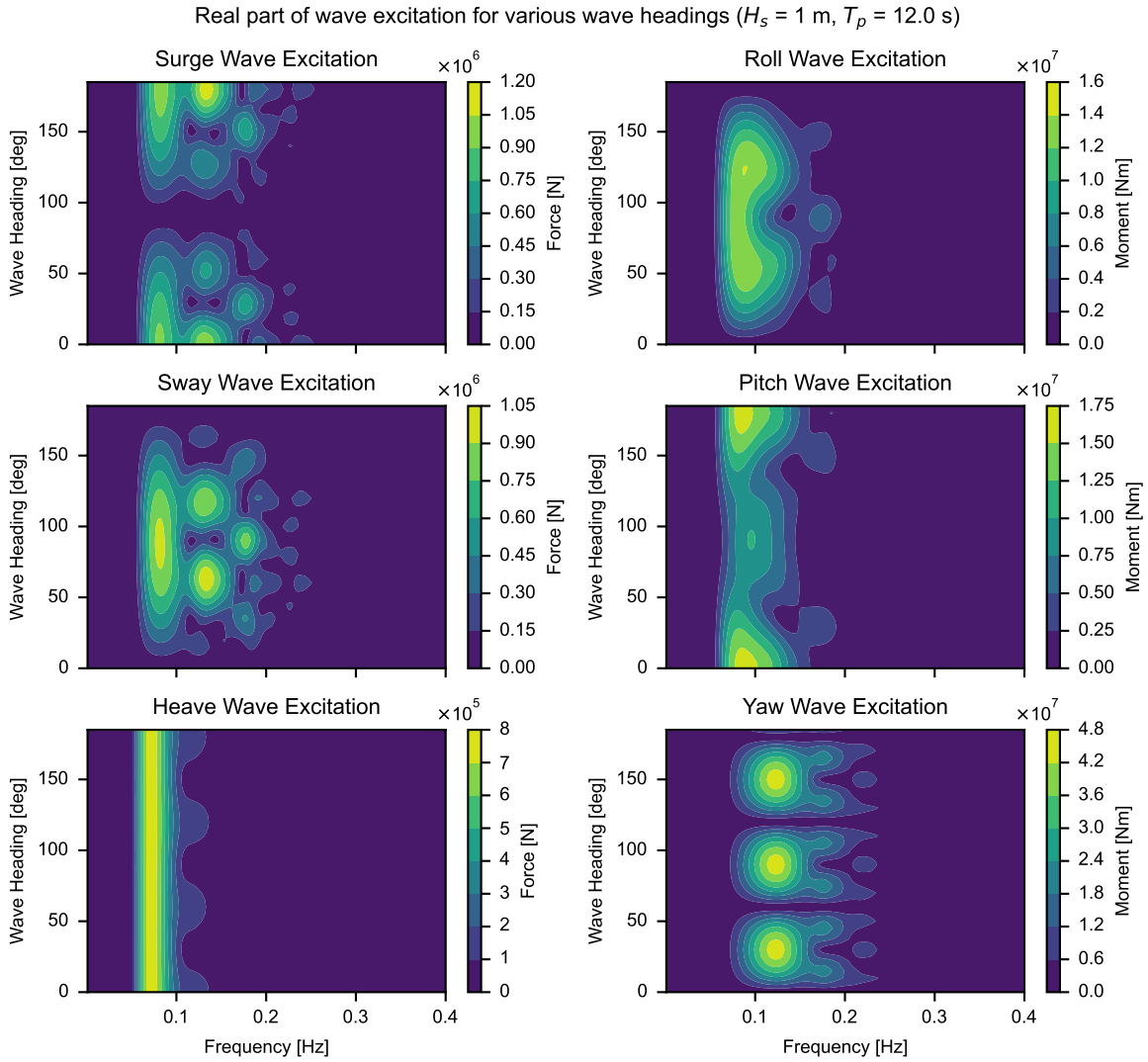

Figure B.10: Wave excitation RAO for 6 DOF's, multiplied by wave elevation from JONSWAP ($T_p = 12.0$, $H_s = 1$, $\gamma = 1$).

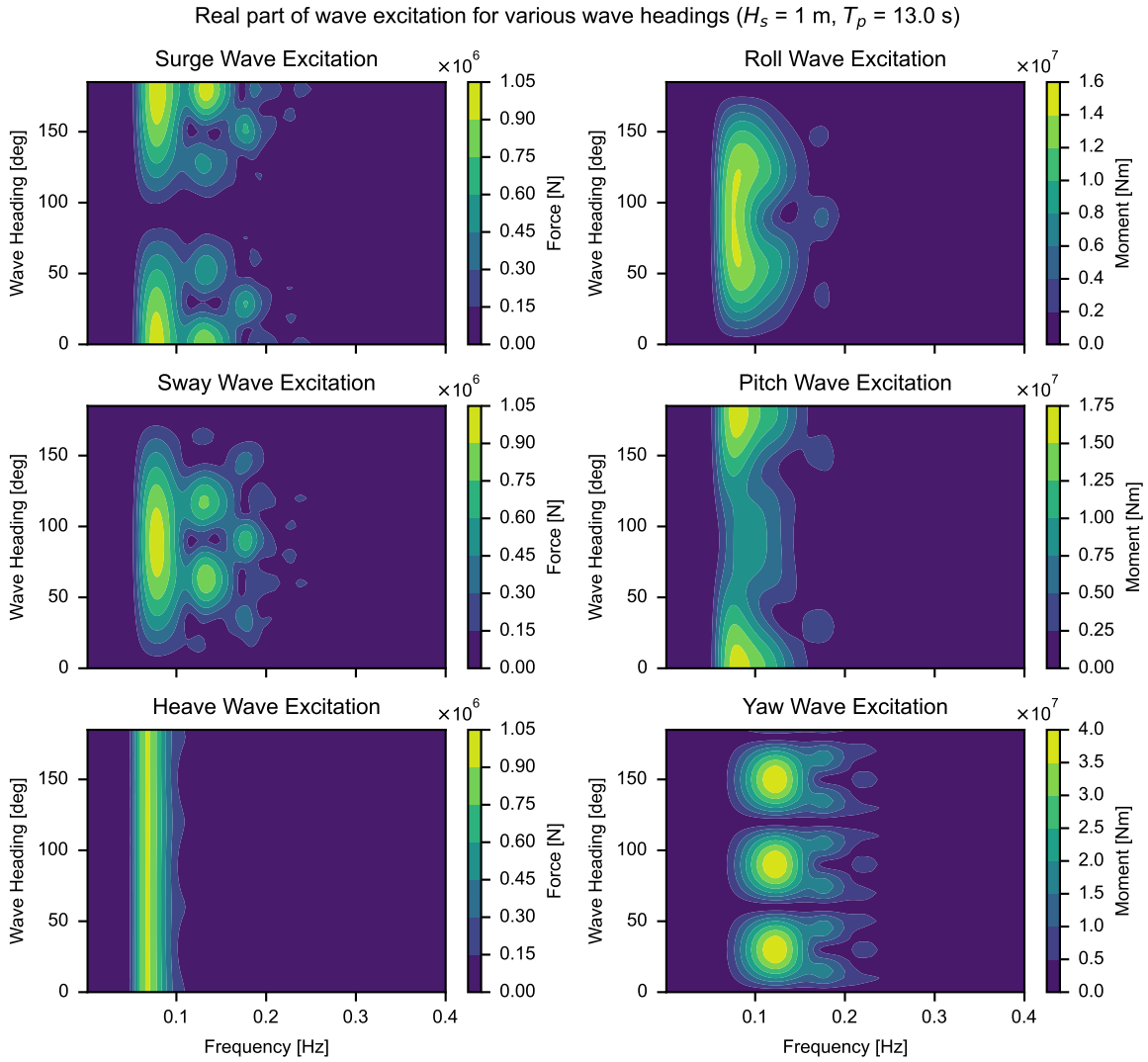

Figure B.11: Wave excitation RAO for 6 DOF's, multiplied by wave elevation from JONSWAP ($T_p = 13.0$, $H_s = 1$, $\gamma = 1$).

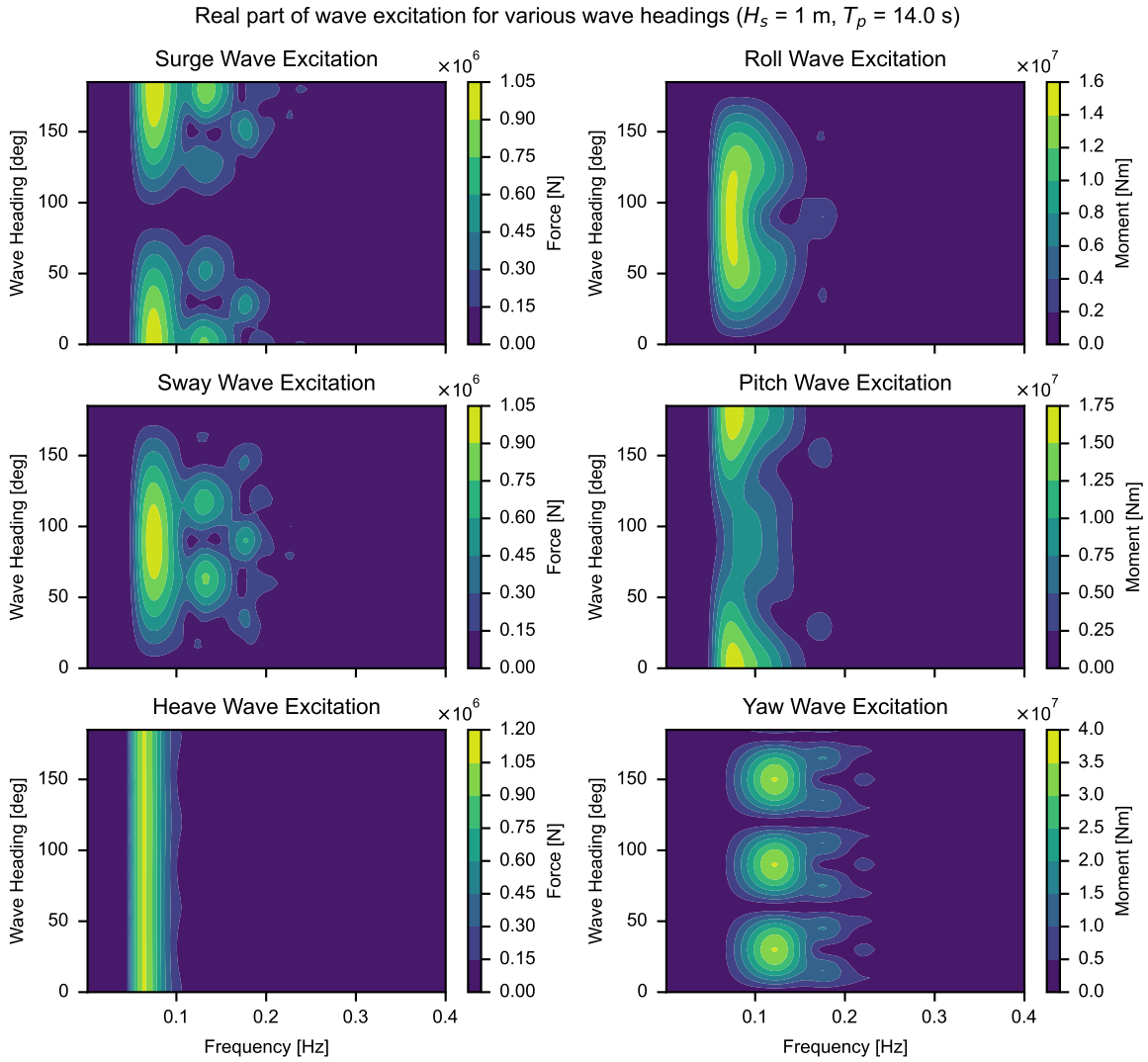

Figure B.12: Wave excitation RAO for 6 DOF's, multiplied by wave elevation from JONSWAP ($T_p = 14.0$, $H_s = 1$, $\gamma = 1$).

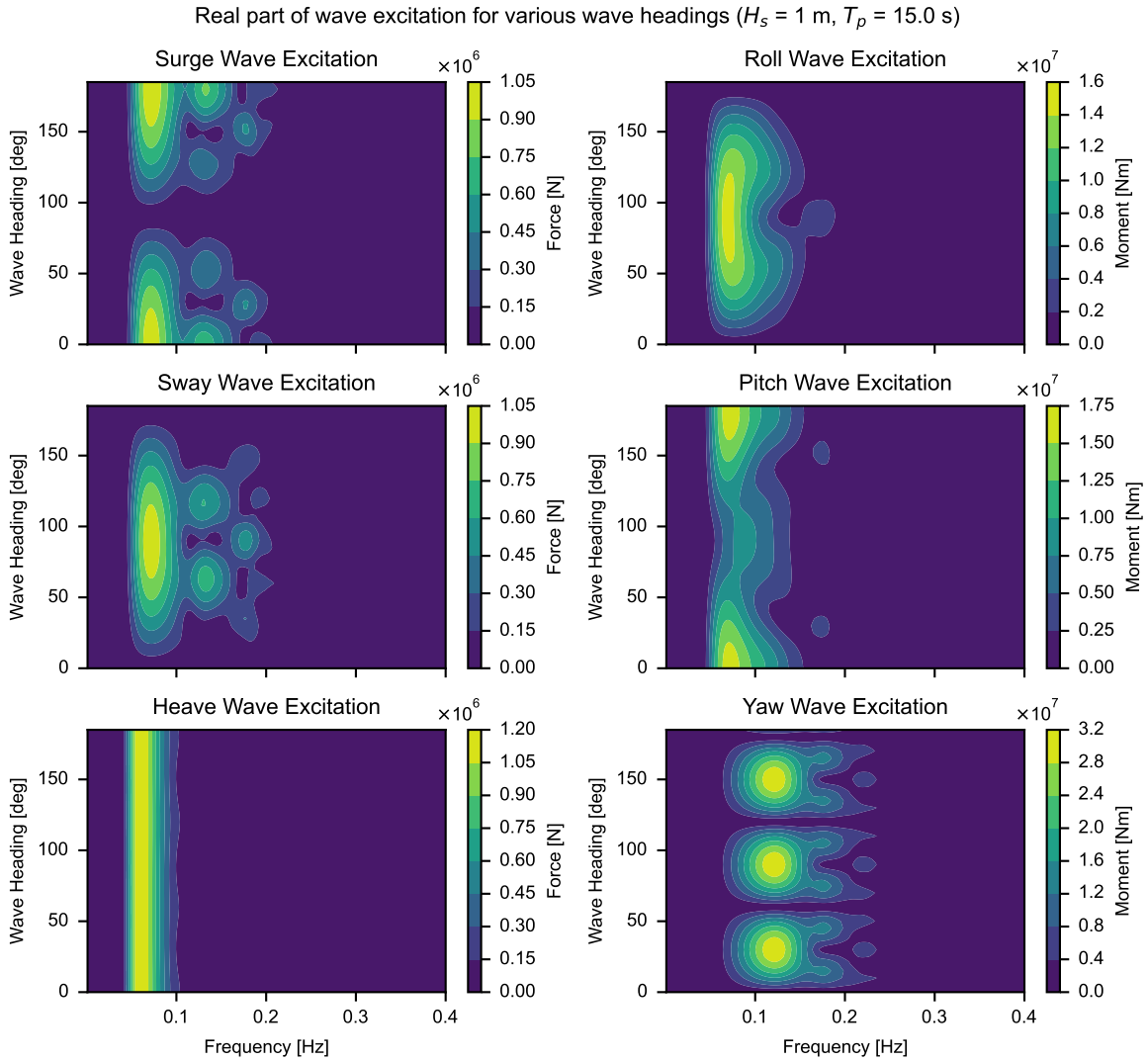

Figure B.13: Wave excitation RAO for 6 DOF's, multiplied by wave elevation from JONSWAP ($T_p = 15.0$, $H_s = 1$, $\gamma = 1$).

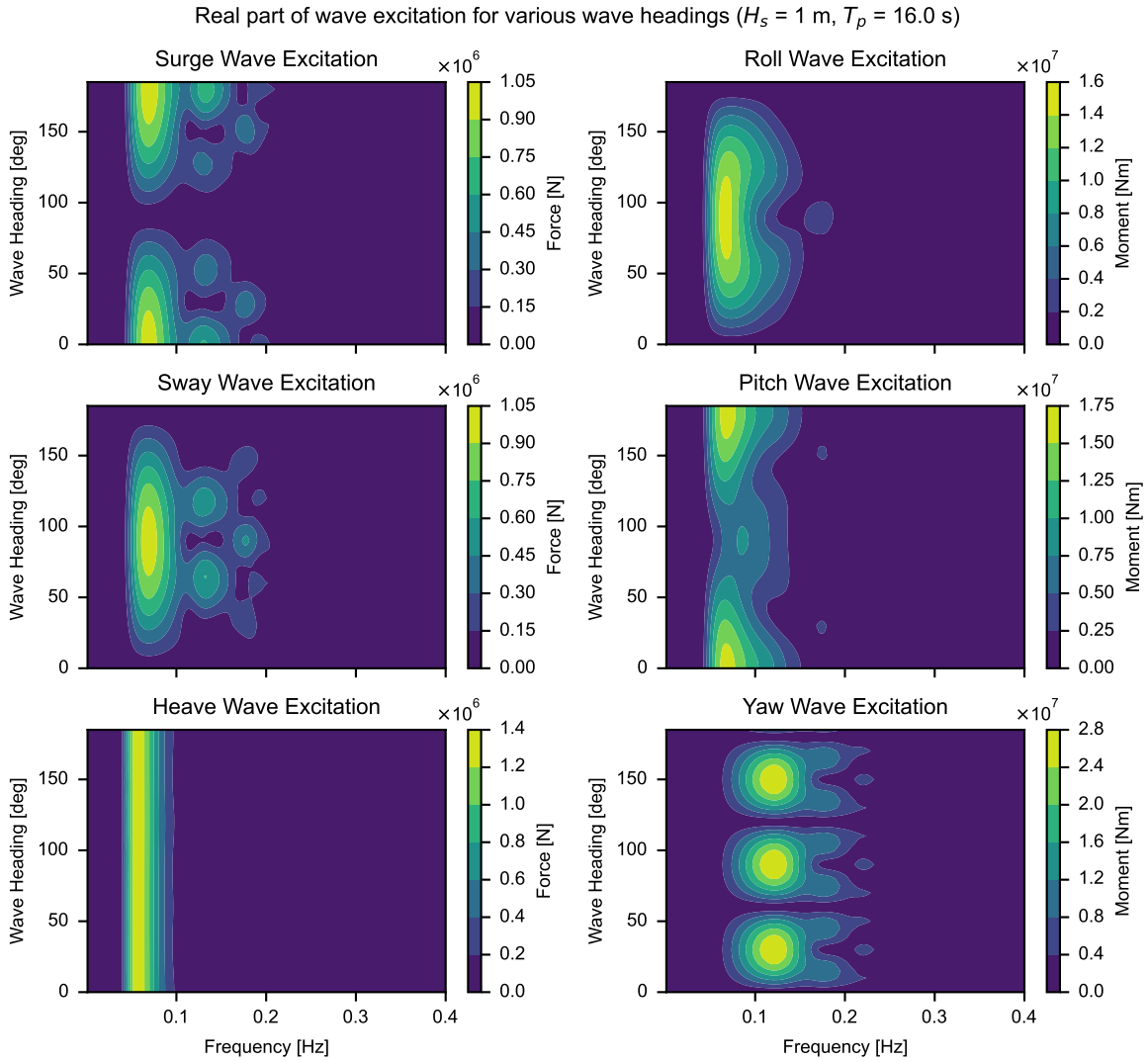

Figure B.14: Wave excitation RAO for 6 DOF's, multiplied by wave elevation from JONSWAP ($T_p = 16.0$, $H_s = 1$, $\gamma = 1$).

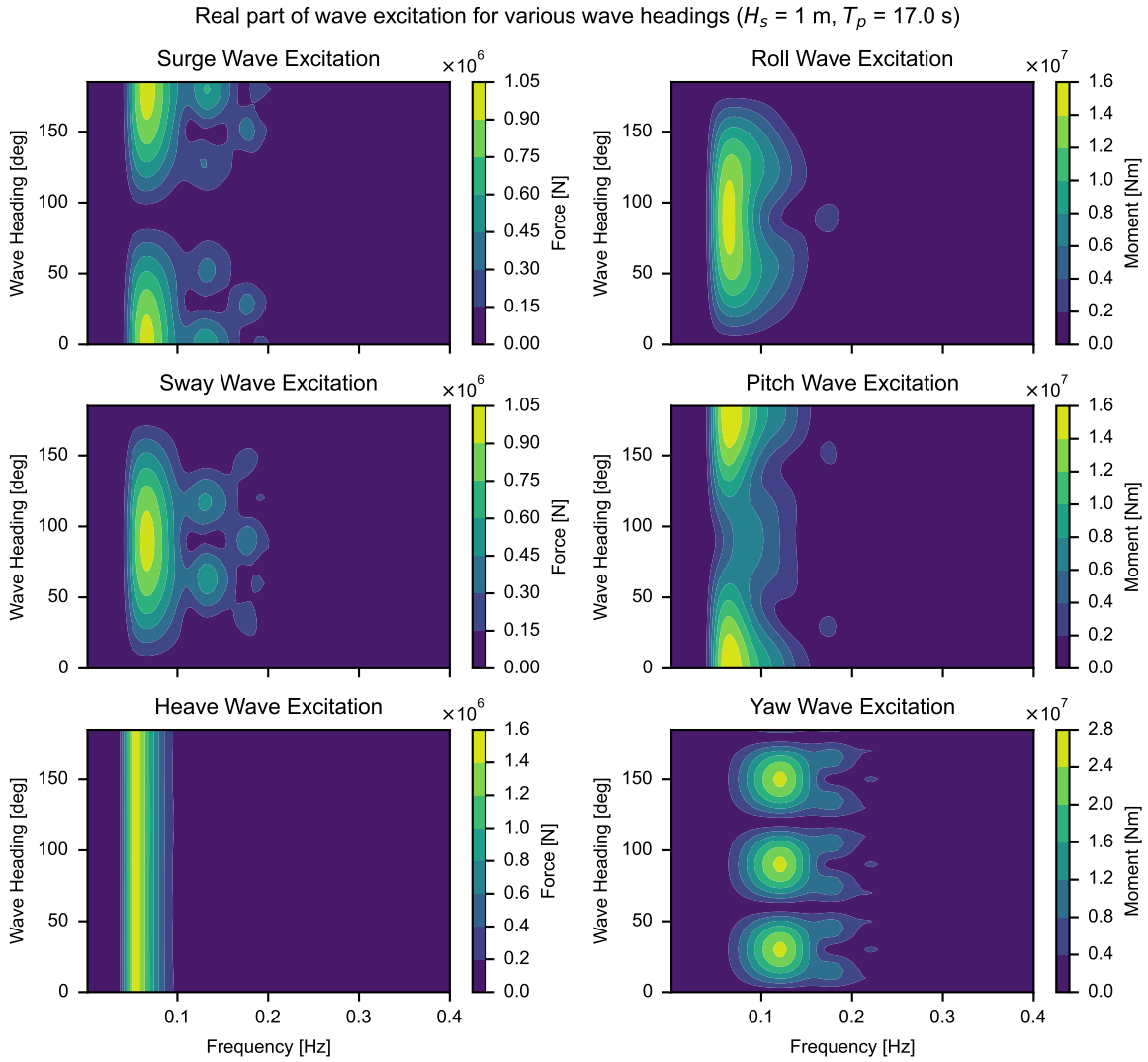

Figure B.15: Wave excitation RAO for 6 DOF's, multiplied by wave elevation from JONSWAP ($T_p = 17.0$, $H_s = 1$, $\gamma = 1$).

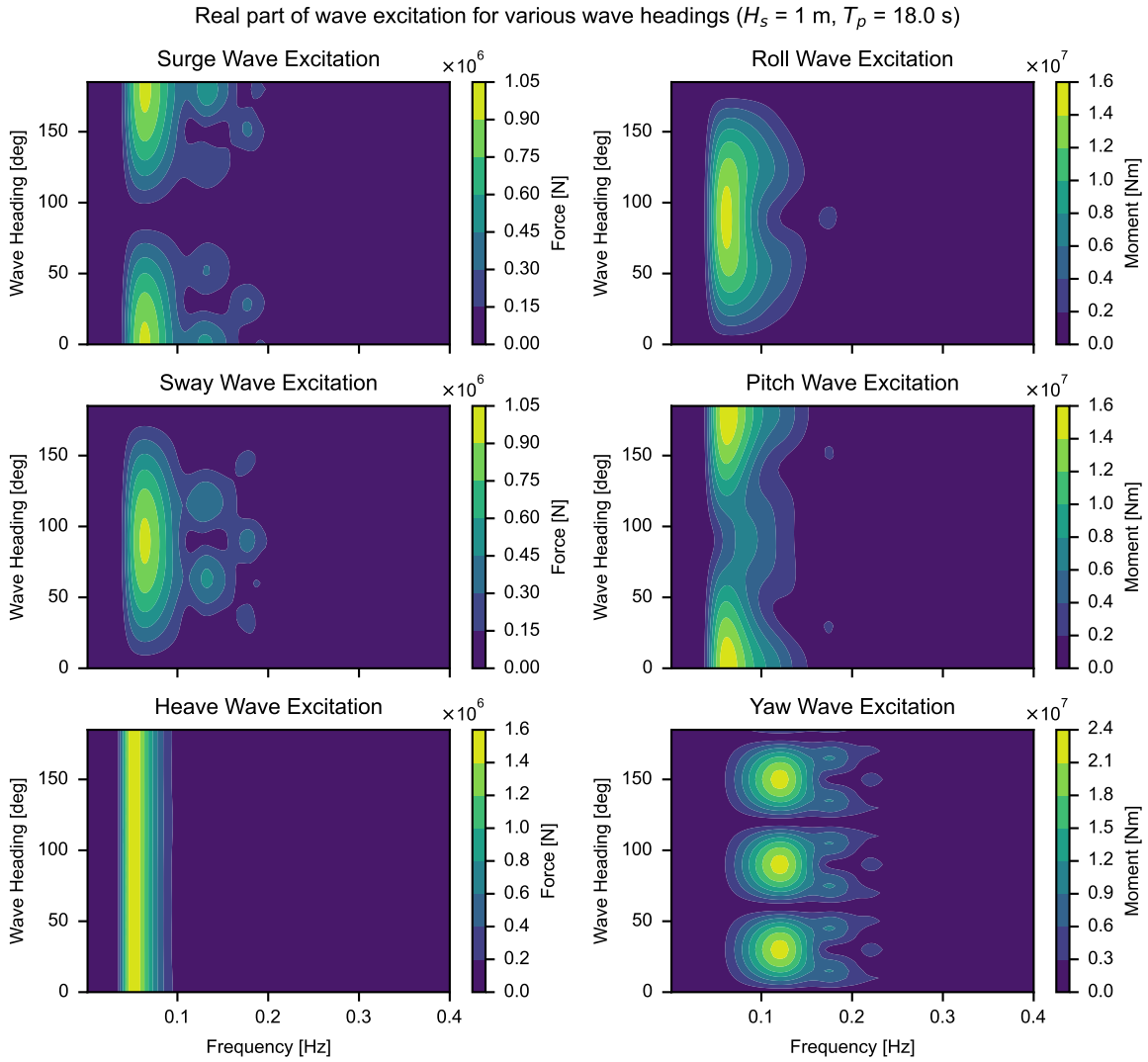

Figure B.16: Wave excitation RAO for 6 DOF's, multiplied by wave elevation from JONSWAP ($T_p = 18.0$, $H_s = 1$, $\gamma = 1$).

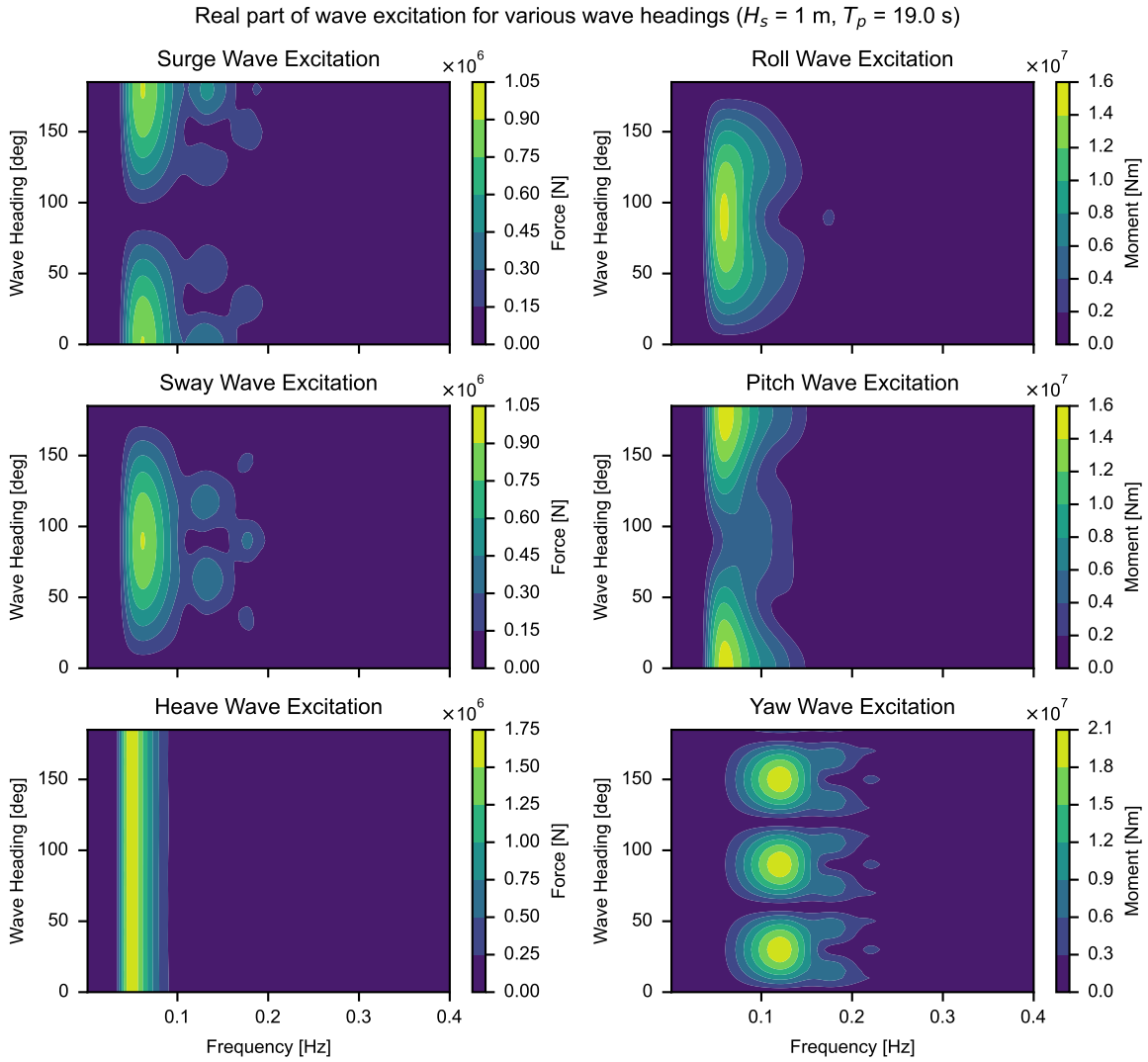

Figure B.17: Wave excitation RAO for 6 DOF's, multiplied by wave elevation from JONSWAP ($T_p = 19.0$, $H_s = 1$, $\gamma = 1$).

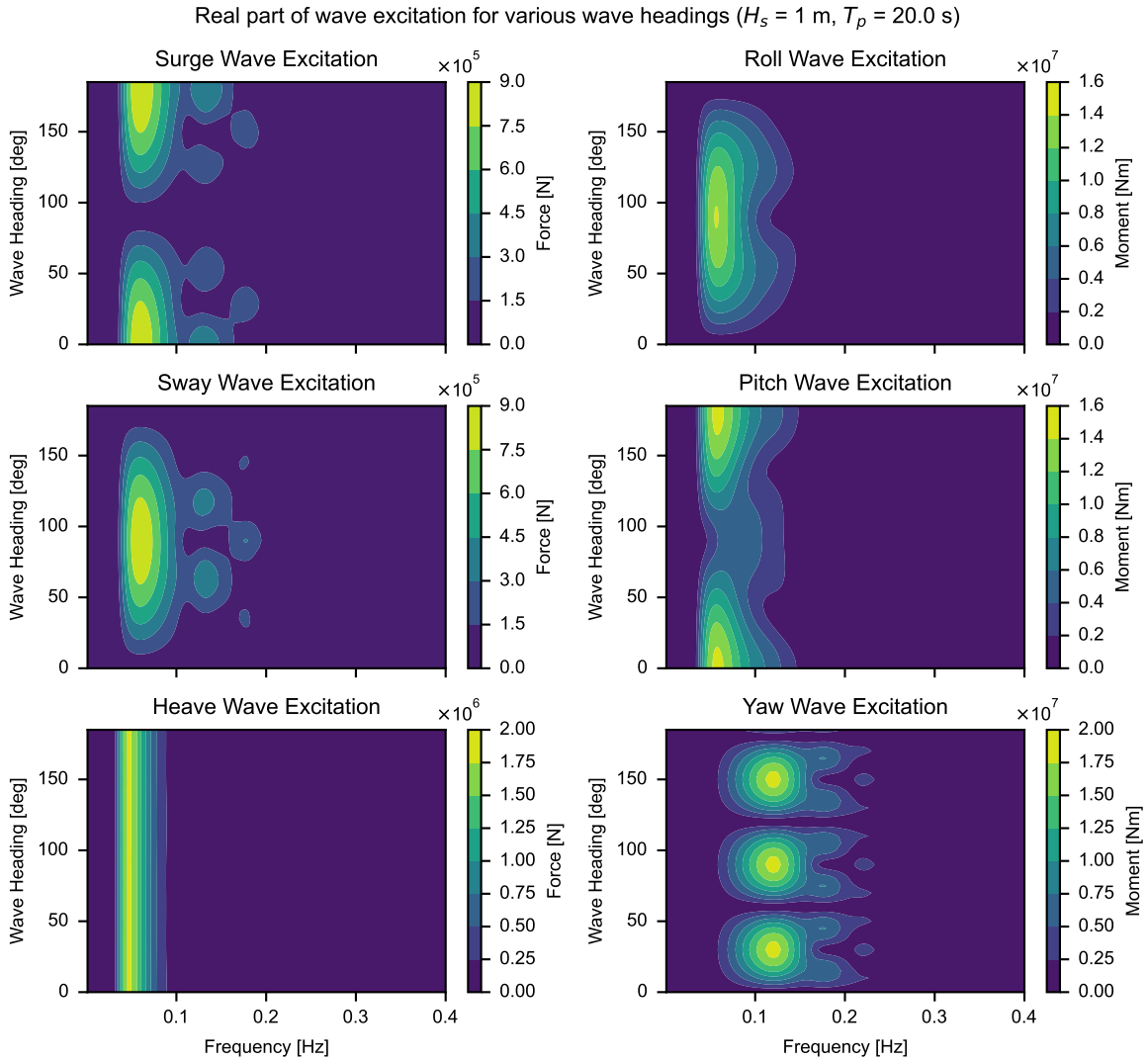

Figure B.18: Wave excitation RAO for 6 DOF's, multiplied by wave elevation from JONSWAP ($T_p = 20.0$, $H_s = 1$, $\gamma = 1$).

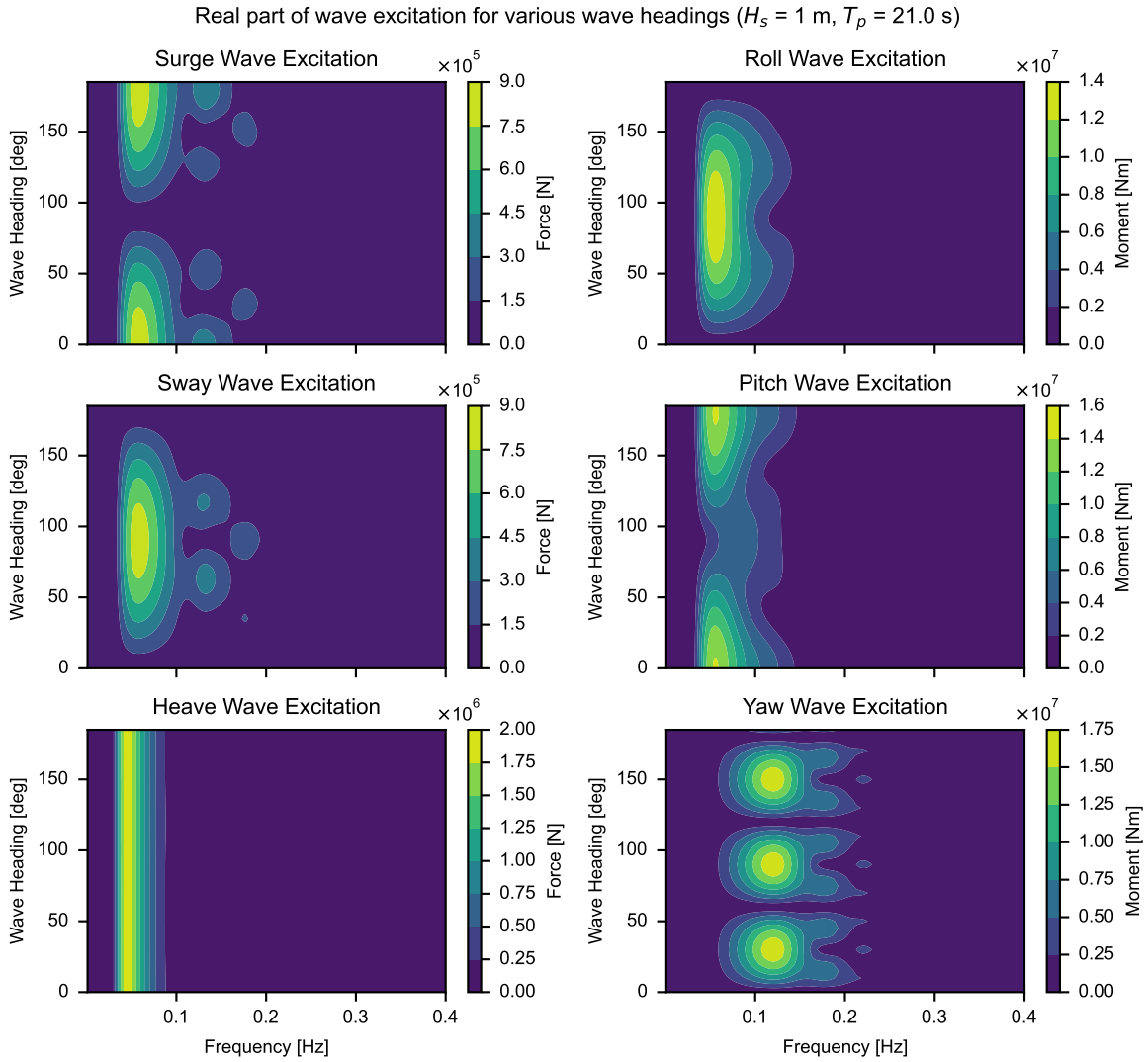

Figure B.19: Wave excitation RAO for 6 DOF's, multiplied by wave elevation from JONSWAP ($T_p = 21.0$, $H_s = 1$, $\gamma = 1$).

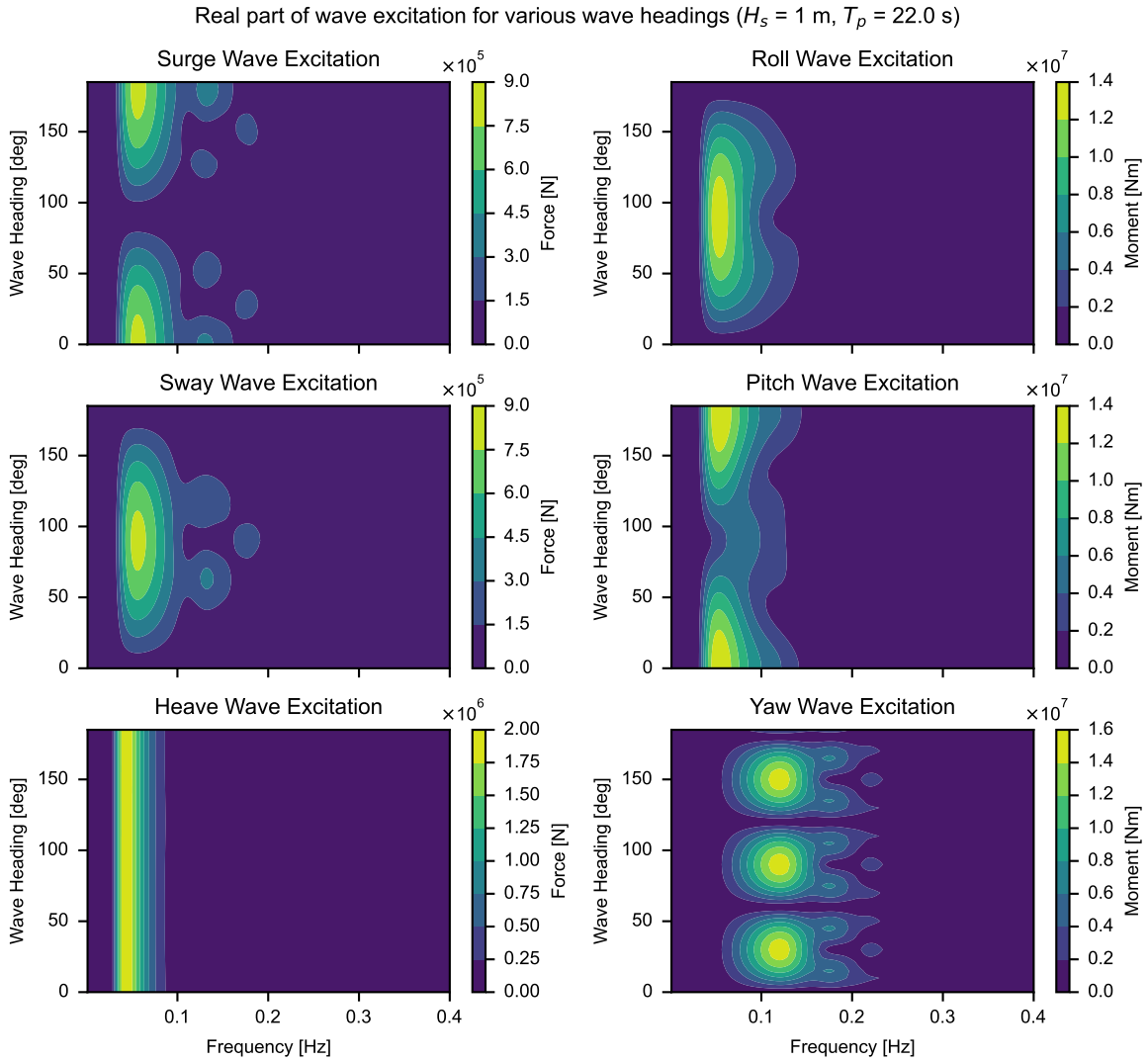

Figure B.20: Wave excitation RAO for 6 DOF's, multiplied by wave elevation from JONSWAP ($T_p = 22.0$, $H_s = 1$, $\gamma = 1$).

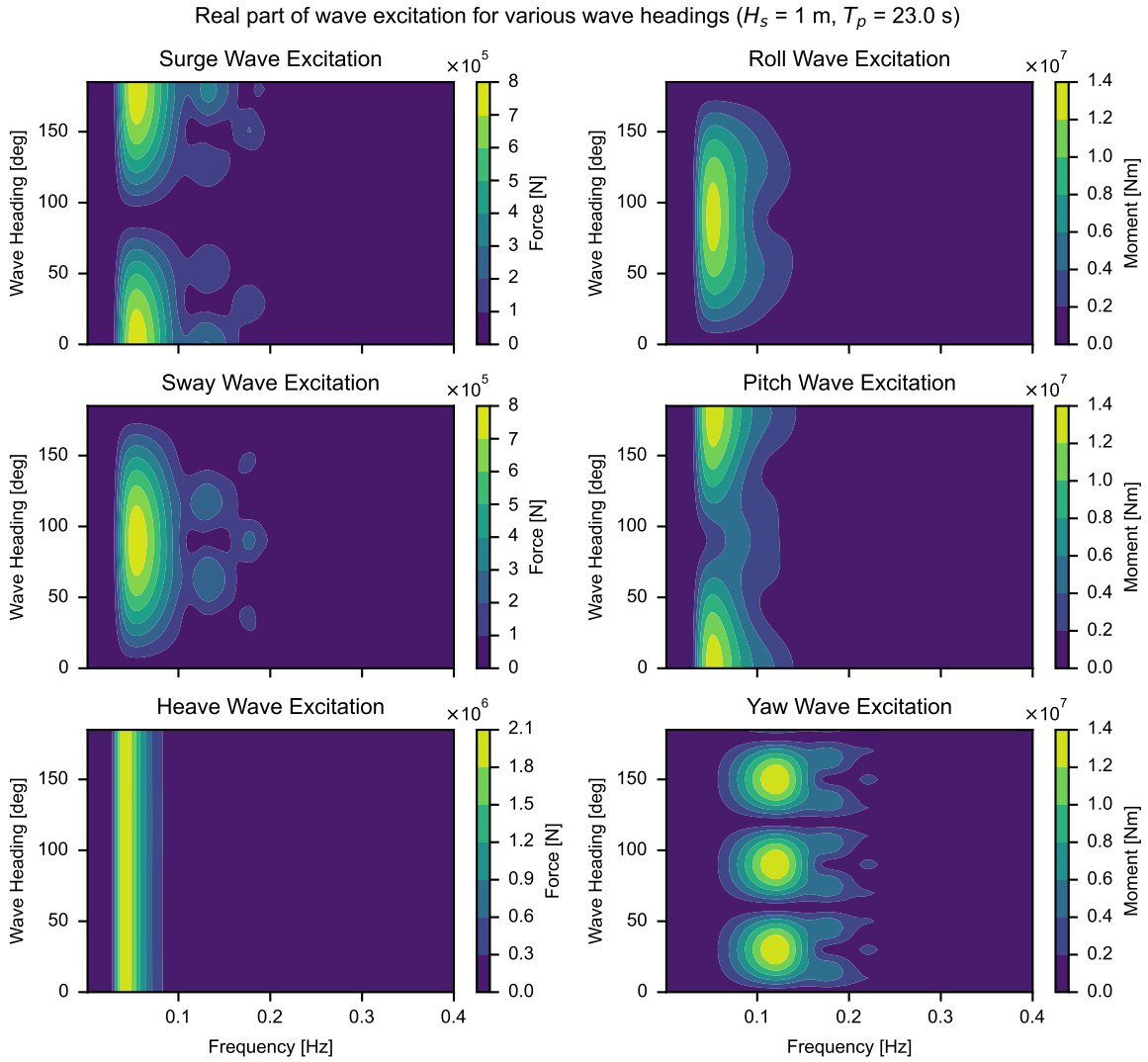

Figure B.21: Wave excitation RAO for 6 DOF's, multiplied by wave elevation from JONSWAP ($T_p = 23.0$, $H_s = 1$, $\gamma = 1$).

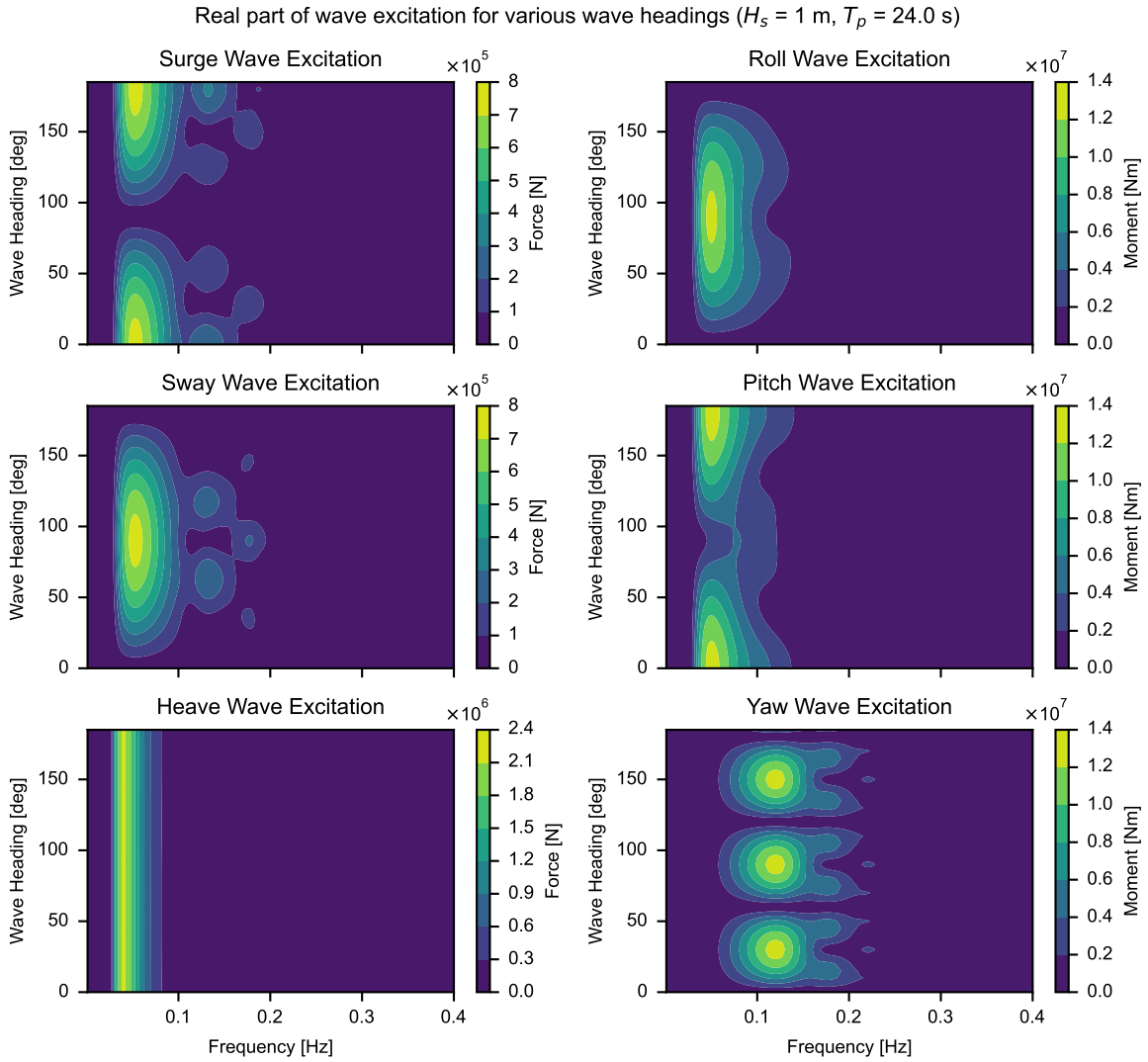

Figure B.22: Wave excitation RAO for 6 DOF's, multiplied by wave elevation from JONSWAP ($T_p = 24.0$, $H_s = 1$, $\gamma = 1$).

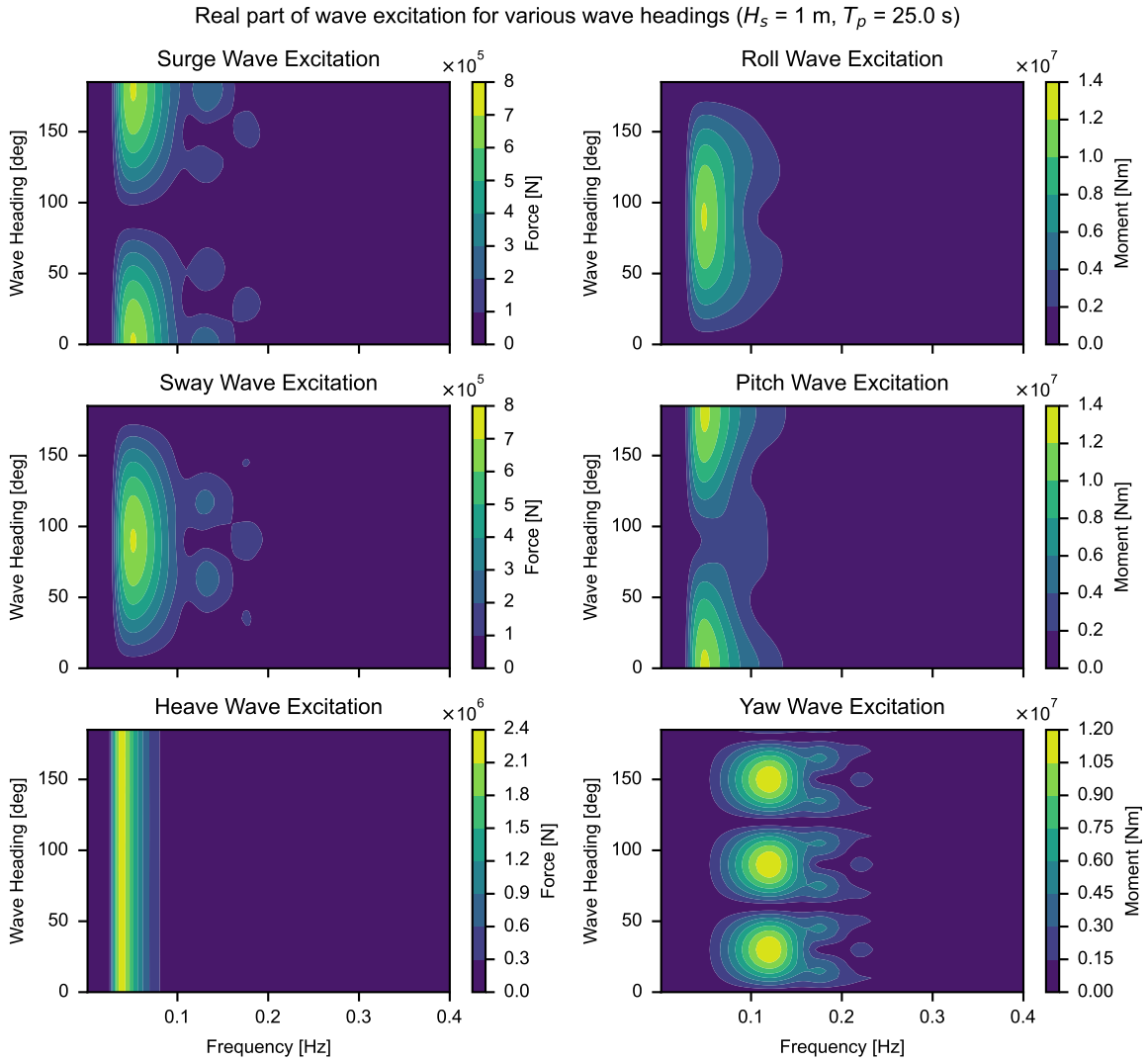

Figure B.23: Wave excitation RAO for 6 DOF's, multiplied by wave elevation from JONSWAP ($T_p = 25.0$, $H_s = 1$, $\gamma = 1$).

C

System Matrices DLC cases.

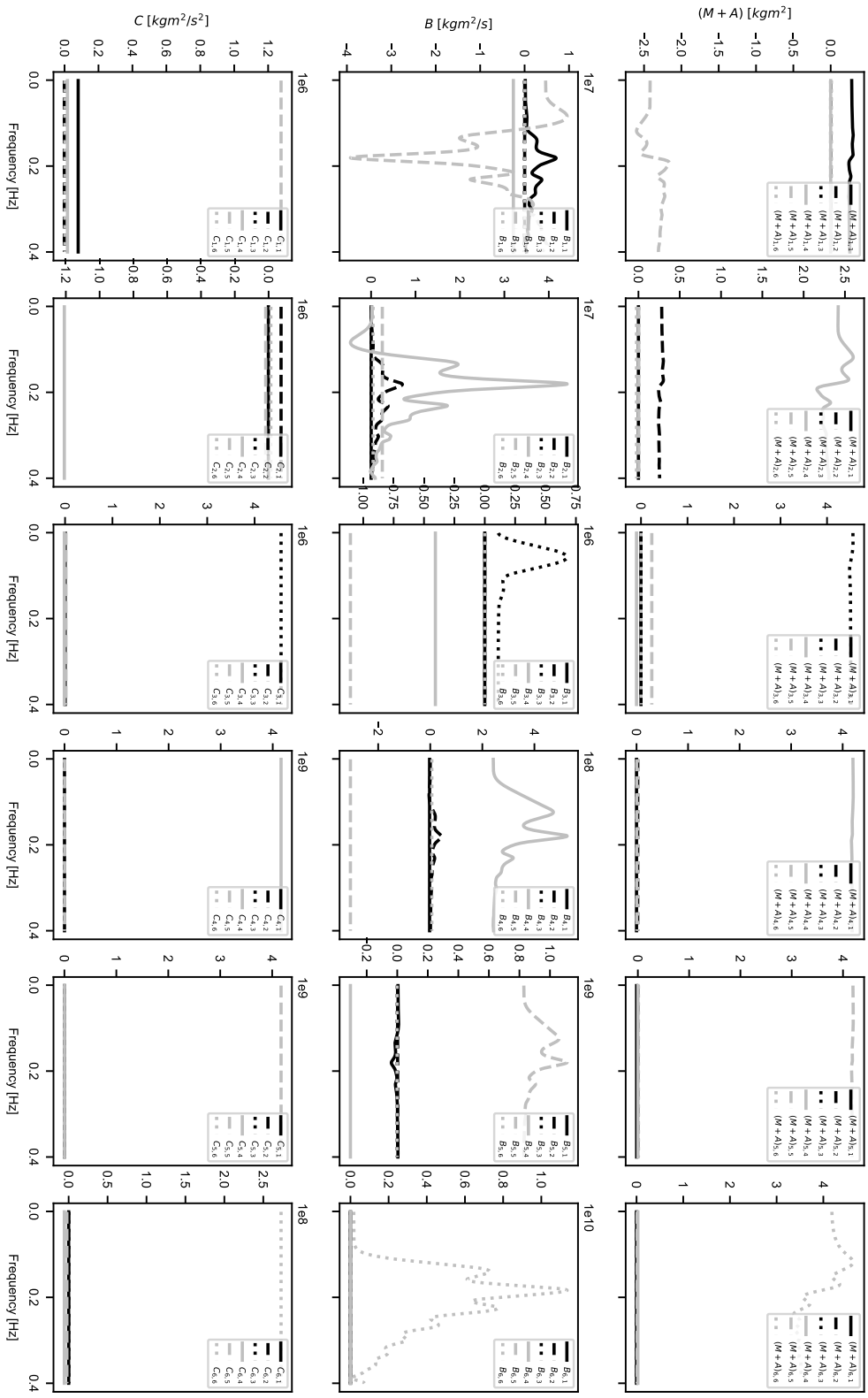

Figure C.1: DLC comparison case 1 system matrices.

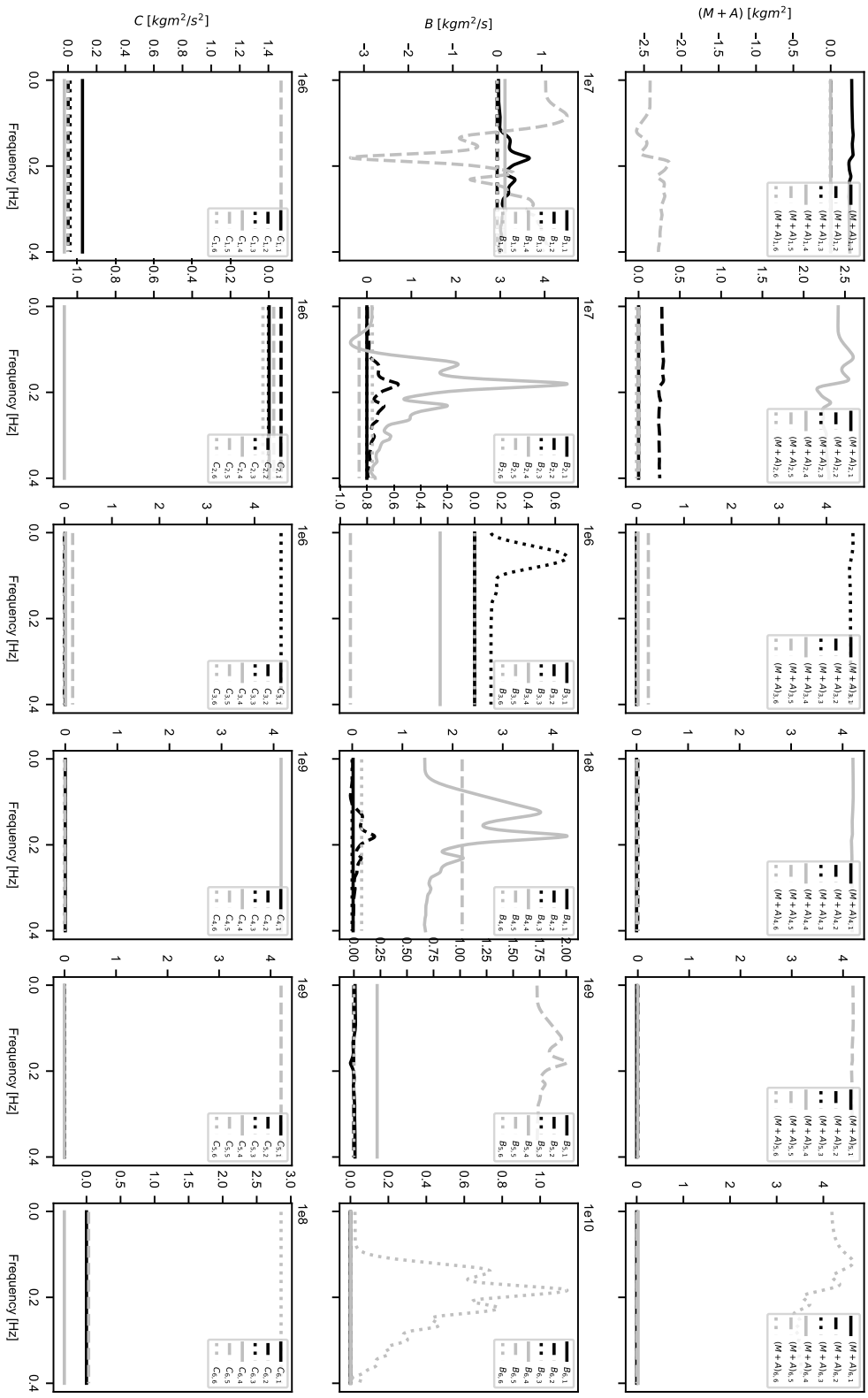

Figure C.2: DLC comparison case 2 system matrices.

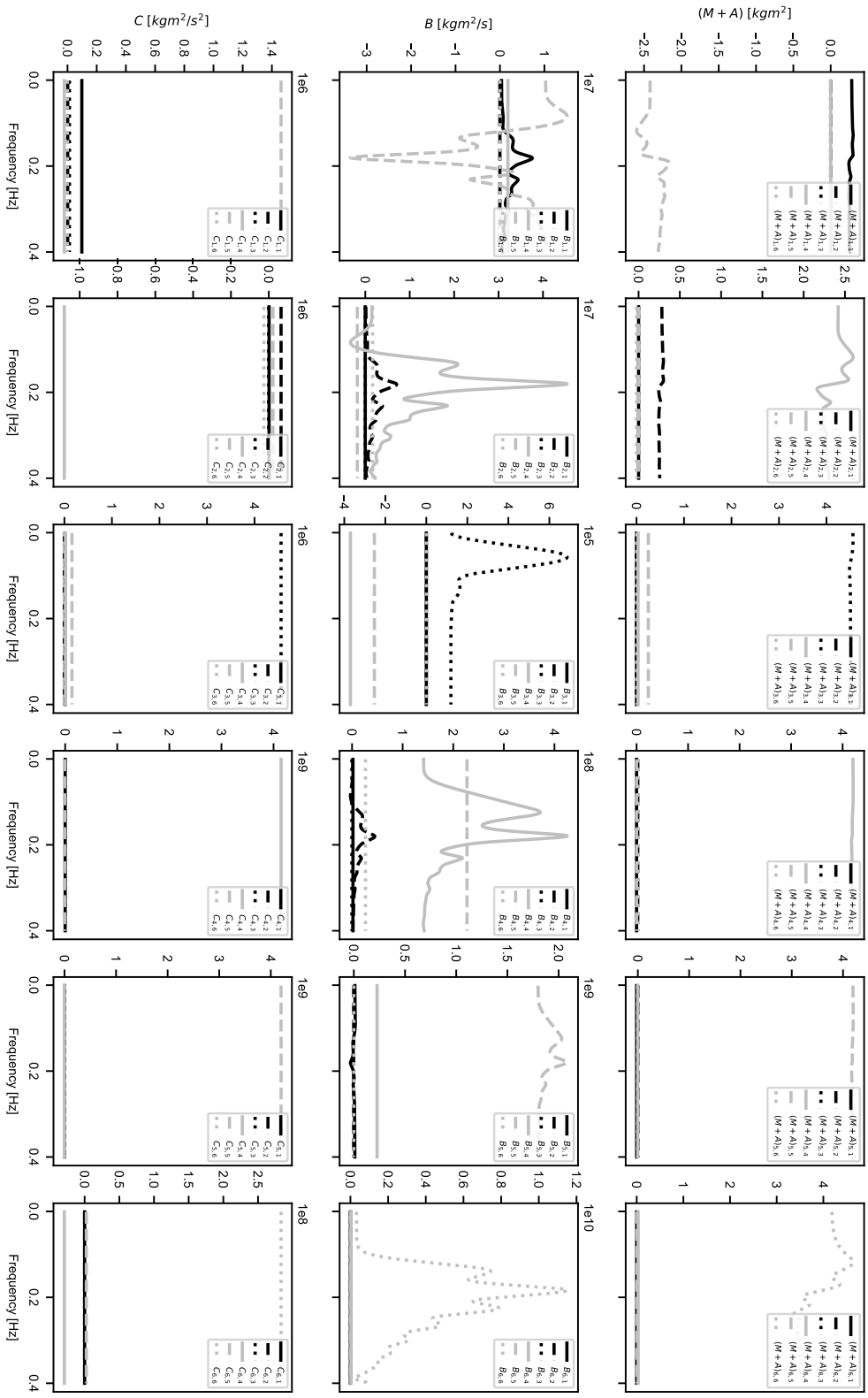

Figure C.3: DLC comparison case 3 system matrices.

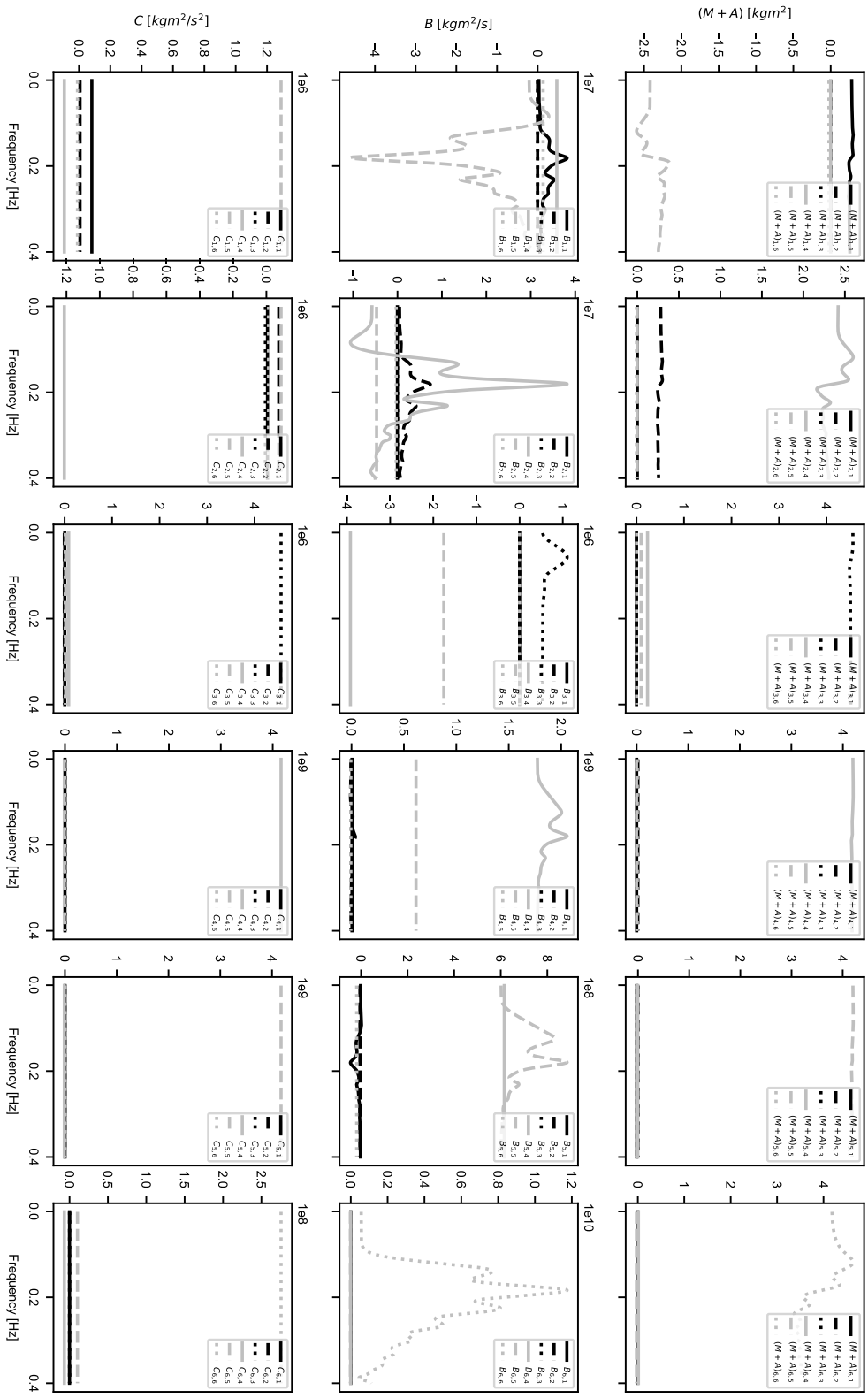

Figure C.4: DLC comparison case 4 system matrices.

D

Tower base bending comparison

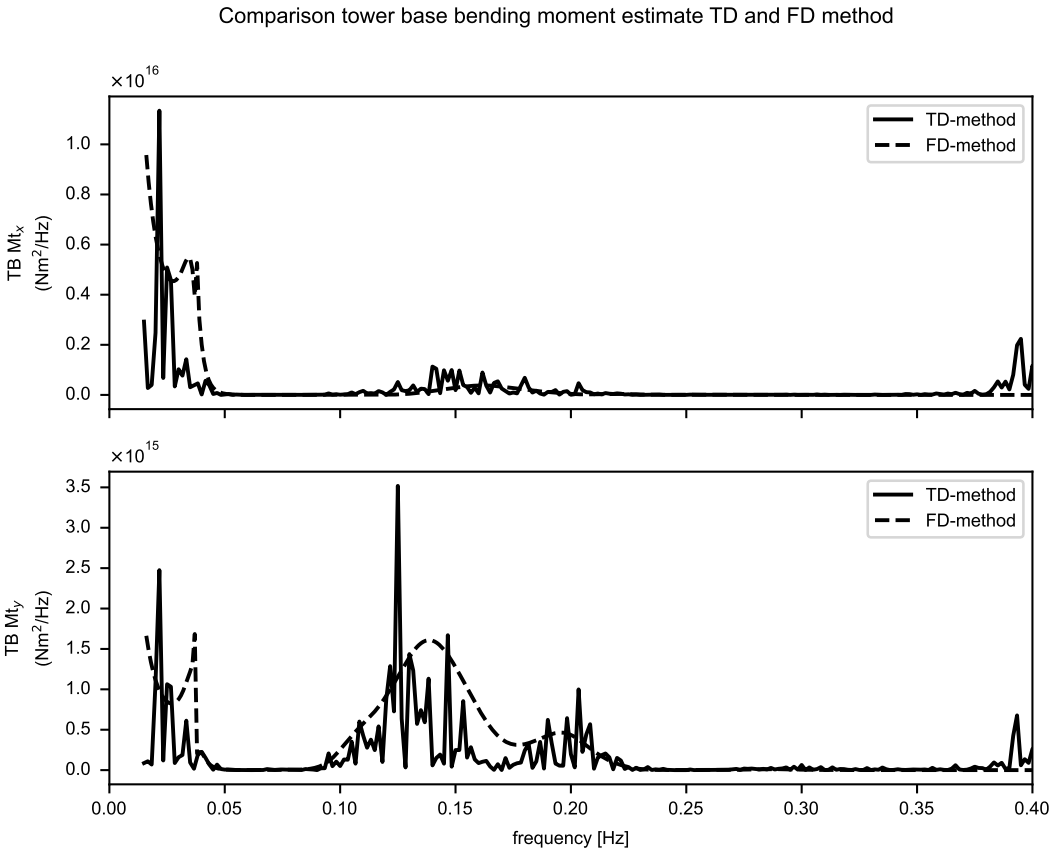

Figure D.1: Tower base bending PSD's (case 2).

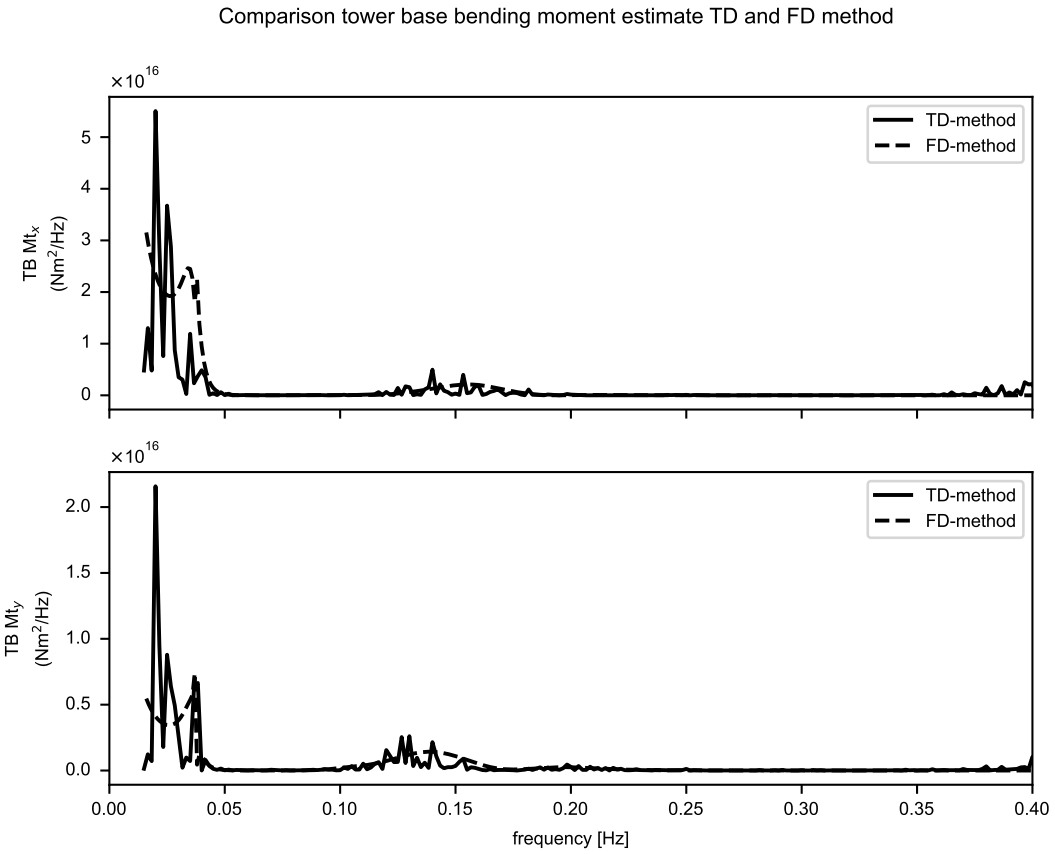

Figure D.2: Tower base bending PSD's (case 3).

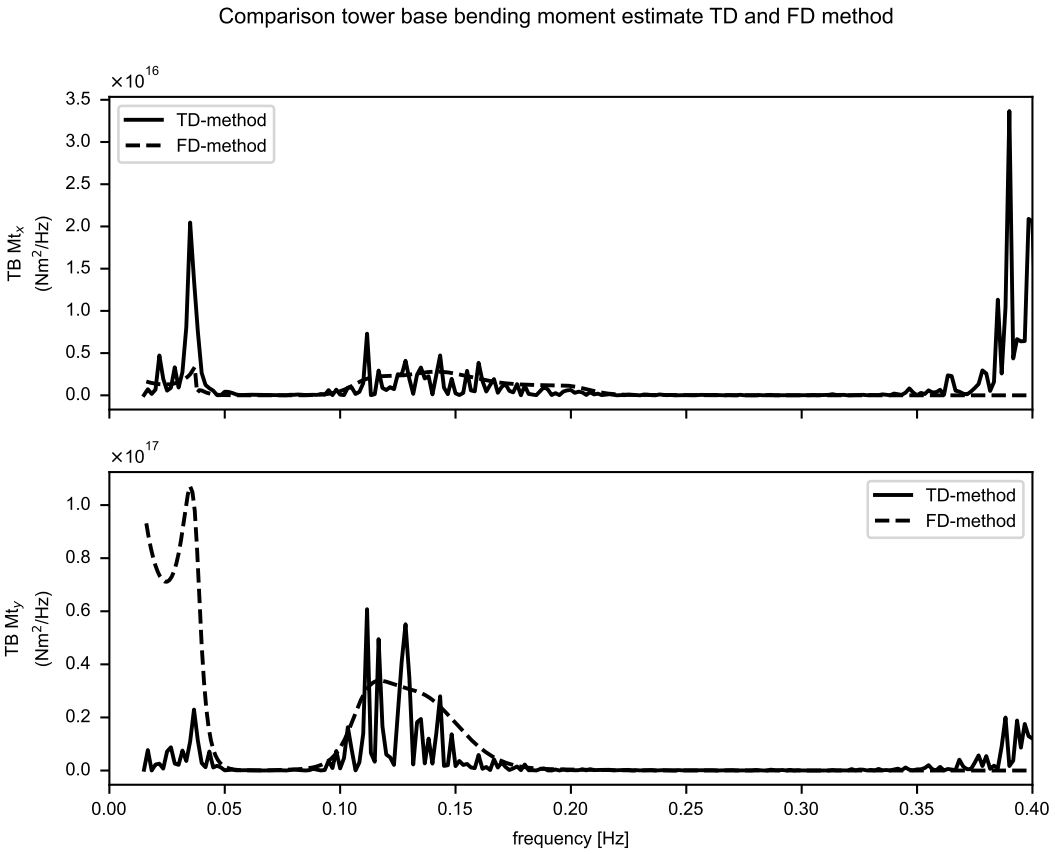

Figure D.3: Tower base bending PSD's (case 4).